

# **Computational Models for Dissolution-based Plastic Recycling**

by

Panzheng Zhou

A dissertation submitted in partial fulfillment of  
the requirements for the degree of

Doctor of Philosophy

(Chemical Engineering)

at the

UNIVERSITY OF WISCONSIN–MADISON

2025

Date of final oral examination: 03/11/2025

The dissertation is approved by the following members of the Final Oral Committee:

Reid C. Van Lehn, Associate Professor, Chemical & Biological Engineering

George W. Huber, Professor, Chemical & Biological Engineering

Styliani Avraamidou, Assistant Professor, Chemical & Biological Engineering

David M. Lynn, Professor, Chemistry





*To my parents, for their unwavering support and endless encouragement.*

## ACKNOWLEDGMENTS

---

This PhD would not have been possible without the support of my mentors, group members, family, and friends. I am deeply grateful for all the help I received throughout this journey. I have been inspired and guided by many great academic minds, and I have found strength in the support and encouragement of many caring hearts during difficult times. These invaluable gifts have made my PhD both enjoyable and memorable, and I express my heartfelt gratitude here.

First and foremost, I would like to thank my advisor, Prof. Reid Van Lehn. I consider Reid not only an outstanding advisor, but also a supportive friend and an academic role model. His brilliant and insightful guidance has been invaluable to my research projects, many of which form key parts of this thesis. He has always listened carefully to my research ideas, and has taken all of them seriously, no matter how bold or eccentric they might be. In the past several years, I have conducted my thesis research and several side projects with Reid, I have also sat in his classroom as a student, served as teaching assistant for his course, and attended academic conferences with him. I have benefited a lot from these valuable interactions with Reid and was very lucky to receive such quality academic training. I am very grateful for all the mentorship and care of him, and I wish to carry on many of his admirable qualities in my future career and life.

I am also thankful to my other mentors: Prof. George Huber and Prof. Victor Zavala. I enjoyed our collaborative projects, which have elevated my research to the next level and expanded my knowledge in different scientific areas. Both professors are world-class experts in their fields, and have provided great expertise and suggestions to my research. In addition to the professors, I also want to thank the outstanding graduate students and postdocs in their groups, especially Jiuling Yu, Kevin Sánchez-Rivera, Aurora del Carmen Munguía-López, Raka Dastidar, and Tianwei Yan. They have made a lot of helpful conversations, insights and contributions to many of the projects that I was part of.

I would also like to thank my fellow group members and other graduate students in our department. Our group members have made it a great pleasure to work in the office, and have formed a wonderful team in every conference trip and social event. I have learned a lot from the knowledge sharing and practice talks within the group. I am also grateful to the companion and support of many fellow graduate students in

the department, which helped me through many difficult challenges in this journey.

I am grateful to my PhD defense committee members: Prof. Reid Van Lehn, Prof. George Huber, Prof. Styliani Avraamidou, and Prof. David Lynn. I appreciate your time and effort in reviewing and improving my dissertation. I also want to thank Prof. Marcel Schreier and Prof. Victor Zavala for your valuable advice as committee members of my preliminary exam and research progress meeting.

I also want to thank the advisors of my undergraduate studies, Prof. Yijun He, Prof. Christos Maravelias, and Prof. Nikolaos Sahinidis, who have inspired and encouraged me to pursue a PhD.

Finally, I would not have been able to achieve anything without the help of my family and friends, who provided endless support not only in my PhD journey, but in my entire life.

I am grateful for the support by (1) the Department of Chemical and Biological Engineering at the University of Wisconsin-Madison, (2) the Center for Chemical Upcycling of Waste Plastics, and (3) the Bioenergy Technologies Office in the Office of Energy Efficiency and Renewable Energy at the Department of Energy, under award number DE-EE0009285.

## CONTENTS

---

<b>Contents</b>	<b>iv</b>
<b>List of Tables</b>	<b>viii</b>
<b>List of Figures</b>	<b>xi</b>
<b>Abstract</b>	<b>xvii</b>
<b>1 Introduction</b>	<b>1</b>
1.1 Motivation . . . . .	1
1.2 Solubility prediction methods for polymer-solvent systems . . . . .	3
1.2.1 Background . . . . .	3
1.2.2 Research questions . . . . .	5
1.3 Solvent screening and process development for dissolution-based plastic recycling processes . . . . .	6
1.3.1 Background . . . . .	6
1.3.2 Research questions . . . . .	8
1.4 Outline of this dissertation . . . . .	8
1.5 References . . . . .	10
<b>2 Molecular-scale models for temperature-dependent polymer solubility predictions</b>	<b>14</b>
2.1 Introduction . . . . .	14
2.2 Methods . . . . .	17
2.2.1 Summary of computational approach . . . . .	17
2.2.2 Molecular dynamics simulations . . . . .	18
2.2.3 Conformational sampling and conformer selection . . . . .	20
2.2.4 Density functional theory calculations . . . . .	21
2.2.5 Solubility prediction with COSMO-RS . . . . .	22
2.2.6 Experimental measurements of solubility . . . . .	23
2.3 Results and discussion . . . . .	24
2.3.1 Conformational sampling methods . . . . .	24
2.3.2 Experimental solubility data . . . . .	27

2.3.3	HSP-based solvent screening . . . . .	28
2.3.4	COSMO-RS calculations . . . . .	30
2.3.5	PE solubility predictions . . . . .	32
2.3.6	EVOH solubility predictions . . . . .	35
2.3.7	Computational screening of selective solvents . . . . .	39
2.4	Summary . . . . .	41
2.5	References . . . . .	42
<b>3</b>	<b>Large-scale computational polymer solubility predictions and applications to dissolution-based plastic recycling</b>	<b>47</b>
3.1	Introduction . . . . .	48
3.1.1	Literature reports of solvents/non-solvents for common polymers	51
3.1.2	Industrial projects . . . . .	53
3.1.3	Limitations of existing methods . . . . .	53
3.2	Methods . . . . .	55
3.2.1	Summary of approach . . . . .	55
3.2.2	Computational simulations for solubility prediction . . . . .	56
3.2.3	Experimental solubility measurements and polymer separations	59
3.3	Results and discussion . . . . .	62
3.3.1	Creation of the polymer solubility database . . . . .	62
3.3.2	Analysis of polymer solubility trends . . . . .	65
3.3.3	Polymer separation sequence and solvent screening . . . . .	68
3.3.4	Case study: separation of binary polymer mixtures . . . . .	70
3.3.5	Case study: separation of ternary polymer mixtures . . . . .	75
3.3.6	Case study: improving polymer recovery process via temperature-controlled precipitation . . . . .	79
3.3.7	Case study: separation of a post-industrial film with 5 polymer components . . . . .	81
3.3.8	Case study: separation of 10-polymer mixtures . . . . .	85
3.3.9	Case study: potential THP applications in plastic dissolution .	91
3.4	Summary . . . . .	97
3.5	References . . . . .	98
<b>4</b>	<b>Integrated optimization framework for the design of dissolution-based plastic recycling processes</b>	<b>106</b>

4.1	Introduction . . . . .	107
4.2	Methods . . . . .	109
4.2.1	STRAP process description and assumptions . . . . .	109
4.2.2	Computational framework . . . . .	112
4.3	Results and discussion . . . . .	118
4.3.1	Case study: recycling a multilayer film of 4 polymers . . . . .	119
4.3.2	Case study: recycling mixed plastic waste stream of 7 polymers	121
4.3.3	Case study: guiding the design of easy-to-recycle plastic products	123
4.3.4	Case study: separation difficulty of different polymer combina- tions . . . . .	125
4.4	Summary . . . . .	128
4.5	References . . . . .	130
<b>5</b>	<b>Contaminant removal strategies for plastic products based on computa- tional property prediction and solvent screening</b>	<b>136</b>
5.1	Introduction . . . . .	137
5.2	Computational framework . . . . .	139
5.3	Results and discussion . . . . .	142
5.3.1	Case study: BFR removal from plastic products . . . . .	142
5.3.2	Case study: phthalates removal from PVC . . . . .	144
5.3.3	Case study: PFAS removal from LDPE . . . . .	149
5.3.4	Case study: ink removal from printed multilayer plastic films	152
5.4	Summary . . . . .	163
5.5	References . . . . .	164
<b>6</b>	<b>Conclusion and future research</b>	<b>169</b>
6.1	Contributions . . . . .	169
6.2	Future research directions . . . . .	170
6.2.1	Improvement and extension of current property prediction workflow for polymer-solvent systems . . . . .	170
6.2.2	Identification of green alternative solvents for solvent-mediated processes . . . . .	172
6.2.3	Computational tool development for all-atom MD simulations of complex polymers . . . . .	173

6.2.4	Supercritical fluids as tunable solvents and pressure effect on polymer-solvent interactions . . . . .	174
6.3	References . . . . .	175

## LIST OF TABLES

2.1	Coverage (quantified by the convex hull hypervolume) of reduced $\sigma$ -profile spaces for 6 conformation sets. Maximum values for each number of reduced dimensions are bolded. . . . .	27
2.2	Experimental measurement of EVOH and PE solubilities. . . . .	28
2.3	HSP values for PE and EVOH (multiple versions for PE were found). . .	29
2.4	HSP-based solvent screening for PE and EVOH. A green value indicates that the HSP prediction is consistent with the experimentally determined solubilities in Table 2.2, whereas a red value indicates that the HSP prediction is inconsistent with the experimentally determined solubilities. . . .	30
2.5	COSMO-RS solubility predictions for PE compared to experimental measurements. Results from two different $\Delta G_{fus}$ options are listed. 10-conformer set of 12-carbon PE oligomers were used. . . . .	31
2.6	COSMO-RS solubility predictions for EVOH compared to experimental measurements. Results from two different $\Delta G_{fus}$ options are listed. 20-conformer set of 14-carbon block structure EVOH oligomers were used. .	31
2.7	COSMO-RS solubility predictions for PE compared to experimental measurements. Toluene is used as a reference and hence its prediction is exact. . . . .	35
2.8	COSMO-RS solubility predictions for EVOH compared to experimental measurements. Three different copolymer structures are compared. . . .	39
2.9	COSMO-RS solvent screening for PE and EVOH. 524 solvents at two temperatures (room temperature and near each solvent's boiling point) were considered. Nine selective solvents are presented as examples (no PE-selective solvents were identified at room temperature). . . . .	40
3.1	A selected list of solvents and non-solvents for the polymers considered in this work. . . . .	52
3.2	Representative industrial processes for dissolution-based plastic recycling.	53
3.3	Modeling information and reference experimental input for each polymer.	58
3.4	Selected results from the solubility database. Each polymer-solvent system is studied at a room temperature (RT) and a higher temperature ( $T_h$ ). $T_h$ is set as 1 °C lower than the boiling point of the solvent with an upper bound of 120 °C. . . . .	64



3.5	Experimental verification of solubility predictions. The solubility of each polymer is measured in a good solvent and a non-solvent (distinguished by a threshold of 3 wt% in predicted values). Among the 14 available test results, 11 computational predictions are in good agreement with experimental data (denoted by the green color), 2 predictions are acceptable as they correctly identify good/non-solvents but have some deviations in solubility values (yellow color), and 1 prediction is inconsistent with experiment (red color). . . . .	65
3.6	Analysis of functional groups associated with the top solvents for each polymer. Top solvents are defined as those ranked within the top 10% of solvents ranked by solubility and with a minimum predicted solubility of at least 5 wt% at any temperature. . . . .	68
3.7	Results from all separation case studies. . . . .	72
3.8	Examples of other possible separation strategies for PP/EVOH/PET mixture. Selective solvents and the corresponding solubility predictions are listed for 4 different separation sequences. Each solvent selectively dissolves a target polymer at a high temperature and precipitates the polymer at room temperature. . . . .	78
3.9	COSMO-RS and HSP solubility predictions for PETG. . . . .	82
3.10	Recovery of polymers from the multilayer film with the STRAP process. . . . .	84
3.11	COSMO-RS predicted polymer solubilities for each STRAP step at the specified temperature. . . . .	87
3.12	STRAP steps for the recovery of 10 common packaging polymers from a physical mixture, with an initial amount of 1 g for each polymer and 30 g of the corresponding solvent. . . . .	89
3.13	Some similar and dissimilar solvents of THP. . . . .	94
3.14	Predicted solubilities of 8 polymers in THP and its 10 most similar solvents. . . . .	95
5.1	Comparison of our log P calculation results and literature experiment observations of BFR removal from several different polymers. Red color indicate inconsistency between computational data and experimental results, green color means they align with each other. . . . .	144
5.2	The phthalates considered in this work, and their applications in plastic products [28]. . . . .	146

5.3	COSMO-RS prediction results for solvent screening of phthalates removal from PVC. The elevated temperature $T_h$ is defined to be 1°C lower than the boiling point (BP) of the solvent, with an upper bound of 120°C. . .	147
5.4	Experimental phthalate removal result for sample 1. . . . .	149
5.5	Experimental phthalate removal result for sample 2. . . . .	149
5.6	Solvent screening result for the 4 groups of 33 PFAS identified by FDA. .	151
5.7	Example results of solvent selection for a more general study that divided 15000 PFAS compounds into 7 groups. . . . .	152
5.8	COSMO-RS solubility predictions for PE, EVOH and PET in 30 common solvents. . . . .	157
5.9	HSP data for some solvents, PET, and 11 PU polymers. . . . .	158
5.10	HSP calculations for some solvents and 11 PU resins . . . . .	159
5.11	HSP calculations for solvents considered for ink removal from PET . . .	159
5.12	Yield of components from a printed multilayer film with the STRAP process. The component yields are the recovered mass of each component divided by the multilayer feed mass in each experiment. The overall mass balance can be improved to near 100 wt% when accounting for material left in the equipment and residual ink in the deinking solvent. . . . .	161

## LIST OF FIGURES

---

1.1	Theories and models to predict polymer solubility in various solvents. The schematic at right illustrates types of solvents able to dissolve example polymers. The sizes of the circles indicates the number of associated solvents, and the widths of the lines indicates solubility trends. These data and trends are possible due to the availability of modern, large-scale computational solubility prediction methods [8]. . . . .	3
1.2	The STRAP process. . . . .	7
2.1	Flow diagram summarizing the methods for computational polymer solubility prediction and experimental validation. . . . .	18
2.2	Three types of structures of EVOH oligomer with 2 ethylene units (red) and 4 vinyl alcohol units (blue). Oligomers are modeled to have end methyl groups (black) that are deactivated such that they do not contribute to the COSMO-RS calculations. . . . .	19
2.3	R <sub>g</sub> -SASA plot of an EVOH oligomer in MD simulation. Each blue dot represents a conformer, red dots are selected samples. The structures of two extreme conformations are shown: the folded one represents a bottom left dot, the elongated one represents a top right dot. . . . .	21
2.4	Conformers selected by random sampling (left) and greedy sampling (right). . . . .	25
2.5	Conformers selected by grid sampling (left) and cluster sampling (right). . . . .	26
2.6	Conformers selected by greedy-grid hybrid sampling (left) and greedy-cluster hybrid sampling (right). . . . .	26
2.7	Variation in the solubility prediction error and computational cost with PE oligomer length. Three conformers are used for the solubility predictions for each data point. . . . .	33
2.8	Variation in the solubility prediction error and computational cost with the number of PE conformers used. All points represent an average over 10 subsets of conformers for a PE oligomer with a 12-carbon chain length. . . . .	34
2.9	Variation in the solubility prediction error and computational cost with EVOH oligomer length. Three conformers in the block copolymer structure are used for the solubility predictions for each data point. . . . .	36

2.10	Variation in the solubility prediction error and computational cost with the number of EVOH conformers used. All points represent an average over 10 subsets of conformers for a EVOH oligomer with a 14-carbon chain length and block copolymer structure. . . . .	37
2.11	Temperature-dependent solubility prediction for EVOH in DMSO with different conformer sets. The light blue, light green, and deep blue regions show the range of predicted solubilities obtained from 10 predictions using subsets of 1, 5, or 20 conformers, respectively. Red dots are experimental data. All predictions used an EVOH oligomer with a 14-carbon chain length and block copolymer structure. . . . .	38
3.1	Summary of computational and experimental approach for large-scale polymer solubility prediction, validation and application. . . . .	56
3.2	Computational examples of using reference experimental data as input to calibrate models and predict polymer solubilities. Left: example COSMO-RS screening charge distributions (colored surface) of PE and nylon models. Oligomer molecules with end groups neglected (gray surface) are used to represent longer polymer chains. Middle: the same molecular model can be calibrated with different reference experimental data to represent different materials (e.g. PE model for LDPE and HDPE, PA model for PA 6 and PA 66). Right: example calculation results of temperature-dependent solubilities of LDPE, HDPE and PP in o-xylene. Dashed lines refer to different temperatures suggested for experiments. . . . .	59
3.3	Some structures obtained from conformational sampling and corresponding COSMO-RS representations (colored surfaces) for 3 polymers: (a) PP, (b) PS, and (c) PVC. End groups of these oligomer molecules (black atoms) are neglected in the COSMO-RS calculations (gray surfaces) to represent the chemical properties of longer polymer chains. . . . .	63
3.4	Polymer solubilities in their top 5% solvents at (a) room temperature (b) and elevated temperatures. The dataset for each polymer is displayed as a box plot, which contains five horizontal lines that represent the minimum, lower quartile, median, upper quartile, and the maximum values. The box denotes the range from lower quartile to higher quartile, which is the middle half of the dataset. . . . .	66
3.5	An example of generating separation sequences for polymer mixtures. .	69

3.6	Results from the separation of case 1 (mixture PE/PS, sequence PE → PS) via selective dissolution. Dodecane at 120 °C is used to selectively dissolve PE. FTIR spectrum verified the purity of both recovered polymers. . . . .	73
3.7	Separation result of case 1 (mixture PE/PS, sequence PE → PS) using an alternative precipitation method. . . . .	73
3.8	Separation result of case 2 (mixture PE/PS, sequence PS → PE). . . . .	74
3.9	Separation result of case 3 (mixture PVC/PET, sequence PVC → PET). . . . .	74
3.10	Separation result of case 4 (mixture EVOH/PP/PET, sequence EVOH → PP → PET). The white arrows in the photo of recovered PET point to the impurities. . . . .	75
3.11	FTIR analysis of the undissolved solid impurity in sequence EVOH → PP → PET. The spectrum of the impurity is mainly similar to that of EVOH virgin. The vertical lines showed two peaks that indicate the existence of PP in the solid. This result suggests that the undissolved solid impurity is a mixture of EVOH and PP resins. . . . .	76
3.12	Separation result of case 5 (mixture EVOH/PP/PET, sequence PP → EVOH → PET). . . . .	76
3.13	Schematic of a proposed separation process for the PP/EVOH/PET mixture using solvents and temperatures optimized for selective dissolution. . . . .	77
3.14	COSMO-RS solubility predictions for EVOH in DMSO-water mixtures. Two EVOH recovery processes are shown by arrows. The STRAP-A process dissolves EVOH in pure DMSO at 95°C (predicted solubility 22.77 wt%) and precipitates the EVOH in 81.5% water at 48°C (predicted solubility 1.23 wt%). The STRAP-B process dissolves EVOH in 40% water at 95°C (predicted solubility 10.45 wt%) and precipitates the EVOH by reducing the temperature to 35°C (predicted solubility 1.72 wt%). . . . .	80
3.15	STRAP process schematic for the separation and recovery of the polymer components in a multilayer film manufactured by Amcor. . . . .	83
3.16	ATR-FTIR spectra of the virgin resins and polymers recovered from multilayer film through STRAP process: a) PETG, b) PE, c) EVOH, d) EVA and e) PET. . . . .	85
3.17	IR spectra of the recovered STRAP polymers from the physical mixture (in red) and the virgin polymers (in black): (a) PS, (b) PVC, (c) LDPE, (d) HDPE, (e) PP, (f) EVOH, (g) PA66/6, (h) PET, (i) PA6, and (j) PA66. . . . .	90

3.18	Solvent-targeted recovery and precipitation STRAP with post-industrial mixed plastic waste MPW from packaging waste that includes multilayer films. . . . .	91
3.19	Computational methods used in this section. (a) COSMO-RS screening charge distributions (colored surfaces) of THP, THF and a PE oligomer. Short oligomers with end groups neglected (gray surface) are used to represent the chemical properties of longer polymer chains. The intermolecular interactions between polymers and solvents are quantified by the interactions of screening charges, as schematically indicated by dashed lines. (b) MD simulation of a PE oligomer in a dilute THP solution. . . .	92
3.20	$\sigma$ -profiles of THP, THF and DCM. . . . .	93
3.21	Molecular structures of the five solvents most similar to THP. . . . .	93
3.22	$R_g$ -SASA scatter plot of PE oligomer in THP, water. . . . .	96
4.1	Schematic representation of the STRAP process. (A) Simplified representation of the process considering a multilayer film with three components (in this case, each component represents only one polymer). (B) Separation process represented as a binary tree. . . . .	110
4.2	Simplified process flow diagram of the STRAP process for one separation module. . . . .	111
4.3	General steps of the proposed computational framework. . . . .	113
4.4	Visualization of solvent candidates for EVOH (green lines), LDPE (grey lines), PET (orange lines), and nylon 6 (black lines); their chemical structures are drawn at right. Line widths and node sizes denote the number of solvents able to dissolve each polymer. Each solvent class has an associated chemical structure motif drawn next to it, with key atoms highlighted with different colors. For example, nitrogen atoms are highlighted in blue. . .	116
4.5	Minimum selling price (MSP) and climate change impact (CCI) of the STRAP process configurations with the lowest impacts in Case Study 1. The separation sequences are denoted by $S_1$ - $S_4$ . Note that the impacts are given per separation step. For instance, for $S_1$ , the MSP when only LDPE is recovered is 0.48 USD/kg. Then, if LDPE and EVOH are recovered, the MSP is 0.77 USD/kg. Finally, if all the polymers are recovered, the MSP is 0.82 USD/kg. . . . .	120

4.6	Minimum selling price (MSP) and climate change impact (CCI) of the STRAP process configurations with the lowest impacts in Case Study 2. The presented impacts are the total cost and emissions of separating the seven polymers. . . . .	122
4.7	Minimum selling price (MSP) and climate change impact (CCI) of the STRAP process configurations with the lowest impacts in Case Study 3A. The separation sequences are denoted by $S_1$ - $S_4$ . Note that the impacts are given per separation step. For instance, for $S_1$ , the MSP when only LDPE is recovered is 0.43 USD/kg. If all the polymers are recovered, the MSP is 0.51 USD/kg. . . . .	124
4.8	Minimum selling price (MSP) and climate change impact (CCI) of the STRAP process configurations with the lowest impacts in Case Study 3B. The separation sequences are denoted by $S_1$ - $S_4$ . Note that the impacts are given per separation step. For instance, for $S_1$ , the MSP when only LDPE is recovered is 0.41 USD/kg. If all the polymers are recovered, the MSP is 0.52 USD/kg. . . . .	125
4.9	Separation difficulty in binary polymer mixtures. Difficulty refers to the number of feasible separation sequences and potential solvent candidates.	127
5.1	Example structures of a phthalate, a PFAS, and a BFR molecules. . . . .	137
5.2	Molecular-scale illustrations of two contaminant removal strategies. (a) Leaching, where contaminant molecules migrate from solid polymer phase into liquid solvent phase. (b) Simultaneous STRAP and contaminant removal, it first dissolves the polymer and contaminant together in a solvent, and then selectively precipitate the polymer into solid phase. . .	140
5.3	Chemical structures of some example brominated flame retardants. . . .	143
5.4	Photos of the experimental material before and after the phthalate removal experiments. Sample 1 is an extruded material based on the mixture of PVC powder and liquid BBP. Sample 2 is the extruded material after an additional processing step of hot pressing. . . . .	148
5.5	Examples of some PFAS compounds and their chemical structures . . . .	150
5.6	Simplified structure of a printed multilayer film composed of PE, EVOH, PET, and PU-based inks, manufactured by Amcor . . . . .	153

5.7	Computational methods used in this work. (a) Screening of PE-selective solvents in the presence of PU-based inks using HSPs. The HSPs for the PE polymer, two representative PU polymers, and 3 example solvents are indicated as points in HSP space, with the soluble regions for each polymer drawn as spheres centered on the corresponding polymer HSPs. Dodecane lies within the PE sphere but outside of the PU spheres and is thus predicted to be a selective solvent for PE. (b) COSMO-RS screening charge distributions (colored surfaces) of GVL and a PET oligomer. Oligomer molecules with end groups neglected (gray surface) are used to represent the chemical properties of longer polymer chains. The intermolecular interactions between polymers and solvents are quantified by the interaction of screening charges, as schematically indicated by dashed lines. . . . .	154
5.8	Temperature-dependent solubility prediction of PET in GVL. Dashed line is the dividing value to distinguish between a good solvent and a poor solvent (5 wt%). . . . .	160
5.9	(a) Solvent-targeted recovery and precipitation (STRAP) of a printed multilayer film composed of PE, EVOH, PET, and PU-based inks, (b) Photos of each polymer after the STRAP process. . . . .	162
5.10	STRAP deinking step with gamma-valerolactone (GVL) to separate white, black, and yellow ink from PET of a printed multilayer film. . . . .	163



## ABSTRACT

---

Dissolution-based plastic recycling is a promising approach to separate and recover high-quality polymers from multicomponent plastic waste by exploiting differences in polymer solubility. The design of these recycling processes requires determination of polymer separation sequence, appropriate solvent/nonsolvent systems, and operating conditions of dissolution/precipitation steps. To address these challenges, we developed a series of computational models for polymer solubility prediction, solvent screening, contaminant removal, and process optimizations.

In this dissertation, we first present a computational approach to rapidly predict temperature-dependent polymer solubilities. We employed molecular dynamics simulations and the conductor-like screening model for real solvents (COSMO-RS), and performed systematic study on simulation parameters. Predicted solubilities showed good agreement with experimental measurements.

With the established molecular models for quantitative polymer solubility prediction, we developed a joint computational and experimental workflow to improve the model performance and conduct large-scale predictions. We established a computational solubility database for common polymers and solvents and validated the data with experiments. We also developed automated tools for solvent selection of different polymer separation sequences. We demonstrated the application of these methods via experimental case studies on both physical mixtures and industrial products of polymers.

The polymer solubility database and solvent screening program have led to the development of a process design and optimization framework for dissolution-based plastic recycling. This framework combines the solubility database with process simulation models to evaluate the economic and environmental impacts of different processes. It can not only suggest favorable process designs, but also offers insights into the manufacturing of easy-to-recycle plastic products.

Apart from polymer separation, contaminant removal is also a critical part of plastic recycling. With molecular models and computational property predictions, we developed solvent screening methods for different contaminant removal processes. We investigated the removal of plastic additives including brominated flame retardants, phthalates, and per- and polyfluoroalkyl substances. We also presented an ink removal process to recover pure polymers from a printed multilayer plastic film.

The dissertation concludes by summarizing the key findings and contributions of these studies, highlighting advances in quantitative prediction of polymer-solvent interactions and the design of dissolution-based plastic recycling processes. Future research directions to further innovate and expand the field are also discussed.

# Chapter 1

## Introduction

In this chapter, we outline the key components of this dissertation, including its background, motivation, core research questions, and objectives. We begin by introducing the current state of the plastic industry and existing plastic recycling technologies, highlighting recent advances in dissolution-based recycling processes. This leads to a discussion of two critical challenges in developing effective dissolution-based recycling: determining polymer solubility in various solvent systems and establishing efficient tools for solvent screening and process development. Finally, we provide an overview of the dissertation's structure, summarizing the chapters that follow.

### 1.1 Motivation

Plastic products, which are synthetic materials that use polymers as a main ingredient, are ubiquitous materials in our daily lives. Multicomponent plastics have been developed to meet the increasing demand for multifunctional engineering polymeric materials with reduced processing cost and broad utilization ability obtained from the mixture of different polymers [1]. Such polymers are often blended to develop an optimized product that can fulfill certain complex industrial demands. For example, multiplayer plastic film is a common type of multicomponent material that has been widely used in the packaging industry with global production exceeding 100 million tons each year [2]. There are many different manufacturing methods to combine different polymers and produce multilayer plastic films: co-extrusion, layer-by-layer assembly, extrusion lamination, extrusion coating, adhesive lamination, solvent casting, etc. [3]. Such products often provides a wide range of useful functions that

originate from the physical properties of different polymer components, for example, moisture/gas barrier, puncture/impact resistance, and chemical inertness [4].

However, multicomponent plastic materials are extremely difficult to recycle. Due to their complex compositions and the variant properties of their different polymer components, traditional plastic recycling technologies based on mechanical or chemical methods are incapable of handling such mixture of polymers [5]. For example, single-component plastic bottles have a recycle rate of over 29% in the U.S. in 2018, but only 8.7% of all plastic municipal solid waste was recycled and most multilayer films are diverted to landfills [6]. Therefore, there is an urgent need to develop new recycling technologies for multicomponent plastic materials.

Recent advances of dissolution-based plastic recycling approaches made it a promising approach to deal with multicomponent plastic materials. The dissolution-based recycling process utilizes the differences in polymer solubility to achieve the separation and recovery of pure polymer resins from carefully chosen solvent systems that dissolve only target polymers [7]. This recycling method has several advantages over traditional chemical or mechanical recycling methods: it can process multicomponent plastic mixtures, it maintains the chemical structures and properties of recovered polymers, and it does not require a high-purity input stream because impurities and additives can be removed by selective dissolution [8]. Dissolution-based recycling is also a green process that has over 40% lower greenhouse gas emissions than producing virgin resins, saving 3–6 tons CO<sub>2</sub> for each ton of plastic waste [9]. In addition, dissolution-based technologies can reduce emissions to an extent comparable to closed-loop mechanical recycling, and have 65–75% less environmental impact than incineration [10, 11, 12].

There are several critical technical challenges to the successful development of a dissolution-based recycling process that can effectively separate and recover pure polymer components from complex multicomponent plastic materials. Solvent screening determines which solvents and nonsolvents can be used to separate and recover target polymer components from the waste. Process design involves the decision and parameter optimization of polymer separation sequence and operation conditions. Contaminant removal is also often a necessary step for the recycled polymers to meet certain industrial criteria. In the following sections, we will discuss these research questions and introduce corresponding solution methods in detail.

## 1.2 Solubility prediction methods for polymer-solvent systems

### 1.2.1 Background

The information of temperature-dependent polymer solubilities in different solvent systems allows for the selection of a suitable solvent and operation conditions for dissolution and precipitation. While some solvents and nonsolvents have been identified and tabulated for common polymers [13], identifying solvents that enable the selective dissolution of a single polymer component from a multicomponent mixture of plastic waste remains a challenge. Figure 1.1 summarizes four broad categories of theories and computational models that can efficiently guide solvent selection by predicting polymer solubility.

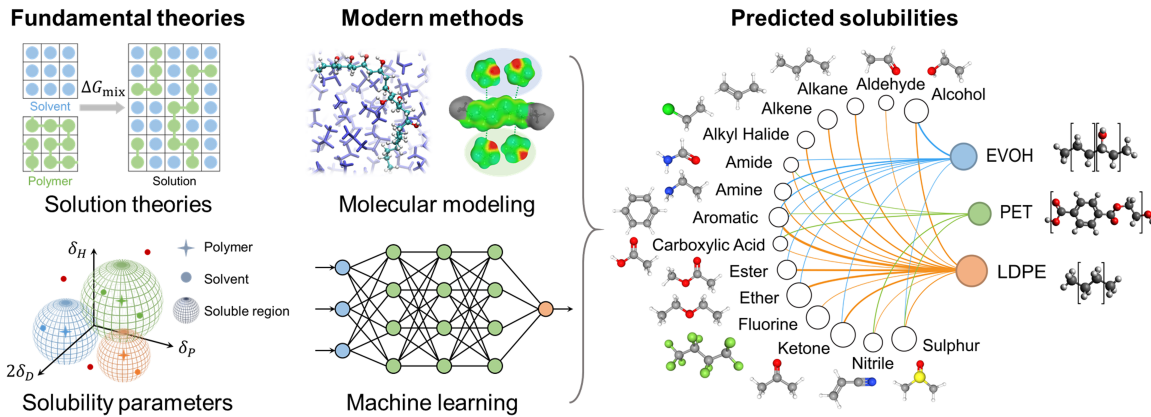


Figure 1.1: Theories and models to predict polymer solubility in various solvents. The schematic at right illustrates types of solvents able to dissolve example polymers. The sizes of the circles indicates the number of associated solvents, and the widths of the lines indicates solubility trends. These data and trends are possible due to the availability of modern, large-scale computational solubility prediction methods [8].

Classical solution theories for polymers focus on the thermodynamics of polymer-solvent mixing, which is governed by the Gibbs free energy of mixing  $\Delta G_{\text{mix}} = \Delta H_{\text{mix}} - T\Delta S_{\text{mix}}$ , where  $\Delta H_{\text{mix}}$  is the enthalpy of mixing and  $\Delta S_{\text{mix}}$  is the entropy of mixing. A polymer and a solvent will mix if  $\Delta G_{\text{mix}} < 0$ . Flory-Huggins theory [8]

is the most prominent solution theory and uses a mean-field lattice model to derive Equation 1.1

$$\Delta G_{\text{mix}} = RT [n_1 \ln \phi_1 + n_2 \ln \phi_2 + n_1 \phi_2 \chi_{12}] \quad (1.1)$$

In this equation, component 1 is the solvent, component 2 is the polymer.  $n_i$  is the number of moles, and  $\phi_i$  is the volume fraction. The first two terms account for the combinatorial entropy contribution to  $\Delta S_{\text{mix}}$ , while the third term uses the parameter  $\chi_{12}$  to account for polymer-solvent interactions that contribute to  $\Delta H_{\text{mix}}$ . Phase diagrams based on Flory-Huggins theory have provided physical insight into the key contributions to  $\Delta G_{\text{mix}}$  at different temperatures and compositions. However, Flory-Huggins theory is a highly simplified physical model and cannot capture all features of a polymer solution, such as the volume change of mixing, the energetically favorable arrangements of molecule segments, or the composition dependence of the interaction parameter [14].

Solubility parameters are another powerful tool to predict polymer dissolution. Most solubility parameter systems adopt the “like dissolves like” concept and postulate that materials with similar parameter values will be miscible [15]. Notable examples include the Hildebrand parameter and Hansen solubility parameters (HSPs) [16]. The Hildebrand solubility parameter is derived from a material’s cohesive energy density and has reasonable predictive accuracy for non-polar systems but is limited when there are strong polar or specific interactions such as hydrogen bonds. HSPs extend this concept to three parameters that assess the chemical similarity between a polymer and a solvent based on dispersion ( $\delta_D$ ), polar ( $\delta_P$ ), and hydrogen-bonding ( $\delta_H$ ) interactions. Polymer-solvent interactions are quantified by their virtual distance  $R_a$  as shown in Equation 1.2.

$$R_a^2 = 4 \left( \delta_D^{\text{solv}} - \delta_D^{\text{poly}} \right)^2 + \left( \delta_P^{\text{solv}} - \delta_P^{\text{poly}} \right)^2 + \left( \delta_H^{\text{solv}} - \delta_H^{\text{poly}} \right)^2 \quad (1.2)$$

Each polymer has an interaction radius  $R_0$ ; solvents with  $R_a < R_0$  are predicted to dissolve the polymer. HSPs are tabulated for a wide range of polymers and solvents and have been a benchmark method for screening solvents to dissolve polymers. [17] While parameter systems such as HSPs have many successful applications, they only qualitatively predict whether a polymer should or should not dissolve in a target solvent, and generally are less accurate at temperatures other than room temperature.

Recent studies have applied modern molecular models and computational methods to evaluate polymer solubility in various solvent systems. Molecular dynamics (MD) simulations and conductor-like screening model for real solvents (COSMO-RS) have been employed to predict polymer solubilities. COSMO-RS is a statistical thermodynamics model that can perform solid-liquid and liquid-liquid equilibrium calculations to calculate polymer solubilities. This approach can rapidly predict quantitative polymer solubilities at different temperatures and in both single- and multicomponent solvent systems. For example, Soyemi et al. [18] established a solvent library that contains over 9000 glycerol derivatives and predicted their physicochemical properties using quantum chemical methods, COSMO-RS, and machine learning models. The predicted properties included densities, dipole moments, water solubilities, octanol-water partition coefficients, melting points, and HSP values. Potential solvent candidates and dissolution strategies for 6 common polymers were identified based on the predicted data.

Most recently, machine learning methods have been developed to predict properties relevant to polymer dissolution. Chandrasekaran et al. [19] introduced a solvent/antisolvent classification model using a deep neural network, which Aoki et al. [20] extended to predict temperature-dependent Flory-Huggins interaction parameters. Ethier et al. [21] combined Flory-Huggins theory with neural networks to improve model interpretability and accuracy. Sanchez-Lengeling et al. [22] introduced the Gaussian process HSP, a Bayesian method for HSP determination. Kurotani et al. [23] used an in-phase deep neural network to predict solubility parameters. Kern et al. [24] proposed fingerprints of polymers and solvents for room-temperature solubility prediction. These studies largely focus on qualitatively classifying solvents and antisolvents for target polymers or predicting solubility parameters, but a research gap remains in developing machine learning models to *quantitatively* predict polymer solubilities. Training these models also requires large-scale and high-quality data of polymer solubility, requiring the development of standardized, high-throughput experimental solubility measurement approaches [25].

### 1.2.2 Research questions

To address the limitations of the previously mentioned methods, we aim to develop computational models that can rapidly and efficiently predict temperature-dependent polymer solubilities in different solvent systems. We hypothesize that MD simulations

of polymer-solvent systems encode information about the polymer chain conformations and interactions of the polymer with its surrounding solvation environment. We also hypothesize that the COSMO-RS screening charge distribution profiles of polymer and solvent molecules encode their intermolecular interaction properties and can provide thermodynamic properties in solid-liquid equilibrium systems. We seek to answer the following research questions:

1. How do we develop appropriate and efficient models for long polymer molecules and use classical MD simulations to represent real-world polymer-solvent systems?
2. How do we use MD simulations to obtain molecular configurations of the polymer chain to properly represent the physical behavior of the polymer molecule in solution systems?
3. How do we leverage MD simulations and COSMO-RS models to calculate polymer solubilities in different solvents and temperatures?
4. How do we deal with the resin-specific properties of different polymer materials and apply our computational models to practical plastic products?

## **1.3 Solvent screening and process development for dissolution-based plastic recycling processes**

### **1.3.1 Background**

Apart from polymer solubility data, there are many other considerations to develop an effective and economic dissolution-based plastic recycling process. In this section, we will discuss the challenges and key research questions for dissolution-based recycling processes with a focus on multilayer packaging films.

Multilayer films are formed from several layers of common polymers, each of which is selected to contribute useful properties to the film. For example, polyethylene (PE) is chemically inert and serves as a good moisture barrier; ethylene vinyl alcohol (EVOH) is a good gas barrier but a poor moisture barrier; polyvinyl chloride (PVC) has good cling behavior and puncture resistance but is oxygen permeable; and polyethylene terephthalate (PET) is rigid and impact resistant but has poor alkali



resistance [4, 26, 27]. To separate and recover pure polymer resins that a multilayer plastic film is composed of, we have developed a dissolution-based process called Solvent-Targeted Recovery and Precipitation (STRAP) [7]. As shown in Figure 1.2, a suitable solvent selectively dissolves a target polymer from the multilayer film at a defined temperature, the mixture is filtered to separate the dissolved polymer from the residual film components, and the polymer is precipitated and recovered by adding nonsolvent (also referred to as antisolvent, a solvent in which the polymer is insoluble) and/or decreasing the temperature. This process is then repeated sequentially for each target polymer until all resins have been recovered from the film.

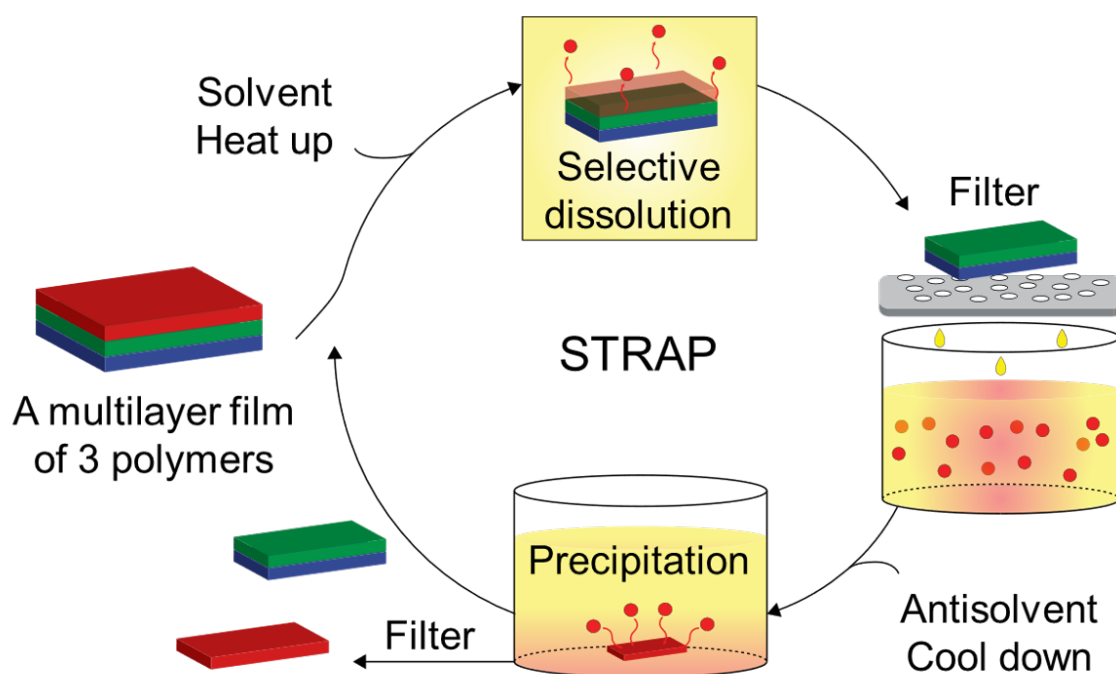


Figure 1.2: The STRAP process.

In the previous section, we have discussed the importance of polymer solubility data in the design of a dissolution-based polymer recycling process. With this information, the selection of an appropriate solvent (and nonsolvent in some cases) for each polymer of interest, temperatures for dissolution and precipitation, and the amount of solvent will then need to be investigated. The determination of these parameters require an efficient tool to screen selective solvents along with a large polymer solubility database. These considerations affect the efficiency, economics, and environmental impact of the process, process simulation models, techno-economic

analysis (TEA), and life-cycle assessment (LCA) are then needed to study the performance of the proposed processes. [28, 29] Apart from identifying selective solvents to separate target polymers from multicomponent plastics, we sometimes also want to develop strategies that can separate hazardous contaminants from target polymers. Therefore, computational models on phase equilibrium and partitioning properties will be needed.

### 1.3.2 Research questions

To develop feasible dissolution-based plastic recycling processes, we will need to first establish a large-scale polymer solubility database based on the molecular models mentioned above, then develop computational tools for efficient solvent screening. We will also need to investigate different possible separation sequences given a certain set of polymer mixtures, as well as the related process economics and environmental impacts. These objectives lead us to the following research questions:

1. How do we utilize the current molecular models to establish a workflow that can perform solubility calculations for various polymer-solvent combinations at scale?
2. How do we integrate experimental measurements with computational workflow to calibrate and validate the solubility predictions?
3. How do we efficiently screen solvents for a given set of polymers and identify favorable sequences of separation?
4. How do we evaluate the feasibility and performance of a dissolution-based plastic recycling process?
5. Are the dissolution processes we developed for physical mixtures of polymers transferrable to waste streams of commercial plastic products?
6. How do we remove undesirable contaminants from plastic products, and what models or properties should we consider?

## 1.4 Outline of this dissertation

The structure of this dissertation is outlined as follows:

**Chapter 2** focuses on the method development of polymer solubility predictions. We introduced a series of computational approaches including molecular dynamics simulations, conformational sampling methods, density functional theory calculations, and the conductor-like screening model for real solvents. We achieved quantitative prediction of temperature-dependent polymer solubilities in different solvent systems, and demonstrated its potential applications in solvent screening for dissolution-based plastic recycling processes.

**Chapter 3** extended the polymer solubility predictions to a wide range of solvent candidates and common polymers in the packaging industry with a joint computational and experimental workflow. Experimental data can be used for calibration and validation of the predictions, which improved the accuracy and applicability of the computational models. This new workflow enabled the establishment of a large-scale polymer solubility database, which lay the foundation for efficient solvent screening and convenient integration with process models. Approaches developed in this chapter have been shown to effectively separate physical mixtures of polymers, post-industrial multilayer films, and complex mixed plastic waste.

**Chapter 4** discussed an integrated computational framework that can assist the design and optimization of dissolution-based plastic recycling processes. We discussed the combination of large-scale polymer solubility database, solvent screening tools, and process simulation models. We incorporated techno-economic analysis and life-cycle assessment into the framework to analyze the economics and environmental impacts of different processes. This framework can not only provide suggestions on favorable ways to recycle multicomponent plastic wastes, but also offers insights on the manufacturing of easy-to-recycle plastic products.

**Chapter 5** focuses on contaminant removal methods for plastic products. We introduced several contaminant removal processes that utilize leaching, extraction, and precipitation to either reduce the contaminant concentration in target polymer resins, or directly recover the target polymers in high-quality forms. We discussed different cases where common contaminants including brominated flame retardants (BFRs), phthalates, PFAS, and inks are taken into consideration.

**Chapter 6** provides a summary of the key findings from this dissertation and potential avenues of future research.

## 1.5 References

- [1] Jin Kuk Kim, Sabu Thomas, and Prosenjit Saha. Multicomponent polymeric materials, 2016.
- [2] Delilah Lithner, Åke Larsson, and Göran Dave. Environmental and health hazard ranking and assessment of plastic polymers based on chemical composition. *Science of the total environment*, 409(18):3309–3324, 2011.
- [3] Deepak Langhe and Michael Ponting. *Manufacturing and novel applications of multilayer polymer films*. William Andrew, 2016.
- [4] Dorel Feldman. Polymer barrier films. *Journal of Polymers and the Environment*, 9:49–55, 2001.
- [5] Jeannette M Garcia and Megan L Robertson. The future of plastics recycling. *Science*, 358(6365):870–872, 2017.
- [6] U.S. Environmental Protection Agency. Containers and packaging: Product-specific data, Jan 2021.
- [7] Theodore W Walker, Nathan Frelka, Zhizhang Shen, Alex K Chew, Jesse Banick, Steven Grey, Min Soo Kim, James A Dumesic, Reid C Van Lehn, and George W Huber. Recycling of multilayer plastic packaging materials by solvent-targeted recovery and precipitation. *Science advances*, 6(47):eaba7599, 2020.
- [8] Panzheng Zhou, Jiuling Yu, Kevin L Sánchez-Rivera, George W Huber, and Reid C Van Lehn. Large-scale computational polymer solubility predictions and applications to dissolution-based plastic recycling. *Green Chemistry*, 25(11):4402–4414, 2023.
- [9] Ina Vollmer, Michael JF Jenks, Mark CP Roelands, Robin J White, Toon van Harmelen, Paul de Wild, Gerard P van Der Laan, Florian Meirer, Jos TF Keurentjes, and Bert M Weckhuysen. Beyond mechanical recycling: Giving new life to plastic waste. *Angewandte Chemie International Edition*, 59(36):15402–15423, 2020.
- [10] Dominik Triebert, Hagen Hanel, Marlen Bundt, and Klaus Wohnig. Solvent-based recycling. In *Circular Economy of Polymers: Topics in Recycling Technologies*, pages 33–59. American Chemical Society, 2021.

- [11] Daniel Maga, Markus Hiebel, and Nils Thonemann. Life cycle assessment of recycling options for polylactic acid. *Resources, Conservation and Recycling*, 149:86–96, 2019.
- [12] AE Schwarz, TN Ligthart, D Godoi Bizarro, Paul De Wild, Berend Vreugdenhil, and Toon van Harmelen. Plastic recycling in a circular economy; determining environmental performance through an lca matrix model approach. *Waste management*, 121:331–342, 2021.
- [13] Houqian Li, Horacio A Aguirre-Villegas, Robert D Allen, Xianglan Bai, Craig H Benson, Gregg T Beckham, Sabrina L Bradshaw, Jessica L Brown, Robert C Brown, Victor S Cecon, et al. Expanding plastics recycling technologies: chemical aspects, technology status and challenges. *Green Chemistry*, 24(23):8899–9002, 2022.
- [14] Joel R Fried. *Polymer science and technology*. Pearson Education, 2014.
- [15] Allan FM Barton. Solubility parameters. *Chemical Reviews*, 75(6):731–753, 1975.
- [16] Beth A Miller-Chou and Jack L Koenig. A review of polymer dissolution. *Progress in polymer science*, 28(8):1223–1270, 2003.
- [17] Charles M Hansen. *Hansen solubility parameters: a user's handbook*. CRC press, 2007.
- [18] Ademola Soyemi and Tibor Szilvási. Calculated physicochemical properties of glycerol-derived solvents to drive plastic waste recycling. *Industrial & Engineering Chemistry Research*, 62(15):6322–6337, 2023.
- [19] Anand Chandrasekaran, Chiho Kim, Shruti Venkatram, and Rampi Ramprasad. A deep learning solvent-selection paradigm powered by a massive solvent/non-solvent database for polymers. *Macromolecules*, 53(12):4764–4769, 2020.
- [20] Yuta Aoki, Stephen Wu, Teruki Tsurimoto, Yoshihiro Hayashi, Shunya Minami, Okubo Tadamichi, Kazuya Shiratori, and Ryo Yoshida. Multitask machine learning to predict polymer–solvent miscibility using flory–huggins interaction parameters. *Macromolecules*, 56(14):5446–5456, 2023.

- [21] Jeffrey G Ethier, Debra J Audus, Devin C Ryan, and Richard A Vaia. Integrating theory with machine learning for predicting polymer solution phase behavior. *Giant*, 15:100171, 2023.
- [22] Benjamin Sanchez-Lengeling, Loïc M Roch, José Darío Perea, Stefan Langner, Christoph J Brabec, and Alán Aspuru-Guzik. A bayesian approach to predict solubility parameters. *Advanced Theory and Simulations*, 2(1):1800069, 2019.
- [23] Atsushi Kurotani, Toshifumi Kakiuchi, and Jun Kikuchi. Solubility prediction from molecular properties and analytical data using an in-phase deep neural network (ip-dnn). *ACS omega*, 6(22):14278–14287, 2021.
- [24] Joseph Kern, Shruti Venkatram, Manali Banerjee, Blair Brettmann, and Rampi Ramprasad. Solvent selection for polymers enabled by generalized chemical fingerprinting and machine learning. *Physical Chemistry Chemical Physics*, 24(43):26547–26555, 2022.
- [25] Mona Amrihesari, Amari Murry, and Blair Brettmann. Towards standardized polymer solubility measurements using a parallel crystallizer. *Polymer*, 278:125983, 2023.
- [26] Dukjoon Kim and Seong Woo Kim. Barrier property and morphology of polypropylene/polyamide blend film. *Korean Journal of Chemical Engineering*, 20:776–782, 2003.
- [27] K Khanah Mokwena, Juming Tang, and Marie-Pierre Laborie. Water absorption and oxygen barrier characteristics of ethylene vinyl alcohol films. *Journal of food engineering*, 105(3):436–443, 2011.
- [28] Aurora del Carmen Munguía-López, Dilara Göreke, Kevin L Sánchez-Rivera, Horacio A Aguirre-Villegas, Styliani Avraamidou, George W Huber, and Victor M Zavala. Quantifying the environmental benefits of a solvent-based separation process for multilayer plastic films. *Green Chemistry*, 25(4):1611–1625, 2023.
- [29] Kevin L Sánchez-Rivera, Panzheng Zhou, Min Soo Kim, Leonardo D González Chávez, Steve Grey, Kevin Nelson, Shao-Chun Wang, Ive Hermans, Victor M Zavala, Reid C Van Lehn, et al. Reducing antisolvent use in the strap

process by enabling a temperature-controlled polymer dissolution and precipitation for the recycling of multilayer plastic films. *ChemSusChem*, 14(19):4317–4329, 2021.

## Chapter 2

# Molecular-scale models for temperature-dependent polymer solubility predictions

In this chapter, we focus on the method development of polymer solubility predictions. We will introduce a series of computational approaches, including molecular dynamics simulations, conformational sampling methods, density functional theory calculations, and the conductor-like screening model for real solvents. We will show quantitative predictions of temperature-dependent polymer solubilities in various solvent systems. We will also test the accuracy and applicability of our computational models on practical challenges of dissolution-based plastic recycling processes.

### 2.1 Introduction

Multilayer plastic films are widely used materials in the packaging industry [1] with global production exceeding 100 million tons each year [2]. Multilayer films are formed from several layers of common polymers, each of which is selected to contribute useful properties to the film. For example, polyethylene (PE) is chemically

---

This chapter is based on the following publication: Zhou, P., Sánchez-Rivera, K. L., Huber, G. W., & Van Lehn, R. C. (2021). Computational approach for rapidly predicting temperature-dependent polymer solubilities using molecular-scale models. *ChemSusChem*, 14(19), 4307-4316.



inert and serves as a good moisture barrier; ethylene vinyl alcohol (EVOH) is a good gas barrier but a poor moisture barrier; polyvinyl chloride (PVC) has good cling behavior and puncture resistance but is oxygen permeable; and polyethylene terephthalate (PET) is rigid and impact resistant but has poor alkali resistance [3, 4, 5]. The manufacture of multilayer films employs methods such as co-extrusion, layer-by-layer assembly, extrusion lamination, extrusion coating, adhesive lamination and solvent casting to combine different polymers for various applications [6, 7]. Unfortunately, the resulting materials are extremely challenging to recycle because of their complex compositions and the incompatibility of their different polymer components [8]. Current plastic recycling technologies based on mechanical or chemical methods are designed for single-component materials and are unable to recycle multi-layer films into new products [9, 10, 11]. As a result, large amounts of multilayer plastic films accumulate as solid waste, including post-industrial waste that is unutilized during industrial fabrication processes (up to 40% of all films [12]) and municipal post-consumer waste. Only 13% of plastic municipal solid waste in the U.S. has been recycled with the majority of these films being landfilled [13]. There is thus an urgent need for new technologies for recycling multilayer plastic films.

Solvent-based polymer recycling processes are promising, near-term approaches that exploit differences in polymer solubility to recover polymer resins in pure form from carefully chosen solvent systems that dissolve only target polymers. A few solvent-based plastic recycling processes are being developed industrially. A German company, APK AG, developed a process called Newcycling to recycle LDPE/PA films [14, 15]. A solvent-based PVC purification project, VinyLoop, was launched in Italy in 2002 but terminated in 2018 due to challenges in separating hazardous plasticizer additives [16, 17]. Unilever and the Fraunhofer Institute launched a pilot project called CreaSolv that aims to recycle PE from packaging materials [18, 19]. A Canadian startup called Polystyvert uses essential oils to recycle polystyrene [20]. These examples demonstrate the industrial relevance and broad applicability of solvent-based polymer recycling technologies. However, limited information is available regarding the processing conditions and solvents used in these processes.

Recently, we developed the solvent-targeted recovery and precipitation (STRAP) process to recycle multiple polymer components from a multilayer plastic film [8]. The STRAP process selectively dissolves constituent polymers through a series of solvent washes, each designed to dissolve only a single polymer component. Pure

resins are then precipitated from solution by changing the temperature and/or adding antisolvents [21]. We demonstrated that the STRAP process can successfully recover PE, EVOH and PET resins from a post-industrial waste film using two solvent washes [8]. In the first solvent wash, toluene was used as a selective solvent and acetone as an antisolvent to recover PE. In the second solvent wash, dimethyl sulfoxide (DMSO) was used as a selective solvent and water as an antisolvent to recover EVOH. The remaining polymer component of the film was PET, which was recovered after removal of the other polymer components. The STRAP process highlights the feasibility of recycling multiple polymers from complex multilayer films.

There are several important design considerations underlying a solvent-based polymer recycling process like STRAP, including the selection of an appropriate solvent and antisolvent for each polymer component, the choice of temperature for dissolution and precipitation, and the selection of an optimal solvent/antisolvent ratio for precipitation. These considerations impact process design and corresponding process economics. The key information needed to quantify tradeoffs between different operating conditions and solvent systems is the temperature-dependent solubility of each polymer in a proposed solvent system. Experimental data on the solubility of common polymers in some solvents are readily available. For example, Bloch summarized solvents and non-solvents for a large library of polymers [22], while Zhao et al. reviewed solvent-based methods for waste plastics recycling [23] and listed solvents and nonsolvents for polystyrene (PS), polycarbonate (PC), PE, PP, PET, acrylonitrile butadiene styrene (ABS) and polyvinyl chloride (PVC) with detailed experimental conditions. However, experimental collection of solubility data in the large number of possible solvents is prohibitively time-consuming, limiting the design of solvent systems for selective dissolution.

To more rapidly screen potential solvent systems, various empirical solvent parameters are available to identify possible solvents/nonsolvents for a given polymer; examples include Hildebrand [24], Hansen [25], Kamlet-Taft [26], Gutmann [27], and Swain [28] parameters. Among these, Hansen solubility parameters (HSPs) are the most widely used for selecting solvents for polymer dissolution. Tabulated HSP values are available for most common polymers and solvents and solvent screening based on HSPs has many successful applications [29]. Computational methods can also be utilized for solvent selection. For example, Chandrasekaran et al. trained a deep neural network for the binary classification of solvents/nonsolvents using

over 4500 homopolymers and 24 common solvents with an accuracy of 93.8% [30]. In general, these various approaches focus on qualitatively distinguishing solvents and nonsolvents for a given polymer at room temperature and are most accurate for single-component solvent systems. Quantitatively predicting temperature-dependent solubilities remains a challenge, which is the gap this research aims to fill.

Herein, we demonstrate a computational approach to quantitatively predict temperature-dependent polymer solubilities in different solvent systems. This approach improves upon the methodology that we previously employed to guide solvent design for the STRAP process [8], which was suitable for qualitatively identifying potential solvent systems but overestimated polymer solubilities. Our approach employs classical molecular dynamics (MD) simulations and the Conductor-like Screening MOdel for Real Solvents (COSMO-RS). We first model a polymer as a single oligomer molecule and simulate its motion in a dilute solution by MD simulation to obtain various conformations of the oligomer molecule. From this trajectory, we select representative conformations that span a range of structural parameters and use these as input to COSMO-RS for solubility calculations. We show that systematic variation of numerous simulation parameters leads to solubility predictions in good agreement with experimental solubility measurements for PE and EVOH in DMSO, water, tetrahydrofuran (THF), hexane, ethyl acetate, ethanol, acetone, toluene and dimethylformamide (DMF). These predictions also outperform qualitative solubility predictions obtained from analysis with HSPs. We then demonstrate the applicability of the approach by screening a large library of 524 solvents at different temperatures to identify selective solvents for PE and EVOH dissolution. This computational approach thus can be used to screen solvents for solvent-based polymer recycling schemes and can be performed rapidly enough to guide process design.

## 2.2 Methods

### 2.2.1 Summary of computational approach

A series of computational methods were used to evaluate polymer solubilities and compare them to experimental measurements for validation. Figure 2.1 summarizes this process in 5 steps:

1. A MD simulation of a single oligomer was performed in dilute solution to obtain

a simulation trajectory of various oligomer conformations.

2. A set of conformers was selected from the MD trajectory to span a range of representative oligomer structures.
3. Density functional theory (DFT) calculations were performed for the selected conformers to obtain corresponding screening charge density profiles.
4. Screening charge density profiles were input for COSMO-RS solubility calculations.
5. Experimental solubility measurements were to benchmark the computational predictions.

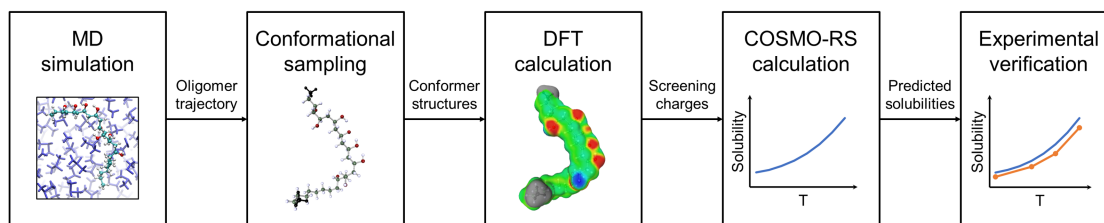


Figure 2.1: Flow diagram summarizing the methods for computational polymer solubility prediction and experimental validation.

This procedure was performed for two polymers: a homopolymer (PE) and copolymer (EVOH). Each step is detailed in the sections below.

## 2.2.2 Molecular dynamics simulations

Atomistic MD simulations were performed in the isothermal-isobaric ensemble using *Gromacs 2016* [31]. Each MD simulation contained 1 oligomer molecule (PE or EVOH) and 216 solvent molecules. PE was simulated in toluene and EVOH in water. All polymer and solvent molecules were parameterized using Antechamber and the Generalized AMBER force fields [32, 33]. The simulation system was initialized with a cubic box containing a single polymer. The system was then solvated, energy minimized, and equilibrated for 2 ns in an *NPT* simulation at 300 K and 1 bar using a velocity-rescale thermostat and Berendsen barostat. A 10 ns *NPT* simulation

was then performed at the same temperature and pressure using the Nose-Hoover thermostat and Parrinello-Rahman barostat. All simulations were performed using a leapfrog integrator with a 2-fs timestep. Verlet lists were generated using a 1.2 nm neighbor list cutoff. Van der Waals interactions were modeled with a shifted Lennard-Jones potential and Verlet cutoff-scheme that was smoothly shifted to zero at 1.2 nm. Electrostatic interactions were calculated using the smooth Particle Mesh Ewald method with a short-range cutoff of 1.2 nm, grid spacing of 0.14 nm, and 4<sup>th</sup> order interpolation. Bonds were constrained using the LINCS algorithm. All thermostats used a 2.0 ps time constant and all barostats used a 2.0 ps time constant with an isothermal compressibility of  $3.0 \times 10^{-5} \text{ bar}^{-1}$ .

The chain lengths of the PE oligomers studied in this work range from 4 to 24 carbon atoms, whereas the chain lengths of EVOH range from 8 to 32 carbon atoms. EVOH is a copolymer that has two different monomer units (ethylene and vinyl alcohol). The EVOH studied experimentally (described below) has a molar ratio of 35%:65% ethylene:vinyl alcohol. Therefore, we modeled EVOH oligomers using a 1:2 ethylene:vinyl alcohol ratio and tested 3 different structures (block, alternating and random) as shown in Figure 2.2.

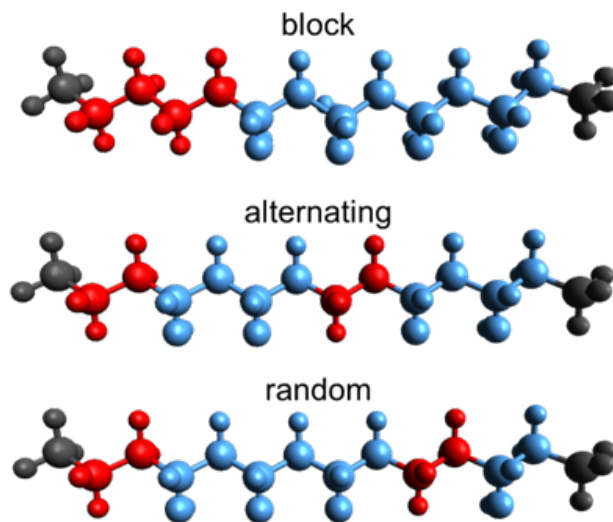


Figure 2.2: Three types of structures of EVOH oligomer with 2 ethylene units (red) and 4 vinyl alcohol units (blue). Oligomers are modeled to have end methyl groups (black) that are deactivated such that they do not contribute to the COSMO-RS calculations.

### 2.2.3 Conformational sampling and conformer selection

The MD trajectory of the oligomer molecule samples a large number of conformations as a function of simulation time. Since it is prohibitive to input all these conformers to COSMO-RS, we selected a set of representative conformers based on two structural parameters: the radius of gyration ( $R_g$ ) and the solvent-accessible surface area (SASA). We hypothesized that sampling conformers that capture a range of these parameters would provide reliable data to COSMO-RS for solubility predictions (see below). Figure 2.3 shows values in the two-dimensional  $R_g$ -SASA space generated from the MD trajectory of an EVOH oligomer.  $R_g$  and SASA values are normalized to a range from 0 to 1. Each blue dot corresponds to a conformer. We systematically investigated several sampling methods, and chose grid sampling in this work. The grid sampling method selected a set of conformers from this space by superimposing a square grid over the point cloud and selecting conformers closest to each grid intersection; sampled points are shown in red in Figure 2.3. The grid density can be tuned to control the number of conformer samples. In this work, 30 conformers of PE and 40 conformers of EVOH were studied.

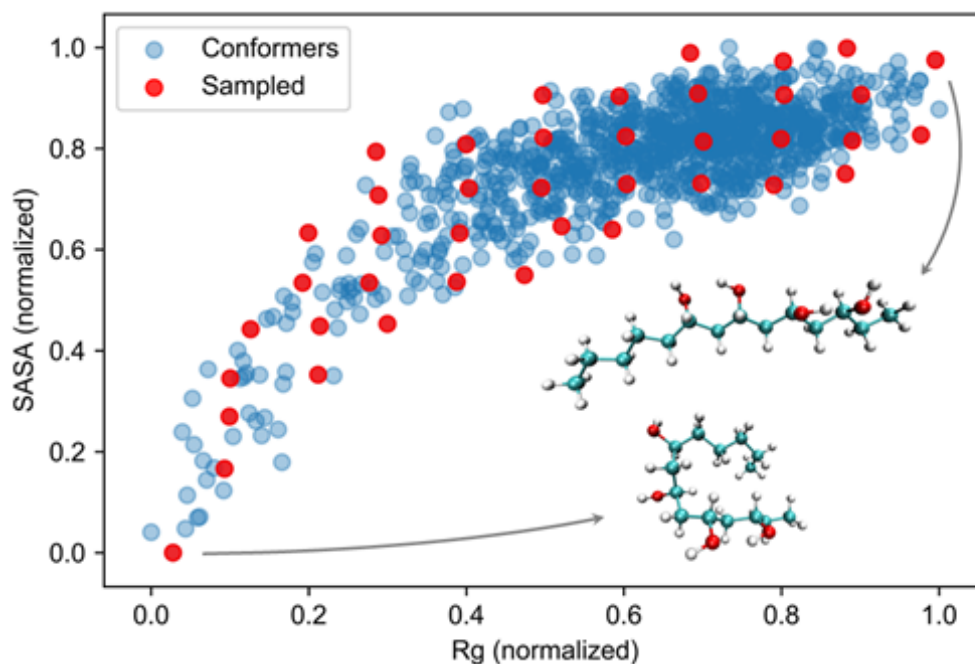


Figure 2.3:  $R_g$ -SASA plot of an EVOH oligomer in MD simulation. Each blue dot represents a conformer, red dots are selected samples. The structures of two extreme conformations are shown: the folded one represents a bottom left dot, the elongated one represents a top right dot.

## 2.2.4 Density functional theory calculations

Each conformer chosen from the MD trajectory was input to a DFT calculation to generate screening charge densities (COSMO files) using *Gaussian 16* [34]. Geometry optimization was first performed in implicit water using the conductor-like polarizable continuum model (CPCM) at the BVP86/TZVP/DGA1 level of theory. A single-point calculation with the same DFT level was then performed to obtain screening charges in the infinite dielectric constant limit. COSMO files for the 9 solvents (DMSO, water, THF, hexane, ethyl acetate, ethanol, acetone, toluene and DMF) studied in this work were also obtained using the same DFT calculations. For the 524 solvents involved in the large-scale solvent screening application, we used pre-calculated COSMO files from the database COSMObase-1901-BP-TZVP.

### 2.2.5 Solubility prediction with COSMO-RS

COSMO files from the DFT calculations were input to COSMO-RS for property evaluation. COSMO-RS predicts the thermodynamic properties of multicomponent systems based on quantum mechanical calculations and statistical thermodynamics methods [35, 36]. The chemical properties of each molecule are represented by the probability distribution of the screening charge densities (called the  $\sigma$ -profile). The  $\sigma$ -profiles of the oligomer molecules with deactivated terminal groups were used to approximate the  $\sigma$ -profile of a polymer [37]. Since the screening charge density and resulting  $\sigma$ -profile depend on the specific molecular conformation, the MD simulation and conformational sampling steps described above were used to generate a set of oligomer conformations that span a range of possible  $\sigma$ -profiles. The  $\sigma$ -profiles were then used to calculate the chemical potential of the polymer to enable predictions of polymer solubility via a solid-liquid equilibrium calculation. This calculation requires the polymer melting temperature and either the heat of fusion or an experimentally measured solubility as input. All COSMO-RS calculations were performed using the *COSMOtherm 19* software with the BP\_TZVP\_19 parameterization [38, 39]. Detailed information is presented below.

COSMO-RS was originally developed for liquid-liquid and liquid-vapor systems, and has been extended to solid compounds [39, 38] and polymers [40]. Polymers were treated as one or several repeat units with end methyl groups. These end methyl groups are deactivated by being assigned zero weight in the calculations [37]. PE and EVOH were respectively represented as  $-(\text{C}_2\text{H}_4)_n-$  and  $-(\text{CH}_2\text{CH}(\text{OH}))_{2n}(\text{C}_2\text{H}_4)_n-$ .

In *COSMOtherm*, the solubility of a solid solute,  $x_j$ , is calculated using Equation 2.1

$$x_j = \exp \left( \frac{\mu_j^{\text{pure}} - \mu_j^{\text{solvent}} - \Delta G_{\text{fus}}}{RT} \right) \quad (2.1)$$

where  $\mu_j^{\text{pure}}$  is the chemical potential of the pure compound  $j$  and  $\mu_j^{\text{solvent}}$  is the chemical potential of compound  $j$  in solvent at infinite dilution.  $\Delta G_{\text{fus}}$  is the free energy of fusion for compound  $j$  and accounts for the free energy difference between the subcooled liquid state and ordered solid state. *COSMOtherm* supports 3 options for the calculation of  $\Delta G_{\text{fus}}$  [41]:



1. By using the the Schröder-van Laar equation (Equation 2.2):

$$\Delta G_{fus} = \Delta H_{fus} \left( 1 - \frac{T}{T_{melt}} \right) - \Delta C_{p,fus} (T_{melt} - T) + \Delta C_{p,fus} T \ln \frac{T_{melt}}{T} \quad (2.2)$$

where  $\Delta H_{fus}$  is enthalpy of fusion,  $T_{melt}$  is melting temperature, and  $\Delta C_{p,fus}$  is the heat capacity difference between the liquid and solid phases. The heat capacity difference is generally assumed to be zero or can be approximated as  $\Delta H_{fus}/T_{melt}$ .

2. By using an experimental solubility as reference. *COSMOtherm* offers an option to input a reference solubility so that the  $\Delta G_{fus}$  can be fitted to experimental data.
3. By using the embedded quantitative structure-property relationship method in *COSMOtherm*.  $\Delta G_{fus}$  can be estimated based on the input structure of the compound. This option can be used when the enthalpy of fusion or solubility data are not available.

Note that Options 2 and 3 do not use  $T_{melt}$  for  $\Delta G_{fus}$ , but  $T_{melt}$  is still required for temperature-dependent solubility prediction. The melting temperatures used for PE and EVOH were 414.6 K and 450 K [42]. In our solubility calculations, we tested Option 1 using  $\Delta H_{fus}$  data from the literature with  $\Delta C_{p,fus} = 0$  (an approximation used in our previous study that led to reasonable results [8]) and Option 2 with our own experimental data. For Option 1, literature  $\Delta H_{fus}$  data for PE and EVOH are 293 J/g and 140 J/g [42]. For Option 2, the experimental solubility of PE in toluene at 110 °C and EVOH in DMSO at 95 °C were used as reference values.

## 2.2.6 Experimental measurements of solubility

Experimental solubility measurements for PE and EVOH in DMSO, water, THF, hexane, ethyl acetate, ethanol, acetone, toluene and DMF were performed to benchmark the computational predictions. The resins are low-density polyethylene (LDPE) and EVOH35 (molar ratio 35%:65% ethylene:vinyl alcohol). The experimental set up consisted of a 250 mL round bottom flask connected to a reflux condenser with a cold-water supply line. The round bottom flask contained a specific solvent amount

for the experiment (around 30 g). In each experiment, the round bottom flask was partially submerged in a 1500 mL dish containing silicone oil as a heat transfer fluid. The system was heated to the desired polymer dissolution temperature with an electric heat plate equipped with a magnetic stir drive and the stirring rate was adjusted to have constant mixing. After the solvent reached the dissolution temperature, 1 wt% of polymer virgin pellets (with respect to the solvent) were added to the round bottom flask and mixed at a constant rate. If the polymer or part of the polymer was dissolved after 30 minutes, an additional 1 wt% of polymer pellets was added to the solvent. This procedure was repeated every 30 minutes. Once no further polymer could be dissolved, an additional 1 wt% was added to ensure an excess of undissolved polymer. After the final 30 minutes, the round bottom flask was removed from the oil. The liquid contents were poured into an antisolvent, either acetone or water, to precipitate the dissolved polymer. The precipitated material was filtered out of the solvent mixture, washed with water, and vacuum dried overnight. The undissolved solids remaining in the flask were also washed with water and vacuum dried overnight. The fractions were weighed after drying and the solubility was determined based on the amount of dissolved polymer with respect to the amount of solvent used. In some cases, the solubilities were regarded as a lower limit since there was a viscosity increase of the solvent (such cases are indicated below). The mass of the undissolved solids was included to complete the mass balance in each experiment.

## 2.3 Results and discussion

### 2.3.1 Conformational sampling methods

A critical input for COSMO-RS calculations is a set of molecular conformations that are used to generate  $\sigma$ -profiles. Since  $\sigma$ -profiles are affected by conformer structures, different conformers will lead to different solubility predictions. Conformers can be obtained from MD simulations of oligomers, but many such conformers are sampled during a MD simulation so a rational framework to select representative conformers is required. To select a set of conformers as input structures for COSMO-RS, we hypothesized that conformers that span a representative space of structural parameters would similarly cover the range of possible  $\sigma$ -profiles to generate suitable COSMO-RS input. We quantified oligomer structures based on two structural parameters,  $R_g$  and SASA. We assume that conformers that span a range of  $R_g$  and SASA values will

span a range of possible  $\sigma$ -profiles. We tested several methods to select 40 conformers (out of 1,000 sampled conformers) from a MD trajectory of the 14-carbon EVOH oligomer with block structure. We describe each strategy in the sections below. In Figures 2.4-2.6,  $R_g$  and SASA values for the 1,000 sampled conformers are shown as a point-cloud of blue points. Conformers selected according to different methods are shown in red.

Figure 2.4 compares conformers selected by random sampling and greedy sampling. Random sampling randomly chooses 40 points from the 1,000 options. As a result, the conformers selected by random sampling mostly cluster in the densest region of the  $R_g$ -SASA point cloud and represent the most probable conformations of the molecule. Greedy sampling seeks to identify a set of points such that each point added to the set is as different as possible from current points in the set. In this approach, an extreme point in the 2D space is selected first, then points are iteratively selected by maximizing the sum of the log-distance to all previously selected points. This approach leads to the selection of points on the edge of the point cloud, which represents the least probable conformations of the molecule.

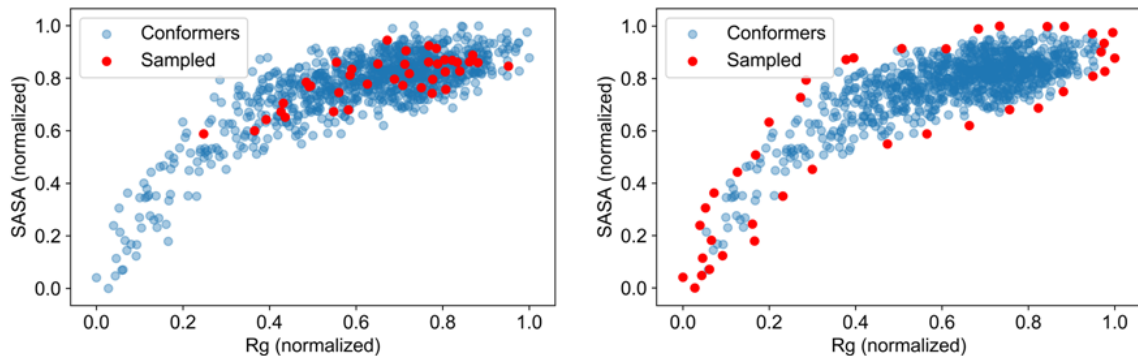


Figure 2.4: Conformers selected by random sampling (left) and greedy sampling (right).

Figure 2.5 compares conformers selected by grid sampling and cluster sampling. Grid sampling superimposes a square grid on the  $R_g$ -SASA space and selects conformers closest to each grid intersection. Cluster sampling first applies k-means clustering to the points, then selects the closest conformer to each cluster center. k-means clustering is a common data analysis method that partitions the 1000 points into 40 clusters by minimizing within-cluster variances [43]. Grid and cluster sampling both aim to

identify a sample set that reasonably cover the  $R_g$ -SASA point cloud.

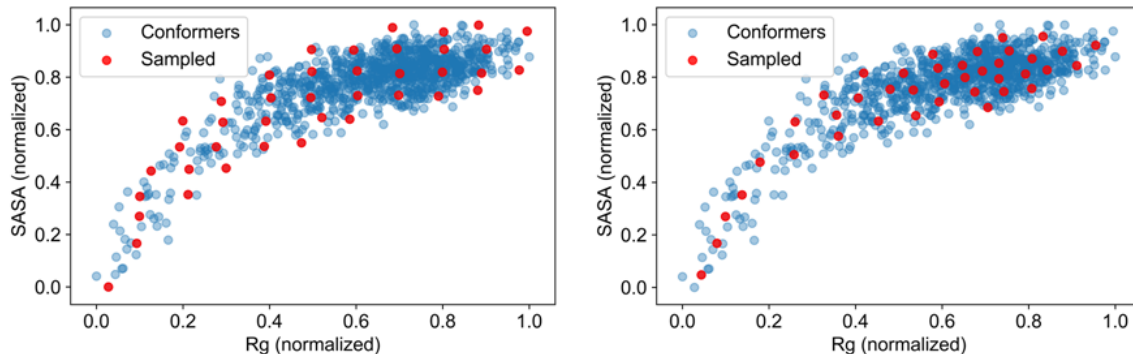


Figure 2.5: Conformers selected by grid sampling (left) and cluster sampling (right).

A potential problem of the cluster sample set is that no edge point is included because cluster centers are mostly located in the main body of the point cloud. Therefore, a hybrid sampling method that combines cluster sampling with greedy sampling was studied. A hybrid of grid sampling and greedy sampling was also generated for comparison. Figure 2.6 shows two hybrid sampling results.

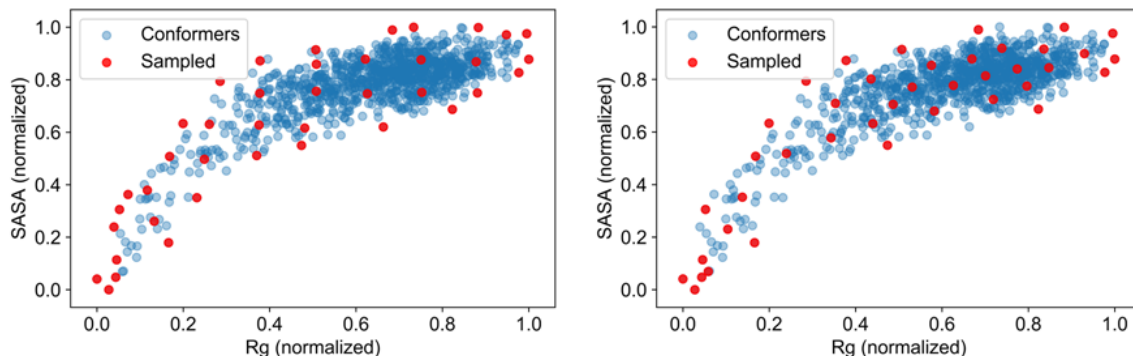


Figure 2.6: Conformers selected by greedy-grid hybrid sampling (left) and greedy-cluster hybrid sampling (right).

To assess these conformer sets, we generated  $\sigma$ -profiles for all selected conformers and calculated the resulting coverage of  $\sigma$ -profile space, which we defined as the hypervolume of the convex hull of conformer  $\sigma$ -profiles. A convex hull is the smallest polytope that contains all the points. In 2D, the convex hull is the smallest polygon

that contains all the points, and its hypervolume is simply the polygon area. In *COSMOtherm 19*,  $\sigma$ -profiles are 61-dimensional vectors, so computing the hypervolume of the convex hull for 40 points in this space is inaccurate because the points are too sparse. Therefore, we used principal component analysis to reduce the dimensionality of the 61-dimension  $\sigma$ -profile space to 2-8 dimensions. The sum of explained variance ratio reaches 95% for 8 dimension, suggesting that maximizing coverage of a 8-dimensional space would reasonably approximate coverage of the complete 61-dimensional  $\sigma$ -profile space. Table 2.1 shows the convex hull hypervolumes calculated in 2 to 8 dimensions for each conformational selection method. Grid sampling has the highest coverage for 5 to 8 dimensions, and thus the highest coverage of the complete  $\sigma$ -profile space. Therefore, we selected grid sampling as the conformational sampling approach in this work.

Table 2.1: Coverage (quantified by the convex hull hypervolume) of reduced  $\sigma$ -profile spaces for 6 conformation sets. Maximum values for each number of reduced dimensions are bolded.

Dimensions	Sum of explained variance ratio	Convex hull hypervolume					
		Random	Greedy	Grid	Cluster	Greedy-grid hybrid	Greedy-cluster hybrid
2	73.5%	148.5	152.1	146.3	<b>152.8</b>	151.9	148.5
3	82.1%	484.6	479.7	515.3	<b>550.7</b>	541.4	543.5
4	87.9%	1155.2	1253.6	1289.7	1076.1	<b>1327.3</b>	1285.0
5	91.5%	1387.7	2087.8	<b>2697.3</b>	1584.2	1923.7	2194.8
6	93.3%	1276.5	2117.3	<b>2623.8</b>	1776.7	1883.5	2231.5
7	94.7%	858.5	1137.3	<b>1592.6</b>	1410.0	1009.5	1319.9
8	95.7%	516.4	579.8	<b>915.4</b>	813.9	416.5	534.1

### 2.3.2 Experimental solubility data

To develop a new workflow for quantitative polymer solubility prediction, we first present experimental measurements of PE and EVOH solubility in nine common solvents to provide benchmarks for comparison to COSMO-RS and HSP predictions. Table 2.2 shows experimental measurements of polymer solubility at elevated temperatures (close to the boiling point of each solvent).

Table 2.2: Experimental measurement of EVOH and PE solubilities.

Solvent	Temperature (°C)	PE solubility (wt%)	EVOH solubility (wt%)
DMSO	95	0.040	24.020
water	95	0.002	0.000
THF	65	0.018	0.019
hexane	65	0.031	0.000
ethyl acetate	77	0.004	0.053
ethanol	78	0.011	0.000
acetone	55	0.001	0.001
toluene	110	14.56*	0.000
DMF	100	0.009	30.63*

\*these values represent the lower limits of polymer solubilities in the selected solvents because higher polymer concentrations resulted in a viscous solution that was difficult to stir.

### 2.3.3 HSP-based solvent screening

We first utilized HSPs to qualitatively identify good and poor solvents for PE and EVOH to compare against the measured solubility data. The HSP system assigns each compound (polymer and solvent) three parameters that account for dispersion ( $\delta_D$ ), polar ( $\delta_P$ ), and hydrogen-bonding forces ( $\delta_H$ ). Solvent-polymer interactions are measured by their distance ( $R_a$ ) in the HSP space ( $2\delta_D$ - $\delta_P$ - $\delta_H$  space). Each polymer has an additional radius parameter,  $R_0$ , that defines a sphere in the HSP space. Solvents within this sphere ( $R_a/R_0 < 1$ ) are expected to dissolve the polymer, whereas solvents outside of this sphere ( $R_a/R_0 > 1$ ) are not expected to dissolve the polymer. HSPs for a wide range of polymers and solvents have been tabulated in the HSP handbook [29]. However, there are multiple sets of HSP values for PE. Table 2.3 shows 7 sets of room-temperature HSP values that are listed for PE in the handbook as well as values for EVOH. The different HSP values for PE resins reflect differences in properties such as crystallinities and molecular weight distributions. Unfortunately, little information is provided in this literature regarding the most appropriate set of parameters.

Table 2.4 shows  $R_a/R_0$  values for the 9 solvents tested experimentally for PE and for EVOH. Each value is colored green based on comparison to the experimental

solubility data: values of  $R_a/R_0 < 1$  are green if the experimental solubility is greater than 1 wt% and red if the experimental solubility is less than 1 wt%, whereas values of  $R_a/R_0 > 1$  are green if the experimental solubility is less than 1 wt% and red if the experimental solubility is greater than 1 wt%. Excluding DMSO, the HSP values for EVOH generally were good predictors of experimental solubility data. The room-temperature DMSO value is also near the threshold and would likely be identified as a good solvent if temperature effects were included. However, different sets of HSPs for PE lead to different solvent screening results. Surprisingly, the HSPs of HDPE resulted in a perfect match with the experiments, even though the polymer used experimentally was actually LDPE. The data for PE (1) and LDPE (2) correctly classify 8/9 solvents, but PE (2), LDPE (1), and LDPE (3) perform worse with only 5-6 correct classifications each. Moreover, the errors are generally due to HSP values identifying poor solvents as good (i.e., HSP values are erroneously low) which cannot be attributed to temperature effects. Since it can be unclear which of these values to select in advance, there are clear deficiencies with using HSP values for screening solvents for these polymers. Similarly, the solubilities of EVOH in DMSO and DMF are substantially higher than that of PE in toluene even though the ratio  $R_a/R_0$  for PE in toluene tends to be much lower, highlighting that HSPs cannot provide quantitative information on solubility predictions. These observations motivate the need for alternative methods for solubility predictions.

Table 2.3: HSP values for PE and EVOH (multiple versions for PE were found).

Polymer	HSP data			
	$\delta_D$	$\delta_P$	$\delta_H$	$R_0$
PE (1)	16.0	0.8	2.8	3.2
PE (2)	16.5	2.7	6.1	7.9
LDPE (1)	16.3	5.9	4.1	8.2
LDPE (2)	16.5	4.5	0.5	6.0
LDPE (3)	15.3	5.3	2.5	10.1
HDPE	18.0	0.0	2.0	2.0
HDPE/LDPE	17.5	4.3	8.3	3.9
EVOH	20.5	10.5	12.3	7.3

\*data source: Hansen, Charles M. Hansen solubility parameters: a user's handbook. CRC press, 2007.

Table 2.4: HSP-based solvent screening for PE and EVOH. A green value indicates that the HSP prediction is consistent with the experimentally determined solubilities in Table 2.2, whereas a red value indicates that the HSP prediction is inconsistent with the experimentally determined solubilities.

Solvent	HSP			Solvent-polymer $R_a/R_0$							
	$\delta_D$	$\delta_P$	$\delta_H$	PE (1)	PE (2)	LDPE (1)	LDPE (2)	LDPE (3)	HDPE	HDPE/LDPE	EVOH
DMSO	18.4	16.4	10.2	5.60	1.87	1.57	2.64	1.47	9.18	3.17	1.03
water	15.5	16	42.3	13.23	4.89	4.82	7.23	4.08	21.82	9.28	4.40
THF	16.8	5.7	8.0	2.29	0.46	0.49	1.27	0.62	4.31	0.51	1.34
hexane	14.9	0.0	0.0	1.14	0.94	0.94	0.92	0.59	3.26	2.74	2.69
ethyl acetate	15.8	5.3	7.2	1.97	0.40	0.40	1.15	0.48	4.32	0.95	1.63
ethanol	15.8	8.8	19.4	5.76	1.86	1.90	3.24	1.71	9.99	3.19	1.63
acetone	15.5	10.4	7.0	3.29	1.01	0.68	1.50	0.67	6.29	1.90	1.55
toluene	18.0	1.4	2.0	1.29	0.66	0.73	0.76	0.66	0.70	1.80	2.00
DMF	17.4	13.7	11.3	4.91	1.56	1.32	2.38	1.27	8.30	2.53	0.97

### 2.3.4 COSMO-RS calculations

Solubility calculations for PE are shown in Table 2.5 (for PE) and Table 2.6 (for EVOH). These tables compare solubilities predicted using Option 1 and Option 2 as described previously and indicate that results obtained with Option 2 are more consistent with the experimental data. The larger deviation from experiments identified for solubilities predicted using Option 1 is likely because  $\Delta H_{fus}$  can substantially vary between different polymer resins due to differences in crystallinity, composition, or branching (in the case of PE). Therefore,  $\Delta H_{fus}$  data from the literature may not be a good reference for the actual resins we used.



Table 2.5: COSMO-RS solubility predictions for PE compared to experimental measurements. Results from two different  $\Delta G_{fus}$  options are listed. 10-conformer set of 12-carbon PE oligomers were used.

Solvent	Temperature (°C)	Experimental solubility (wt%)	COSMO-RS predictions (wt%)	
			Option 1 (literature $\Delta H_{fus}$ as input)	Option 2 (expt. toluene solubility as reference)
DMSO	95	0.04	1.02	0.34
water	95	0.002	0	0.00
THF	65	0.018	14.95	0.54
hexane	65	0.031	20.18	0.85
ethyl acetate	77	0.004	5.44	0.52
ethanol	78	0.011	1.17	0.20
acetone	55	0.001	2.88	0.06
toluene	110	14.56	16.02	14.56*
DMF	100	0.009	4.00	1.85

\*toluene is used as a reference and hence its prediction is exact.

Table 2.6: COSMO-RS solubility predictions for EVOH compared to experimental measurements. Results from two different  $\Delta G_{fus}$  options are listed. 20-conformer set of 14-carbon block structure EVOH oligomers were used.

Solvent	Temperature (°C)	Experimental solubility (wt%)	COSMO-RS predictions (wt%)	
			Option 1 (literature $\Delta H_{fus}$ as input)	Option 2 (expt. DMSO solubility as reference)
DMSO	95	24.02	27.33	24.02*
water	95	0.00	0.01	0.01
THF	65	0.02	17.83	5.53
hexane	65	0.00	0.23	0.02
ethyl acetate	77	0.05	7.61	2.47
ethanol	78	0.00	15.37	7.63
acetone	55	0.00	13.71	1.81
toluene	110	0.00	3.85	4.49
DMF	100	30.63	28.19	27.49

\*DMSO is used as a reference and hence its prediction is exact.

In the following sections, the data presented in Figure 2.7 to Figure 2.11 were generated via Option 1 to ensure consistent  $\Delta H_{\text{fus}}$  data consistent while different simulation parameters were tested. These comparisons were used to show the effect of simulation parameters on the resulting prediction error and notably that error could be systematically decreased. The solubility predictions presented in Table 2.7 and Table 2.8 were obtained using Option 2.

### 2.3.5 PE solubility predictions

We sought to develop a quantitative solubility prediction workflow using COSMO-RS to improve upon the deficiencies of HSPs noted above. We first systematically compared the impact of several parameters by predicting solubilities for PE as a simple homopolymer for which HSPs were shown to be inaccurate. Since the computational modeling of a full-length polymer molecule is formidable, the polymers were modeled as oligomers. The oligomer chain length was thus the first parameter we considered: increasing the chain length will increase the computational cost of the DFT calculations (the most time-consuming step in the COSMO-RS workflow) but could increase prediction accuracy. Consequently, there is a potential tradeoff between prediction accuracy and computational time that must be quantified to guide the solubility prediction workflow.

To select a reasonable chain length, PE oligomers with 4, 8, 12, 16, 20, and 24 carbon atoms were selected. MD simulations were performed of each oligomer and 3 conformers of each length were randomly selected. Each conformer was then input separately to DFT and COSMO-RS solubility calculations, with the latter using literature values for the melting point and heat of fusion of PE [42]. Prediction accuracy was quantified by calculating the mean prediction error relative to the experimentally measured solubilities in 9 solvents listed in Table 2.2. The CPU time of the DFT calculation was used to quantify computational cost because the MD simulation time is not substantially affected by the chain length and the COSMO-RS calculation time is minimal. Figure 2.7 shows the mean prediction error and DFT calculation CPU time as a function of oligomer chain length. As the PE oligomer length increases, the mean solubility prediction error decreases and DFT CPU time increases, illustrating the hypothesized tradeoff between accuracy and computational cost. This result also confirms that the COSMO-RS prediction accuracy can be systematically improved. We selected the PE oligomer with 12 carbon atoms (corresponding to 5 ethylene

units and 2 methyl end groups) for further workflow development because it has an acceptable prediction error with relatively short computational time.

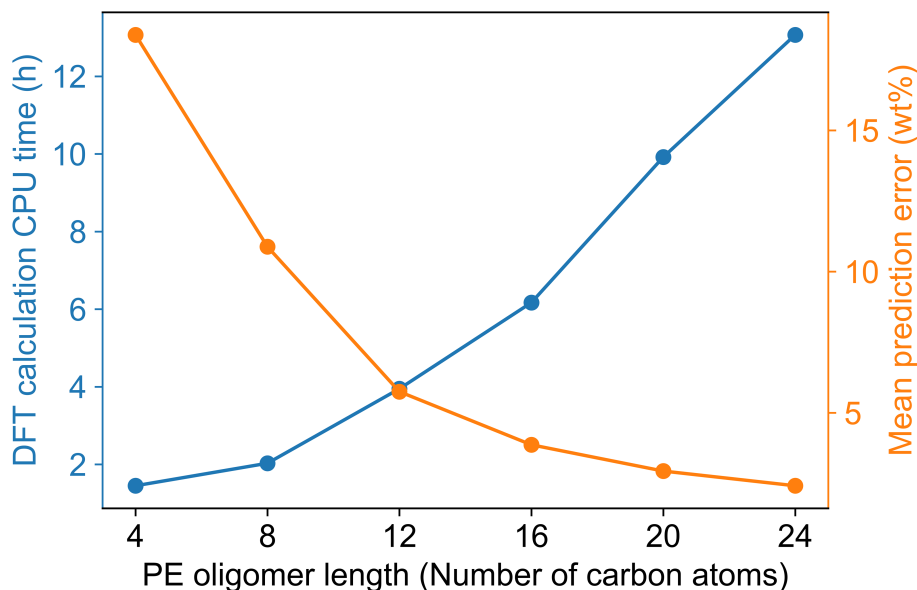


Figure 2.7: Variation in the solubility prediction error and computational cost with PE oligomer length. Three conformers are used for the solubility predictions for each data point.

With the oligomer chain length determined, we next studied the impact of the number of conformers on the tradeoff between prediction accuracy and computational cost. Different chain conformations have different screening charge density profiles that can influence the solubility prediction results, with substantial differences possible given conformational flexibility of the oligomers. From the MD trajectory, we selected a set of 30 representative conformations that span a range of  $R_g$  and SASA values for the 12-carbon PE oligomer using the grid sampling method. A series of subsets of different sizes (1, 3, 5, 10, and 20 conformers) were then generated by randomly selecting each number of conformers from the 30. 10 subsets were generated for each chosen subset size. Figure 2.8 shows the mean prediction error and DFT calculation CPU time as a function of the number of conformers (defined following the approach of Figure 2.7), with each point representing the average over all 10 subsets. The computational time required to generate a conformer set linearly scales with the set size. The mean prediction error decreases as more conformers are used and the error values tend to plateau as the number of conformers increases, again

indicating that the COSMO-RS predictions can be systematically improved. Based on this comparison, the conformer number was selected to be 10 for the final solubility predictions.

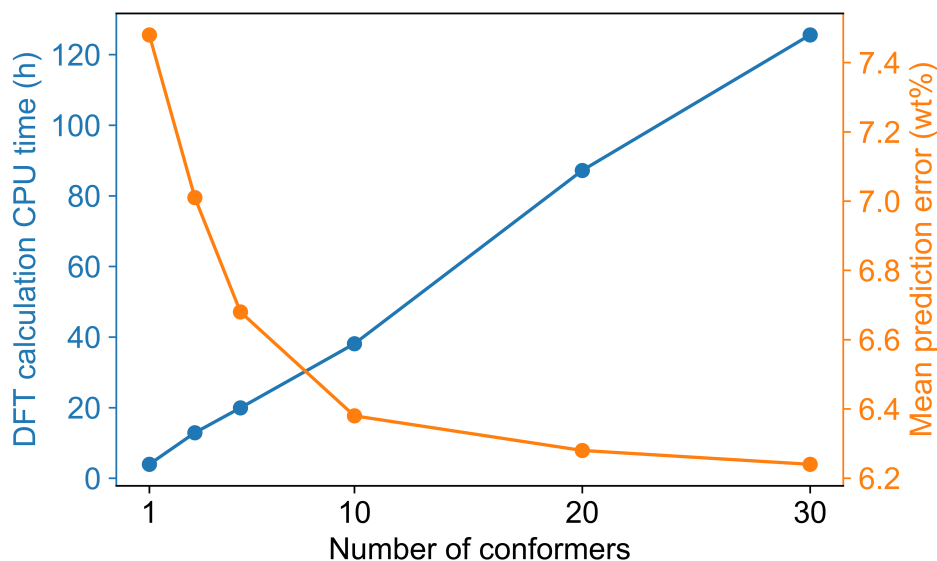


Figure 2.8: Variation in the solubility prediction error and computational cost with the number of PE conformers used. All points represent an average over 10 subsets of conformers for a PE oligomer with a 12-carbon chain length.

The 10-conformer set of the 12-carbon PE oligomer was used for final solubility predictions to compare to the experimental data. The solubility predictions in Figures 4 and 5 used the melting temperature and heat of fusion data of PE from literature sources, which leads to a relatively large error [42]. However, the properties of PE resins could vary substantially between different samples, particularly since the heat of fusion will depend on polymer crystallinity. Therefore, we instead utilized the experimental solubility of PE in toluene at 110°C as a reference value for the solid-liquid equilibrium calculation for all solvents. Table 2.7 shows corresponding predicted and experimental solubilities. As expected, the COSMO-RS protocol predicts near-zero solubilities for all solvents other than toluene in good agreement with the experimental measurements. Notably, several of these solvents are predicted by some sets of HSPs to be good solvents (e.g., hexane, THF, and ethyl acetate; see Table 2.4), indicating that the COSMO-RS approach qualitatively outperforms the HSP approach as well as providing quantitative solubility estimates. The COSMO-RS approach does slightly overestimate solubilities in nonsolvents, but these results are

highly consistent with the experimental benchmarks if 2 wt% is used as a threshold to distinguish solvents and nonsolvents.

Table 2.7: COSMO-RS solubility predictions for PE compared to experimental measurements. Toluene is used as a reference and hence its prediction is exact.

Solvent	Temperature (°C)	Experimental solubility (wt%)	COSMO-RS predictions (wt%)
DMSO	95	0.040	0.34
water	95	0.002	0.00
THF	65	0.018	0.54
hexane	65	0.031	0.85
ethyl acetate	77	0.004	0.52
ethanol	78	0.011	0.20
acetone	55	0.001	0.06
toluene	110	14.56	14.56
DMF	100	0.009	1.85

### 2.3.6 EVOH solubility predictions

We performed a similar process to compare the influence of oligomer length and the number of conformers on solubility predictions for EVOH. Since EVOH is a copolymer, we utilized the block copolymer oligomer structure for predictions when varying these parameters, then compared predictions using the block, alternating and random copolymer structures (Figure 2.2). Figure 2.9 shows the mean prediction error and computational cost as a function of oligomer chain lengths between 8 to 32 carbon atoms in increments of 6 carbon atoms. This increment corresponds to 3 monomer units to maintain the 1:2 ethylene:vinyl alcohol ratio. For each oligomer length there are 3 conformers randomly selected from the MD trajectories. Based on the tradeoff between prediction accuracy and computational cost shown in this figure, the 14-carbon EVOH oligomer was selected because of the relatively low error values in a short computational time. This oligomer has 2 ethylene units, 4 vinyl alcohol units, and 2 methyl end groups.

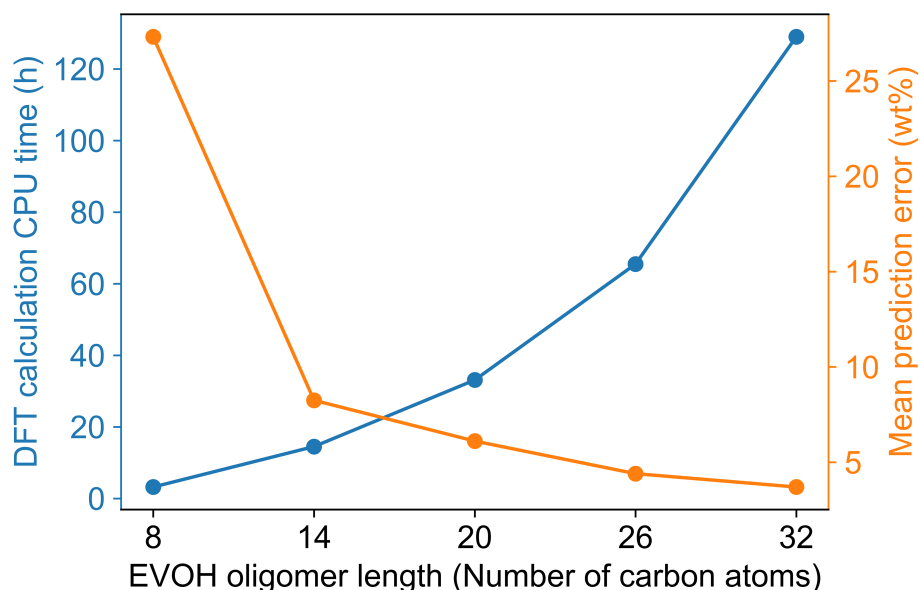


Figure 2.9: Variation in the solubility prediction error and computational cost with EVOH oligomer length. Three conformers in the block copolymer structure are used for the solubility predictions for each data point.

The number of conformers was then investigated for EVOH. A set of 40 representative conformations with various  $R_g$  and SASA values were selected using the grid sampling method and split into subsets of 1, 5, 10, 20, and 30 conformers. 10 distinct subsets were generated for each number of conformers. Figure 2.10 shows the mean prediction error and computational cost as a function of the number of conformers with each point representing the average over all 10 subsets. The scale of the vertical axis for mean prediction error is larger than that in Figure 2.8, indicating that the effect of the number of conformers is more significant for EVOH than for PE, but still plateaus as expected. Based on this comparison, the conformer number for EVOH was selected to be 20.

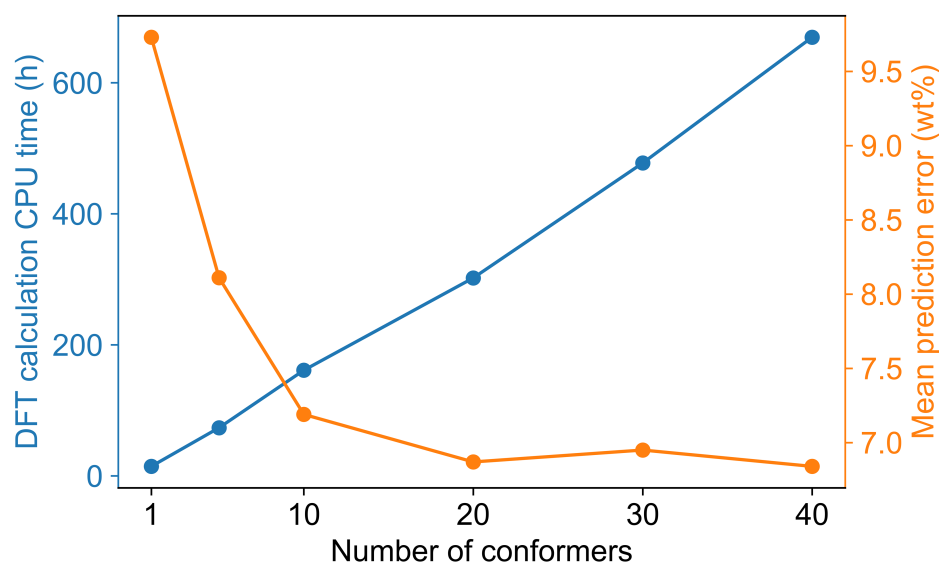


Figure 2.10: Variation in the solubility prediction error and computational cost with the number of EVOH conformers used. All points represent an average over 10 subsets of conformers for a EVOH oligomer with a 14-carbon chain length and block copolymer structure.

To further illustrate the effect of conformers on solubility predictions, Figure 2.11 shows the predicted EVOH solubility in DMSO as a function of temperature. Experimental data at four temperatures are included for reference. Predictions were based on either 1, 5, or 20 EVOH conformers, with 10 separate subsets of conformers used for predictions. Predicted solubilities with only a single conformer varied substantially and lie with the region indicated by the light blue color. The region bounding the solubility predictions decreased substantially for the 5-conformer sets (light green region). For the 20-conformer sets, the solubility calculations are highly consistent leading to a deep blue region that nearly converges to a solid line such that variations are difficult to discern by eye. These results indicate that increasing the number of conformers both leads to a decrease in prediction accuracy (Figure 2.10) and decreases the variation between different subsets of conformers, suggesting more robust results. Moreover, all conformer sets exhibit reasonable agreement with experiments, with the final results (for 20 conformers) slightly overestimating the measured solubilities but exhibiting similar trends.

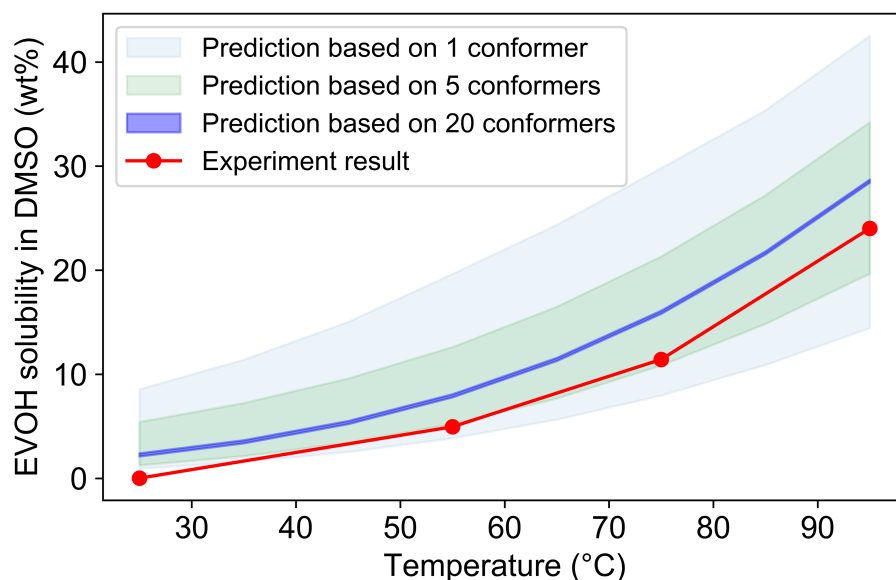


Figure 2.11: Temperature-dependent solubility prediction for EVOH in DMSO with different conformer sets. The light blue, light green, and deep blue regions show the range of predicted solubilities obtained from 10 predictions using subsets of 1, 5, or 20 conformers, respectively. Red dots are experimental data. All predictions used an EVOH oligomer with a 14-carbon chain length and block copolymer structure.

Unlike PE, EVOH is a copolymer that has two different monomer units. The arrangement of these units leads to different types of structures. As shown in Figure 2.2, three types of structures were compared using oligomers with 14-carbon chain lengths and 20 conformers per oligomer. For this comparison, the experimental solubility of EVOH in DMSO at 95 °C was used as the reference for the solid-liquid equilibrium calculation. Table 2.8 compares solubility predictions to the experimental data. Clearly, DMF was recognized as a good solvent in all three cases, but only the block structure result correctly identifies it as the best solvent in the list. Solubilities are somewhat overpredicted for experimentally identified nonsolvents, with ethanol being the most notable deviation. However, the values clearly differentiate solvents and nonsolvents, with a slightly higher threshold (3 wt%) required to distinguish these categories than is necessary for PE. With respect to quantitative predictions, the random structure has the lowest overall mean prediction error, which is consistent with the fact that EVOH is a random copolymer [44].



Table 2.8: COSMO-RS solubility predictions for EVOH compared to experimental measurements. Three different copolymer structures are compared.

Solvent	T (°C)	Expt. solubility (wt%)	COSMO-RS solubility predictions		
			Block (wt%)	Alternating (wt%)	Random (wt%)
DMSO	95	24.02*	24.02	24.02	24.02
water	95	0.00	0.01	0.03	0.03
THF	65	0.02	5.53	2.06	1.78
hexane	65	0.00	0.02	0.00	0.00
ethyl acetate	77	0.05	2.47	0.66	0.49
ethanol	78	0.00	7.63	3.94	2.98
acetone	55	0.00	1.81	0.58	0.45
toluene	110	0.00	4.49	0.64	0.39
DMF	100	30.63	27.49	21.19	20.48

\*experimental data in this solvent was used as reference for the solid-liquid equilibrium calculation, so all three structures have the same calculated solubility.

### 2.3.7 Computational screening of selective solvents

To demonstrate the power of the proposed computational solubility prediction method, we applied the COSMO-RS protocol to identify selective solvents for PE and EVOH from a large library of 524 solvents. We note that the results in Tables 2.7 and 2.8 (and corresponding experiments) indicate that DMSO and DMF are selective solvents for EVOH (by promoting high EVOH solubility and low PE solubility) whereas toluene is a selective solvent for PE; the screening procedure thus seeks to identify additional selective solvents beyond these examples. As above, a 10-conformer set of 12-carbon PE oligomers and a 20-conformer set of 14-carbon EVOH oligomers were used. The solubilities were computed at room temperature and 1 °C below the boiling points of the respective solvents. For this screening procedure, we define selective solvents as solvents with a solubility greater than 10 wt% for one polymer and lower than 1 wt% for the other. Table 2.9 shows some selected examples of identified selective solvents. At room temperature, the PE solubility was  $< 1$  wt% in all solvents considered, so no PE-selective solvents were found in this condition. PE-selective solvents were identified when temperatures were increased near the solvents' boiling

points. EVOH-selective solvents were found at both room temperature and elevated temperatures. The calculations for this large-scale solvent screening were completed within two hours since no new MD or DFT calculations were required, demonstrating the efficiency of this computational approach.

Table 2.9: COSMO-RS solvent screening for PE and EVOH. 524 solvents at two temperatures (room temperature and near each solvent’s boiling point) were considered. Nine selective solvents are presented as examples (no PE-selective solvents were identified at room temperature).

Solvent	Temperature (°C)	PE solubility (wt%)	EVOH solubility (wt%)	Comment
hydrazine	25	0.00	26.38	Room temperature, EVOH-selective
ethylenediamine	25	0.00	24.40	
n-butylamine	25	0.00	15.26	
octane	124.6	45.40	0.13	Near boiling point, PE-selective
1-octene	120.2	35.22	0.21	
tetrachloroethylene	120.3	21.34	0.08	
methylhydrazine	86.5	0.23	34.21	Near boiling point, EVOH-selective
acetic acid	116.9	0.62	25.46	
formic acid	100	0.02	24.42	

The computational efficiency of this solvent screening approach enables its application to the selection of solvents for solvent-mediated plastic recycling processes, such as the STRAP process described in our previous work. In our first STRAP process, pure DMSO was used to dissolve EVOH from a multilayer plastic film, and then water was added as an antisolvent to precipitate the polymer [8]. The computational approach presented in this work is more accurate than the prior approach due to the newly developed methods for conformational screening and oligomer length selection, suggesting that it can be applied to improve the recovery of polymers in revised STRAP processes. For example, our prior work selected solvents for STRAP based primarily on solubility considerations; technoeconomic analysis was then performed to evaluate the minimum selling price of the recovered materials necessary for economic feasibility. The computational screening approach could instead be applied to identify solvents that both selectively dissolve target polymers and reduce

downstream costs associated with polymer recovery and solvent recycling, leveraging the computational efficiency and improved accuracy described in this work. The computational approach could also be utilized to identify temperature-controlled polymer dissolution and precipitation at fixed solvent compositions to reduce the use of antisolvent and improve process economics [21]. Another example application would be to search for green solvents (quantified by metrics such as energy demand and greenhouse gas emissions in solvent production or environmental health and safety rankings [45, 46]) as potential replacements for common industrial solvents, permitting quantification of tradeoffs between greenness and solubility behavior of the solvents. There are thus multiple opportunities to apply the computational protocol developed in this work to efficiently identify solvent systems that improve selective dissolution processes for plastic recycling.

## 2.4 Summary

In this work, we present a computational approach to quantitatively predict temperature-dependent polymer solubilities in various solvents. Our approach employs MD simulations and COSMO-RS calculations. The MD simulation models a polymer as an oligomer and simulates its motion in a dilute solution to generate various chain conformations. Representative oligomer conformers that span a range of  $R_g$  and SASA values are then used as input structures to COSMO-RS solubility calculations. We studied the effects of oligomer length, conformer numbers, and copolymer structures on the accuracy of solubility predictions. We show that increasing the oligomer length and number of conformers can systematically improve prediction accuracy, albeit with increased computational cost. By selecting a reasonable oligomer length and number of conformers, the proposed approach leads to solubility predictions in good agreement with experimental measurements for PE and EVOH in DMSO, water, THF, hexane, ethyl acetate, ethanol, acetone, toluene and DMF. These predictions outperform qualitative HSP-based solubility predictions while also enabling predictions of temperature-dependent behavior, and lead to more accurate predictions than the protocol employed in our past work [8]. We demonstrated the applicability and efficiency of the new computational approach by screening 524 solvents to identify selective solvents for the dissolution of PE and EVOH at two temperatures. Future work will apply this protocol to additional polymers, including both industrially

relevant polymers and biopolymers (e.g., lignin) that must be solubilized prior to depolymerization. A current limitation of the method is the need for a single experimental solubility measurement as input to account for sample-specific parameters. We will thus continue to improve the protocol by incorporating explicit consideration of polymer molecular weight and crystallinity to reduce the amount of needed experimental input.

## 2.5 References

- [1] Liesl K Massey. *Permeability properties of plastics and elastomers: a guide to packaging and barrier materials*. Cambridge University Press, 2003.
- [2] Delilah Lithner, Åke Larsson, and Göran Dave. Environmental and health hazard ranking and assessment of plastic polymers based on chemical composition. *Science of the total environment*, 409(18):3309–3324, 2011.
- [3] Dukjoon Kim and Seong Woo Kim. Barrier property and morphology of polypropylene/polyamide blend film. *Korean Journal of Chemical Engineering*, 20:776–782, 2003.
- [4] Dorel Feldman. Polymer barrier films. *Journal of Polymers and the Environment*, 9:49–55, 2001.
- [5] K Khanah Mokwena, Juming Tang, and Marie-Pierre Laborie. Water absorption and oxygen barrier characteristics of ethylene vinyl alcohol films. *Journal of food engineering*, 105(3):436–443, 2011.
- [6] Deepak Langhe and Michael Ponting. *Manufacturing and novel applications of multilayer polymer films*. William Andrew, 2016.
- [7] Jin Kuk Kim, Sabu Thomas, and Prosenjit Saha. Multicomponent polymeric materials, 2016.
- [8] Theodore W Walker, Nathan Frelka, Zhizhang Shen, Alex K Chew, Jesse Banick, Steven Grey, Min Soo Kim, James A Dumesic, Reid C Van Lehn, and George W Huber. Recycling of multilayer plastic packaging materials by solvent-targeted recovery and precipitation. *Science advances*, 6(47):eaba7599, 2020.

- [9] Jeannette M Garcia and Megan L Robertson. The future of plastics recycling. *Science*, 358(6365):870–872, 2017.
- [10] Oksana Horodytska, Francisco Javier Valdés, and Andres Fullana. Plastic flexible films waste management—a state of art review. *Waste management*, 77:413–425, 2018.
- [11] Peter Lacy and Jakob Rutqvist. *Waste to wealth: The circular economy advantage*. Springer, 2016.
- [12] Richard Coles and Mark J Kirwan. *Food and beverage packaging technology*. John Wiley & Sons, 2011.
- [13] U.S. Environmental Protection Agency. Containers and packaging: Product-specific data, Jan 2021.
- [14] Maurizio Crippa, Bruno De Wilde, Rudy Koopmans, Jan Leyssens, Mats Linder, Jane Muncke, Anne-Christine Ritschkoff, Karine Van Doorselaer, Costas Velis, and Martin Wagner. *A circular economy for plastics: Insights from research and innovation to inform policy and funding decisions*. European Commission EC, 2019.
- [15] Maija Pohjakallio and Tommi Vuorinen. Chemical routes for recycling—dissolving, catalytic, and thermochemical technologies. In *Plastic Waste and Recycling*, pages 359–384. Elsevier, 2020.
- [16] Jean M Hoffman. Vinyloop pvc recycling’s online. *Machine Design*, 75(11):79–79, 2003.
- [17] Jens Hartmann. Vinyloop: Closure of operation in italy / phthalates issue under reach brings down european pvc recycling project, Apr 2018.
- [18] Ina Vollmer, Michael JF Jenks, Mark CP Roelands, Robin J White, Toon van Harmelen, Paul de Wild, Gerard P van Der Laan, Florian Meirer, Jos TF Keurentjes, and Bert M Weckhuysen. Beyond mechanical recycling: Giving new life to plastic waste. *Angewandte Chemie International Edition*, 59(36):15402–15423, 2020.
- [19] Martin Schlummer, Fabian Wolff, and Andreas Mäurer. Recovery of pc/abs from weee plastic shred by the creasolv® process. In *2016 Electronics Goes Green 2016+(EGG)*, pages 1–6. IEEE, 2016.

- [20] CÔTÉ Roland. Processes for recycling polystyrene waste, October 19 2017. US Patent App. 15/515,817.
- [21] Kevin L Sánchez-Rivera, Panzheng Zhou, Min Soo Kim, Leonardo D González Chávez, Steve Grey, Kevin Nelson, Shao-Chun Wang, Ive Hermans, Victor M Zavala, Reid C Van Lehn, et al. Reducing antisolvent use in the strap process by enabling a temperature-controlled polymer dissolution and precipitation for the recycling of multilayer plastic films. *ChemSusChem*, 14(19):4317–4329, 2021.
- [22] Daniel R Bloch. Solvents and non solvents for polymers. *The Wiley Database of Polymer Properties*, 2003.
- [23] Yi-Bo Zhao, Xu-Dong Lv, and Hong-Gang Ni. Solvent-based separation and recycling of waste plastics: A review. *Chemosphere*, 209:707–720, 2018.
- [24] Joel H Hildebrand. Factors determining solubility among non-electrolytes. *Proceedings of the National Academy of Sciences*, 36(1):7–15, 1950.
- [25] Charles M Hansen and Lisbeth Just. Prediction of environmental stress cracking in plastics with hansen solubility parameters. *Industrial & engineering chemistry research*, 40(1):21–25, 2001.
- [26] Robert W Taft, Jose-Luis M Abboud, Mortimer J Kamlet, and Michael H Abraham. Linear solvation energy relations. *Journal of Solution Chemistry*, 14(3):153–186, 1985.
- [27] V Gutmann. Empirical parameters for donor and acceptor properties of solvents. *Electrochimica Acta*, 21(9):661–670, 1976.
- [28] C Gardner Swain, Marguerite S Swain, Arnet L Powell, and Sergio Alunni. Solvent effects on chemical reactivity. evaluation of anion-and cation-solvation components. *Journal of the American Chemical Society*, 105(3):502–513, 1983.
- [29] Charles M Hansen. *Hansen solubility parameters: a user's handbook*. CRC press, 2007.
- [30] Anand Chandrasekaran, Chiho Kim, Shruti Venkatram, and Rampi Ramprasad. A deep learning solvent-selection paradigm powered by a massive solvent/non-solvent database for polymers. *Macromolecules*, 53(12):4764–4769, 2020.

- [31] Mark James Abraham, Teemu Murtola, Roland Schulz, Szilárd Páll, Jeremy C Smith, Berk Hess, and Erik Lindahl. Gromacs: High performance molecular simulations through multi-level parallelism from laptops to supercomputers. *SoftwareX*, 1:19–25, 2015.
- [32] Junmei Wang, Wei Wang, Peter A Kollman, and David A Case. Automatic atom type and bond type perception in molecular mechanical calculations. *Journal of molecular graphics and modelling*, 25(2):247–260, 2006.
- [33] Junmei Wang, Romain M Wolf, James W Caldwell, Peter A Kollman, and David A Case. Development and testing of a general amber force field. *Journal of computational chemistry*, 25(9):1157–1174, 2004.
- [34] MJ Frisch, GW Trucks, HB Schlegel, GE Scuseria, MA Robb, JR Cheeseman, G Scalmani, VPGA Barone, GA Petersson, HJRA Nakatsuji, et al. Gaussian 16 revision c. 01, 2016. *Gaussian Inc. Wallingford CT*, 1:572, 2016.
- [35] Andreas Klamt. Conductor-like screening model for real solvents: a new approach to the quantitative calculation of solvation phenomena. *The Journal of Physical Chemistry*, 99(7):2224–2235, 1995.
- [36] Andreas Klamt, Volker Jonas, Thorsten Bürger, and John CW Lohrenz. Refinement and parametrization of cosmo-rs. *The Journal of Physical Chemistry A*, 102(26):5074–5085, 1998.
- [37] Jens Kahlen, Kai Masuch, and Kai Leonhard. Modelling cellulose solubilities in ionic liquids using cosmo-rs. *Green Chemistry*, 12(12):2172–2181, 2010.
- [38] Frank Eckert and Andreas Klamt. Fast solvent screening via quantum chemistry: Cosmo-rs approach. *AIChE Journal*, 48(2):369–385, 2002.
- [39] Andreas Klamt, Frank Eckert, Martin Hornig, Michael E Beck, and Thorsten Bürger. Prediction of aqueous solubility of drugs and pesticides with cosmo-rs. *Journal of computational chemistry*, 23(2):275–281, 2002.
- [40] Christoph Loschen and Andreas Klamt. Prediction of solubilities and partition coefficients in polymers using cosmo-rs. *Industrial & Engineering Chemistry Research*, 53(28):11478–11487, 2014.

- [41] F Eckert. Cosmotherm reference manual, release 19. 2019.
- [42] Bernhard Wunderlich. *Thermal analysis*. Elsevier, 2012.
- [43] Kevin P Murphy. *Machine learning: a probabilistic perspective*. MIT press, 2012.
- [44] Caroline Maes, Wout Luyten, Geert Herremans, Roos Peeters, Robert Carleer, and Mieke Buntinx. Recent updates on the barrier properties of ethylene vinyl alcohol copolymer (evoh): A review. *Polymer Reviews*, 58(2):209–246, 2018.
- [45] Philip G Jessop. Searching for green solvents. *Green Chemistry*, 13(6):1391–1398, 2011.
- [46] Fergal P Byrne, Saimeng Jin, Giulia Paggiola, Tabitha HM Petchey, James H Clark, Thomas J Farmer, Andrew J Hunt, C Robert McElroy, and James Sherwood. Tools and techniques for solvent selection: green solvent selection guides. *Sustainable Chemical Processes*, 4:1–24, 2016.



## Chapter 3

# Large-scale computational polymer solubility predictions and applications to dissolution-based plastic recycling

We have developed an approach for rapid quantitative prediction of temperature-dependent polymer solubility predictions. In this chapter, we will further improve the prediction workflow and apply it to real-world plastic recycling challenges. Here, we report a joint computational and experimental workflow that was conducted for a

---

This chapter is based on the following publications

1. Zhou, P., Yu, J., Sánchez-Rivera, K. L., Huber, G. W., & Van Lehn, R. C. (2023). Large-scale computational polymer solubility predictions and applications to dissolution-based plastic recycling. *Green Chemistry*, 25(11), 4402-4414.
2. Sánchez-Rivera, K. L., Zhou, P., Kim, M. S., González Chávez, L. D., Grey, S., Nelson, K., ... & Huber, G. W. (2021). Reducing antisolvent use in the STRAP process by enabling a temperature-controlled polymer dissolution and precipitation for the recycling of multilayer plastic films. *ChemSusChem*, 14(19), 4317-4329.
3. Sánchez-Rivera, K. L., Zhou, P., Radkevich, E., Sharma, A., Bar-Ziv, E., Van Lehn, R. C., & Huber, G. W. (2025). A solvent-targeted recovery and precipitation scheme for the recycling of up to ten polymers from post-industrial mixed plastic waste. *Waste Management*, 194, 290-297.
4. Dastidar, R. G., Kim, M. S., Zhou, P., Luo, Z., Shi, C., Barnett, K. J., McClelland, D. J., Chen, E. Y. X., Van Lehn, R. C., & Huber, G. W. (2022). Catalytic production of tetrahydropyran (THP): a biomass-derived, economically competitive solvent with demonstrated use in plastic dissolution. *Green Chemistry*, 24(23), 9101-9113.

large scale of polymer-solvent systems at multiple temperatures. We will establish a polymer solubility database and an efficient solvent screening tool using this workflow. We also show that experimental measurement of polymer solubility in carefully selected reference solvents can be used by the computational models for calibration and validation. The predicted polymer solubility data will be tested on pure single polymers, physical mixtures of polymers, post-industrial multilayer plastic films, and complex mixed plastic waste.

### 3.1 Introduction

Seven billion tons of plastic waste have been generated globally to date, but less than 10% of these materials has been recycled [1]. The estimated annual loss due to plastic packaging, which is the largest constituent of plastic waste, during sorting and processing alone is 80-120 billion dollars [2]. A key factor that contributes to the low rate of plastic recycling is that current plastic recycling technologies are mostly designed for single-component plastics and are unable to deal with multicomponent plastics due to their complex compositions and the incompatibility of different polymers [3, 4, 5]. For example, multilayer plastic films are widely used in the packaging industry and over 100 million tons are produced worldwide each year [6, 7]. These films are made of several layers of different polymers that each contributes useful functional properties (*e.g.*, mechanical stiffness, barrier properties) [8, 9, 10]. However, the concomitant heterogeneity of such multicomponent materials hinders their recycling [11]. As a result, while over 29% of some single-component plastic bottles was recycled in the U.S. in 2018, only 8.7% of all plastic municipal solid waste was recycled and most multilayer films are diverted to landfills [12].

A promising, near-term approach to recycle multicomponent plastics is dissolution-based polymer recycling. In this approach, differences in polymer solubility permit the separation and recovery of pure polymer resins from carefully chosen solvent systems that dissolve only target polymers [11, 13]. Dissolution-based plastic recycling has several advantages over traditional chemical or mechanical recycling methods: it can process multicomponent plastic mixtures, it maintains the chemical structures and properties of recovered polymers, it does not require a high-purity input stream because impurities and additives can be removed by selective dissolution, and it has lower greenhouse gas emissions than producing the virgin resin [14, 15, 16, 17, 18, 19].

Recently, we proposed a dissolution-based process called Solvent-Targeted Recovery and Precipitation (STRAP) to recycle multilayer plastic films [11, 20]. In STRAP, a suitable solvent selectively dissolves a target polymer from the multilayer film at a defined temperature, the mixture is filtered to separate the dissolved polymer from the residual film components, and the polymer is precipitated and recovered by adding non-solvent (a solvent in which the polymer is insoluble) and/or decreasing the temperature. This process is then repeated sequentially for each target polymer until all resins have been recovered from the film. We have demonstrated the recovery of high-density polyethylene (HDPE), ethylene vinyl alcohol (EVOH), and polyethylene terephthalate (PET) resins from post-industrial waste films via STRAP [11, 20, 21]. Some dissolution-based plastic recycling technologies are also being developed industrially, although limited information about their process conditions and solvent selections is openly available [5, 13, 16]. These processes highlight the feasibility and broad applicability of recycling polymers from complex input streams via dissolution-based approaches.

The design of a successful dissolution-based polymer recycling process requires the selection of an appropriate solvent (and non-solvent in some cases) for each polymer of interest, temperatures for dissolution and precipitation, and the amount of solvent. These considerations affect the efficiency, economics, and environmental impact of the process [18, 20]. The key information needed to guide these choices is the temperature-dependent solubilities of polymers in different solvent systems. Several past studies have reported known solvents and non-solvents for some common polymers at various temperatures [22, 23]; examples are included in Table 3.1. However, solvent selection for complex input streams containing multiple polymers often requires consideration of a broader range of possible solvents, and the experimental collection of polymer solubility data at a large scale is prohibitively time-consuming. Alternatively, computational methods can enable effective, large-scale solvent screening which can be valuable for process design as well as for evaluating alternative sets of solvents based on cost, sustainability, or toxicity. For example, tabulated solubility parameters are often used to identify possible solvents/non-solvents for a given polymer with minimal computational effort. Examples of solubility parameters include Hildebrand [24], Hansen [25], Kamlet-Taft [26], Gutmann [27], and Swain [28] parameters. In particular, Hansen solubility parameters (HSPs) are widely used to guide solvent selection for polymers because tabulated HSP values are available

for a great number of solvents and polymers. There are many successful applications of solvent screening with HSPs [25, 29]. Machine learning methods have also been developed for solvent selection. For example, a recent study trained a deep neural network for binary solvents/non-solvent classification with over 4500 homopolymers and 24 common solvents with an accuracy of 93.8% [30]. While valuable, these prior computational methods generally focus on qualitatively distinguishing good and non-solvents for a given polymer at room temperature as opposed to quantitatively predicting solubility as a function of temperature. These drawbacks limit their applicability to the design of dissolution-based processes, which require quantitative values of polymer solubility (to determine the amount of solvent needed) as a function of temperature (to determine operating temperatures). Another challenge with HSPs is uncertainty in the selection of HSPs for specific polymer resins. The lack of computational methods to predict temperature-dependent polymer solubilities in a wide range of solvents, and for specific polymer resins, is thus the gap that we seek to address.

In this work, we address this gap by using molecular-scale models to generate quantitative, temperature-dependent, and large-scale solubility predictions for 8 common polymers in 1007 solvents at multiple temperatures [11, 31]. Our approach utilizes classical molecular dynamics (MD) simulations to sample representative oligomer conformations as input for Conductor-like Screening Model for Real Solvents (COSMO-RS) solubility calculations, which are calibrated by an experimentally measured solubility for each polymer in a reference solvent. We perform such solubility predictions for polymers that are common components of plastic waste, including EVOH, PE, PET, polypropylene (PP), polystyrene (PS), polyvinyl chloride (PVC), nylon 6 and nylon 66. Experimental measurements are subsequently performed to validate the computational predictions. Using this database, we provide chemical insights into solvent preferences for polymers based on functional group analysis. We then show how computational tools can aid the design of STRAP processes by evaluating feasible solvents for all possible separation sequences (*i.e.*, sequences of successive solvent washes, each designed to selectively dissolve a single target polymer) for systems representative of multicomponent plastic waste. Specifically, we demonstrate the applicability of the computational methods through the successful experimental separation of three different physical mixtures of polymers (PE/PS, PVC/PET, and PP/EVOH/PET) via multiple separation sequences. These compu-

tational methods have the ability to rapidly guide the design of dissolution-based plastics recycling processes to accelerate their application to new waste feedstocks and have the potential to identify green solvents as replacements for solvents utilized in existing selective dissolution processes [17, 20, 31, 32].

### **3.1.1 Literature reports of solvents/non-solvents for common polymers**

Table 3.1 includes a selected list of known solvent and non-solvents for some common polymers studied in this work. While valuable, this list of solvents it is not sufficient for designing selective dissolution processes complex, multicomponent input streams; when there are multiple polymers present in an input stream, finding a selective solvent only using literature information is challenging. Moreover, this list does not consider a wide range of temperatures unlike the computational predictions performed in this work.

Table 3.1: A selected list of solvents and non-solvents for the polymers considered in this work.

Polymer	Solvents	Nonsolvents
EVOH	acetamide DMF DMSO (hot) glycerol (hot)	carboxylic acids esters hydrocarbons lower alcohols
PE	xylene (100 °C) THF toluene 1,2,4-trichlorobenzene	propanol hexane methanol
PP	benzene diethyl ether tetrachloroethylene (121 °C) xylene (135 °C)	acetone hexane
PS	carbon disulfide chloroform cyclohexane (>35 °C) DCM (100 °C)	acetone phenol methanol hexane
PET	benzyl alcohol (180 °C) NMP (160 °C) $\gamma$ -valerolactone DMSO (hot)	aliphatic alcohols hydrocarbons ethers ketones
PVC	chlorobenzene DMF MEK THF	hexane methanol acetic anhydride alcohols
Nylon 6	DMSO acetic acid chlorophenol <i>m</i> -cresol	MEK chloroform esters ethers
Nylon 66	formic acid chloral hydrate (RT) acetic acid benzyl alcohol (120-180 °C)	aliphatic alcohols chloroform diethyl ether hydrocarbons

### 3.1.2 Industrial projects

Table 3.2 summarizes some dissolution-based plastic recycling processes being adopted at industrial scale. These processes indicate the feasibility of scaling-up selective dissolution processes, but limited information on the solvents and operating conditions used in these processes is openly available

Table 3.2: Representative industrial processes for dissolution-based plastic recycling.

Company	Process description
APK AG (Germany)	Newcycling®: combines mechanical and solvent-based processes to recycle plastic materials such as LDPE/PA films.
VinyLoop (Italy)	Solvent-based PVC purification. Launched in 2022 but terminated in 2018 due to challenges in separating hazardous plasticizer additives.
Unilever (U.K.), Fraunhofer Institute (Germany)	CreaSolv®: Solvent-based process to recycle polymers including PP, PS, PVC, ABS and PC from plastic waste (pilot plant opened in Indonesia).
Polystyvert (Canada)	PS recycling through dissolution in essential oil.

### 3.1.3 Limitations of existing methods

As described previously, various solubility parameter systems have been developed to predict polymer dissolution behaviors in different solvents; machine learning techniques have also been employed to facilitate solvent screening for polymers. Here we discuss the limitations of existing methods and the advantages of our approach in several aspects:

1. Quantitative prediction of polymer solubility. Both the HSP and the machine learning classification methods mentioned above provide qualitative predictions of polymer behaviors in solvents, i.e., they predict that a polymer should either dissolve or not. However, the amount of solvent usage is an important design parameter for dissolution-based processes [33]. The determination of this

parameter requires quantitative data on polymer solubility, which is the gap that this work aims to fill.

2. Temperature dependence of polymer solubility. As shown in Table 3.1, the literature reports on known solvents and non-solvents for polymers typically provide only one temperature for the system, or simply assume room temperature [22, 23]. Computational methods also typically assume room temperature [29, 30]. However, operation temperatures are also critical considerations in selective dissolution and temperature-induced precipitation processes [20, 11]. HSPs at other temperatures can be calculated based on room temperature HSPs and thermal expansion coefficients of the compounds [25, 29], but the qualitative nature of HSP predictions still limits its ability to provide temperature-dependent information on quantitative polymer solubilities. Our approach, however, can predict the full temperature-dependent profile of polymer solubility in various solvents.
3. Solvent mixtures. The solvent screening methods above are mostly designed for pure solvents. In practical applications, a solvent mixture may be useful in terms of solubility, selectivity, viscosity, boiling temperature (bubble point), etc. For example, in our previous study, a DMSO/water mixture was designed to recover EVOH from a multilayer plastic film and a THF/DMF mixture was designed for selective PETG dissolution [20]. Therefore, predicting polymer solubility in solvent mixtures can enable the design of solvent systems in a larger search space. Although solubility predictions in this work are for pure solvents, our proposed workflow can also be applied to solvent mixtures with trivial modifications, as shown in our previous work [20].
4. Polymer types and properties. As shown in an example, there can be multiple versions of the same kind of polymers in the HSP database. In reality, the same polymers purchased from different suppliers can have different properties such as crystallinities and molecular weight distributions. The solubility of these resins could differ greatly. In this work, we address this problem by using an experimentally measured solubility for each polymer as a reference input to the computational model so that the solubility prediction has a single resin-specific calibration. We do note, however, that this experimental calibration is also a limitation of our approach as we do not explicitly include molecular



weight or the degree of crystallinity as input parameters, although HSPs also have the same limitation. Future work is needed to explicitly incorporate these parameters in our computational workflow without experimental input.

## 3.2 Methods

### 3.2.1 Summary of approach

Our approach employs a series of computational methods to predict polymer solubilities in conjunction with experimental measurements of solubility for calibration and validation. This workflow is designed to address limitations with conventional solvent selection based on HSPs, which cannot provide quantitative predictions of polymer solubility as a function of temperature. Another challenge with HSPs addressed by our approach is the potential uncertainty when selecting specific HSP values for a given resin. Like predictions based on HSPs, our approach does not explicitly use resin molecular weight or crystallinity as inputs for solubility predictions; however, we do use experimental input to calibrate the model, thereby accounting for these resin-specific properties. Further discussion comparing our approach to existing methods is discussed in a later section.

Figure 3.1 summarizes the general workflow for solubility predictions and the application of these predictions to STRAP processes in 5 steps:

1. Using the molecular structure of the chosen polymer (modeled as an oligomer) and solvent, perform an MD simulation of a single oligomer in dilute solution to obtain a simulation trajectory that samples a wide range of chain conformations.
2. Select a set of conformers from the MD trajectory to span a range of representative oligomer structures.
3. Based on the selected conformers and a reference experimentally measured solubility for the target polymer, perform COSMO-RS solubility calculations to establish a polymer solubility database.
4. Verify selected values from the database with experimental measurements.
5. Based on the predicted solubilities, identify selective solvents for STRAP processes for plastic waste that contains multiple polymers. Test the proposed

polymer recycling process by using model systems consisting of physical mixtures of polymers.

The computational solubility database established via this approach contains 8 common polymers (EVOH, PE, PP, PS, PET, PVC, nylon 6, and nylon 66) and 1007 solvents. We then demonstrate the STRAP polymer recycling processes for 3 different physical mixtures of polymers (PE/PS, PVC/PET, and PP/EVOH/PET) which are common components of multilayer films. Details of the specific methods for each step are described in the following sections.

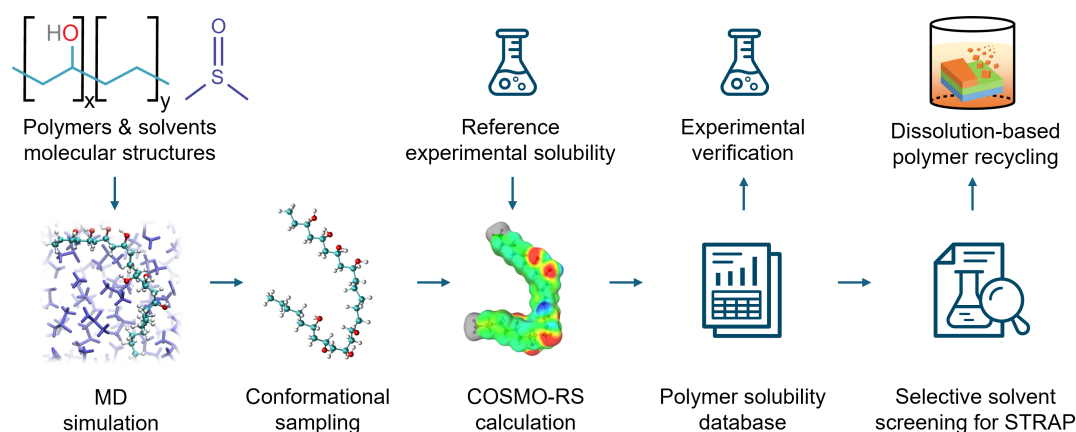


Figure 3.1: Summary of computational and experimental approach for large-scale polymer solubility prediction, validation and application.

### 3.2.2 Computational simulations for solubility prediction

We first model the polymers as oligomer molecules and perform MD simulations of these oligomers in dilute solutions to obtain trajectories of representative oligomer conformations, following the workflow established in our previous work [31]. Table 3.3 shows detailed information on the polymer structures and number of monomers included in the corresponding oligomers. Atomistic MD simulations were performed in the isothermal-isobaric ensemble using *Gromacs 2016* [34]. Each MD simulation contained 1 oligomer molecule and 216 solvent molecules. Solvents were selected for these simulations based on literature reports of good solvents for the target polymers [22, 23]. Specifically, EVOH was simulated in dimethyl sulfoxide (DMSO); PE, PP and PS were simulated in toluene; PVC and PET were simulated in dichloromethane;

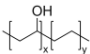
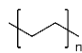
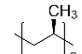
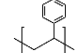
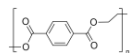
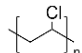
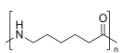
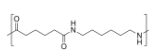
and nylon 6 and nylon 66 were simulated in tetrahydrofuran (THF). All molecules were parameterized using Antechamber and the Generalized AMBER force fields [35, 36]. The simulation system was initialized with a cubic box containing a single polymer. The system was then solvated, energy minimized, and equilibrated for 2 ns in an *NPT* simulation at 300 K and 1 bar using a velocity-rescale thermostat and Berendsen barostat. A 10 ns *NPT* simulation was then performed at the same temperature and pressure using the Nosé-Hoover thermostat and Parrinello-Rahman barostat. All simulations were performed using a leapfrog integrator with a 2-fs timestep. Verlet lists were generated using a 1.2 nm neighbor list cutoff. Van der Waals interactions were modeled with a shifted Lennard-Jones potential and Verlet cutoff-scheme that was smoothly shifted to zero at 1.2 nm. Electrostatic interactions were calculated using the smooth Particle Mesh Ewald method with a short-range cutoff of 1.2 nm, grid spacing of 0.14 nm, and 4<sup>th</sup> order interpolation. Bonds were constrained using the LINCS algorithm. All thermostats used a 2.0 ps time constant and all barostats used a 2.0 ps time constant with an isothermal compressibility of  $3.0 \times 10^{-5} \text{ bar}^{-1}$ .

We then sampled representative oligomer structures (referred to as conformers) from the MD trajectories based on two structural parameters: the radius of gyration ( $R_g$ ) and the solvent-accessible surface area (SASA). Sampling conformers that cover a range values of these two parameters can provide reliable input for COSMO-RS solubility estimations [31, 37]. We thus selected conformers by superimposing a square grid over the two-dimensional  $R_g$ -SASA scatter plot and choosing conformers closest to grid intersections following our previous work [31]. The number of sampled conformers for each polymer is listed in Table 3.3. The selected conformers were input to density functional theory (DFT) calculations to obtain screening charge densities (COSMO files). The DFT calculations included a geometry optimization in implicit water using the conductor-like polarizable continuum model and a single-point calculation in the infinite dielectric constant limit. These DFT calculations were performed with *Gaussian 16* at the BVP86/TZVP/DGA1 level of theory [38]. Precalculated COSMO files for the solvents were obtained from the database *COSMObase-1901-BP-TZVP*.

COSMO files from the DFT calculations were input to COSMO-RS for solubility calculations. COSMO-RS predicts the thermodynamic properties of multicomponent systems based on quantum mechanical calculations and statistical thermodynamics

methods [39, 40]. The chemical properties of each molecule are represented by the probability distribution of the screening charge densities (called the  $\sigma$ -profile).  $\sigma$ -profiles of all oligomer conformations with deactivated terminal groups were used to approximate the  $\sigma$ -profile of the corresponding polymer [41]. The  $\sigma$ -profiles were then used to calculate the chemical potential of the polymer to enable predictions of solubility via a solid-liquid equilibrium calculation [42]. This calculation requires the polymer melting temperature and an experimentally measured solubility as reference input. Table 3.3 shows the reference experimental solubilities used in this work (measured following the methods described below). Melting temperatures were taken from literature sources [43, 44]. All COSMO-RS calculations were performed using the COSMOtherm 19 software with the BP\_TZVP\_19 parameterization [45, 46, 42].

Table 3.3: Modeling information and reference experimental input for each polymer.

Polymer	Modeling information	Number of conformers	Reference experimental input		
			Solvent	T (°C)	Solub (wt%)
EVOH 	6-mer (4VA:2E), random copolymer structure	24	DMSO	95	19.4
PE 	6-mer	31	Toluene	110	23.1
PP 	6-mer, isotactic	25	Toluene	110	31.2
PS 	6-mer, atactic	29	Toluene	110	41.2
PET 	4-mer	22	DMSO	135	13.3
PVC 	6-mer, atactic	27	THF	50	14.9
Nylon 6 	4-mer	20	Acetic acid	90	10.8
Nylon 66 	2-mer	28	DMSO	135	3.1

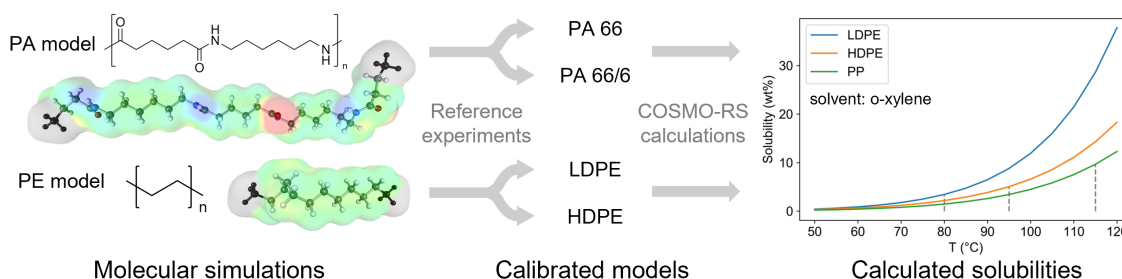


Figure 3.2: Computational examples of using reference experimental data as input to calibrate models and predict polymer solubilities. Left: example COSMO-RS screening charge distributions (colored surface) of PE and nylon models. Oligomer molecules with end groups neglected (gray surface) are used to represent longer polymer chains. Middle: the same molecular model can be calibrated with different reference experimental data to represent different materials (e.g. PE model for LDPE and HDPE, PA model for PA 6 and PA 66). Right: example calculation results of temperature-dependent solubilities of LDPE, HDPE and PP in o-xylene. Dashed lines refer to different temperatures suggested for experiments.

### 3.2.3 Experimental solubility measurements and polymer separations

Experimental solubility measurements for all eight polymers in multiple solvents were performed to calibrate and validate the computational solubility predictions. PP (isotactic, weight-average molecular weight  $\sim 12,000$ , number-average molecular weight  $\sim 5,000$ ) and PVC (high molecular weight) were purchased from Sigma-Aldrich (St. Louis, Missouri, USA). PS was purchased from Goodfellow Cambridge Ltd. (Huntingdon, UK). Low density PE (DOWTM 608A), EVOH (32 mol% ethylene content, CCP EV3251), PET (DAK Americas Laser+® C 9921), nylon 6 (BASF Ultramid® B36), and nylon 66 (DuPont Zytel® FG42A) resins were purchased and provided by Amcor Flexibles. These resins were selected because they are used commonly in industry and by major manufacturers [11, 20]. Consequently, we expect their solubilities to be representative of the solubilities of components of common commercial plastic materials. Each polymer was separately dissolved in a reference solvent to support the creation of the computational solubility database. To validate computational predictions, each polymer was also dissolved in predicted good and non-solvents.

Experiments to measure individual polymer solubilities were performed in a three-necked 100 mL round bottom flask which was equipped with a reflux condenser, a

thermometer, and a glass stopper. Approximately 40 g solvent and a magnetic stir bar were put into the flask, which was then immersed in a 1000 mL silicon oil bath with continuous agitation and heated to the target temperature. When the target temperature was reached, 1 wt% (with respect to the solvent mass) of polymer resin was added into the heated solvent and the solvent and polymer were stirred for 0.5 h to permit dissolution. If the polymer resin dissolved completely, another 1 wt% of polymer resin was added, and the above process was repeated until no further resin could be dissolved after 0.5 h mixing. The undissolved resin was filtered from the solvent, washed with DI water, dried in a vacuum oven at 100 °C for 3 h, and weighed to determine its mass after drying. The solubility was then computed as shown in Equation 3.1.

$$\text{Solubility (wt\%)} = \frac{m_{\text{added polymer}} - m_{\text{undissolved polymer}}}{m_{\text{solution}}} \times 100\% \quad (3.1)$$

It should be noted that for some polymer resins, the solubility is regarded as a lower limit because the high viscosity of the solution at the measured value inhibited further dissolution. More details regarding experimental procedures are available in the end of this section.

Physical mixtures of polymers were experimentally separated by sequential dissolution to show the feasibility of our polymer separation strategies. Three polymer mixtures were studied, including a PE/PS mixture, PET/PVC mixture, and PP/EVOH/PET mixture. Around 3 g of the desired mixtures (with a 1:1 mass ratio for the 2-component mixtures and 1:1:1 mass ratio for the 3-component mixture) were added into ~30 g of the selected solvents in a round bottom flask and heated to the desired temperature under stirring using a 1000 mL silicon oil bath. After 1 h dissolution, the flask was removed from the oil bath and emptied into a 250 mL beaker using a hot stainless wire cloth as the filter. The undissolved polymer was collected from the surface of stainless wire cloth and washed with DI water. A same amount of the non-solvent (if applicable) was added into the beaker to precipitate the dissolved polymer. The precipitated polymer was filtered with a Büchner funnel. Both dissolved and undissolved polymers were dried at 100 °C for 3 h in a vacuum oven. The mass balance was calculated based on the mass of dried polymers. For the 3-component mixture, the aforementioned dissolution step was repeated twice with different solvents.

The handling of polymer solutions in this work can sometimes be challenging. Here, we summarize some notes about the stirring, filtration, and precipitation procedures used during the experimental measurements.

**Stirring.** All experiments were performed at lab-scale within three-neck flasks. The amount of solvent used in each experiment was 30-40 g.

- In experiments to measure polymer solubilities, the viscosity of the solution can get high as the concentration of dissolved polymer increases. If the system became so viscous that the magnetic stir bar could not spin smoothly, we stopped adding more polymer and used the current concentration as a lower limit of the polymer's solubility, following the same approach as in our previous studies [11, 31].
- In the polymer separation case studies, the viscosity of the system was often low because excess solvent was used. Therefore, the solutions could be easily stirred with the magnetic stir bar.

**Filtration.** There were two types of filtration performed in our experiments:

- Hot filtration with a stainless wire cloth. This filtration procedure was used to separate undissolved polymer(s) from solution in the separation case studies. The stainless wire cloth used in this work had an opening size of 0.0277 inch and an open area of 44.2%. This cloth was selected based on the size of the polymer pellets. Note that the undissolved PS resin in case 1 is in a powder form, but it aggregates during the experiments and thus can still be filtered by the stainless wire cloth. Compared to regular filtration with filter paper, filtration with the stainless wire cloth is much faster, which minimizes the precipitation of the dissolved polymer. In addition, excess solvent was used during the experiments performed for the case studies to reduce the polymer concentration, which avoids immediate polymer precipitation during filtration after the heat is removed.
- Vacuum filtration with a Büchner funnel. This filtration procedure was performed after the precipitation step to obtain the precipitated resins. This filtration uses filter paper with 11  $\mu\text{m}$  pore size. Note that some solutions may cause the filter paper to break easily, as described in case 2. Therefore, caution

is needed in this process and the usage of alternative solvents or the addition of another solvent may also be needed.

**Precipitation.** We used two different methods to precipitate the dissolved polymers:

- Adding a non-solvent (case 1, 2 and 3). Room temperature non-solvents were added to hot solutions to precipitate dissolved polymers. The precipitated resins were then filtered (as described above) and dried in a vacuum oven at 100 °C. Note that the drying temperature should not exceed the melting temperature of the resins, otherwise the resins may melt and adhere to the filter paper.
- Evaporation (case 4 and 5). To compare the yields of case 4 and case 5, we used evaporation to precipitate the polymers in a vacuum oven. To avoid solvent bumping, the temperature was increased gradually until reaching a final temperature of 100 °C.

### 3.3 Results and discussion

#### 3.3.1 Creation of the polymer solubility database

We developed a database of computationally predicted polymer solubilities following the approach detailed in the Methods section. We modeled polymers as short oligomers, performed MD simulations of these oligomers in dilute solution to obtain various chain configurations, selected 20-31 conformers from the MD trajectories for each polymer (Table 3.3), and calculated screening charges for each of these conformers [31]. Figure 3.3 shows some example conformers sampled from the MD simulations following this approach and their corresponding screening charge densities. Screening charge densities serve as the input to solid-liquid equilibrium calculations using COSMO-RS to evaluate polymer solubilities in various solvents. Solubilities were calculated for each polymer-solvent system at room temperature (RT) and a higher temperature ( $T_h$ ) because solubilities generally increase with temperature. The higher temperature is determined by the boiling point of the solvent: if the boiling point is greater than 120 °C,  $T_h = 120$  °C; otherwise,  $T_h$  was selected as the temperature 1 °C lower than the boiling point. The upper bound on temperature enables calculations of polymer solubility at elevated temperatures while avoiding



temperatures that are too high, which may lead to melting or thermal degradation and thereby influence the properties of the recovered materials [43, 47]. Using this approach, we performed large-scale solubility predictions for 8 polymers and 1007 solvents at both temperatures, establishing a solubility database with over 16,000 data points. Table 3.4 shows some selected results from these solubility predictions for 25 common polymer-solvent systems.

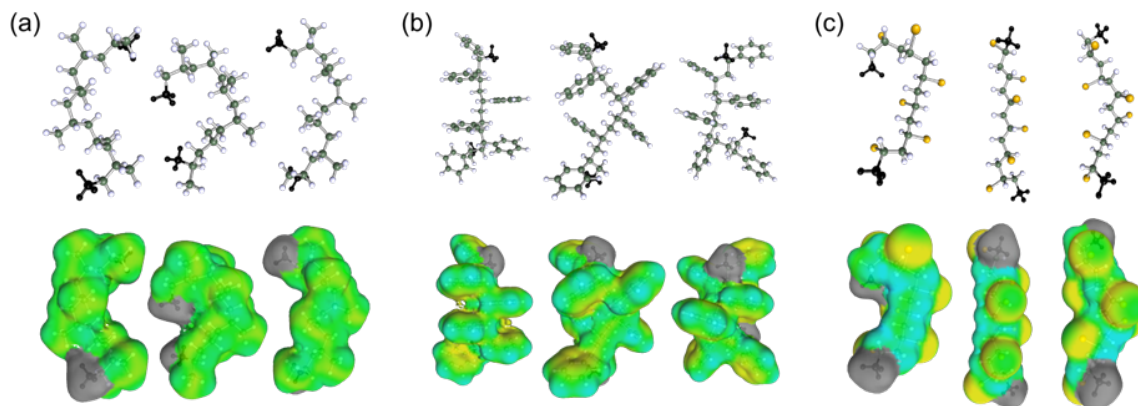


Figure 3.3: Some structures obtained from conformational sampling and corresponding COSMO-RS representations (colored surfaces) for 3 polymers: (a) PP, (b) PS, and (c) PVC. End groups of these oligomer molecules (black atoms) are neglected in the COSMO-RS calculations (gray surfaces) to represent the chemical properties of longer polymer chains.

To verify the computational predictions, we conducted experimental measurements to determine polymer solubilities in one predicted good solvent and one predicted non-solvent for each polymer. We define good solvents of a polymer as solvents with predicted solubilities  $> 3$  wt% and non-solvents as those with predicted solubilities  $\leq 3$  wt%. For the experiments, we prioritized common laboratory solvents to avoid concerns of toxicity or safety [31].

Table 3.4: Selected results from the solubility database. Each polymer-solvent system is studied at a room temperature (RT) and a higher temperature ( $T_h$ ).  $T_h$  is set as 1 °C lower than the boiling point of the solvent with an upper bound of 120 °C.

Solvent	Boiling point (°C)	Predicted polymer solubility (wt%)									
		EVOH		PE		PET		PS		PVC	
		RT	Th	RT	Th	RT	Th	RT	Th	RT	Th
Methanol	64.6	0.0	0.8	0.0	0.1	0.0	0.0	0.0	0.0	0.1	0.8
Toluene	110.6	0.0	0.3	0.1	22.6	0.0	2.5	3.6	41.0	0.7	14.8
THF	65	0.1	0.9	0.1	1.7	0.0	0.8	14.0	31.3	8.9	19.1
Water	100	0.0	0.0	0.0	0.0	0.0	0.0	0.0	0.0	0.0	0.0
Benzene	80	0.0	0.0	0.0	3.1	0.0	0.9	5.3	29.3	1.0	8.1

Table 3.5 summarizes the polymer-solvent systems and compares solubilities measured experimentally and predicted computationally. There are 2 experiments (nylon 6 and nylon 66 in DMF) for which accurate solubilities could not be measured due to the retention of the (good) solvent in the polymer. These values thus qualitatively support the prediction of high solubility, but numerical solubilities are not provided in the table. Among the 14 systems that have available experimental data points, 11 of them demonstrate good agreement between computations and experiments with the average absolute difference between predicted and experimental solubilities equal to 1.3 wt%. Two systems (PP in THF and PS in THF) have acceptable accuracy, as the computational predictions correctly identify good/non-solvents but exhibit some deviations from experimental data. Only 1 system (PET in DMF) has a computational result that is qualitatively inconsistent with the experiment. In this system, DMF was predicted to be a good solvent for PET but proved to be a non-solvent experimentally. However, we note that PET is known to be challenging to dissolve and that it is possible that kinetic effects associated with a slow rate of dissolution could inhibit accurate solubility measurements [48, 15]. Overall, the experimental verification of the database identified 11/14 good, 2/14 acceptable, and 1/14 incorrect predictions. This overall good agreement between computational and experimental solubilities validates the suitability of the solubility database for further investigation.

Table 3.5: Experimental verification of solubility predictions. The solubility of each polymer is measured in a good solvent and a non-solvent (distinguished by a threshold of 3 wt% in predicted values). Among the 14 available test results, 11 computational predictions are in good agreement with experimental data (denoted by the green color), 2 predictions are acceptable as they correctly identify good/non-solvents but have some deviations in solubility values (yellow color), and 1 prediction is inconsistent with experiment (red color).

Polymer	Good solvent	T (°C)	Pred solub (wt%)	Expt solub (wt%)	Non-solvent	T (°C)	Pred solub (wt%)	Expt solub (wt%)
EVOH	DMF	120	30.8	27.3	acetone	55	0.2	0
PE	dodecane	120	32.5	30.1	acetone	55	0.3	0
PP	THP	87	20.9	6.4	acetone	55	1.4	0
PS	THF	25	14.0	24.4	2-propanol	82	1.2	0.01
PET	DMF	120	18.4	0.5	acetone	55	0.7	0.01
PVC	THP	87	17.9	14.7	ethylene glycol	122	1.6	< 0.46
Nylon 6	DMF	120	7.3	*	acetone	55	0.2	0.01
Nylon 66	DMF	120	4	*	acetone	55	0.1	0.01

\*data unavailable due to solvent retention

### 3.3.2 Analysis of polymer solubility trends

Based on the large-scale solubility prediction results, we next analyzed the complete set of solvents to identify sets of good and non-solvents for each polymer by rank-ordering predicted solubilities. To provide heuristics regarding the feasibility of dissolving different polymers, we first defined a set of “top” solvents for each polymer. Here, we define the top solvents as the top 5% of all solvents ranked by solubility. The statistics of these solvents gives a general idea of the difficulty to dissolve each polymer. Figure 3.4 shows the distributions of polymer solubilities in their top solvents at room temperature and at elevated temperatures. As expected, polymer solubilities are mostly low at room temperature and increase at higher temperatures. Accordingly,

dissolution-based recycling processes typically dissolve the resins in a heated solvent and precipitate in a cooled system [20]. For example, Figure 3.4 indicates that there are very few good solvents for PE at room temperature but such solvents are easy to identify at higher temperatures. As a comparison, PET, nylon 6 and nylon 66 have relatively low solubilities even in their high-temperature top solvents. This comparison indicates that the dissolution of PET and nylons can be challenging in general, and if possible, dissolution-based recycling processes should be designed to avoid dissolving these components. Indeed, we have recently developed STRAP processes for multilayer plastic films containing PET which was often the last in the separation sequence and thus was recovered as a residual solid without being dissolved [11, 20].

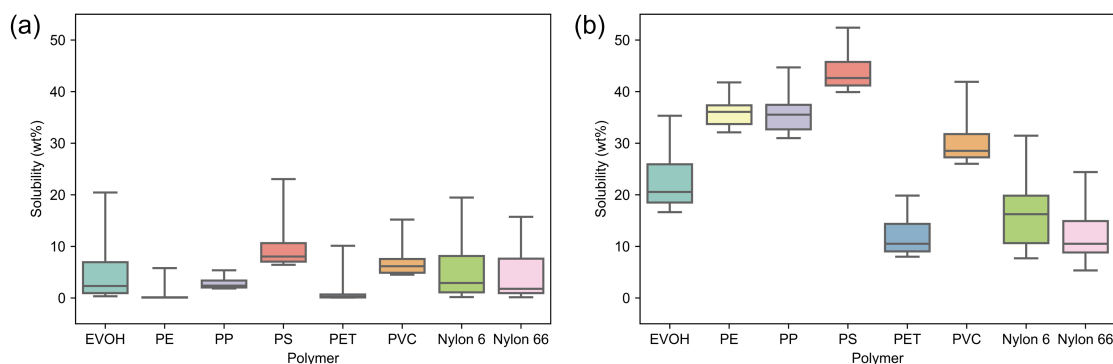


Figure 3.4: Polymer solubilities in their top 5% solvents at (a) room temperature (b) and elevated temperatures. The dataset for each polymer is displayed as a box plot, which contains five horizontal lines that represent the minimum, lower quartile, median, upper quartile, and the maximum values. The box denotes the range from lower quartile to higher quartile, which is the middle half of the dataset.

The solubility database can also provide chemical heuristics on polymer dissolution. To study the general relationship between the molecular structures of polymers and solvents, we analyzed the occurrence of different functional groups in the top solvents of each polymer. For this comparison, we define the top solvents of a polymer as those within the top 10% of all solvents ranked by solubility while also having a minimum solubility of 5 wt% at any temperature. The 5 wt% threshold is to guarantee that the set of top solvents only includes solvents with appreciable solubility values. We then performed functional group analysis for these solvents based on their molecular structures and assign each solvent to one or more classes based on their

functional groups. For example, toluene is considered to be part of the “aromatic” class and glycol is considered part of the “alcohol” class. This analysis was performed with SMILES string representation of molecules and SMARTS substructure matching syntax via RDKit [49, 50, 51].

Table 3.6 summarizes the analysis of top solvent classes. We first notice that the sets of top solvents for these polymers can include a different number of solvents. PET, nylon 6 and nylon 66 have fewer top solvents than the other polymers, indicating that the dissolution of these three polymers is generally more challenging, which is consistent with our observations of Figure 3.4. The table also lists the top solvent classes and example solvents for each polymer. Solvent classes are sorted by what percentage of the top solvents are in each class; only solvent classes that represent at least 10% of the top solvents are listed in Table 3.6. The list of functional groups aligns with our chemical intuition of “like dissolves like” as many top solvent classes share the same functional groups with the polymers. For example, alcohol is the most common solvent class for EVOH, which is a polymer with hydroxy groups; alkane and alkene are top classes for PE and PP; and aromatic compounds are the best for PS and PET. These solvent class rankings provide a general solvent selection guide for polymer dissolution and can also serve to guide the selection or design of new solvent systems with tuned chemical moieties. However, we note that these ranking results do not assert any absolute conclusion such as which class is always better for dissolution, since ranking classes by what percentage of the top solvents are in each class is not sufficiently comprehensive. For example, the aromatic class ranks quite high for multiple polymers, which can be partially attributed to the fact that it is the most common class (23%) in the solvent library.

Table 3.6: Analysis of functional groups associated with the top solvents for each polymer. Top solvents are defined as those ranked within the top 10% of solvents ranked by solubility and with a minimum predicted solubility of at least 5 wt% at any temperature.

Polymer	EVOH	PE	PP	PS	PET	PVC	Nylon 6	Nylon 66
Number of top solvents	100	100	100	100	95	100	84	49
Top solvent classes	alcohol amine aromatic carboxylic acid amide ether	aromatic ester ether ketone alkene alkane	aromatic alkane ketone ether alkene ester	aromatic ketone alkene ester ether sulfide	aromatic amine nitrile alkyl halide alkene	ether ketone alcohol amide amine	aromatic carboxylic acid alkyl halide alcohol	carboxylic acid aromatic nitrogen alkene alkyl halide
Example solvents	glycol triethylamine phenol	toluene dibutyl ether 4-heptanone octene	p-xylene cycloheptane 4-heptanone dibutyl ether	styrene toluene cyclohexanone	1-naphthol 3-chloroaniline butyronitrile	1,4-dioxane ethoxyethanol cyclohexanone	2-chlorophenol formic acid chloroform	acrylic acid m-cresol pyrrole

### 3.3.3 Polymer separation sequence and solvent screening

A typical STRAP process employs a sequential series of solvent washes with each solvent selected to selectively dissolve a target polymer from the mixture. An important consideration in designing such a process is the sequence in which polymers are dissolved and separated because different separation sequences for the same mixture of polymers lead to different requirements for selectivity. For example, a STRAP process involving sequential dissolution of each component of mixed plastic waste containing 3 polymers can have 6 possible sequences. As noted above, each sequence can impact the selection of solvents (*e.g.*, by leading to a small number of possible options for sequences that target hard-to-dissolve polymers first) and similarly influence process economics and life cycle metrics.

To guide the design of dissolution-based plastic recycling processes and automate solvent screening, we developed a tool to generate all possible sequence and screen suitable solvents for each solvent based on the computational solubility predictions. Figure 3.5 shows an example of generating separation sequences for a polymer mixture containing PE, EVOH and PET, which are the constituents of a multilayer plastic packaging film studied in our previous work [11]. The tool first generates all 6

possible separation sequences for the polymer mixture under the assumption that only one polymer is to be selectively dissolved in each step. It then provides ranked lists of solvent candidates for all steps in all separation sequences. For example, in the first separation sequence, EVOH is the first polymer to be dissolved, PE is the second, and PET is then recovered as a residual component that is not dissolved because solvents for its dissolution are rare (Figure 3.4). Step 1 of this sequence requires a solvent that selectively dissolves EVOH but not PE or PET and Step 2 requires a solvent that dissolves PE but not PET. A few top-ranked solvents for each of these steps are shown in Figure 3.5 as an example. This ranking is based on the solubility difference between the target polymer and other polymers. Each separation sequence has its own selectivity requirements and therefore leads to different sets of eligible solvents. Some separation sequences will have a wide range of solvent candidates, while some sequences have few possible solvents (*e.g.*, when a rarely soluble polymer like PET is the first in the sequence). Our program can thus provide results as input for process simulation and technoeconomic analysis to compare and determine suitable separation sequences and selective solvents. Below, we further demonstrate the applicability of this tool in several experimental case studies.

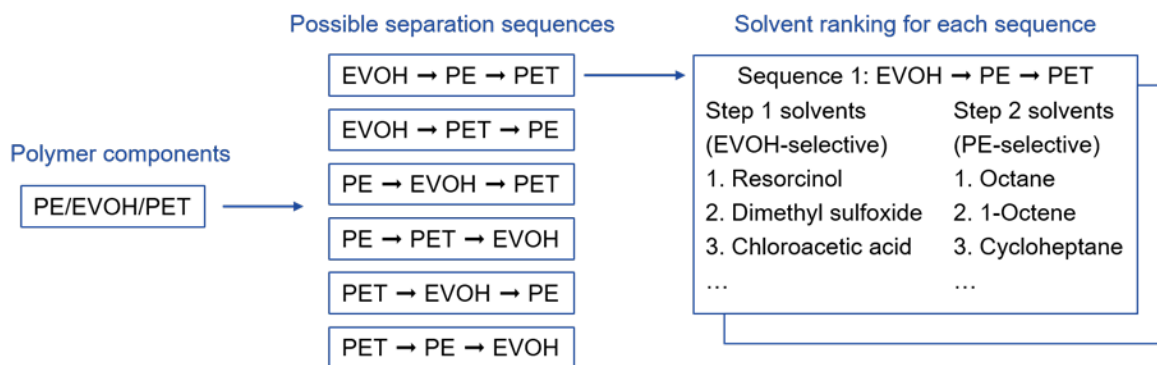


Figure 3.5: An example of generating separation sequences for polymer mixtures.

Only solvents that meet the following criteria are included in the ranking:

1. The boiling point of the solvent must be at least 25 °C;
2. The solubility of the target polymer (the one to be selectively dissolved) at  $T_h$  is at least 5 wt%;
3. The solubility of the target polymer in the solvent at RT is at most 10 wt%;

4. The solubility of other polymer(s) in the solvent at  $T_h$  is at most 10 wt%;

Here, “target polymer” and “other polymers” refer to different resins in different sequences and steps, thus the set of eligible solvents may also differ. Note that the value thresholds of these rules are quite loose and they do not guarantee selective dissolution of the target polymer. Therefore, the program will then rank these solvents in descending order by their selectivity score, which is defined as target polymer solubility minus average solubility of other polymers at  $T_h$ . As a result, the top-ranked solvents will have the largest solubility difference between target polymer and other polymers at  $T_h$ , thus it is likely to achieve the selective dissolution of target polymer. We also want to note that this program does not directly provide precipitation strategy for dissolved polymers. This is because precipitation is often less challenging and can be carried out in a variety of ways, as shown in the Table 3.7.

### 3.3.4 Case study: separation of binary polymer mixtures

To demonstrate the applicability of our computational approaches in dissolution-based polymer recycling, we perform case studies on the experimental separation of several physical mixtures of polymers. These mixtures include PE/PS, PVC/PET and a 3-component mixture of EVOH/PP/PET which are representative of common real-world plastic products or application scenarios. For example, PE/PS is the composition of a commercial laminated plastic sheet [52], the PVC/PET mixture represents a typical separation challenge in water bottle recycling processes where PVC is often a contaminant in PET [53, 54], and EVOH/PP/PET can be made into a food packaging material [55]. We use physical mixtures for these case studies to ensure that the system composition is controlled. Our past studies of multilayer plastic packaging materials have demonstrated that computational tools for solubility prediction can be applied to more realistic plastic materials [11, 20, 21]. We note that the time required for the dissolution of physical mixtures may differ from that of manufactured plastic materials (*e.g.*, multilayer films) that may have components in nanoscale contact, but we focus only on solubility as opposed to dissolution kinetics in this work.

In these case studies, we first select solvents and dissolution temperatures for different mixtures and separation sequences based on computational solubility predictions. To achieve selective dissolution, solvents are selected to have a high solubility



for the target polymer and a low solubility for the other polymers in the mixture. As in the prior validation experiments, we preferentially select common laboratory solvents (even if they are not optimal according to computational predictions) to avoid concerns with toxicity. We then conduct experiments to perform the separation of polymers. The separation result is evaluated by the yield and Fourier transform infrared spectroscopy (FTIR) of virgin and recovered resins to confirm resin purity.

The PE/PS mixture is separated in two different sequences. In the first sequence (PE→PS), dodecane at 120 °C is used to selectively dissolve PE but not PS. After 1 h of dissolution, the solid PS is separated by filtering it from the liquid solution of PE. Isopropyl alcohol is then added as a non-solvent (*i.e.*, a solvent with low predicted solubility for the target polymer) to precipitate the PE. Figure 3.6 shows photos and FTIR spectra of the virgin and recovered resins. The physical morphologies of the recovered resins change due to the dissolution and precipitation processes, as shown in the photos; the PE resin changes from pellets to flakes while the PS resin changes from a powder to a chunk. However, the FTIR spectra of the recovered resins are highly consistent with the virgin ones, indicating that the chemical structures of the polymers remain unaffected and that the recovered resins each contain a single polymer component as expected. The yields of the recovered PE and PS are 99.18% and 99.96%, respectively. In the other separation sequence, ethyl acetate is used to selectively dissolve PS, and isopropyl alcohol is used for precipitation. Changing the order of dissolution leads to different yields of 100.21% of PE and 93.84% of PS (Table 3.7). FTIR analysis further indicates that the recovered resins are similar to the virgin resins (Figure 3.9). This example shows how separation sequence impacts the performance of the dissolution-based recycling process.

We also performed an experiment that used a different non-solvent. As Figure 3.7 shows, the dissolved PE was precipitated by adding room-temperature water. Note that water is not miscible with dodecane, so the precipitation of PE was mainly attributed to the temperature change of the system. We also observed a similar morphology change of the resins, and verified the purity of the recovered resins through FTIR characterization. The yields of the recovered PE and PS are 93.26% and 109.75%, respectively. The yield of PS is slightly higher than 100%, which is possibly attributed to its physical aggregation during the contact with the solvent; some solvent might have been retained within the aggregated PS resin, leading to a mass increase.

Similar experiments and analysis were performed for the PVC/PET mixture. Only one separation sequence (PVC→PET) was experimentally tested because the other sequence involves the selective dissolution of PET, which has a very limited number of solvent candidates, and most of them are quite uncommon and hazardous (*e.g.*, hexafluoro-2-propanol). In this case study, the physical mixture of PVC/PET was separated by selective dissolution of PVC in THF at 65 °C. Room temperature water was then used as the non-solvent for precipitation. Figure 3.9 shows the photo and FTIR spectra of virgin and recovered resins. As shown in the photos, the morphology of PVC changed, while the PET resin was unaffected. The consistent FTIR result shows the purity of the recovered resins.

Table 3.7 summarizes the selected solvents and conditions. We obtain over 90% yield of both polymers using THF as a selective solvent at a relatively low temperature (65 °C), which eliminates concerns with thermal degradation and the production of potentially hazardous products from PVC [56, 57].

Table 3.7: Results from all separation case studies.

Polymer mixture	Separation sequence	Selective solvent	Temperature and time	Precipitation	Recovery yield
PE/PS	PE→PS	Dodecane (PE)	120 °C 1 h	Non-solvent: isopropyl alcohol	PE: 99.18 % PS: 99.96%
	PS→PE	Ethyl acetate (PS)	75 °C 20 min	Non-solvent: isopropyl alcohol	PE: 100.21% PS: 93.84%
PVC/PET	PVC→PET	THF (PVC)	65 °C 2 h	Non-solvent: water	PVC: 90.61% PET: 94.25%
EVOH/PP/PET	EVOH→PP →PET	EG (EVOH) THP (PP)	120 °C, 1 h 88 °C, 1.5 h	Evaporation	EVOH: 97.6% PP: 78.3% PET: 100.95%
	PP→EVOH →PET	THP (PP) EG (EVOH)	88 °C, 1 h 120 °C, 2 h	Evaporation	EVOH: 98.61% PP: 96.77% PET: 94.23%

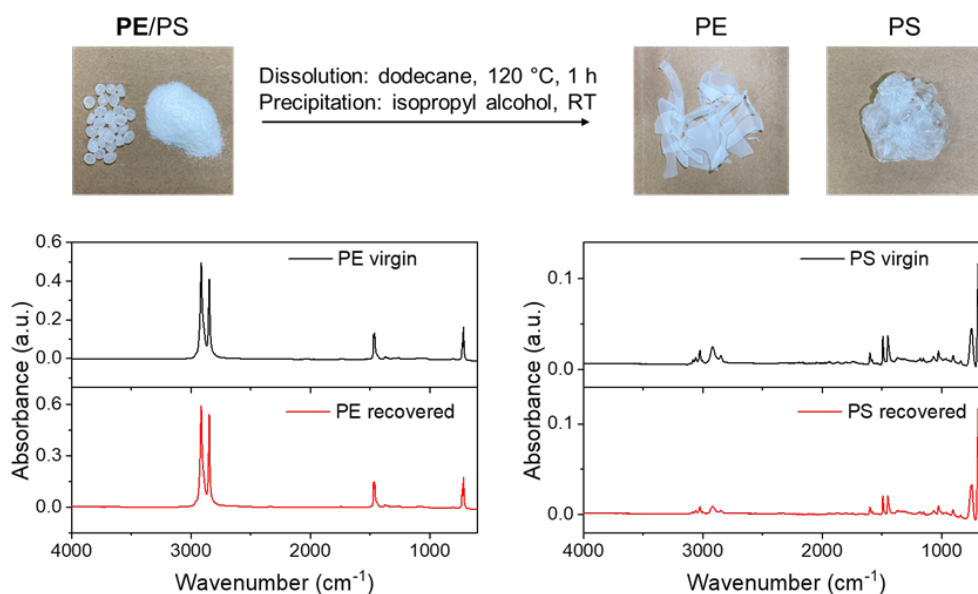


Figure 3.6: Results from the separation of case 1 (mixture PE/PS, sequence PE  $\rightarrow$  PS) via selective dissolution. Dodecane at 120 °C is used to selectively dissolve PE. FTIR spectrum verified the purity of both recovered polymers.

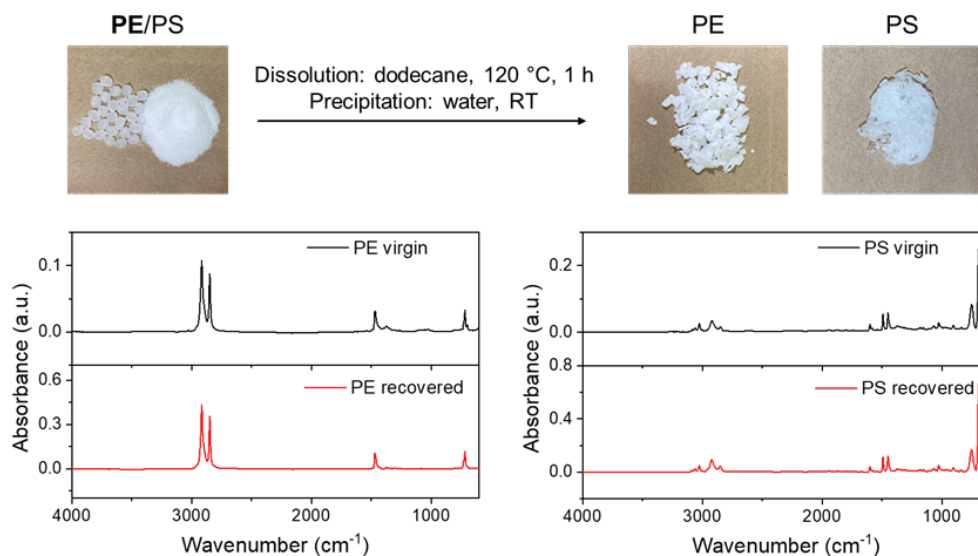


Figure 3.7: Separation result of case 1 (mixture PE/PS, sequence PE  $\rightarrow$  PS) using an alternative precipitation method.

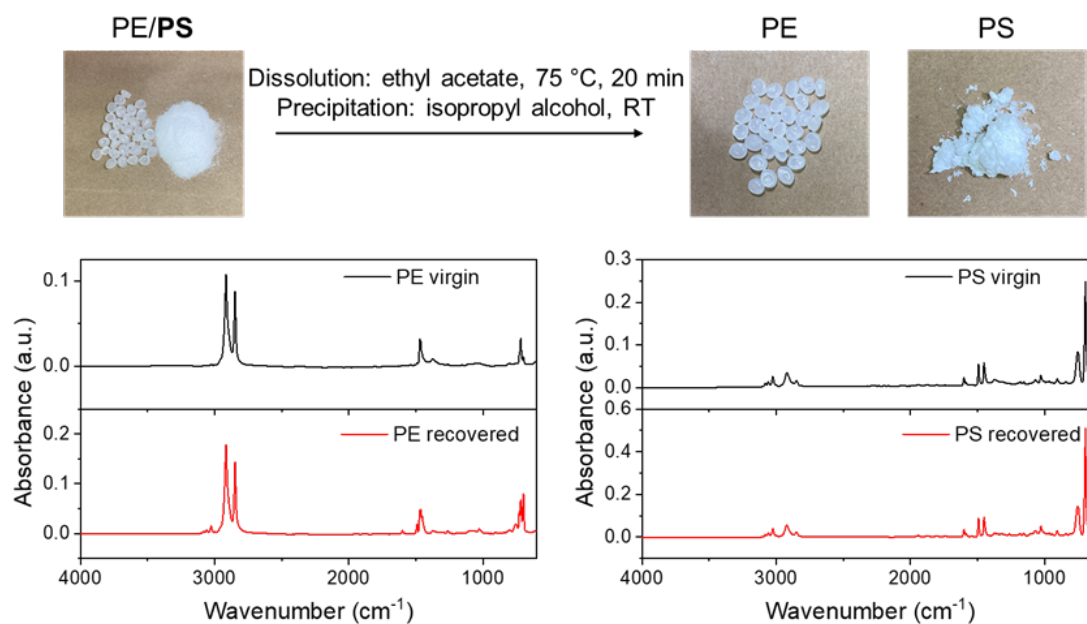


Figure 3.8: Separation result of case 2 (mixture PE/PS, sequence PS → PE).

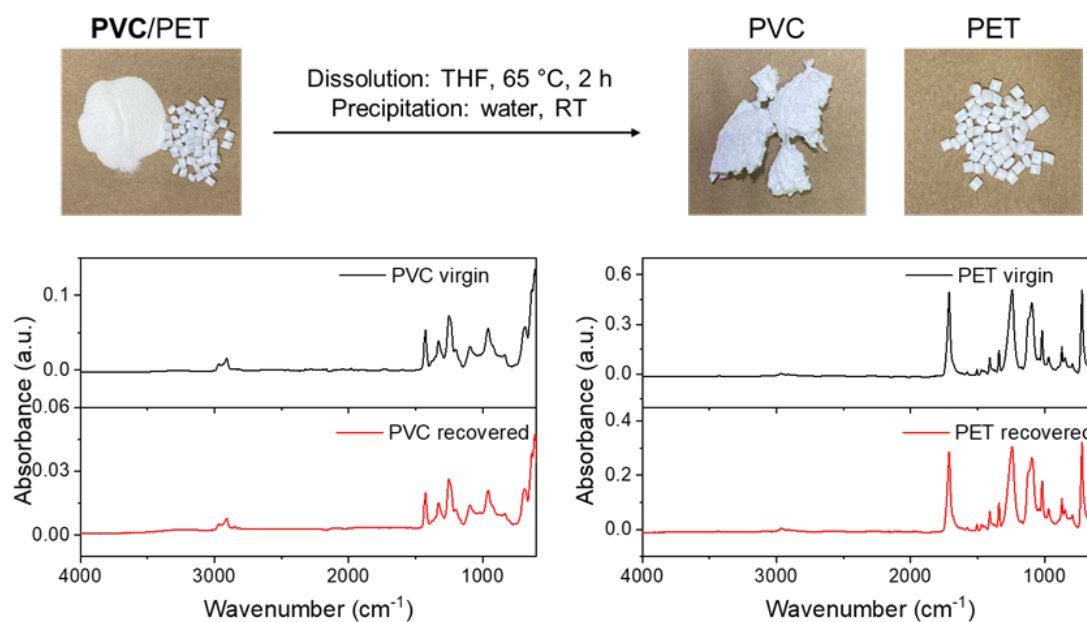


Figure 3.9: Separation result of case 3 (mixture PVC/PET, sequence PVC → PET).

### 3.3.5 Case study: separation of ternary polymer mixtures

For the 3-component mixture (EVOH/PP/PET), we first study the separation sequence  $\text{EVOH} \rightarrow \text{PP} \rightarrow \text{PET}$ , in which ethylene glycol (EG) is used as an EVOH-selective solvent in the first step, then tetrahydropyran (THP) is used as the PP-selective solvent in the second step. With this sequence, it was found that the yield of PP is low (78.3%) and we observe an undissolved solid which clearly differs from the PET resin. The FTIR spectra suggest that the undissolved solid is a mixture of PP and EVOH. We speculate that some EVOH and PP agglomerate in the presence of EG at the first step and remain undissolved throughout the remaining selective dissolution process. Therefore, a different separation sequence ( $\text{PP} \rightarrow \text{EVOH} \rightarrow \text{PET}$ ) was tested with the same solvents and temperatures. In this sequence, PP is the first to be separated to avoid its contact with EG. With this sequence, we observe no undissolved solid and the yields for all three polymers are excellent ( $>94\%$ , Table 3.7). This example shows how unexpected effects can arise during selective dissolution processes to further demonstrate the value of assessing alternative separation sequences.

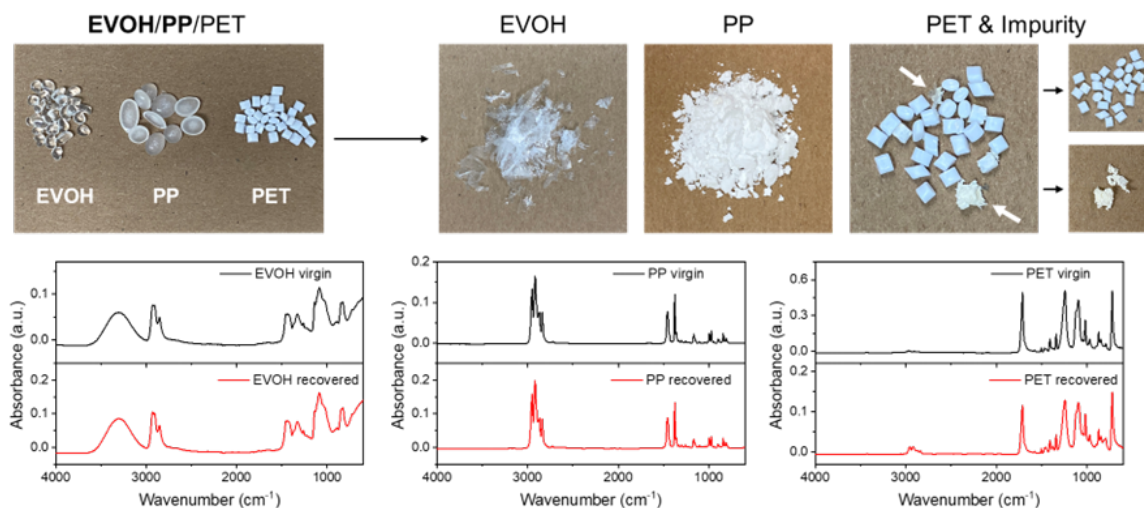


Figure 3.10: Separation result of case 4 (mixture EVOH/PP/PET, sequence  $\text{EVOH} \rightarrow \text{PP} \rightarrow \text{PET}$ ). The white arrows in the photo of recovered PET point to the impurities.

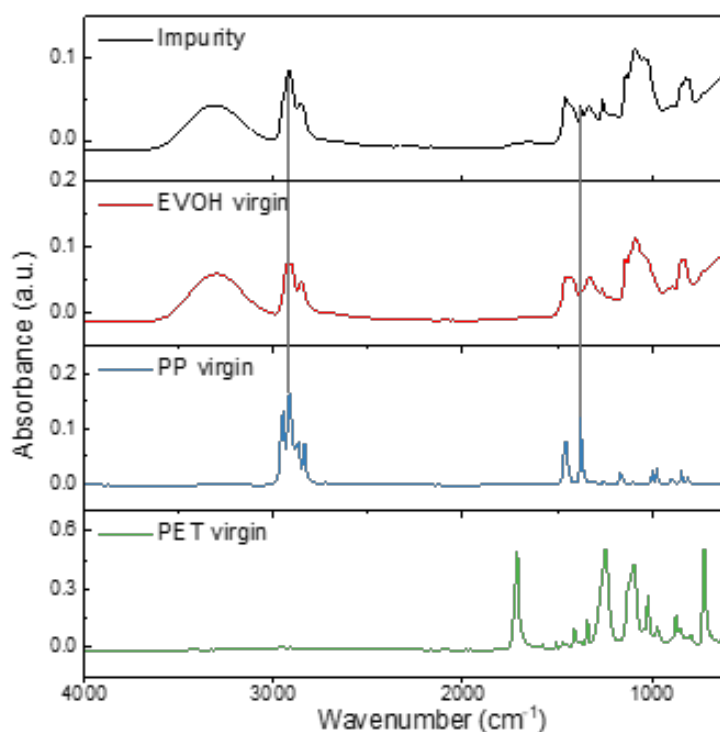


Figure 3.11: FTIR analysis of the undissolved solid impurity in sequence EVOH → PP → PET. The spectrum of the impurity is mainly similar to that of EVOH virgin. The vertical lines showed two peaks that indicate the existence of PP in the solid. This result suggests that the undissolved solid impurity is a mixture of EVOH and PP resins.

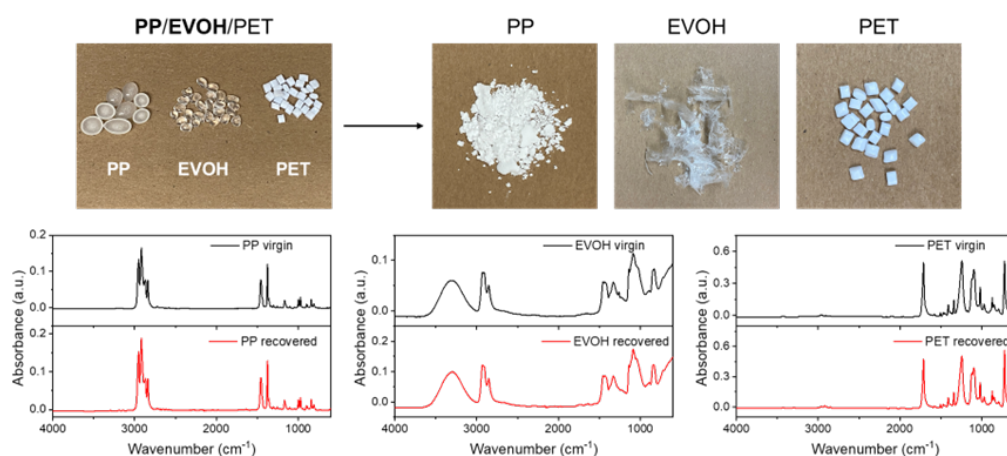


Figure 3.12: Separation result of case 5 (mixture EVOH/PP/PET, sequence PP → EVOH → PET).

There are multiple other possible separation sequences for this 3-polymer mixture EVOH/PP/PET. We did not test all sequences experimentally, but instead propose some applicable solvent selections here. Table 3.8 presents four more separation strategies for this polymer mixture. In these strategies, we specifically focus on enabling temperature-controlled precipitation, in which a target polymer is dissolved at a high temperature and precipitated at a low temperature (as opposed to being precipitated through addition of a non-solvent). Temperature-controlled precipitation has been shown to be preferred in STRAP processes based on prior technoeconomic analysis [18, 20]. We selected solvents from those that satisfy the following rules: the predicted solubility of the polymer to be dissolved must be greater than 5 wt% while the solubility of other polymers must be lower than 3 wt%, the difference in the predicted solubilities must be greater than 5 wt% to achieve selectivity, and the predicted solubility of the dissolved polymer at room temperature must be 80% lower than its solubility at high temperature to assure the feasibility of temperature-controlled precipitation. Figure 3.13 provides an illustrative example of the workflow of the first proposed separation strategy, in which EVOH is first dissolved in resorcinol and PET is then dissolved in pyrrole. These examples demonstrate the capability of the computational methods to rapidly generate potential separation sequences for further evaluation experimentally or as input for further technoeconomic/life cycle analysis.

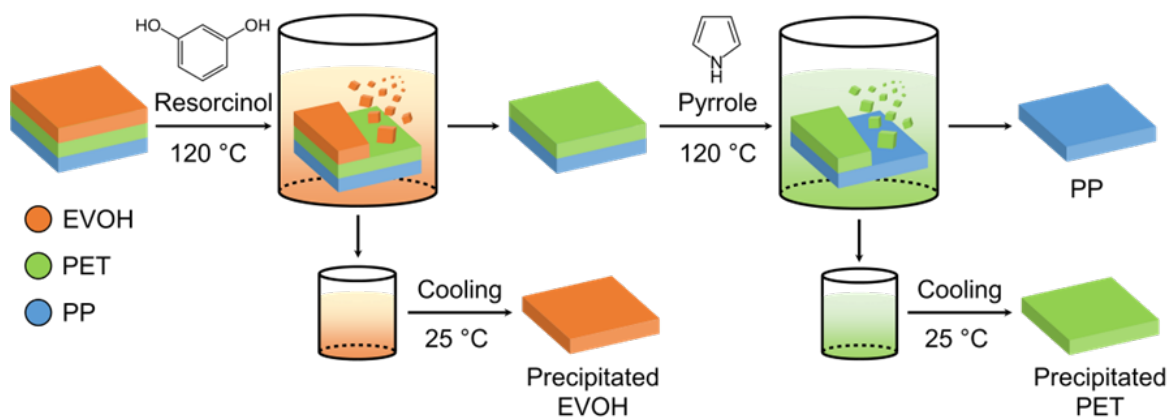


Figure 3.13: Schematic of a proposed separation process for the PP/EVOH/PET mixture using solvents and temperatures optimized for selective dissolution.

Table 3.8: Examples of other possible separation strategies for PP/EVOH/PET mixture. Selective solvents and the corresponding solubility predictions are listed for 4 different separation sequences. Each solvent selectively dissolves a target polymer at a high temperature and precipitates the polymer at room temperature.

Separation sequence	Predicted solubilities			
	Solvent	Polymer	T (°C)	Solubility (wt%)
EVOH→PET→PP	Resorcinol	EVOH	120	31.2
			25	3.7
		PET	120	2.2
		PP	120	0.2
	Pyrrole	PET	120	15.8
			25	0.1
PP		120	1.3	
PP→PET→EVOH	Cycloheptane	PP	117	44.7
			25	3.0
		PET	117	0.0
		EVOH	117	0.1
	Methyl isothiocyanate	PET	118	19.8
			25	0.1
EVOH		118	1.6	
PET→PP→EVOH	Propionitrile	PET	96	9.1
			25	0.1
		PP	96	1.4
		EVOH	96	2.0
	1-Octene	PP	120	42.0
			25	2.3
EVOH		120	0.1	
PET→EVOH→PP	Dibromomethane	PET	96	6.9
			25	0.4
		EVOH	96	0.1
		PP	96	0.5
	DMSO	EVOH	120	35.3
			25	1.3
PP		120	1.7	



### 3.3.6 Case study: improving polymer recovery process via temperature-controlled precipitation

We previously reported a STRAP process that could separate PE, EVOH, and PET resins from a multi-layer plastic film [11]. In this process, EVOH was dissolved in hot DMSO solvent, then precipitated by adding water to the solution. In this case study, we want to explore other possibilities in the precipitation strategy of EVOH solution with the help of our computational tools. Here, COSMO-RS predictions were performed to identify potential solvent compositions for the EVOH recovery, leveraging the ability of this method to capture temperature-dependent solubilities.

Figure 3.14 shows COSMO-RS predictions of EVOH solubility as a function of temperature and DMSO-water compositions. For comparison, the predicted EVOH solubility in pure DMSO at 95°C is 22.77 wt%, which is similar to the experimentally measured solubility of 24.02 wt%. This comparison supports the validity of COSMO-RS to predict EVOH solubilities. The STRAP-A process dissolves EVOH in pure DMSO at 95°C. Water is then added as the antisolvent to achieve a final 20% DMSO-80% water (v/v) mixture at a lower temperature, reducing the EVOH solubility to trigger its precipitation. These steps are indicated by the labeled white arrow in Figure 3.14. This first process takes advantage of the large solubility difference (as predicted by COSMO-RS and measured experimentally) between the two states to achieve high EVOH recovery.

Figure 3.14 indicates that the STRAP-B process could achieve the same decrease in solubility to precipitate the polymer by reducing the temperature without varying the solvent composition. The COSMO-RS solubility calculations indicate that EVOH recovery should be possible in pure DMSO, which is consistent with the inability of pure DMSO to dissolve EVOH at room temperature. However, the experimental recovery of EVOH upon cooling EVOH dissolved in pure DMSO was low. Therefore, different mixture compositions were tested. A 60% DMSO-40% water mixture (v/v) was selected for EVOH recovery since it was predicted to have a satisfactory solubility (10.45 wt%) at 95°C and low solubility (1.72 wt%) at 35°C; the latter value is comparable to the predicted EVOH solubility for the final step of the STRAP-A process. Experimental values indicated a solubility of 7.17 wt% at 95 °C and 0.01 wt% at 35 °C, leading to a high EVOH recovery. We note that COSMO-RS overpredicts the experimental solubility, but general trends are correctly captured. Process simulations and techno-economic analysis have shown that the temperature-controlled

STRAP-B process can reduce costs and make dissolution-based recycling processes more attractive [20].

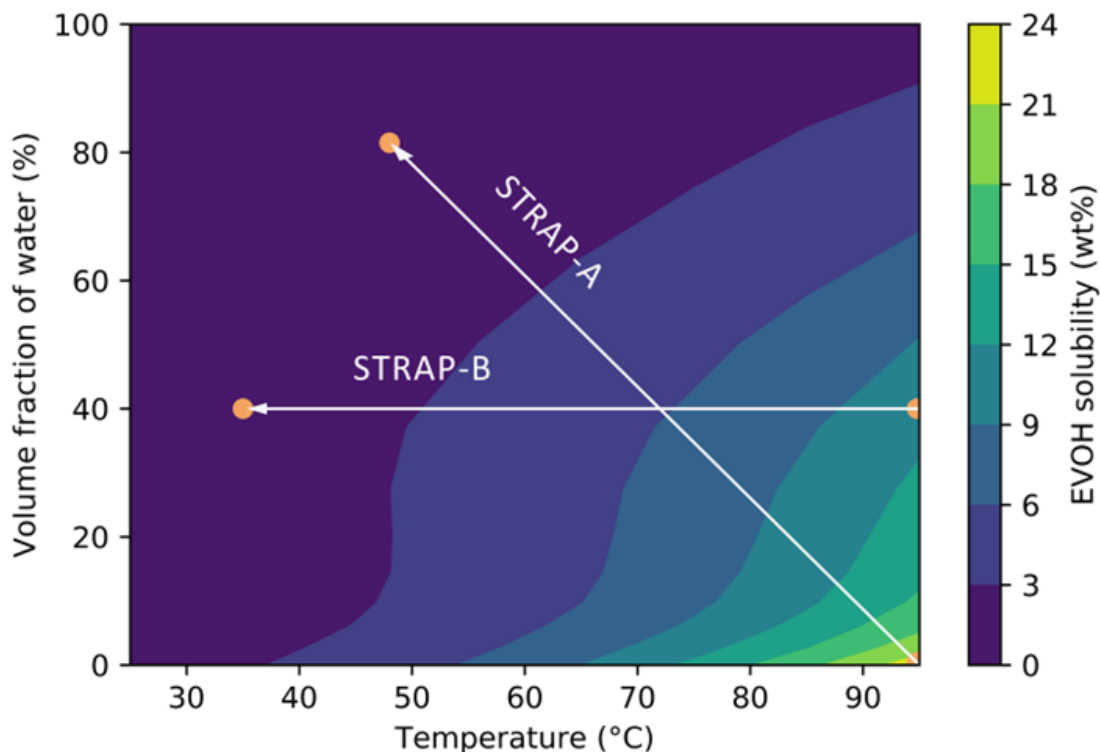


Figure 3.14: COSMO-RS solubility predictions for EVOH in DMSO-water mixtures. Two EVOH recovery processes are shown by arrows. The STRAP-A process dissolves EVOH in pure DMSO at 95°C (predicted solubility 22.77 wt%) and precipitates the EVOH in 81.5% water at 48°C (predicted solubility 1.23 wt%). The STRAP-B process dissolves EVOH in 40% water at 95°C (predicted solubility 10.45 wt%) and precipitates the EVOH by reducing the temperature to 35°C (predicted solubility 1.72 wt%).

Similar COSMO-RS solubility predictions were computed for PE in various toluene-acetone mixtures to identify if any mixtures were suitable for recovery. The experimental solubility of PE in pure toluene (14.56 wt% at 110 °C) was used as a reference input to the COSMO-RS calculations. The computational results indicate that PE solubility in 90% toluene-10% acetone (v/v) is 0.02 wt% at 55 °C. This result suggests that adding only a small fraction of acetone to toluene makes PE insoluble in the mixture, even at elevated temperatures; similar results were obtained for other volume fractions of acetone. This low solubility was verified experimentally, where none of

the tested toluene-acetone mixtures could dissolve the PE. Therefore, pure toluene was still used in order to ensure initial PE dissolution. Pure toluene still allowed the PE precipitation to occur with a decrease in temperature.

### 3.3.7 Case study: separation of a post-industrial film with 5 polymer components

The sections above have reported the application of our computational methods on physical mixtures of up to 3 polymer components. We have also shown that our computational data has been utilized to design and improve STRAP processes for post-industrial multilayer plastic films with 3 polymers. In this section, we will investigate a post-industrial film that has 5 different polymers, manufactured by Amcor. The film is composed of PE, EVOH, PET, EVA and PETG resins. If the same STRAP process developed for the previous PE/EVOH/PET/EVA films were applied to the current 5-component film, both PETG and PE would be dissolved by toluene. Therefore, we used the computational approach to identify alternative solvents capable of dissolving PETG to develop a new STRAP process. Since PETG is a special polymer that was not included in the computational polymer solubility database. Therefore, a few case-specific calculations and simulations were performed to facilitate the solubility estimation and solvent screening.

We first obtained HSPs for 850 solvents and calculated each solvent's distance in HSP space ( $R_a$ ) to the HSPs of PETG. Each value of  $R_a$  was then normalized by the radius of the PETG solubility sphere ( $R_0$ ). Only solvents with values of  $R_a/R_0$  less than 1 are expected to dissolve PETG. Table 3.9 includes HSP values for common, readily available solvents. Toluene, cyclohexanone, 1,4-dioxane and triethylamine are recognized as good candidates with  $R_a/R_0$  values less than 0.7. THF, 1,1-dichloroethane and ethyl acetate have  $R_a/R_0$  values between 0.9 and 1, indicating probable dissolution. DMF and ethanol are identified as poor solvents with  $R_a/R_0$  values greater than 2. However, PETG is a copolymer that is typically synthesized from terephthalic acid (TPA), ethylene glycol (EG) and 1,4-cyclohexanedimethanol (CHDM), with the ratio of EG:CHDM influencing its properties [58]. Unfortunately, available HSP values for PETG do not provide any information on its composition [25]; consequently, we also performed COSMO-RS solubility calculations, which consider both the structure and composition of this copolymer, to identify solvents capable of dissolving PETG. In this case, PETG was modeled as a random copolymer with a 2:1

molar ratio of EG:CHDM based on known information on the PETG component in the film. Table 3.9 shows that the HSP and COSMO-RS results agree with each other for toluene, cyclohexanone, 1,4-dioxane, THF and ethanol; these solvents have large COSMO-RS predicted solubilities and low values of  $R_a/R_0$ . However, the COSMO-RS results also identify DMF as a potential good solvent. Based on these results, toluene, cyclohexanone, dioxane, DMF, and THF could all be good solvents for PETG dissolution. Toluene was eliminated as a possible solvent for STRAP-B because it also dissolves PE. We also eliminated dioxane as a solvent due to potential health hazards and eliminated cyclohexanone because ketones can be unstable. We thus selected THF and DMF as possible solvents for further experimental investigation.

Table 3.9: COSMO-RS and HSP solubility predictions for PETG.

Solvent	COSMO-RS predicted solubility (wt%)	HSP values ( $R_a/R_0$ )	Boiling point (°C)	Temperature for COSMO-RS prediction (°C)
toluene	47.82	0.43	110.6	110
cyclohexanone	36.80	0.58	155.4	100
1,4-dioxane	35.80	0.69	101.2	100
DMF	14.41	2.17	152.8	100
THF	10.21	0.90	66	65
1,1-dichloroethane	1.43	0.96	56.3	55
triethylamine	0.19	0.66	88.8	85
ethanol	0.15	2.84	78.2	78
ethyl acetate	0.04	0.98	77.1	75

After the solvent selection for the PETG component, the STRAP process was applied experimentally to the multilayer film (Figure 3.15). The PETG dissolution was done at 65 °C for 4 hours using THF, before any other polymer component. Separating the PETG entirely from the film using THF was difficult, as some polymer was left behind after the dissolution time was completed. This was not improved with different polymer/solvent ratios or a longer dissolution time. This separation inefficiency was attributed to the film strips being glued together possibly due to the presence of THF. This behavior was not observed whenever DMF was used for

the PETG separation. Since DMF also dissolved the EVOH component, different THF/DMF mixtures were tested to decrease the EVOH solubility. A 40% THF-60% DMF (v/v) solvent mixture was determined to selectively dissolve PETG and not EVOH, by measuring experimental solubilities. This mixture was used for the actual film and the PETG recoveries improved from 15.28 to 20.83 wt%. 1-propanol was selected as an antisolvent to precipitate the PETG, although future work could consider solvent compositions to dissolve and precipitate the PETG component without the addition of an antisolvent. For the remaining polymer components which were PE, EVOH, PET and EVA, the steps from STRAP-B were used. The results are presented in Table 3.10.

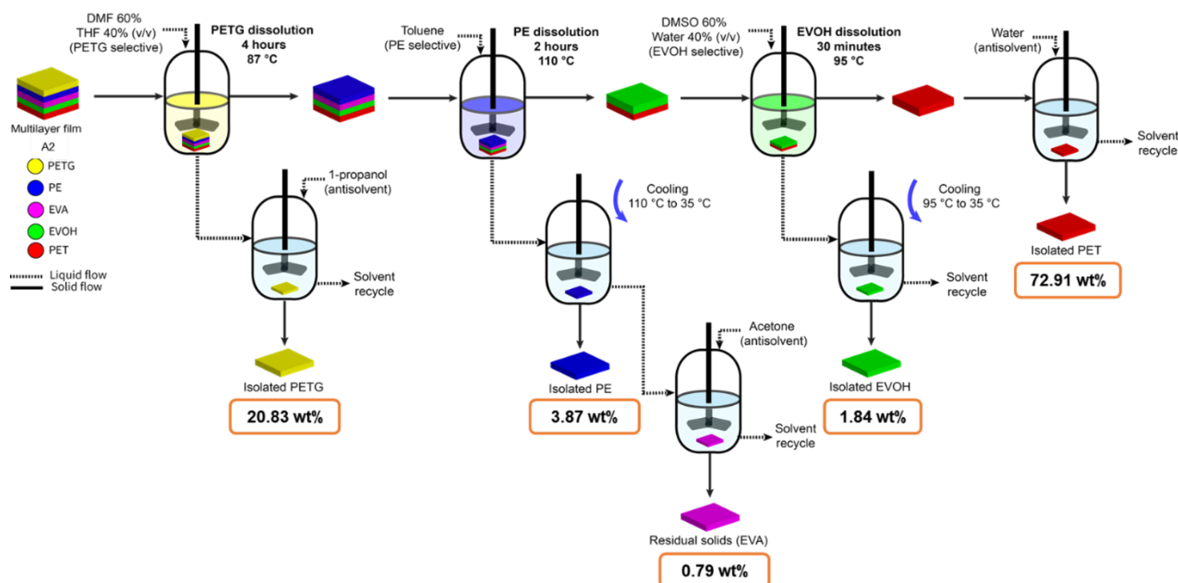


Figure 3.15: STRAP process schematic for the separation and recovery of the polymer components in a multilayer film manufactured by Amcor.

Table 3.10: Recovery of polymers from the multilayer film with the STRAP process.

Experiment	Initial Film Mass (g)	Polymer Recovered from STRAP (wt %)					Overall Mass Balance (%)
		PETG	PE	EVOH	EVA	PET	
1	38.61	21.04%	3.74%	2.05%	0.0031%	73.11%	99.94%
2	38.53	21.00%	3.48%	1.93%	0.99%	73.25%	100.65%
3	38.66	20.44%	4.39%	1.55%	0.59%	72.39%	99.35%
Average	38.60	20.83%	3.87%	1.84%	0.79%	72.91%	99.98%
STDEV	0.07	0.34%	0.47%	0.26%	0.28%	0.46%	0.65%

The FTIR spectra of the PETG, EVOH, EVA and PET recovered using STRAP looked mostly similar to the corresponding virgin resins (Figure 3.16). Some notable differences were observed in the PE spectra, where additional peaks were present at 1740, 1370, 1240, and 1020  $\text{cm}^{-1}$ . These could be due to PETG remnants that were not separated in the first dissolution step. A quantitative measurement would be needed to determine if the PETG amounts in the PE could affect its properties. Dissolution times and solvent amounts could be further adjusted to improve the purity of the PE and remove more of the PETG.

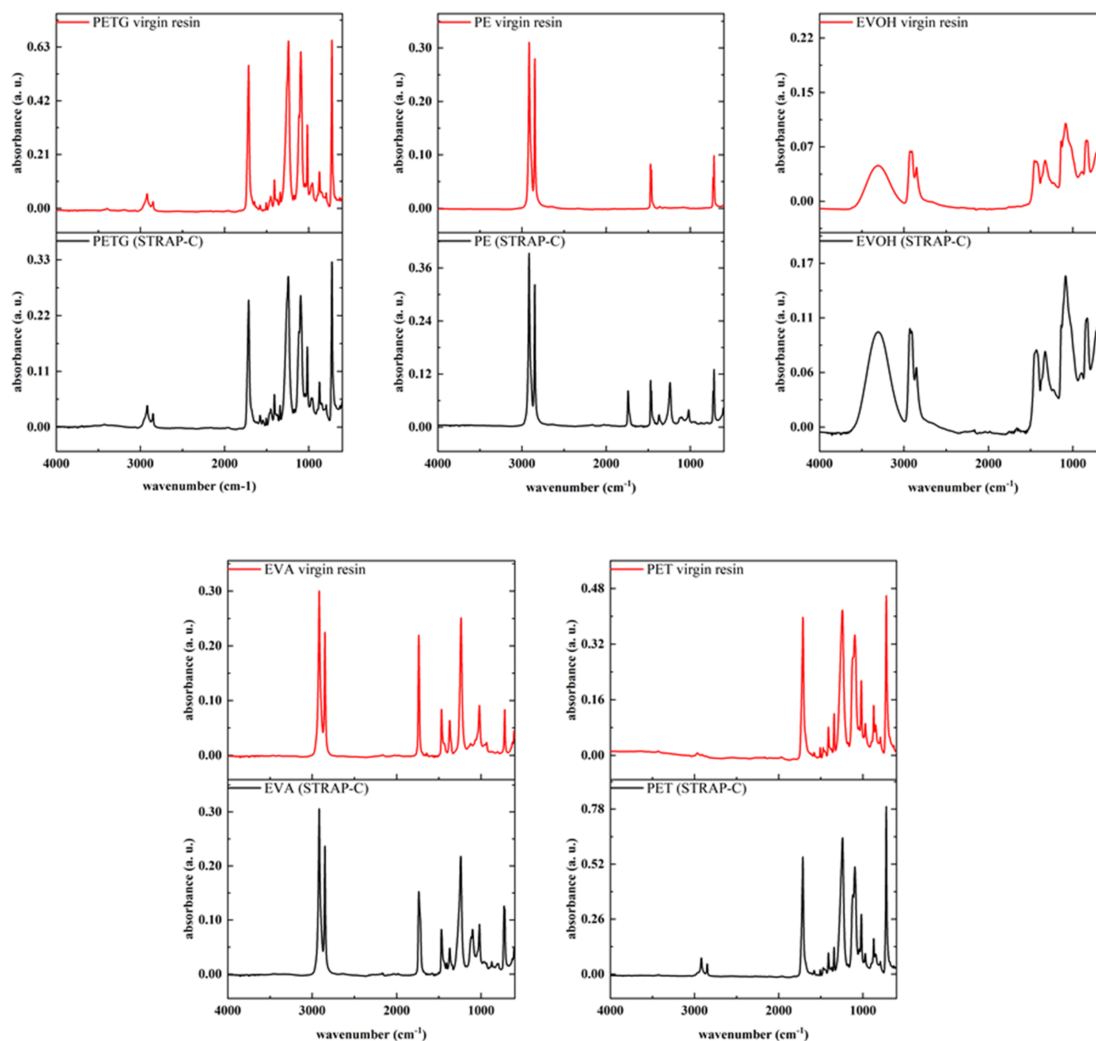


Figure 3.16: ATR-FTIR spectra of the virgin resins and polymers recovered from multilayer film through STRAP process: a) PETG, b) PE, c) EVOH, d) EVA and e) PET.

### 3.3.8 Case study: separation of 10-polymer mixtures

In this section, STRAP was applied to recover different constituent polymeric materials from an unknown post-industrial mixed plastic waste (MPW) stream. Our computational and experimental tools allowed us to develop a series of steps to selectively separate 10 different polymers by selective dissolution, both with physical mixtures of pure polymer pellets and MPW. The polymers considered in this

study were LDPE, HDPE, PS, PVC, EVOH, PET, PP, polyamide 6 (PA6), PA66, and PA66/6. The application of the selected solvents can recover valuable plastic materials from MPW, which can serve as a pretreatment for other recycling technologies or to determine which components are present in majority within the waste.

COSMO-RS calculation results and experimental demonstrations were used to identify potential solvent candidates for selective polymer dissolutions in each step and to determine the separation sequence of the ten polymers. The primary goal of solvent selection in each step was to obtain a higher solubility of the target polymer in the selected solvent than all other polymers, enabling selective dissolution. Table 3.11 summarizes the steps, selected solvents, and the COSMO-RS predicted solubilities of both the target polymer and other polymers for each step.

In general, polymers like PS and PVC can be dissolved at relatively low temperatures in different solvents [40, 58, 59, 60]. For this reason, these two polymers were selected for the first two steps in STRAP with the 10-component physical mixture. For example, toluene, tetrahydrofuran (THF), and styrene have been previously identified as good solvents for PS [35]. Solubility calculations in these solvents show that toluene has excellent selectivity for PS at a low temperature. Therefore, toluene at 35 °C was selected as the solvent for PS, and this dissolution was placed as the first in the separation process. Since only PVC was predicted to have high solubility in THF at its boiling temperature, THF was selected as the solvent for the second step (Table 3.11). Following these first steps, one difficult separation to achieve with dissolution is between polyolefins like PE and PP due to their similar structures. In previous studies, PE and PP have been effectively separated by chromatographic methods and gravity separation and ozonation [45, 46]. Normally, when it comes to separation by dissolution, the same solvents can dissolve both polymers and different temperatures can be used to achieve the desired separation. For example, p-cymene can dissolve both PE and PP at 95 and 120 °C, respectively. Other solvents like toluene, xylene, and THF have been disclosed to be selective for PP, LDPE, and HDPE at different temperatures, ranging from 50 to 160 °C [44]. In our 10-step system, o-xylene was selected for the sequential dissolution of LDPE, HDPE, and PP at different temperatures. According to our solubility predictions, o-xylene can target LDPE, HDPE, and PP at 80, 95, and 115 °C, respectively, in steps 3, 4, and 5 (Table 3.11). After the dissolution steps for the polyolefins, in step 6, EVOH was dissolved in a 60% DMSO-40% water (v/v) mixture, which has been used effectively for STRAP with other materials like



rigid and flexible multilayer packaging films in the recovery of EVOH [61, 29].

Table 3.11: COSMO-RS predicted polymer solubilities for each STRAP step at the specified temperature.

Step	Solvent	T (°C)	Polymers and their solubilities (unit: wt%, bolded values are target polymers)									
			PS	PVC	LDPE	HDPE	PP	EVOH	PA66/6	PET	PA6	PA66
1	toluene	35	<b>5.72</b>	1.12	0.13	0.11	1.74	0.00	0.01	0.01	0.00	0.00
2	THF	67		<b>19.10</b>	2.09	1.45	2.88	1.12	1.33	0.99	0.52	0.26
3	o-xylene	80			<b>3.43</b>	2.17	1.46	0.01	0.14	0.18	0.12	0.03
4	o-xylene	95				<b>5.04</b>	3.42	0.04	0.39	0.53	0.35	0.09
5	o-xylene	115					<b>9.65</b>	0.33	1.29	1.88	1.23	0.33
6	DMSO/water	95						<b>7.67</b>	0.03	0.00	0.01	0.00
7	1,2-PDO	125							<b>3.35</b>	0.05	2.17	0.92
8	GVL	160								<b>12.45</b>	7.71	4.14
9	DMSO	145									<b>8.41</b>	3.56
10	formic acid	90										<b>16.90</b>

Another difficult separation is for the three PAs in the physical mixture: PA6, PA66, and PA66/6. Common solvents that have been used for the dissolution of PAs are DMSO and formic acid, along with diols [42, 43]. To support our solubility predictions, these solvents were tested experimentally to observe potential dissolutions and determine the proper steps to dissolve each PA separately. As seen in Table S1, PA6 was only soluble in DMSO and formic acid, at 145 °C and 60 °C, respectively. PA66 was only soluble in formic acid at 60 °C, and PA 66/6 was soluble in DMSO at 145 °C, 1,2-propanediol (1,2-PDO) at 125 °C, and gamma-valerolactone (GVL) at 160 °C. Based on these observations, the steps needed to achieve selective dissolution of the different PAs in the physical mixture were: PA66/6 dissolution in 1,2-propanediol at 125 °C, PA6 dissolution in DMSO at 145 °C, and PA66 dissolution in formic acid between 60 and 90 °C, according to experiments and solubility predictions. The solubility predictions for these steps indicated preferential dissolution for each PA (Table 3.11). The last polymer in the 10-component physical mixture was PET, for which solvents like GVL, NMP, and DMSO have been used for its dissolution in the

literature [62, 63, 64]. To ensure optimal selectivity, the PET was dissolved before PA6 and PA66, at 160 °C in GVL.

After the solvent selection for each step was completed, the overall procedure was demonstrated with the 10-component physical mixture of pure polymer pellets. Table 3.12 shows the results for the recovery of the polymers after each step in STRAP. Ideally, polymer precipitation should be achieved via a reduction in temperature since this has economic and environmental benefits [61, 65]. However, both PVC and PS required the addition of an antisolvent for their respective precipitation after dissolution. The recovery was 89 wt% or higher for each polymer, confirming the separation of one component per step. This was further confirmed with the FTIR of each recovered fraction, which was for the most part comparable to the pure polymer before STRAP (Figure 3.17). As seen in Figure 3.17(h), the only polymer that presented possible cross contamination after STRAP was PET. Additional peaks were detected after 3000 cm<sup>-1</sup>, one of these pertaining to an N-H stretch at around 3300 cm<sup>-1</sup>, which is characteristic of PA [66]. These peaks indicate contamination of the PET with PA66/6 residue from the previous step, since that polymer is also soluble in GVL at 160 °C. The rest of the recovered polymers showed comparable IR signatures to the corresponding pure polymers.

Table 3.12: STRAP steps for the recovery of 10 common packaging polymers from a physical mixture, with an initial amount of 1 g for each polymer and 30 g of the corresponding solvent.

Step	Polymer	Solvent	T (°C)	Dissolution time (hr)	Antisolvent	Recovery (wt%)
1	PS	Toluene	35	0.5	IPA	89.06%
2	PVC	THF	67	0.5	IPA	93.16%
3	LDPE	O-xylene	80	0.5	None	90.84%
4	HDPE	O-xylene	95	0.5	None	92.30%
5	PP	O-xylene	115	0.5	None	97.61%
6	EVOH	60% DMSO- 40% water (v/v)	95	1	None	90.60%
7	PA66/6	1,2-PDO	125	1	None	99.30%
8	PET	GVL	160	1	None	106.72%**
9	PA6	DMSO	145	1	None	99.13%
10	PA66*	/	/	/	None	97.03%

\*PA66 was recovered as residue from the physical mixture

\*\*Solvent retention

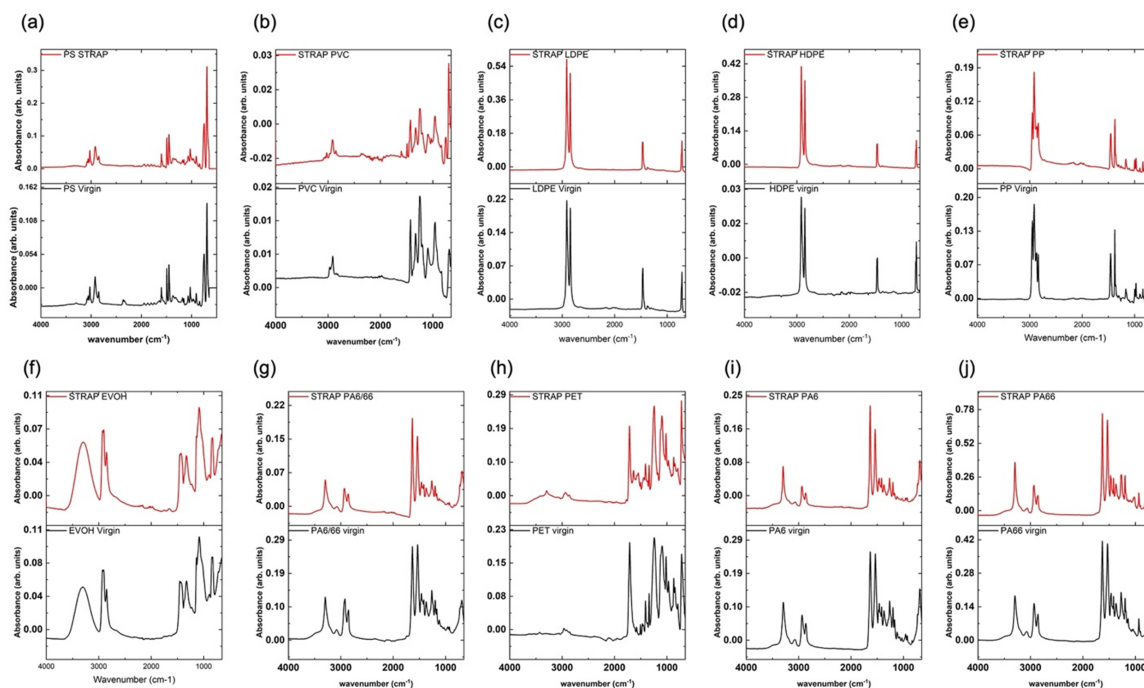


Figure 3.17: IR spectra of the recovered STRAP polymers from the physical mixture (in red) and the virgin polymers (in black): (a) PS, (b) PVC, (c) LDPE, (d) HDPE, (e) PP, (f) EVOH, (g) PA66/6, (h) PET, (i) PA6, and (j) PA66.

The 10 dissolution steps that were developed with the physical mixture targeting PS, PVC, LDPE, HDPE, PP, EVOH, PA66/6, PET, PA6, and PA66, were applied to the post-industrial MPW of interest. For the recovery of PA66, water was used as an antisolvent after its dissolution in formic acid. Figure 3.18 shows the yields of each fraction recovered from the 10 STRAP steps. Majority components were LDPE, HDPE, and PET. The fractions recovered in each STRAP step from the MPW were analyzed with ATR-FTIR to confirm the polymer separations [67].

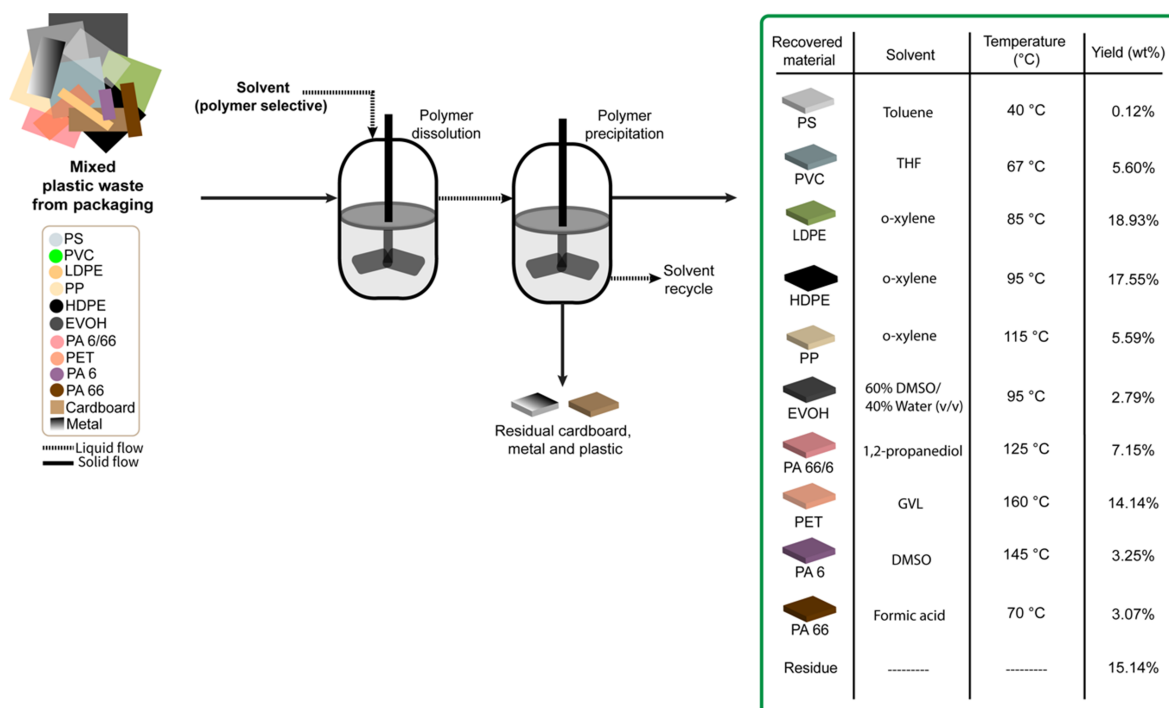


Figure 3.18: Solvent-targeted recovery and precipitation STRAP with post-industrial mixed plastic waste MPW from packaging waste that includes multilayer films.

### 3.3.9 Case study: potential THP applications in plastic dissolution

Tetrahydropyran (THP) is a five-carbon heterocyclic ether that is non-carcinogenic, non-peroxide forming, biodegradable, and economically competitive with tetrahydrofuran (THF) as a solvent, and recent work has reported its synthesis from renewable biomass [17]. In this section, we use our computational tools to identify potential applications of THP as a green alternative solvent in dissolution-based plastic recycling processes.

In previous sections, we used the COSMO-RS model to calculate  $\sigma$ -profiles of over 1000 solvent molecules and for representative polymer conformations; we now use this information to populate the polymer solubility database and to predict polymer solubility in THP and other solvents here. We can also quantify solvent similarity by calculating the Euclidean distance between the  $\sigma$ -profiles of two solvents. We can further perform MD simulations of oligomer molecules in different solvents to support dissolution predictions. The conformations of the oligomer in MD trajectory were used to measure the tendency of the polymer to dissolve in the simulated solvent.

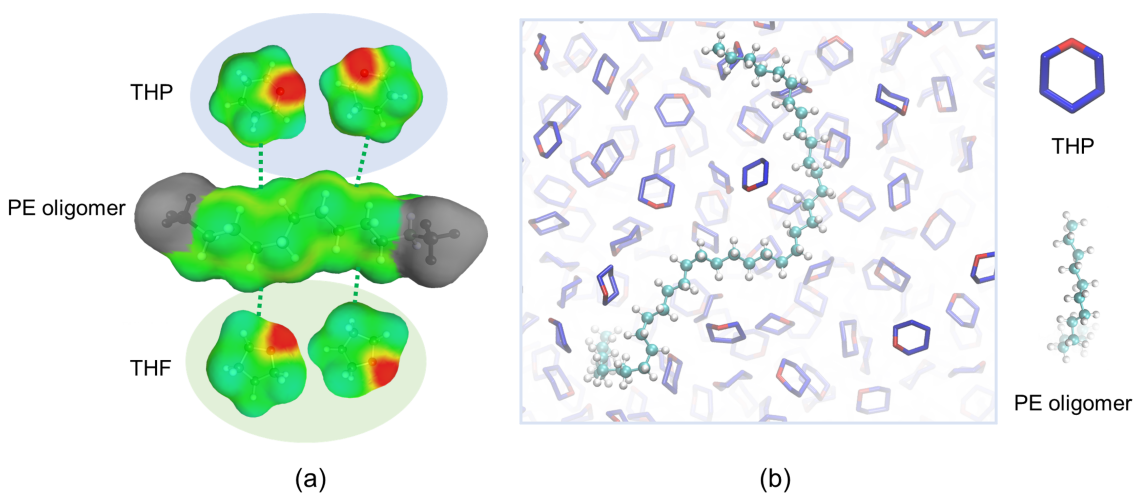


Figure 3.19: Computational methods used in this section. (a) COSMO-RS screening charge distributions (colored surfaces) of THP, THF and a PE oligomer. Short oligomers with end groups neglected (gray surface) are used to represent the chemical properties of longer polymer chains. The intermolecular interactions between polymers and solvents are quantified by the interactions of screening charges, as schematically indicated by dashed lines. (b) MD simulation of a PE oligomer in a dilute THP solution.

To identify potential applications of THP as a solvent, we first analyzed its similarity to other common solvents. Based on the COSMO-RS representation of molecules, the similarity between two molecules can be evaluated by the Euclidean distance between their  $\sigma$ -profiles; this approach thus measures similarity based on the chemical properties of solvents as opposed to their functional groups alone. For example, Figure 3.20 compares the  $\sigma$ -profiles of THP to a similar (THF) and a dissimilar solvent (DCM). THF and THP have highly similar  $\sigma$ -profiles, leading to a small Euclidean distance between these profiles; they are thus considered similar solvents. DCM, however, has a very different profile and is identified as a dissimilar solvent of THP with large distance between  $\sigma$ -profiles. We calculated the Euclidean distances between THP and over 1000 solvents and defined a solvent's similarity score to be its distance to THP normalized by the average distance of all solvents to THP. In this way, we can identify the most THP-like solvents as those with the lowest similarity scores.

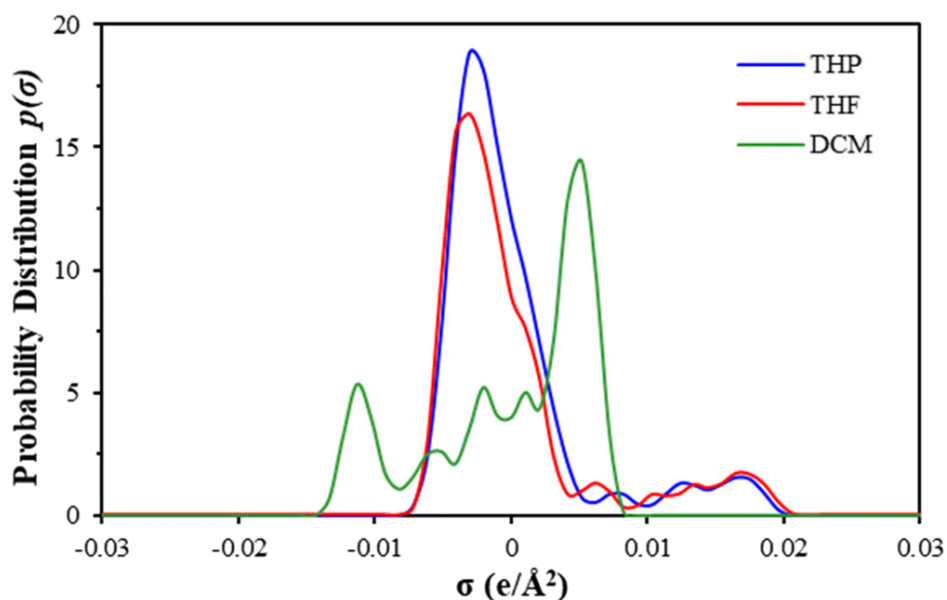


Figure 3.20:  $\sigma$ -profiles of THP, THF and DCM.

Based on the similarity scores, we ranked 1007 solvents by similarity. Table 3.13 shows selected results for the 5 most similar solvents, 3 dissimilar solvents, and 3 common solvents along with their similarity scores and rankings among the whole solvent list. Figure 3.21 shows the chemical structures of the 5 most similar solvents. The similarity of their structures, molecular sizes, and elemental compositions aligns with general chemical intuition for organic compound similarity.

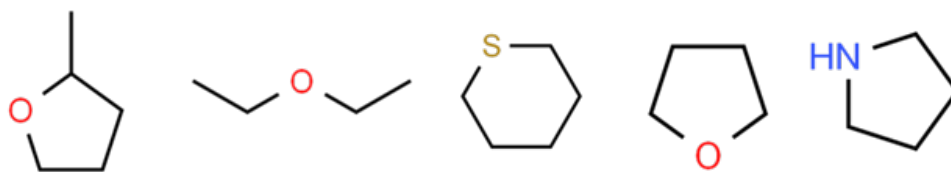


Figure 3.21: Molecular structures of the five solvents most similar to THP.

Table 3.13: Some similar and dissimilar solvents of THP.

Solvent	Similarity score	Similarity ranking	Comment
2-Methyl Tetrahydrofuran	0.14	0.1%	Similar solvents
Diethyl Ether	0.21	0.2%	
Tetrahydrothiapyran	0.24	0.3%	
Tetrahydrofuran (THF)	0.25	0.4%	
Pyrrolidine	0.27	0.5%	
Ethanol	0.66	21.5%	Some common solvents
Toluene	0.87	39.5%	
Phenol	1.10	68.3%	
Dichloromethane (DCM)	1.19	78.8%	Dissimilar solvents
Water	1.27	85.3%	
Eicosane	4.04	99.8%	

To study the applicability of THP as a solvent in dissolution-related polymer processes, we analyzed computationally predicted solubilities of 8 common polymers in THP and its similar solvents. The polymers are ethylene vinyl alcohol (EVOH), polyethylene (PE), polyethylene terephthalate (PET), polypropylene (PP), polystyrene (PS), polyvinyl chloride (PVC), and two polyamides (PA): nylon 6 and nylon 66. Table 3.14 shows the predicted solubilities for these polymers in THP and its 10 most similar solvents. Note that the temperature at which the solubility is predicted is determined by the boiling point of the solvent. Based on the predicted solubilities, THP could serve as a good solvent (defined as a solubility in excess of 3 g/100 g solution) for PE, PP, PS and PVC and as a poor solvent for EVOH, PET, nylon 6 and nylon 66. THP could serve as an alternative to other solvents, especially 2-methyl tetrahydrofuran, THF, and cyclopentyl methyl ether, which have similar predicted solubilities for almost all polymers listed. These values could be used as input parameters in process modeling and techno-economic analyses to study the costs and benefits of using THP as an alternative solvent.



Table 3.14: Predicted solubilities of 8 polymers in THP and its 10 most similar solvents.

Solvent	Similarity score	Temperature of prediction (°C)	Predicted polymer solubility (g/100 g solution)							
			EVOH	PE	PET	PP	PS	PVC	PA 6	PA 66
THP	0.00	87.0	1.1	7.3	0.8	20.9	33.7	17.9	0.7	0.3
2-Methyl Tetrahydrofuran	0.14	77.0	0.5	3.9	0.4	15.1	28.1	14.6	0.4	0.2
Diethyl Ether	0.21	33.5	0.0	0.2	0.0	4.4	10.8	4.0	0.0	0.0
Tetrahydrothiapyran	0.24	120.0	1.3	39.8	5.4	40.3	46.7	26.0	2.5	0.8
Tetrahydrofuran (THF)	0.25	64.0	0.9	1.7	0.8	10.1	31.3	19.1	0.4	0.2
Pyrrolidine	0.27	85.5	19.2	5.7	2.8	15.0	32.2	22.4	2.1	1.2
Dimethyl Ethanolamine	0.27	120.0	17.9	38.5	7.6	37.7	50.3	34.8	6.0	2.9
Methyl Ethyl Ether	0.28	6.4	0.0	0.0	0.0	1.3	9.4	4.2	0.0	0.0
1-Butanol	0.28	116.7	10.1	18.4	0.4	12.4	9.2	10.2	5.4	2.4
Cycloheptanone	0.28	120.0	8.3	30.1	3.9	27.2	41.7	27.9	3.2	1.4
Cyclopentyl Methyl Ether	0.29	105.0	0.9	19.6	0.6	31.3	33.6	14.6	0.8	0.3

Based on the computational solubility predictions, we identified potential applications of THP as selective solvents in dissolution-based polymer recycling processes. We recently developed the solvent-targeted recovery and precipitation (STRAP) process to recycle polymer components from multilayer plastic films [11, 20]. The STRAP process selectively dissolves constituent polymers through a series of solvent washes, each designed to dissolve only a single polymer component. The solubility data in Table 3.14 indicate that THP has potential application as a selective solvent for STRAP processes of many plastic materials. For example, it could be used to selectively dissolve PP from PP/EVOH/PA mixture, which is the composition of an Amcor packaging film [68]; dissolve PS from PS/PET, an UltiDent sealing film [69]; or PVC from PVC/EVOH, a Desu plastic sheet [70]. These proposed applications are based on

commercial products and demonstrate the applicability of THP to possible recycling processes.

THP could also be used to replace hazardous solvents in existing STRAP processes. For example, we recently reported a STRAP process in which toluene is used as a selective solvent to dissolve PE from a PE/EVOH/PET mixture. The predicted solubilities in Table 3.14 indicate that THP should also dissolve PE but not EVOH or PET, and thus could be an alternative selective solvent to toluene. Since the COSMO-RS-predicted solubility of PE in THP is not very large (7.3 g/100 g solution), we performed MD simulations to further support the prediction that THP is a good solvent for PE. A PE oligomer, C<sub>40</sub>H<sub>82</sub>, was simulated in dilute solutions of THP and water, respectively. We calculated the radius of gyration ( $R_g$ ) and the solvent accessible surface area (SASA) of the oligomer molecule from the MD trajectories to evaluate the tendency of the oligomer to collapse into a folded conformation (indicative of poor solvent behavior) or extend into an elongated conformation (indicative of good solvent behavior) [71, 72]. Figure 3.22 shows the oligomer's  $R_g$ -SASA distributions in THP and water. The oligomer molecule in water mostly obtains small values of  $R_g$  and SASA, indicating a preference for folded conformations. In THP, however, the oligomer tends to have large  $R_g$  and SASA, indicating elongated conformations. Since water is a poor solvent for PE, the different behavior of the oligomer chain in THP indicates that it is a good solvent in agreement with COSMO-RS predictions.

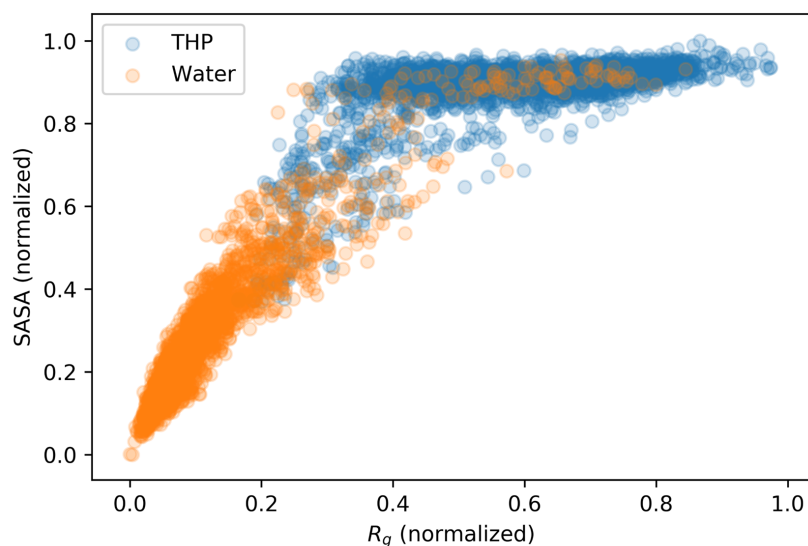


Figure 3.22:  $R_g$ -SASA scatter plot of PE oligomer in THP, water.

### 3.4 Summary

In this work, we established a computational workflow for guiding the design of dissolution-based polymer recycling processes using large-scale, temperature-dependent polymer solubility predictions. Our method integrates MD simulations, conformational sampling, COSMO-RS calculations, as well as experimental calibration. Using MD simulations, we modeled polymers as oligomers in dilute solution and selected representative conformers from the resulting MD trajectories. These conformers, along with an experimentally measured solubility in a reference solvent, were input to COSMO-RS solid-liquid equilibrium calculations to predict polymer solubilities in numerous solvents. We established a solubility database for 11 polymers and 1007 solvents at multiple temperatures and experimentally verified computational predictions for a selected subset of systems. Based on the database, we studied the relationship between polymers and their top solvents via functional group analysis of solvent molecular structures. We further developed a computational tool to automatically select suitable solvents for sequential selective dissolution-based plastic recycling processes (like the STRAP process) while evaluating all possible separation sequences. We demonstrated the applicability of the method using multiple experimental case studies in which physical mixtures and multilayer films of polymers were successfully separated via sequential selective dissolution. This computational approach thus has promise for guiding the design of STRAP processes for multicomponent plastic waste, and could further be used to optimize existing STRAP processes by selecting alternative solvents (*e.g.*, green solvents).

While the approach in this work was demonstrated for sequential selective dissolution processes in which only one polymer was dissolved at each step, future work will continue to develop a combinatorial optimization model that allows for the dissolution of multiple polymers at a time in order to search for the best separation sequence of a STRAP process. The model will also account for factors such as the densities of solvents and the percentage of each polymer in the waste stream when considering challenges that may be faced while scaling up dissolution-based processes. We will further combine these models with technoeconomic analysis and life-cycle assessment tools to evaluate the comprehensive impact of solvents and identify tradeoffs between possible separation sequences. Finally, we envision further expanding the database to consider new classes of green or designer solvents with potential value in polymer dissolution, such as ionic liquids or deep eutectic solvents

[73, 74].

### 3.5 References

- [1] Trevor Letcher. *Plastic waste and recycling: Environmental impact, societal issues, prevention, and solutions*. Academic Press, 2020.
- [2] United Nations Environment Programme. From pollution to solution: A global assessment of marine litter and plastic pollution. 2021.
- [3] Jeannette M Garcia and Megan L Robertson. The future of plastics recycling. *Science*, 358(6365):870–872, 2017.
- [4] Oksana Horodytska, Francisco Javier Valdés, and Andres Fullana. Plastic flexible films waste management—a state of art review. *Waste management*, 77:413–425, 2018.
- [5] Coralie Jehanno, Jill W Alty, Martijn Roosen, Steven De Meester, Andrew P Dove, Eugene Y-X Chen, Frank A Leibfarth, and Haritz Sardon. Critical advances and future opportunities in upcycling commodity polymers. *Nature*, 603(7903):803–814, 2022.
- [6] Delilah Lithner, Åke Larsson, and Göran Dave. Environmental and health hazard ranking and assessment of plastic polymers based on chemical composition. *Science of the total environment*, 409(18):3309–3324, 2011.
- [7] Jin Kuk Kim, Sabu Thomas, and Prosenjit Saha. Multicomponent polymeric materials, 2016.
- [8] Liesl K Massey. *Permeability properties of plastics and elastomers: a guide to packaging and barrier materials*. Cambridge University Press, 2003.
- [9] Camila Távora de Mello Soares, Monica Ek, Emma Östmark, Mikael Gällstedt, and Sigbritt Karlsson. Recycling of multi-material multilayer plastic packaging: Current trends and future scenarios. *Resources, conservation and recycling*, 176:105905, 2022.

- [10] Anja Mieth, Eddo Hoekstra, and Catherine Simoneau. Guidance for the identification of polymers in multilayer films used in food contact materials. *European Commission JRC Technical reports*, 2016.
- [11] Theodore W Walker, Nathan Frelka, Zhizhang Shen, Alex K Chew, Jesse Banick, Steven Grey, Min Soo Kim, James A Dumesic, Reid C Van Lehn, and George W Huber. Recycling of multilayer plastic packaging materials by solvent-targeted recovery and precipitation. *Science advances*, 6(47):eaba7599, 2020.
- [12] U.S. Environmental Protection Agency. Plastics: Material-specific data, 2021.
- [13] Houqian Li, Horacio A Aguirre-Villegas, Robert D Allen, Xianglan Bai, Craig H Benson, Gregg T Beckham, Sabrina L Bradshaw, Jessica L Brown, Robert C Brown, Victor S Cecon, et al. Expanding plastics recycling technologies: chemical aspects, technology status and challenges. *Green Chemistry*, 24(23):8899–9002, 2022.
- [14] Stijn Billiet and Scott R Trenor. 100th anniversary of macromolecular science viewpoint: Needs for plastics packaging circularity. *ACS macro letters*, 9(9):1376–1390, 2020.
- [15] JG Poulakis and CD Papaspyrides. The dissolution/reprecipitation technique applied on high-density polyethylene: I. model recycling experiments. *Advances in Polymer Technology: Journal of the Polymer Processing Institute*, 14(3):237–242, 1995.
- [16] Dominik Triebert, Hagen Hanel, Marlen Bundt, and Klaus Wohnig. Solvent-based recycling. In *Circular Economy of Polymers: Topics in Recycling Technologies*, pages 33–59. American Chemical Society, 2021.
- [17] Raka G Dastidar, Min Soo Kim, Panzheng Zhou, Zaneta Luo, Changxia Shi, Kevin J Barnett, Daniel J McClelland, Eugene Y-X Chen, Reid C Van Lehn, and George W Huber. Catalytic production of tetrahydropyran (thp): a biomass-derived, economically competitive solvent with demonstrated use in plastic dissolution. *Green Chemistry*, 24(23):9101–9113, 2022.
- [18] Aurora del Carmen Munguía-López, Dilara Göreke, Kevin L Sánchez-Rivera, Horacio A Aguirre-Villegas, Styliani Avraamidou, George W Huber, and Victor M

- Zavala. Quantifying the environmental benefits of a solvent-based separation process for multilayer plastic films. *Green Chemistry*, 25(4):1611–1625, 2023.
- [19] Sibel Ügdüler, Kevin M Van Geem, Martijn Roosen, Elisabeth IP Delbeke, and Steven De Meester. Challenges and opportunities of solvent-based additive extraction methods for plastic recycling. *Waste management*, 104:148–182, 2020.
- [20] Kevin L Sánchez-Rivera, Panzheng Zhou, Min Soo Kim, Leonardo D González Chávez, Steve Grey, Kevin Nelson, Shao-Chun Wang, Ive Hermans, Victor M Zavala, Reid C Van Lehn, et al. Reducing antisolvent use in the strap process by enabling a temperature-controlled polymer dissolution and precipitation for the recycling of multilayer plastic films. *ChemSusChem*, 14(19):4317–4329, 2021.
- [21] Kevin L Sánchez-Rivera, Aurora del Carmen Munguía-López, Panzheng Zhou, Victor S Cecon, Jiuling Yu, Kevin Nelson, Daniel Miller, Steve Grey, Zhuo Xu, Ezra Bar-Ziv, et al. Recycling of a post-industrial printed multilayer plastic film containing polyurethane inks by solvent-targeted recovery and precipitation. *Resources, Conservation and Recycling*, 197:107086, 2023.
- [22] Daniel R Bloch. Solvents and non solvents for polymers. *The Wiley Database of Polymer Properties*, 2003.
- [23] Yi-Bo Zhao, Xu-Dong Lv, and Hong-Gang Ni. Solvent-based separation and recycling of waste plastics: A review. *Chemosphere*, 209:707–720, 2018.
- [24] Joel H Hildebrand. Factors determining solubility among non-electrolytes. *Proceedings of the National Academy of Sciences*, 36(1):7–15, 1950.
- [25] Charles M Hansen. *Hansen solubility parameters: a user's handbook*. CRC press, 2007.
- [26] Robert W Taft, Jose-Luis M Abboud, Mortimer J Kamlet, and Michael H Abraham. Linear solvation energy relations. *Journal of Solution Chemistry*, 14(3):153–186, 1985.
- [27] V Gutmann. Empirical parameters for donor and acceptor properties of solvents. *Electrochimica Acta*, 21(9):661–670, 1976.

- [28] C Gardner Swain, Marguerite S Swain, Arnet L Powell, and Sergio Alunni. Solvent effects on chemical reactivity. evaluation of anion-and cation-solvation components. *Journal of the American Chemical Society*, 105(3):502–513, 1983.
- [29] Steven Abbott and Charles M Hansen. *Hansen solubility parameters in practice*. Hansen-Solubility, 2008.
- [30] Anand Chandrasekaran, Chiho Kim, Shruti Venkatram, and Rampi Ramprasad. A deep learning solvent-selection paradigm powered by a massive solvent/non-solvent database for polymers. *Macromolecules*, 53(12):4764–4769, 2020.
- [31] Panzheng Zhou, Kevin L Sánchez-Rivera, George W Huber, and Reid C Van Lehn. Computational approach for rapidly predicting temperature-dependent polymer solubilities using molecular-scale models. *ChemSusChem*, 14(19):4307–4316, 2021.
- [32] Fergal P Byrne, Saimeng Jin, Giulia Paggiola, Tabitha HM Petchey, James H Clark, Thomas J Farmer, Andrew J Hunt, C Robert McElroy, and James Sherwood. Tools and techniques for solvent selection: green solvent selection guides. *Sustainable Chemical Processes*, 4:1–24, 2016.
- [33] Warren D Seider, Daniel R Lewin, JD Seader, Soemantri Widagdo, Rafiqul Gani, and Ka Ming Ng. *Product and process design principles: synthesis, analysis and evaluation*. John Wiley & Sons, 2016.
- [34] Mark James Abraham, Teemu Murtola, Roland Schulz, Szilárd Páll, Jeremy C Smith, Berk Hess, and Erik Lindahl. Gromacs: High performance molecular simulations through multi-level parallelism from laptops to supercomputers. *SoftwareX*, 1:19–25, 2015.
- [35] Junmei Wang, Wei Wang, Peter A Kollman, and David A Case. Automatic atom type and bond type perception in molecular mechanical calculations. *Journal of molecular graphics and modelling*, 25(2):247–260, 2006.
- [36] Junmei Wang, Romain M Wolf, James W Caldwell, Peter A Kollman, and David A Case. Development and testing of a general amber force field. *Journal of computational chemistry*, 25(9):1157–1174, 2004.

- [37] Jianping Li, Christos T Maravelias, and Reid C Van Lehn. Adaptive conformer sampling for property prediction using the conductor-like screening model for real solvents. *Industrial & Engineering Chemistry Research*, 61(25):9025–9036, 2022.
- [38] MJ Frisch, GW Trucks, HB Schlegel, GE Scuseria, MA Robb, JR Cheeseman, G Scalmani, VPGA Barone, GA Petersson, HJRA Nakatsuji, et al. Gaussian 16 revision c. 01, 2016. *Gaussian Inc. Wallingford CT*, 1:572, 2016.
- [39] Andreas Klamt. Conductor-like screening model for real solvents: a new approach to the quantitative calculation of solvation phenomena. *The Journal of Physical Chemistry*, 99(7):2224–2235, 1995.
- [40] Andreas Klamt, Volker Jonas, Thorsten Bürger, and John CW Lohrenz. Refinement and parametrization of cosmo-rs. *The Journal of Physical Chemistry A*, 102(26):5074–5085, 1998.
- [41] Jens Kahlen, Kai Masuch, and Kai Leonhard. Modelling cellulose solubilities in ionic liquids using cosmo-rs. *Green Chemistry*, 12(12):2172–2181, 2010.
- [42] F Eckert. Cosmotherm reference manual, release 19. 2019.
- [43] Bernhard Wunderlich. *Thermal analysis*. Elsevier, 2012.
- [44] Phomma Warangkhan, Magaraphan Rathanawan, et al. Preparation and characterization of reactive blends of poly (lactic acid), poly (ethylene-co-vinyl alcohol), and poly (ethylene-co-glycidyl methacrylate). In *AIP Conference Proceedings*, volume 1664. AIP Publishing, 2015.
- [45] Frank Eckert and Andreas Klamt. Fast solvent screening via quantum chemistry: Cosmo-rs approach. *AIChE Journal*, 48(2):369–385, 2002.
- [46] Andreas Klamt, Frank Eckert, Martin Hornig, Michael E Beck, and Thorsten Bürger. Prediction of aqueous solubility of drugs and pesticides with cosmo-rs. *Journal of computational chemistry*, 23(2):275–281, 2002.
- [47] Victor S Cecon, Greg W Curtzwiler, and Keith L Vorst. A study on recycled polymers recovered from multilayer plastic packaging films by solvent-targeted recovery and precipitation (strap). *Macromolecular Materials and Engineering*, 307(11):2200346, 2022.



- [48] Jian Sun, Dajiang Liu, Robert P Young, Alejandro G Cruz, Nancy G Isern, Timo Schuerg, John R Cort, Blake A Simmons, and Seema Singh. Solubilization and upgrading of high polyethylene terephthalate loadings in a low-costing bifunctional ionic liquid. *ChemSusChem*, 11(4):781–792, 2018.
- [49] David Weininger. Smiles, a chemical language and information system. 1. introduction to methodology and encoding rules. *Journal of chemical information and computer sciences*, 28(1):31–36, 1988.
- [50] Inc. Daylight Chemical Information Systems. Smarts-a language for describing molecular patterns, 2007.
- [51] Greg Landrum. Rdkit: Open-source cheminformatics. 2006. *Google Scholar*, 2006.
- [52] Desu Technology. Laminated plastic sheet ps-pe, 2022.
- [53] Marieke T Brouwer, Fresia Alvarado Chacon, and Eggo Ulphard Thoden van Velzen. Effect of recycled content and rpet quality on the properties of pet bottles, part iii: Modelling of repetitive recycling. *Packaging Technology and Science*, 33(9):373–383, 2020.
- [54] ASG Recycling. Pvc in pet bottle recycling, 2022.
- [55] ROL. Pet evoh pp, 2022.
- [56] Rosa Miranda, H Pakdel, Christian Roy, and C Vasile. Vacuum pyrolysis of commingled plastics containing pvc ii. product analysis. *Polymer degradation and stability*, 73(1):47–67, 2001.
- [57] Ian C McNeill, Livia Memetea, and William J Cole. A study of the products of pvc thermal degradation. *Polymer Degradation and Stability*, 49(1):181–191, 1995.
- [58] Tingting Chen, Jun Zhang, and Hongjun You. Photodegradation behavior and mechanism of poly (ethylene glycol-co-1, 4-cyclohexanedimethanol terephthalate)(petg) random copolymers: correlation with copolymer composition. *RSC advances*, 6(104):102778–102790, 2016.
- [59] Dongda Zhang, Ehecatl Antonio del Rio-Chanona, and Nilay Shah. Life cycle assessment of bio-based sustainable polylimonene carbonate production processes. In *Computer Aided Chemical Engineering*, volume 44, pages 1693–1698. Elsevier, 2018.

- [60] Plastics Technology. Commodity resin prices rise, but pp falls, 2021.
- [61] EB Nauman and JC Lynch. Polymer recycling by selective dissolution. *Patent Number* US 5278282, 1994.
- [62] George S Weeden Jr, Nicholas H Soepriatna, and Nien-Hwa Linda Wang. Method for efficient recovery of high-purity polycarbonates from electronic waste. *Environmental Science & Technology*, 49(4):2425–2433, 2015.
- [63] Sunghoon Kim, Minsoo Kim, Yong Tae Kim, Geunjae Kwak, and Jiyong Kim. Techno-economic evaluation of the integrated polygeneration system of methanol, power and heat production from coke oven gas. *Energy Conversion and Management*, 182:240–250, 2019.
- [64] David CC Habgood, Andrew FA Hoadley, and Lian Zhang. Techno-economic analysis of gasification routes for ammonia production from victorian brown coal. *Chemical Engineering Research and Design*, 102:57–68, 2015.
- [65] Gavin Towler and Ray Sinnott. *Chemical engineering design: principles, practice and economics of plant and process design*. Butterworth-Heinemann, 2021.
- [66] Abhijit Dutta, AH Sahir, Eric Tan, David Humbird, Lesley J Snowden-Swan, Pimphan A Meyer, Jeff Ross, Danielle Sexton, Raymond Yap, and John Lukas. Process design and economics for the conversion of lignocellulosic biomass to hydrocarbon fuels: Thermochemical research pathways with in situ and ex situ upgrading of fast pyrolysis vapors. Technical report, Pacific Northwest National Lab.(PNNL), Richland, WA (United States), 2015.
- [67] Kevin L Sánchez-Rivera, Panzheng Zhou, Elizaveta Radkevich, Anisha Sharma, Ezra Bar-Ziv, Reid C Van Lehn, and George W Huber. A solvent-targeted recovery and precipitation scheme for the recycling of up to ten polymers from post-industrial mixed plastic waste. *Waste Management*, 194:290–297, 2025.
- [68] Amcor. Duplex pp evoh laminates for steam sterilization, 2020.
- [69] UltiDent Scientific. Plateseal™ elisa film, 2022.
- [70] Desu Tech. Pvc-evoh-pvc, 2022.

- [71] Pierre-Gilles De Gennes. Collapse of a polymer chain in poor solvents. *Journal de Physique Lettres*, 36(3):55–57, 1975.
- [72] Michael Rubinstein and Ralph H Colby. *Polymer physics*. Oxford university press, 2003.
- [73] Zeynep Sumer and Reid C Van Lehn. Data-centric development of lignin structure–solubility relationships in deep eutectic solvents using molecular simulations. *ACS Sustainable Chemistry & Engineering*, 10(31):10144–10156, 2022.
- [74] Mood Mohan, Jay D Keasling, Blake A Simmons, and Seema Singh. In silico cosmo-rs predictive screening of ionic liquids for the dissolution of plastic. *Green Chemistry*, 24(10):4140–4152, 2022.

## Chapter 4

# Integrated optimization framework for the design of dissolution-based plastic recycling processes

In this chapter, we present an integrated computation framework that can guide the design and optimization of dissolution-based plastic recycling processes. This framework aims to provide suggestions on the polymer separation sequence and solvent selection given a set of polymer components of a waste stream. We will incorporate the polymer solubility database, solvent screening tool, process simulations models, techno-economic analysis, and life-cycle assessment to solve multiple research challenges of process design and optimization. It will not only provide suggestions on the process design that recycle plastic products, but also offers insights on the manufacturing of easy-to-recycle plastics.

---

This chapter is based on the following publications

1. Ikegwu, U. M., Zhou, P., Van Lehn, R. C., Zavala, V. M., & del Carmen Munguía-López, A. (2025). A Fast Computational Framework for the Design of Solvent-Based Plastic Recycling Processes. Available at ChemRxiv.
2. Zhou, P., Yu, J., Sánchez-Rivera, K. L., Huber, G. W., & Van Lehn, R. C. (2023). Large-scale computational polymer solubility predictions and applications to dissolution-based plastic recycling. *Green Chemistry*, 25(11), 4402-4414.

## 4.1 Introduction

High plastic waste generation and low recycling rates are challenging problems that need to be addressed to mitigate the ongoing plastic waste crisis [1]. One of the main obstacles hindering plastic recycling is that several common plastic materials, such as multicomponent plastics, cannot be processed and repurposed via mechanical recycling [2, 3]. These materials are broadly used in packaging applications, such as food and healthcare [4]. The packaging sector comprises nearly 40% of all plastic produced worldwide, and projections suggest that this share could increase in the future [5]. Proposed alternatives to address the plastic waste crisis include i) developing new and scalable technologies to process difficult-to-recycle plastics and ii) developing new plastics that are compostable or easier to recycle (by design) [6].

Solvent-based technologies are a promising approach for processing multicomponent plastic waste (e.g., mixed post-consumer waste and multilayer film waste) because they can recover/separate their constituent components (e.g., polymers, ink, additives, or other contaminants) [7, 8, 9, 10]. This method allows for the recycling of multilayer films, widely used in food packaging [11, 12]. These films, composed of several layers of different polymers, were pioneered by Howard and Lineburg in 1963 to replace other packaging materials economically and efficiently [13]. The design combined distinct polymer layers to leverage their unique properties to protect food from diverse external factors such as oxygen, water, temperature, and light. Multilayer films revolutionized food packaging by significantly extending shelf life (key for mitigating food waste). Modern multilayer films are highly sophisticated, with a number of layers and polymers tailored to different applications (e.g., fresh meat, frozen food, cheese, coffee, and tea) [14]. Multilayer films with several hundred individual layers are common [12]. Several solvent-based technologies for recycling multicomponent plastics have been investigated in industry and academia [15, 16, 17, 18, 19, 20]. The fundamental principles behind most of these processes are similar, but they differ in the types of feedstocks, products, process conditions, stage of development, and economic and environmental performance [7, 8, 9, 10, 21, 22, 23].

This work focuses on a solvent-based approach known as the Solvent-Targeted Recovery and Precipitation (STRAP) process. The STRAP process uses sequential solvent washes to selectively dissolve and separate different components of multilayer plastic films [11, 18, 7, 24]. The solvents used need to be selected appropriately to dis-

solve only a target component in each step. Therefore, the selected solvent must have a high solubility for the target component and a low solubility for the other components of the film [25, 26]. Identifying appropriate solvents and operating conditions (e.g., temperatures) to dissolve only the target component without dissolving the other components is a non-trivial task. For the STRAP process, molecular-scale thermodynamic models have been employed to predict temperature-dependent polymer solubilities. As part of these efforts, we recently reported a computational workflow that performs large-scale temperature-dependent polymer solubility predictions [26]. This approach also reports a computational solubility database for eight common polymers and more than a thousand solvents at multiple temperatures. To validate such predictions, they measured selected solubilities experimentally. The database has enabled the creation of a computational tool that automates solvent selections for solvent-based processes.

Recycling processes for multicomponent plastics are difficult to design because the number of constituent polymers and contaminants strongly influences their configuration and operating conditions (e.g., solvent types, separation sequence, and dissolution temperatures). Previous process models for solvent-based methods have been reported for specific types of multicomponent plastics. For instance, designs have been reported for a multilayer film composed of four polymers [11], a multilayer film made of three polymers and ink [7], and polypropylene facemasks [8]. These approaches have also conducted economic and environmental analyses of the processes to demonstrate that solvent-based technologies are competitive to virgin resin production. While these efforts have helped estimate the economic and environmental feasibility of processes using specific waste feedstocks and identify process design bottlenecks, they have also revealed a need for general frameworks that can target different types of multilayer films and inform their design. Recent work has also highlighted the importance of considering economic and environmental impacts when selecting solvents for different polymers in solvent-based processes [26, 27]. They also demonstrated that experimentally selecting solvents and operating temperatures is challenging due to the wide range of possibilities originating from the large number of polymer components and available solvent space. Additionally, if the process is designed only considering solubility constraints, it could be economically and environmentally infeasible [22].

There is a need to develop computational design frameworks to quickly evaluate

different separation process designs (including varying separation sequences, solvents, and process conditions). A given process design may include the separation sequence or order (which component is dissolved first), the solvents that enable this sequence, and the required process conditions, such as temperatures. Such insights can also help improve product design by identifying those polymers or components that lead to higher recycling costs and environmental impacts. Packaging designs often only consider economics and desirable properties (e.g., oxygen, water, and temperature barriers). However, the current plastic pollution crisis demands the recyclability of all plastic packaging to be considered in the product design directly [6].

In this work, we present a fast computational framework that integrates molecular-scale models, process modeling, techno-economic analysis (TEA), and life cycle assessment (LCA) to identify sustainable configurations for solvent-based processes. The framework helps estimate the economic and environmental impacts of diverse process design scenarios, including different separation sequences, solvents, and process operating conditions. We also provide guidelines for product design by identifying multilayer film designs that are easier to recycle or have a lower recycling impact. The computational framework developed in this work is general and can be used for complex multilayer films or multicomponent plastic waste streams.

## 4.2 Methods

### 4.2.1 STRAP process description and assumptions

The STRAP process uses selective dissolution and precipitation to recover the constituent components of multilayer films [11, 7, 24]. Figure 4.1 presents a simplified schematic representation of the process considering a multilayer film with three components (in this case, each component represents only one polymer). Here, we can see that the recovery of each component involves a binary separation. That is, the recovery of the first polymer (denoted by  $P_1$  and depicted in yellow) is done by separating this component (via dissolution and precipitation) from the other components. In the same manner, the recovery of the second polymer (denoted by  $P_2$  and depicted in orange) is done by separating this component from the third polymer (denoted by  $P_3$  and depicted in blue). As mentioned previously, this is a simplified representation since common multilayer materials often have more than three components, and the

STRAP process involves many more steps than the ones shown in Figure 4.1. We also note that, even if polymer  $P_1$  was targeted in the first binary separation step, we could also seek to target more than one polymer at a time (e.g., targeting both  $P_1$  and  $P_2$  leaving  $P_3$  undissolved).

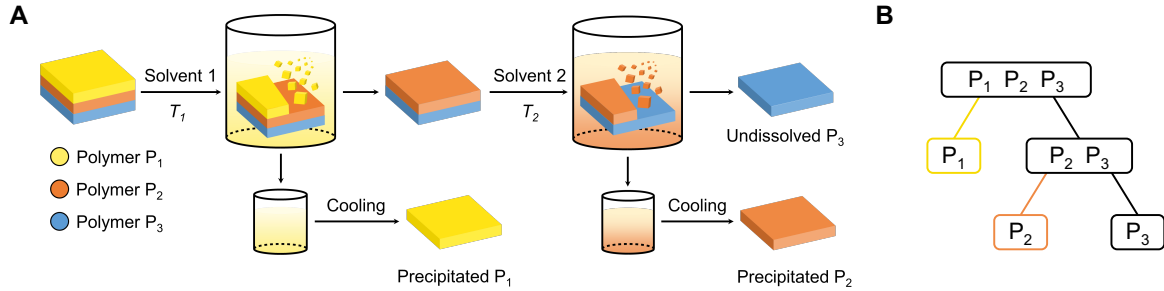


Figure 4.1: Schematic representation of the STRAP process. (A) Simplified representation of the process considering a multilayer film with three components (in this case, each component represents only one polymer). (B) Separation process represented as a binary tree.

Figure 4.2 presents the detailed process flow diagram for each binary separation. Here, we refer to each binary separation as a separation module and present the same example of a three-component material for a given sequence. In this example, each component comprises one polymer, and a couple of separation modules are required to recover all the polymers.

The process steps for each separation module are as follows. The three-component multilayer film (represented as  $P_1, P_2, P_3$ ), initially at temperature  $T_1$  (typically room temperature), is heated to  $T_2$  and mixed with a previously chosen solvent (that selectively dissolves only the target polymer, denoted as  $P_1$ ). The elevated temperature,  $T_2$ , is selected based on the predicted temperature that can dissolve only the target polymer with the chosen solvent [26]. Next, the solution is filtered to separate the undissolved solids (denoted as  $P_2$  and  $P_3$ ). Finally, the target polymer  $P_1$  is precipitated by cooling to the temperature  $T_3$  (typically room temperature), filtered, and recovered. Most of the solvent is also recovered and recycled. The solvent is recovered via filtration (Filter 2) and via a condenser that receives the vapor phase of the dryers. The process is repeated as many times as necessary to separate the remaining components (polymers  $P_2$  and  $P_3$ ), with the choice of solvent and operating temperatures potentially changing for each distinct component. From Figure 4.2, we can see that



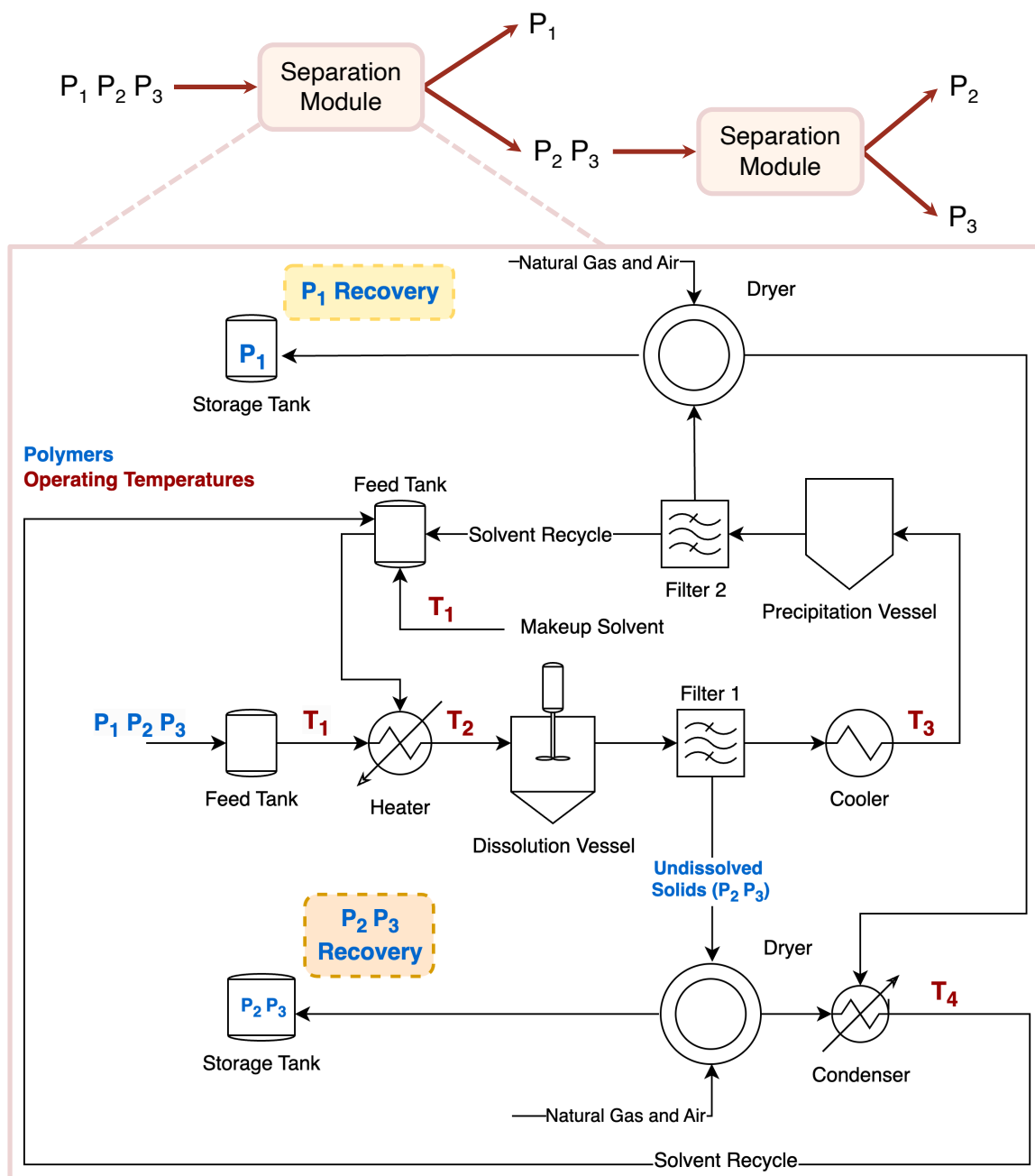


Figure 4.2: Simplified process flow diagram of the STRAP process for one separation module.

separating an  $n$ -component multilayer film requires  $n-1$  separation modules. Hence, for this example, we require two separation modules.

The separation module in Figure 4.2 only considers temperature-controlled precipitation (also known as the cooling method) to recover the target polymer from the solution. This step is usually achieved by reducing the temperature of the polymer solution to room temperature, where the dissolved target polymer becomes insoluble in the solvent. This method is economically and environmentally feasible and can be used for several polymer-solvent combinations [11, 7, 3]. Previous studies have also considered alternative precipitation techniques to recover the target polymer [18]. Another method involves the addition of antisolvent. However, this method leads to higher energy requirements because a distillation unit is needed to separate the resulting mixture of solvents (composed of the solvent used for dissolution and the antisolvent used for precipitation). Furthermore, antisolvent addition requires more solvents because recycling rates are lower [22]. Evaporating the solvent directly from the polymer solution can also be used as an alternative process configuration to separate the target component. A disadvantage of this method is that its environmental impact is higher than the impact of temperature-controlled precipitation [9]. Therefore, it is critical to identify polymer-solvent combinations that allow precipitation via a temperature-controlled process at ambient pressure. Previous studies have concluded that a high solvent recycling rate is needed to ensure the economic and environmental viability of solvent-based processes [28, 29, 30]. Specifically, process costs and overall climate change impacts decrease with solvent recycling rates [31, 7]. Moreover, it has been found that temperature-controlled precipitation can help achieve high recycling rates ( $>90\%$ ) compared to antisolvent-based precipitation [8, 22]. As such, in this work, we only consider solvents that can enable temperature-controlled precipitation and recycling rates higher than  $>95\%$ , which is the lowest reported rate that allows for economic and environmental benefits [7].

#### 4.2.2 Computational framework

We propose a computational framework that integrates molecular-scale models, process modeling, TEA, and LCA to provide fast economic and environmental analyses of different STRAP process design configurations and help identify sustainable designs. The process designs include assessing different separation sequences, solvents for every separation step, and process conditions (e.g., operating temperatures, recycling

rate of solvents, and solid/liquid ratios). The computational framework follows a series of steps, summarized in Figure 4.3 and described in the following subsections.

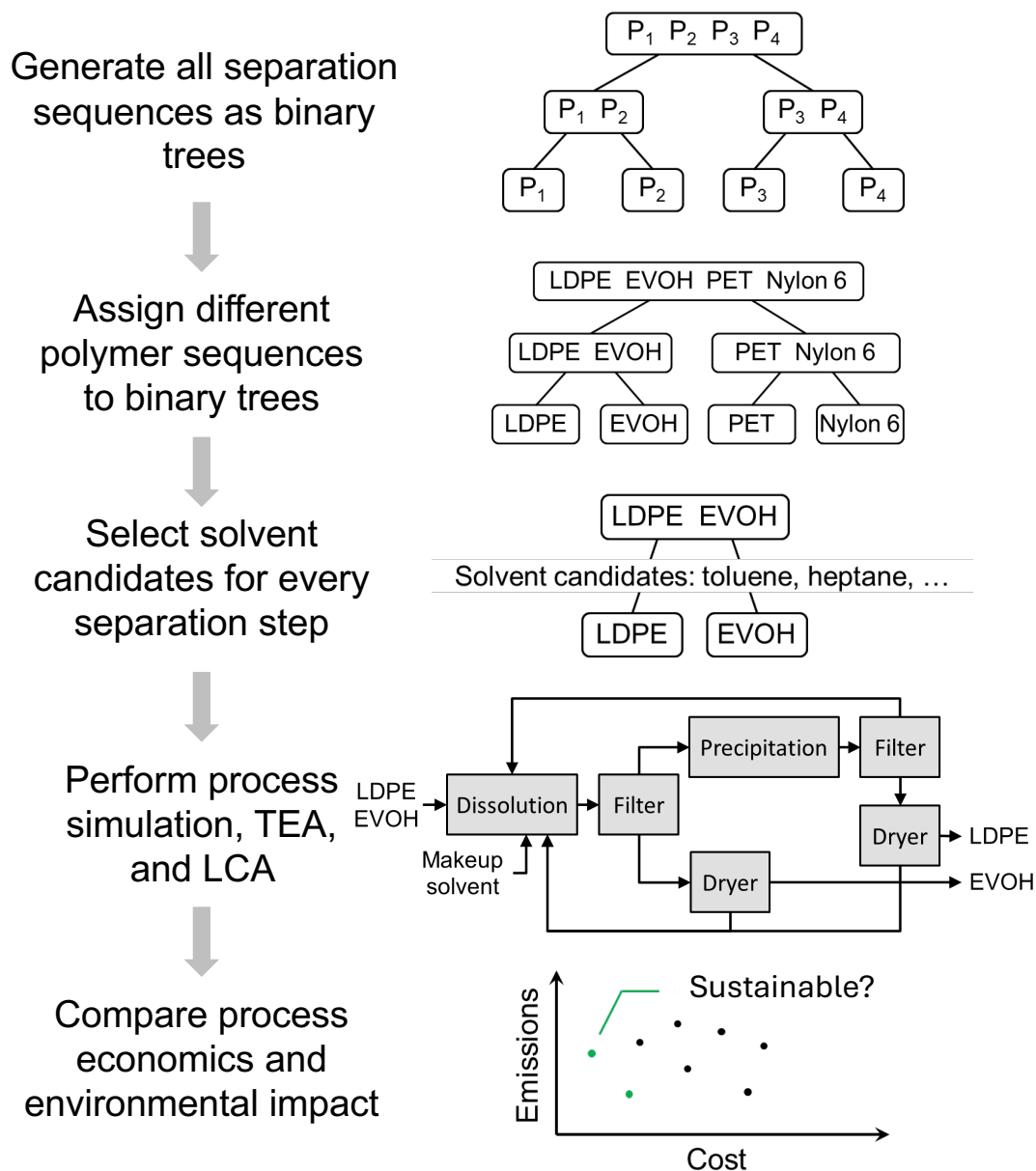


Figure 4.3: General steps of the proposed computational framework.

### Separation sequences as binary trees

The first step consists of generating all the possible separation sequences as binary trees. Figure 4.1B shows an example of the binary trees we use to represent the separation sequences for a multilayer film composed of 3 polymers. Here, we use the left branch to denote the dissolved and precipitated polymer(s) and the right branch to refer to the undissolved polymer(s). For this example, we can see that every separation step only dissolves one polymer. We refer to this as the dissolution number ( $D^n$ ). Therefore, this example has  $D^n = 1$ . Also, this binary tree only shows one separation sequence: dissolving first  $P_1$  and then  $P_2$ . Changing the separation order of the sequence (for example, dissolving first  $P_2$ ) provides all possibilities for the case of  $D^n = 1$ . Therefore, the permutation of the set of polymers ( $P_1$ ,  $P_2$ , and  $P_3$ ) results in 6 different sequences. To determine all the possible sequences, we also consider the binary trees where two polymers are dissolved in a certain step ( $D^n = 2$ ). Considering the permutation of the polymers set, this results in another 6 different sequences. The maximum  $D^n$  for a  $n$ -component multilayer film is given by  $n-1$ . Therefore, the separation of a 3-polymer mixture has 12 possible sequences. Note that this combinatorial complexity increases rapidly with the number of polymers. For example, a 4-polymer mixture will have 120 sequences, and a 5-polymer mixture will have 1680 sequences.

As shown in Figure 4.3, the next step is to assign different polymer sequences to the binary trees. For example, instead of having  $P_1$ ,  $P_2$ ,  $P_3$ , and  $P_4$ , now we will have low-density polyethylene (LDPE), which corresponds to  $P_1$ ; ethylene vinyl alcohol (EVOH), which corresponds to  $P_2$ ; polyethylene terephthalate (PET), which corresponds to  $P_3$ ; and nylon 6 or N6, which corresponds to  $P_4$ . This step is needed to select solvent candidates.

### Solvent selection process

This step includes selecting the solvent candidates for the target polymer(s) in each separation step using molecular-scale models [25]. The selected solvents may vary depending on the separation sequence and the composition of the multicomponent material. For instance, for the multilayer film in Figure 4.3, composed of LDPE, EVOH, PET, and nylon 6, different solvents may be chosen if LDPE or EVOH is dissolved first. In addition, if the multilayer film were composed of only LDPE, EVOH, and PET, the selected solvents might also differ.

The solvent selection is performed based on the previously reported solubility database and the solvent screening tool [26]. For the presented case studies, we consider a library of 60 common solvents selected from the solubility database. The criteria for selecting feasible solvents is that the target polymer(s) solubility should be greater than 10 wt.% at an elevated temperature and less than 3 wt.% at room temperature to enable dissolution and precipitation, respectively. Also, the solubility of the non-target polymer(s) should be lower than 3 wt.%. These criteria were selected because they can lead to reasonable experimental yields, as previously reported [26]. The screening tool identifies all the solvents that can satisfy such criteria. If there are no feasible solvents for a given sequence, this sequence is discarded. Note that, at this point, solvent selection only depends on the temperature-dependent polymer solubilities, and no economic or environmental impacts are considered. Thus, the output of solvent selection only includes the solvent(s) for the target component in each separation step and the dissolution temperature.

The dissolution temperature for each solvent is determined following a previously reported approach [26]. In summary, the dissolution temperature is selected considering the solvent boiling point as follows: if the boiling point is greater than 120 °C, the selected temperature for dissolution is 120 °C. In contrast, if the boiling point is equal to or below 120 °C, the dissolution temperature is set to 1 °C below the solvent boiling point. The reason behind these limits is that the upper bound of 120 °C enables calculations of polymer solubility at a high temperature while limiting the selection of temperatures that may lead to thermal degradation of the target polymers [32]. Also, operating below the solvent's boiling point makes operating at ambient pressure conditions possible.

Figure 4.4 presents a graphical representation of solvent candidates (from the entire solubility database, comprising 1000 solvents) that satisfy the criteria required to selectively dissolve each polymer in a multicomponent plastic containing LDPE, EVOH, PET, and nylon 6 polymers, assuming that the only polymers are present. Nylon 6 and PET have the fewest candidate solvents due to the polymer itself (e.g., not many solvents can dissolve PET) or to the specific combination of polymers in this example since finding solvents that selectively dissolve only one polymer can be challenging. On the contrary, LDPE and EVOH both have many solvents that can be used for their dissolution, which may indicate their ease of recovery. From this visualization (Figure 4.4), we see that targeting either PET or nylon 6 polymers at the

first dissolution step may be impossible or difficult, thereby reducing the separation design space. It is worth highlighting that Figure 4.4 groups the 1,000 solvents into 17 solvent categories (instead of each solvent) to facilitate their visualization, showing the diversity of the solvent database. However, the computational framework can provide the specific solvents for each process design as output.

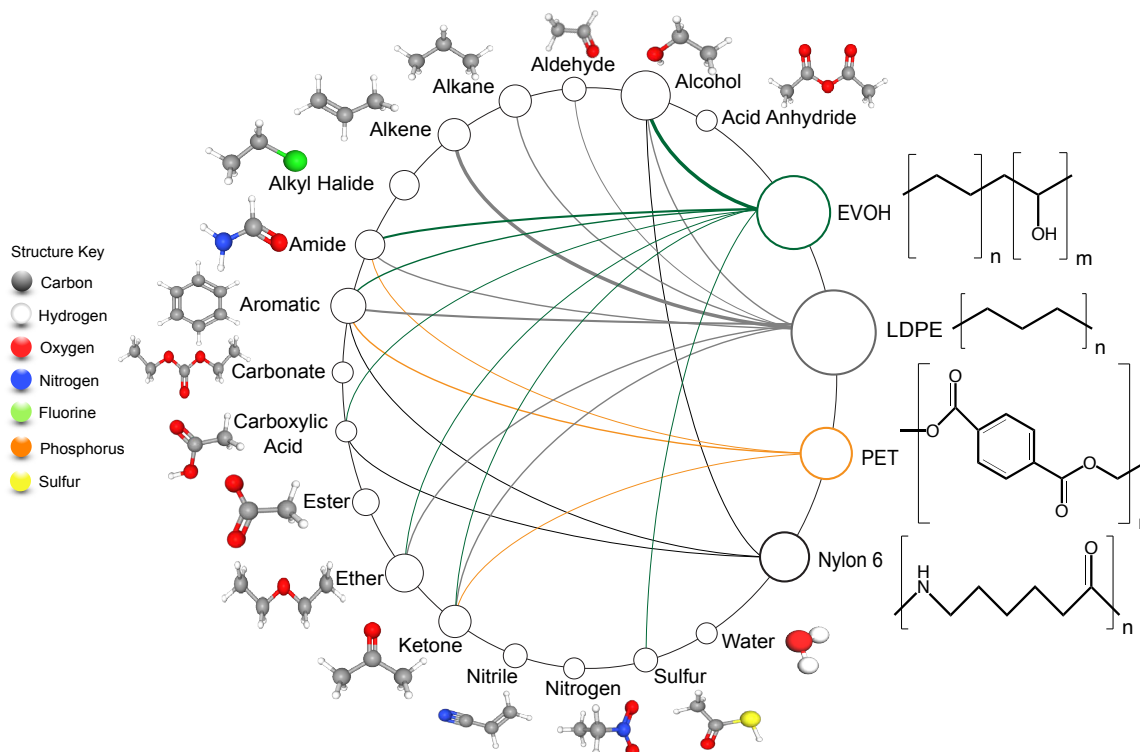


Figure 4.4: Visualization of solvent candidates for EVOH (green lines), LDPE (grey lines), PET (orange lines), and nylon 6 (black lines); their chemical structures are drawn at right. Line widths and node sizes denote the number of solvents able to dissolve each polymer. Each solvent class has an associated chemical structure motif drawn next to it, with key atoms highlighted with different colors. For example, nitrogen atoms are highlighted in blue.

### Process simulation, TEA, and LCA

This step uses the collected inputs from the previous steps (feasible separation sequences, solvents, and dissolution temperature) to perform the process simulation, TEA, and LCA of different STRAP process design configurations. We applied our

framework to different case studies constituting various multicomponent plastic films containing known constituent polymers and mass fractions.

As indicated in previous studies, results have shown that a high solvent recovery ( $>95\%$ ) is required to ensure the economic and environmental feasibility of temperature-controlled precipitation [8, 22]. As shown in Figure 4.2, after precipitation, most of the solvent is recovered after filtering the target polymer (using Filter 2). Then, the target polymer is sent to a dryer to recover the remaining solvent further. Similarly, the undissolved solids ( $P_2$  and  $P_3$ ) are also sent to a dryer to recover the remaining solvent in these components. The vapor phase of both dryers is then sent to a condenser to recover the solvent. Here, the solvent recovery rate is a function of the condenser temperature (represented by  $T_4$  in Figure 4.2). Therefore, we estimate the required temperature ( $T_4$ ) in the condenser to achieve a solvent recovery rate of  $>99.99\%$  in a computational pre-processing step (before applying the proposed computational framework). In this step, we performed the process simulation of a system consisting only of a dryer and a condenser. Several temperature points within a temperature domain (established based on previous work [7, 8]) are sampled and evaluated to achieve the required solvent recovery rate. In the scenario where a  $99.99\%$  recovery can not be obtained, we estimate the temperature to recover  $>98\%$  of solvent to maximize the economic and environmental benefits. The process model simulation is performed in the open-source package BioSTEAM [33]. This Python-based process simulator has been validated against proprietary software (e.g., SuperPro Designer and Aspen Plus).

We use the condenser temperatures previously estimated and perform the process model and TEA of all the feasible STRAP process design configurations in BioSTEAM. Here, mass and energy balances are used to determine the sizing and the energy required by the different process units. It is important to note that the process simulation and TEA are performed for all the feasible sequences and modules (i.e., each binary separation) for the given multicomponent material. For example, given the material presented in Figure 4.2, we simulate two separation modules for that given sequence since it has two binary separation steps. We repeat this step for all the feasible sequences. We use the minimum selling price (MSP) as the economic metric to compare different scenarios. The MSP is also known as the break-even price and is defined as the price per mass of product sold. We report the MSP as USD per kg of recovered polymer.

After performing the process simulation and TEA, we evaluate the environmental impact of each scenario using an LCA methodology. The LCA was performed using the open-source software openLCA v1.10.3 [34], the Environmental Footprint and AGRIBALYSE databases, and the Environmental footprint impact assessment method [35, 36]. We consider all the inputs to the process (electricity, steam, water) and estimate the climate change impact (CCI) for each scenario. Since there are limited data for solvents in the LCA databases and we are considering high recycling rates, we exclude the impact of producing the solvents used in each separation. The environmental impact of the process was analyzed considering a product perspective [37]. From this perspective, the STRAP technology is seen as an alternative process to produce virgin-grade polymers. Therefore, the functional unit considered is the production of 1 kg of recovered polymer. As a result, the CCI is expressed in kg CO<sub>2 eq.</sub> per kg of polymer.

### **Ranking of sustainable process designs**

In this last step, we store the economic (MSP) and environmental (CCI) outputs of all feasible process design scenarios (including different sequences and solvents). Then, we compare and rank the economic and environmental impacts to identify sustainable process design configurations. Each of these configurations provides detailed process information such as solvent types and recycling rates, polymer/solvent ratios, and operating temperatures.

## **4.3 Results and discussion**

We illustrate the applicability of our computational framework by addressing four case studies consisting of different feedstocks that can be processed using different STRAP designs. For case 1, we analyze the economic and environmental impacts of recovering the components of a 4-polymer multilayer film commonly used for food packaging. For case 2, we evaluate a more complicated multicomponent feedstock that consists of 7 polymers that can commonly be found in mixed plastic waste streams. For case 3, we compare the impact of changing the design of a 3-polymer multilayer film often used for food packaging applications. For case 4, we analyze the separation feasibility in polymer mixtures considering various possible combinations between 10 common polymers.



From previous research, we know the range of the required scale to achieve an MSP comparable to average market prices[7]. Therefore, the results presented in this work were obtained for a fixed plant capacity of 6,400 tons per year. For the solvent selection, we consider a library with 60 common solvents based on our previously reported database [26].

### 4.3.1 Case study: recycling a multilayer film of 4 polymers

We applied the proposed computational framework to a multilayer film composed of LDPE (60 wt%), EVOH (5 wt%), PET (25 wt%), and nylon 6 or N6 (10 wt%). This 4-polymer multilayer film is commonly used for food packaging applications, such as ham[12, 38].

We followed the steps in our framework as described and summarized in Figure 4.3. Figure 4.5 summarizes the process designs with the lowest economic and environmental impacts. We only present the feasible sequences based on the 60 common solvents in our database, denoted by  $S_1$ ,  $S_2$ ,  $S_3$ , and  $S_4$ . We include only the solvents that lead to the lowest environmental and economic impacts, which are the same for this case study. The impacts are given per separation step, and the solvent required for each step is also included. As mentioned before, for the binary tree representation, we use the left branch to denote the dissolved and precipitated polymer(s) and the right branch to refer to the undissolved polymer(s). Therefore, we can see that in the first step of  $S_1$ , LDPE is dissolved using p-xylene as a solvent. The only product is LDPE with an MSP of 0.48 USD/kg and a CCI of 0.31 kg CO<sub>2 eq.</sub>/kg. Note that the process could end here if the only product of interest is LDPE. Following the next separation steps, EVOH is recovered in the second step. Since this step depends on the previous one, we estimate the MSP and CCI to be 0.77 USD/kg and 0.41 kg CO<sub>2 eq.</sub>/kg, considering the recovery of both LDPE and EVOH. Finally, in the last step, PET is dissolved, and N6 is recovered via filtration. This step includes the recovery of all polymers, and we refer to these MSP (0.82 USD/kg) and CCI (0.49 kg CO<sub>2 eq.</sub>/kg) as the total impacts.

As a benchmark, we also estimate the CCI of producing the four polymers from fossil sources and their average market prices. We find that the average market MSP of these polymers is 1.2–2.6 USD/kg. Furthermore, the multilayer film addressed in this study has a market price of 2.9 USD/kg [38, 39]. When we compare these costs with the total MSPs of the four sequences in Figure 4.5, we observe that all the

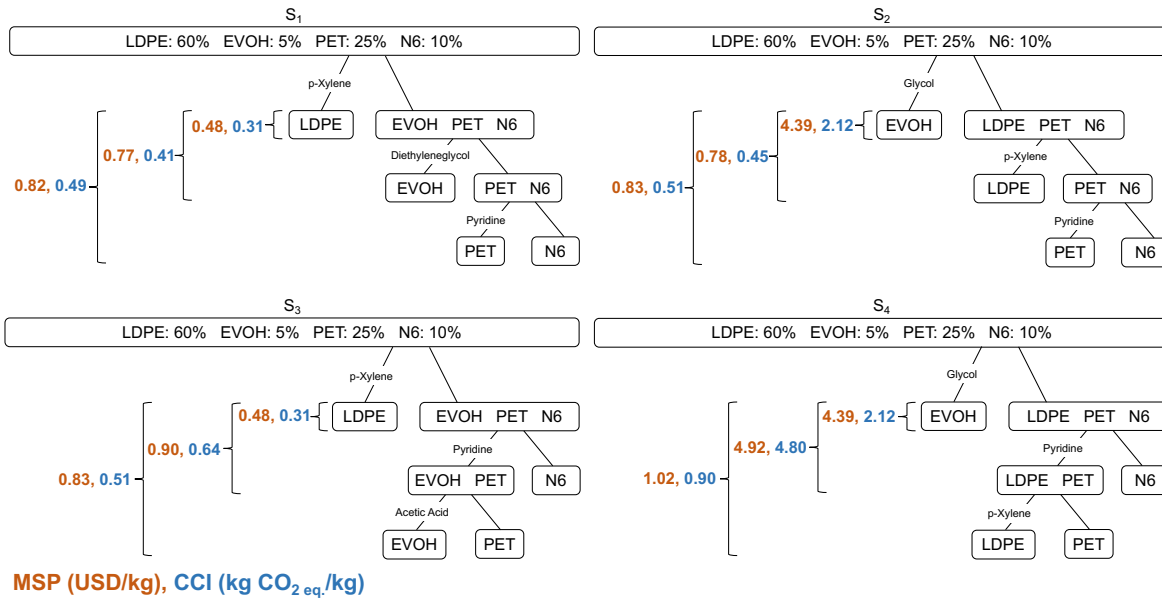


Figure 4.5: Minimum selling price (MSP) and climate change impact (CCI) of the STRAP process configurations with the lowest impacts in Case Study 1. The separation sequences are denoted by S<sub>1</sub>-S<sub>4</sub>. Note that the impacts are given per separation step. For instance, for S<sub>1</sub>, the MSP when only LDPE is recovered is 0.48 USD/kg. Then, if LDPE and EVOH are recovered, the MSP is 0.77 USD/kg. Finally, if all the polymers are recovered, the MSP is 0.82 USD/kg.

STRAP process configurations have lower costs. Regarding the environmental impact of virgin polymers, we estimate the CCI of the production from fossil sources of the multilayer film considered in this case study (LDPE, EVOH, PET, and N6). We find that 4.81 CO<sub>2</sub> eq./kg are generated. Figure 4.5 shows that all the total CCI of the STRAP process configurations are lower than this value, supporting the claim that STRAP offers a better process for plastic production from an environmental standpoint [22].

If we compare the total impacts of each sequence, we can see that S<sub>1</sub> provides the lowest impacts, while S<sub>2</sub> and S<sub>3</sub> have similar impacts. However, if S<sub>4</sub> were chosen as the selected process design, we note that the cost and emissions would be 24% and 84% higher than S<sub>1</sub>, respectively. These differences greatly increase if we compare only the first step, which is the recovery of only one polymer. We compare S<sub>1</sub> and S<sub>3</sub>, which recover LDPE first, with S<sub>2</sub> and S<sub>4</sub>, which recover EVOH first. We find that separating only EVOH is 9 times more expensive and generates 7 times more emissions. When we compare the next separation step, which includes the recovery of two polymers, we find that recovering EVOH and N6 via S<sub>4</sub> results in a 6 times

higher MSP and 12 times higher CCI than using  $S_4$  to recover LDPE and EVOH.

It should be highlighted that each step and sequence has different process parameters (e.g., temperatures, recycling rate, solvent/polymer ratio) that also contribute to the reported impacts. For instance, among all the separation steps, the selective dissolution of LDPE has the lowest MSP and CCI. This is partly due to the high weight percentage of LDPE in the multilayer plastic film (60%) and the high recycling rate (99.98%) of the solvent (p-xylene) used.

From these results, we conclude that recovering all polymers is the best option because it helps reduce the impacts. However, if the objective is to have only the first or second step of the process,  $S_3$  and  $S_4$  should be avoided because these sequences result in higher costs and impacts. In summary, while this analysis shows that a rule of thumb to follow to achieve a low MSP and CCI is to selectively dissolve components from the largest percentage composition to the lowest (taking advantage of the economics of scale), there are other factors and constraints to consider. For instance, although  $S_1$  provides the overall best MSP and CCI by dissolving LDPE first, targeting PET next based on its percentage composition could lead to lower MSP and CCI. However, finding a solvent capable of selectively dissolving and precipitating PET from an EVOH-PET-N6 polymer mix is difficult. The same applies to N6. This shows that other factors related to the solvent also affect the MSP and CCI. For instance, this higher MSP and CCI could be attributed to the fact that only 99.95% of pyridine, which was used to recover N6 in  $S_3$ , can be recycled at a much lower condenser temperature of 243.15 K. In contrast, 99.99% of diethylene glycol that was used to recover EVOH in  $S_1$  could be recovered at a less energy-intensive condenser temperature of 323.15 K. Having identified the influence of the percentage composition, recycling rates, and condenser temperature on the MSP and CCI, other solvent effects like solvent dissolution energy could affect the CCI [27].

#### **4.3.2 Case study: recycling mixed plastic waste stream of 7 polymers**

For this case study, we consider a 7-polymer feedstock commonly found in mixed plastic waste streams. We select the composition based on previous approaches: LDPE (43 wt%), PET (26 wt%), polypropylene (PP) (10 wt%), polycarbonate (PC) (6 wt%), EVOH (5 wt%), polyvinyl chloride (PVC) (5 wt%), and N6 (5 wt%) [12, 40]. Note that the main components are LDPE and PET, similar to Case Study 1. Here, we

do not focus on a specific multilayer film because the goal is to analyze the feasibility and the impacts of recovering the polymers of a mixed waste stream that may contain different types of multilayer films or other multicomponent materials.

We followed the general steps for the proposed computational framework. First, when we evaluated all the possible sequences, we found that 36 different sequences were feasible for this mixture of polymers. In other words, we can recover the seven polymers using any of these 36 separation sequences, where the order of separation changes, as do the other process variables (e.g., solvents and temperatures).

Because different sets of solvents may be used to achieve a complete separation sequence, we select the process designs (i.e., the sequence with its required solvent set) of each of the 36 feasible sequences that lead to the lowest impacts. Figure 4.6 presents the total impacts for all sequences: the cost and emissions of all the steps required to separate the seven polymers. Similar to Case Study 1, when we compare different process conditions (solvents and temperatures) for a given sequence, we find that the process parameters that lead to the lowest MSP also result in the lowest CCI. Therefore, the MSP and CCI presented in Figure 4.6 represent each sequence's lowest economic and environmental impacts.

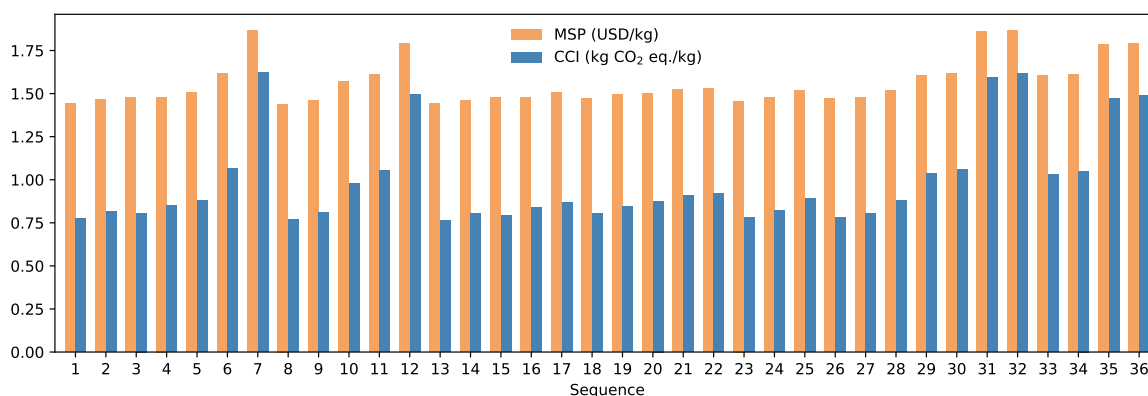


Figure 4.6: Minimum selling price (MSP) and climate change impact (CCI) of the STRAP process configurations with the lowest impacts in Case Study 2. The presented impacts are the total cost and emissions of separating the seven polymers.

When we compare the MSP between the different sequences, we can see that the lowest MSP is given by Sequence 8 with 1.44 USD/kg. Here, the separation order is 1) EVOH, 2) PVC, 3) PP, 4) LDPE, 5) PC, 6) PET, and 7) N6. Then, Sequence 7 provides the highest MSP, resulting in 30% higher costs with 1.87 USD/kg. The

separation order for this sequence is 1) EVOH, 2) PC, 3) PET, 4) N6, 5) PVC, 6) PP, and 7) LDPE. Contrary to Case Study 1, we can see that in this case, recovering the polymers with the highest composition (LDPE-43 wt% and PET-26 wt%) first does not lead to the lowest MSP. This is because the solvents used, which depend on the multilayer/mixed plastic composition, have a greater influence on the costs than the percentage composition; in other words, the solvents and conditions required to recover LDPE in a 4-component film change from the solvents and conditions to recover LDPE in a 7-component mixture to satisfy the selective dissolution criteria.

Similarly to the previous case studies, the same sequences that provide the lowest and highest MSP lead to the lowest and highest CCI. The difference between the minimum and maximum CCI is greater than the difference for the MSP. For Sequence 8, the CCI is 0.77 kg CO<sub>2 eq.</sub>/kg, while for Sequence 7, the CCI is 2.1 times more with 1.62. These results highlight the importance of estimating and comparing the impacts of all the feasible sequences.

### 4.3.3 Case study: guiding the design of easy-to-recycle plastic products

After demonstrating the relevance of evaluating different process designs and identifying the main impact drivers for the STRAP process, we examine the economic and environmental variations when the product design changes. Several companies are working to replace specific polymers in multilayer films used for food packaging to reduce environmental and human health hazards[41, 42]. PVC is of particular concern and has already been replaced in some food packaging applications with EVOH [43, 44]. Therefore, in this case study, we aim to analyze the impacts of changing such packaging designs on the STRAP recycling process. To do that, we compare a multilayer film composed of LDPE (75 wt%), PVC (5 wt%), and N6 (20 wt%) with a similar film where EVOH is used instead of PVC. These multilayer film designs are often used for cheese packaging [43, 12].

We refer to the LDPE/PVC/N6 film as Case Study 3A. Figure 4.7 presents the process designs with the lowest economic and environmental impacts. Here, the impacts and solvents per separation step are shown. If we compare the sequences  $S_1$ - $S_4$ , we can see relevant differences. For instance, when we compare  $S_1$  and  $S_2$ , we can see that recovering only PVC results in a 10 times higher MSP and 5 times higher CCI. Similarly,  $S_3$  and  $S_4$  lead to 4 and 5 times higher costs and emissions than  $S_1$  in

the first separation steps. Note that in  $S_3$  and  $S_4$ , the product is N6, but it is obtained via filtration while the dissolved polymers are LDPE and PVC (the polymers on the right branch of the tree as mentioned above).

Similar to the previous case studies, we observe that the impacts decrease if we consider the recovery of all components. However, there are important differences between the lowest and highest impacts. For instance,  $S_3$  results in 33% and 94% higher MSP and CCI than  $S_1$ .

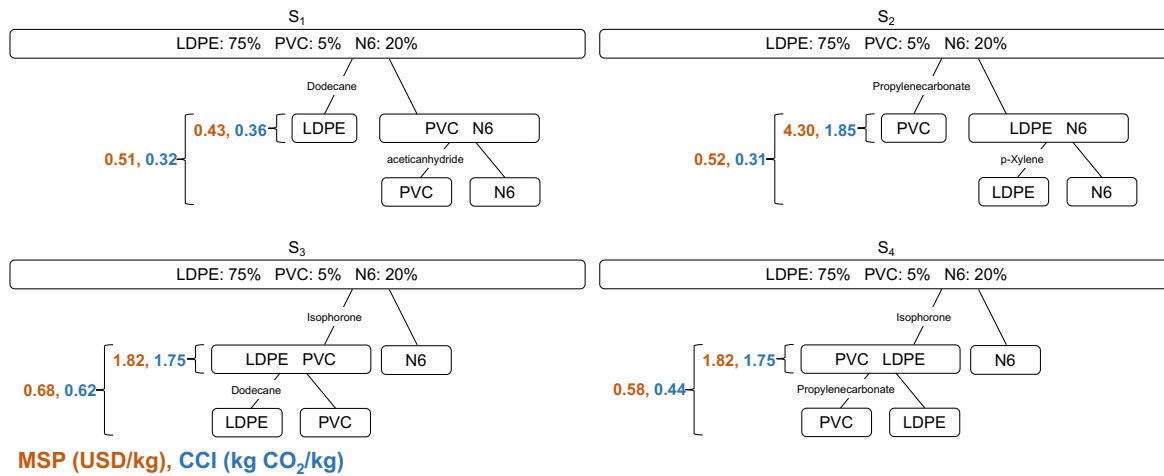


Figure 4.7: Minimum selling price (MSP) and climate change impact (CCI) of the STRAP process configurations with the lowest impacts in Case Study 3A. The separation sequences are denoted by  $S_1$ - $S_4$ . Note that the impacts are given per separation step. For instance, for  $S_1$ , the MSP when only LDPE is recovered is 0.43 USD/kg. If all the polymers are recovered, the MSP is 0.51 USD/kg.

Figure 4.8 presents the process designs with the lowest economic and environmental impacts for the LDPE/EVOH/N6 film, which we refer to as Case Study 3B and represents a re-designed film that replaces PVC with EVOH. We can see some similar trends to Case Study 3A. For instance,  $S_1$  has the lower CCI and MSP. Then, for  $S_2$ , if only EVOH is recovered, the MSP and CCI are 11 and 7 times higher, respectively.  $S_3$  and  $S_4$  also result in higher impacts, but recovering all polymers reduces the impacts.

If we compare the recovery of only PVC (see Figure 4.7) or EVOH (see Figure 4.8) using  $S_2$ , we find that the MSP is similar, but the CCI is 15% higher for the EVOH separation. When considering the recovery of all polymers for both case studies, we observe no significant differences for  $S_1$  and  $S_2$ . However, for  $S_3$ , the film containing EVOH results in 13% and 23% higher MSP and CCI, respectively, compared to the

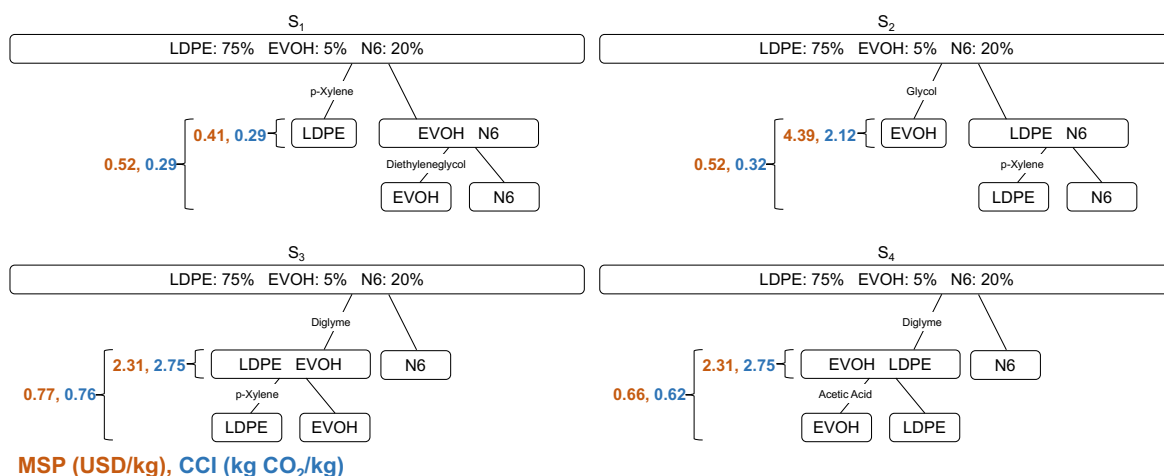


Figure 4.8: Minimum selling price (MSP) and climate change impact (CCI) of the STRAP process configurations with the lowest impacts in Case Study 3B. The separation sequences are denoted by S<sub>1</sub>-S<sub>4</sub>. Note that the impacts are given per separation step. For instance, for S<sub>1</sub>, the MSP when only LDPE is recovered is 0.41 USD/kg. If all the polymers are recovered, the MSP is 0.52 USD/kg.

film containing PVC. For S<sub>4</sub>, the increase in MSP is similar, but the CCI is now 41% higher.

We can conclude that if the best sequence (S<sub>1</sub>) is selected, the impacts of the film with PVC and EVOH are similar. On the other hand, if other sequences with higher impacts are selected, the potential savings for recycling the material via STRAP could be significantly reduced. This analysis shows the applicability of this fast computational framework to guide the product design of easy-to-recycle multilayer plastic film or guide plastic waste sorting by identifying plastic wastes that can be sorted together, reducing the time and cost of sorting plastics (i.e., polymers) into individual bails.

#### 4.3.4 Case study: separation difficulty of different polymer combinations

This last case study aims to investigate the separation difficulty in polymer mixtures. To achieve this, we applied the first three steps of our computational framework and conducted a systematic solvent selection test for various polymer combinations based on our solubility database. Given a polymer mixture and a solvent library, the number

of feasible separation sequences and potential solvent candidates can represent the difficulty of separating the polymers. Smaller values of these two numbers indicate a higher difficulty of separation. Note that difficulty here refers only to the number of feasible sequences (i.e., the number of ways to separate the polymer mixture) and the ease of selecting solvent candidates for their separation. Thus, the last two steps of the framework, which include performing the process simulation, TEA, LCA, and ranking of impacts, were not included (see Figure 4.3). This case study considers ten polymers - LDPE, high-density polyethylene (HDPE), EVOH, PP, polystyrene (PS), PC, PVC, PET, nylon 6 (N6), and nylon 66 (N66) - and the 60-solvent library, as previously mentioned.

We first study all possible binary combinations between these ten polymers. We find that there are 45 unique binary combinations. Every binary mixture has a maximum of two possible separation sequences. For instance, in a mixture of LDPE and PC, one sequence refers to dissolving LDPE and recovering PC via filtration. Thus, the other sequence involves dissolving PC and recovering LDPE via filtration. We identify the solvent candidates available in our database for both sequences. If no solvents are available for a given sequence, we consider that sequence to be unfeasible. The solvent selection process follows the assumptions and steps described previously.

Figure 4.9 presents a visualization of the difficulty for selective separation of all possible binary mixtures comprising the selected ten polymers. Here, we represent the difficulty (easy, medium, hard, and impossible) by lines of different colors (green, blue, yellow, and red) connecting each binary mixture. We determine the difficulty for each binary polymer combination as follows. We sum the number of solvent candidates with the number of feasible separation sequences (which can be one or two for a binary mixture), and we establish a set of ranking criteria based on this value. If the value is  $>10$ , we rank the separation as "easy," but if the value is between 5 and 10, we rank it as "medium." For the mixtures that have a value  $<5$ , they are classified as "hard," while "impossible" means that the value is 0. We specify these constraints based on the observations from the previous case studies. Note that the impossible case here means no solvents can be found to separate the binary polymer combination under the current conditions. The polymer combinations with impossible ratings may still be separable when a larger search space is considered (e.g., more solvents, larger temperature range, other precipitation methods, solvent mixtures). For example, in the case of the PET/PC combination, only PET can be dissolved (we did not find



solvents that can dissolve PC), which means that the number of separation sequences is 1 since PET is dissolved first. The number of candidate solvents for selective PET dissolution in the presence of PC is 9. If we consider the sum of these values, we can see that PET and PC separation has a ranking of 10, which is considered "medium" difficulty (see Figure 4.9).

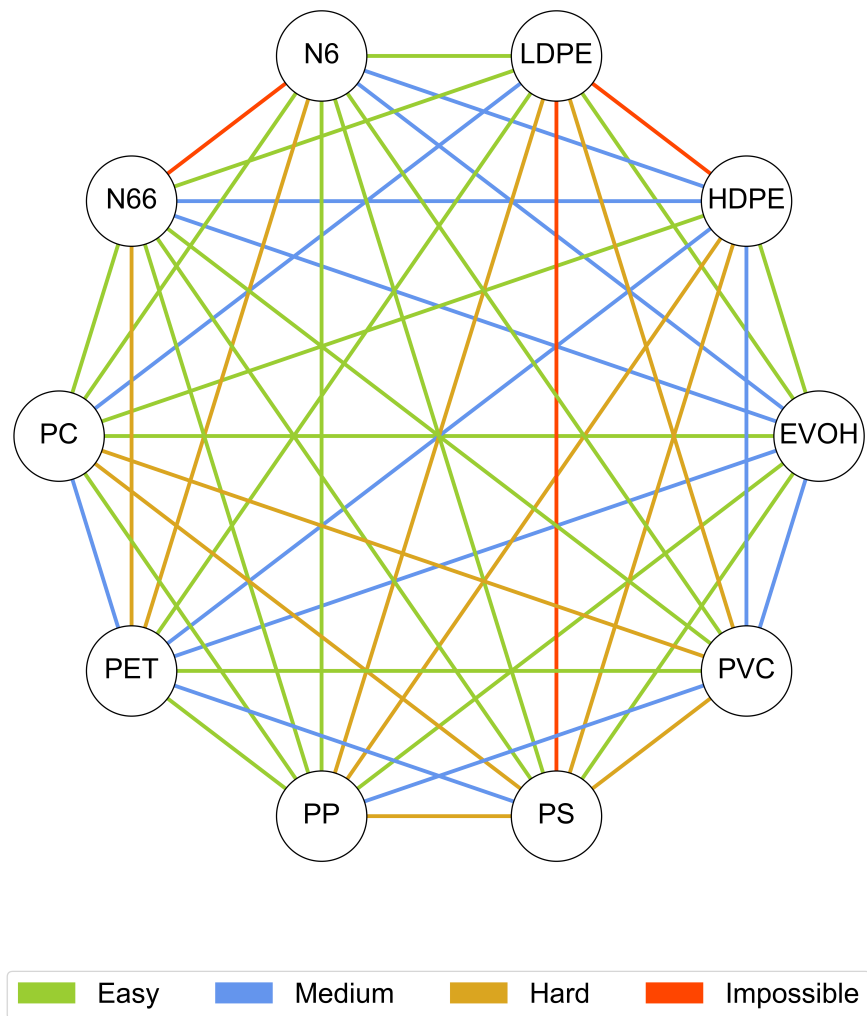


Figure 4.9: Separation difficulty in binary polymer mixtures. Difficulty refers to the number of feasible separation sequences and potential solvent candidates.

From Figure 4.9, we can see that, among all 45 combinations, there are 20 easy, 12 medium, 10 hard, and 3 impossible ratings. The hard and impossible combinations typically comprise two similar polymers: LDPE/PP, LDPE/HDPE, LDPE/PS, N6/N66.

This result aligns with the general chemical idea of “like dissolves like,” as finding a solvent with very different solubility values for similar polymers is challenging. The ratings and the data here not only guide the design of plastic recycling processes but can also help plastic manufacturers design more sustainable and easy-to-recycle products or discover new applications of such inseparable polymers to eliminate the need for their separation.

As a complement to binary combinations, we also conducted similar calculations on combinations of more than two polymers. As mentioned before, we consider the possibility of dissolving two polymers or more in a certain step. Note that several sequences can include the same solvents when these combinations have more than two polymers. The number of solvent candidates here has already excluded such duplicates. An obvious observation of these calculation results is that all impossible polymer combinations here are supersets of an impossible binary combination. Similarly, hard combinations of multiple polymers are often supersets of hard binary combinations. In short, these data can serve as supplementary reference for the design of multicomponent plastic waste recycling processes.

## 4.4 Summary

This study proposed a computational framework that integrates molecular-scale models, process modeling, TEA, and LCA to provide insights into the design of sustainable solvent-based recycling processes and easy-to-recycle multilayer/mixed plastics. The framework provides a fast estimation of the economic and environmental impacts of different process design scenarios for hard-to-recycle plastics (e.g., multilayer films). The framework reports the economic impact as the minimum selling price of the recovered products, while the environmental impact is evaluated as the climate change impact. Each scenario includes different separation sequences, solvents, and process operating conditions (polymer/solvent ratio, dissolution temperature, solvent recycling rate). We also provide guidelines for product design by identifying multilayer film designs with a lower recycling impact. The computational framework is general and can be used for complex multilayer films or multicomponent plastic waste streams.

We focused on a process denominated as the STRAP technology, which can selectively dissolve and separate the constituent polymers of multicomponent plastics.

We addressed 4 case studies to illustrate the applicability of the proposed framework. For Case Study 1, we analyzed the impacts of recycling a multilayer film composed of LDPE, EVOH, PET, and N6. We identified the sequence and process designs that drive the impacts. We found that recovering the component with higher weight composition (LDPE) first led to lower impacts. In addition, when other components were recovered first, the impacts could only be reduced if all the polymers were recovered. Overall, dissolving and recovering LDPE had lower impacts, while dissolving EVOH or recovering N6 via filtration led to higher impacts. For Case Study 2, we evaluated the feasibility and the economic and environmental impacts of recycling a more complex 7-polymer feedstock with LDPE, PET, PP, PC, EVOH, PVC, and N6. Here, we identified 36 feasible sequences and presented the process configurations with the lowest impacts. We found that, in this mixture, recovering the component with the highest weight composition first did not provide the lowest impact. Surprisingly, such sequences that targeted the highest component by weight fraction were not feasible. We also found that the solvents and conditions required to recover LDPE in a 4-component film change from the solvents and conditions to recover LDPE in a 7-component mixture. We conclude that for this more complex mixture, the solvent selection has a greater influence on the impacts than the percentage composition. For Case Study 3, we analyzed how the impacts of the STRAP process changed with different multilayer film designs. We compare a film composed of LDPE, PVC, and N6 with a film containing LDPE, EVOH (instead of PVC), and N6. We presented the configurations with the lowest costs and emissions for both materials. We found that if the best sequence was selected, the impacts of the film with PVC and EVOH were similar. However, if other sequences with higher impacts were chosen, the material containing EVOH could lead to higher impacts. Finally, for case study 4, we ranked the difficulty of separating all possible binary polymer mixtures in a set of 10 common polymers (LDPE, HDPE, EVOH, PP, PS, PC, PVC, PET, N6, and N66). We considered the number of feasible separation sequences and candidate solvents for ranking the separation from "easy" to "impossible." These findings can provide insights into recycling a given material before applying the complete computational framework.

We considered specific assumptions, including the 60-solvent library, fixed processing capacity, and temperature-controlled precipitation. Future work could include varying these parameters and considering other types of multicomponent plastic

feedstocks. As mentioned above, other dissolution methods, such as antisolvent addition, could lead to higher economic and environmental impacts. However, such methods may be required for certain feedstocks or polymers. Therefore, an analysis that proposes the optimal combination of dissolution methods could provide a broader set of possibilities for recycling diverse multicomponent plastics. In addition, the proposed computational framework could be used to generate tailored datasets that can help predict the impacts of different feedstocks.

## 4.5 References

- [1] Kara Lavender Law, Natalie Starr, Theodore R Siegler, Jenna R Jambeck, Nicholas J Mallos, and George H Leonard. The united states' contribution of plastic waste to land and ocean. *Science advances*, 6(44):eabd0288, 2020.
- [2] Jeannette M Garcia and Megan L Robertson. The future of plastics recycling. *Science*, 358(6365):870–872, 2017.
- [3] Ina Vollmer, Michael JF Jenks, Mark CP Roelands, Robin J White, Toon van Harmelen, Paul de Wild, Gerard P van Der Laan, Florian Meirer, Jos TF Keurentjes, and Bert M Weckhuysen. Beyond mechanical recycling: Giving new life to plastic waste. *Angewandte Chemie International Edition*, 59(36):15402–15423, 2020.
- [4] Roland Geyer, Jenna R Jambeck, and Kara Lavender Law. Production, use, and fate of all plastics ever made. *Science advances*, 3(7):e1700782, 2017.
- [5] Paul Stegmann, Vassilis Daioglou, Marc Londo, Detlef P van Vuuren, and Martin Junginger. Plastic futures and their co2 emissions. *Nature*, 612(7939):272–276, 2022.
- [6] Ellen MacArthur Foundation, McKinsey, and Company. The new plastics economy: Rethinking the future of plastics. In *The World Economic Forum: Geneva, Switzerland*, volume 36, 2016.
- [7] Kevin L Sánchez-Rivera, Aurora del Carmen Munguía-López, Panzheng Zhou, Victor S Cecon, Jiuling Yu, Kevin Nelson, Daniel Miller, Steve Grey, Zhuo Xu, Ezra Bar-Ziv, et al. Recycling of a post-industrial printed multilayer plastic film containing polyurethane inks by solvent-targeted recovery and precipitation. *Resources, Conservation and Recycling*, 197:107086, 2023.

- [8] Jiuling Yu, Aurora del Carmen Munguía-López, Victor S Cecon, Kevin L Sánchez-Rivera, Kevin Nelson, Jiayang Wu, Shreyas Kolapkar, Victor M Zavala, Greg W Curtzwiler, Keith L Vorst, et al. High-purity polypropylene from disposable face masks via solvent-targeted recovery and precipitation. *Green Chemistry*, 25(12):4723–4734, 2023.
- [9] Utkarsh S Chaudhari, Daniel G Kulas, Alejandra Peralta, Tasmin Hossain, Anne T Johnson, Damon S Hartley, Robert M Handler, Barbara K Reck, Vicki S Thompson, David W Watkins, et al. Solvent based dissolution–precipitation of waste polyethylene terephthalate: economic and environmental performance metrics. *RSC Sustainability*, 1(7):1849–1860, 2023.
- [10] Taylor Uekert, Avantika Singh, Jason S DesVeaux, Tapajyoti Ghosh, Arpit Bhatt, Geetanjali Yadav, Shaik Afzal, Julien Walzberg, Katrina M Knauer, Scott R Nicholson, et al. Technical, economic, and environmental comparison of closed-loop recycling technologies for common plastics. *ACS Sustainable chemistry & engineering*, 11(3):965–978, 2023.
- [11] Kevin L Sánchez-Rivera, Panzheng Zhou, Min Soo Kim, Leonardo D González Chávez, Steve Grey, Kevin Nelson, Shao-Chun Wang, Ive Hermans, Victor M Zavala, Reid C Van Lehn, et al. Reducing antisolvent use in the strap process by enabling a temperature-controlled polymer dissolution and precipitation for the recycling of multilayer plastic films. *ChemSusChem*, 14(19):4317–4329, 2021.
- [12] John R Wagner Jr. *Multilayer flexible packaging*. William Andrew, 2016.
- [13] Curler Howard and Glenn E Lineburg. *Flexible wrapper*, 1963.
- [14] Camila Távora de Mello Soares, Monica Ek, Emma Östmark, Mikael Gällstedt, and Sigbritt Karlsson. Recycling of multi-material multilayer plastic packaging: Current trends and future scenarios. *Resources, conservation and recycling*, 176:105905, 2022.
- [15] Polstyvert. First commercial polystyrene recycling plant, 2023.
- [16] Andreas Mäurer, Martin Schlummer, Fabian Knappich, FELL Tanja, and Arthur Berrang. Method for recycling polyolefin containing waste, March 2 2021. US Patent 10,934,410.

- [17] Creasolv. Polystyreneloop, 2016.
- [18] Theodore W Walker, Nathan Frelka, Zhizhang Shen, Alex K Chew, Jesse Banick, Steven Grey, Min Soo Kim, James A Dumesic, Reid C Van Lehn, and George W Huber. Recycling of multilayer plastic packaging materials by solvent-targeted recovery and precipitation. *Science advances*, 6(47):eaba7599, 2020.
- [19] Kim Phan, Sibel Ügdüler, Lies Harinck, Ruben Denolf, Martijn Roosen, Galahad O'Rourke, Dirk De Vos, Veronique Van Speybroeck, Karen De Clerck, and Steven De Meester. Analysing the potential of the selective dissolution of elastane from mixed fiber textile waste. *Resources, Conservation and Recycling*, 191:106903, 2023.
- [20] Zhuo Xu, Kevin L Sánchez-Rivera, Panzheng Zhou, Charles Granger, Panzheng Zhou, Aurora del Carmen Munguía-López, Ugochukwu M Ikegwu, Styliani Avraamidou, Victor M Zavala, Reid C Van Lehn, Ezra Bar-Ziv, Steven De Meester, and George W Huber. A review of solvent-based plastic recycling technologies. *submitted to Nature Chemical Engineering*, under revision.
- [21] Daniel Maga, Markus Hiebel, and Nils Thonemann. Life cycle assessment of recycling options for polylactic acid. *Resources, Conservation and Recycling*, 149:86–96, 2019.
- [22] Aurora del Carmen Munguía-López, Dilara Göreke, Kevin L Sánchez-Rivera, Horacio A Aguirre-Villegas, Styliani Avraamidou, George W Huber, and Victor M Zavala. Quantifying the environmental benefits of a solvent-based separation process for multilayer plastic films. *Green Chemistry*, 25(4):1611–1625, 2023.
- [23] Houqian Li, Horacio A Aguirre-Villegas, Robert D Allen, Xianglan Bai, Craig H Benson, Gregg T Beckham, Sabrina L Bradshaw, Jessica L Brown, Robert C Brown, Victor S Cecon, et al. Expanding plastics recycling technologies: chemical aspects, technology status and challenges. *Green Chemistry*, 24(23):8899–9002, 2022.
- [24] Kevin L Sánchez-Rivera, Charles Granger, Harrison Appiah, Kevin Nelson, Steve Grey, David J Sun, John E Estela-García, Edward Chen, Zhuo Xu, Tim A Osswald, et al. Cast film production with polyethylene recycled from a post-industrial printed multilayer film by solvent-targeted recovery and precipitation. *ACS Materials Letters*, 6(9):4042–4050, 2024.

- [25] Panzheng Zhou, Kevin L Sánchez-Rivera, George W Huber, and Reid C Van Lehn. Computational approach for rapidly predicting temperature-dependent polymer solubilities using molecular-scale models. *ChemSusChem*, 14(19):4307–4316, 2021.
- [26] Panzheng Zhou, Jiuling Yu, Kevin L Sánchez-Rivera, George W Huber, and Reid C Van Lehn. Large-scale computational polymer solubility predictions and applications to dissolution-based plastic recycling. *Green Chemistry*, 25(11):4402–4414, 2023.
- [27] Ugochukwu Ikegwu, Victor M Zavala, and Reid Van Lehn. Screening green solvents for multilayer plastic films separation. *Systems and Control Transactions*, 3:763–770, 2024.
- [28] Austin L Lehr, Kayla L Heider, Emmanuel A Aboagye, John D Chea, Jake P Stengel, Pahola Thathiana Benavides, and Kirti M Yenkie. Design of solvent-assisted plastics recycling: Integrated economics and environmental impacts analysis. *Frontiers in Sustainability*, 3:989720, 2022.
- [29] Martin Schlummer, Andreas Mäurer, and Gerald Altnau. Recycling of high performance polymers from electro (nic) scrap. In *2012 Electronics Goes Green 2012+*, pages 1–5. IEEE, 2012.
- [30] Aurora del C Munguía-López, Panzheng Zhou, Ugochukwu M Ikegwu, Reid C Van Lehn, and Victor M Zavala. A fast computational framework for the design of solvent-based plastic recycling processes. *Systems and Control Transactions*, 3:814–819, 2024.
- [31] Sibel Ügdüler, Kevin M Van Geem, Martijn Roosen, Elisabeth IP Delbeke, and Steven De Meester. Challenges and opportunities of solvent-based additive extraction methods for plastic recycling. *Waste management*, 104:148–182, 2020.
- [32] Victor S Cecon, Greg W Curtzwiler, and Keith L Vorst. A study on recycled polymers recovered from multilayer plastic packaging films by solvent-targeted recovery and precipitation (strap). *Macromolecular Materials and Engineering*, 307(11):2200346, 2022.

- [33] Yoel Cortes-Pena, Deepak Kumar, Vijay Singh, and Jeremy S Guest. Biosteam: a fast and flexible platform for the design, simulation, and techno-economic analysis of biorefineries under uncertainty. *ACS sustainable chemistry & engineering*, 8(8):3302–3310, 2020.
- [34] Dr A Citroth, C Di Noi, T Lohse, and M Srocka. openlca 1.10 comprehensive user manual. 2020.
- [35] Simone Fazio, Valentina Castellani, Serenella Sala, Erwin Schau, Michela Secchi, Luca Zampori, Edward Diaconu, et al. Supporting information to the characterisation factors of recommended life cycle impact assessment methods: new methods and differences with ilcd. 2018.
- [36] Vincent Colomb, Samy Ait-Amar, Claudine Basset-Mens, Armelle Gac, Gérard Gaillard, Peter Koch, Jerome Mousset, Thibault Salou, Aurélie Tailleur, and Hayo MG Van Der Werf. Agribalyse®, the french lci database for agricultural products: high quality data for producers and environmental labelling. 2015.
- [37] Harish Jeswani, Christian Krüger, Manfred Russ, Maike Horlacher, Florian Antony, Simon Hann, and Adisa Azapagic. Life cycle environmental impacts of chemical recycling via pyrolysis of mixed plastic waste in comparison with mechanical recycling and energy recovery. *Science of the Total Environment*, 769:144483, 2021.
- [38] Shandong Top Leader Plastic Packing CO. 100mic food packaging pet/pa/evo-h/pe plastic film, 2023.
- [39] S. & P. Global POLYMERSCAN. Commodity insights, 2023.
- [40] Kevin L Sánchez-Rivera, Panzheng Zhou, Elizaveta Radkevich, Anisha Sharma, Ezra Bar-Ziv, Reid C Van Lehn, and George W Huber. A solvent-targeted recovery and precipitation scheme for the recycling of up to ten polymers from post-industrial mixed plastic waste. *Waste Management*, 194:290–297, 2025.
- [41] MO Rodrigues, Nelson Abrantes, FJM Gonçalves, H Nogueira, João Carlos Marques, and Ana MM Gonçalves. Impacts of plastic products used in daily life on the environment and human health: What is known? *Environmental toxicology and pharmacology*, 72:103239, 2019.



- [42] Awuchi Chinaza Godswill and Awuchi Chibueze Godspel. Physiological effects of plastic wastes on the endocrine system (bisphenol a, phthalates, bisphenol s, pbdes, tbbpa). *International Journal of Bioinformatics and Computational Biology*, 4(2):11–29, 2019.
- [43] Amcor. Form-tite™ shrink film, 2024.
- [44] Dorota Napierska. "bye bye " to pvc in food packaging – once and for all. Technical report, [zerowasteeurope.eu](http://zerowasteeurope.eu), 2024.

## Chapter 5

# Contaminant removal strategies for plastic products based on computational property prediction and solvent screening

This chapter focuses on the development of novel contaminant removal methods for plastic products. We will discuss different contaminant removal processes including leaching, extraction, and precipitation. Several types of contaminants, including brominated flame retardants (BFRs), phthalates, perfluoroalkyl and polyfluoroalkyl substances (PFAS) will be studied.

---

This chapter is based on the following publications

1. Zhou, P., Ikegwu U. M., Radkevich, E., Ra, E. C., Liburd, H., Huber, G. W., Zavala, V. M., Van Lehn, R. C. Molecular Models to Guide Contaminant Removal from Plastics. In preparation.
2. Zhou, P., Yu, J., Sánchez-Rivera, K. L., Huber, G. W., & Van Lehn, R. C. (2023). Large-scale computational polymer solubility predictions and applications to dissolution-based plastic recycling. *Green Chemistry*, 25(11), 4402-4414.
3. Sánchez-Rivera, K. L., del Carmen Munguía-López, A., Zhou, P., Cecon, V. S., Yu, J., Nelson, K., Miller, D., Grey, S., Xu, Z., Bar-Ziv, E., Vorst, K. L., Curtzwiler, G. W., Van Lehn, R. C., Zavala, V. M., & Huber, G. W. (2023). Recycling of a post-industrial printed multilayer plastic film containing polyurethane inks by solvent-targeted recovery and precipitation. *Resources, Conservation and Recycling*, 197, 107086.

## 5.1 Introduction

Most plastic products are made from base polymer resins mixed with a complex blend of materials collectively known as additives. These additives enhance plastic products by making them safer, more durable, and visually appealing [1]. They also reduce production costs and extend the lifespan of plastic materials [2]. However, some additives raise concerns due to their persistence in the environment and potential health impacts.

There are many different types of plastic additives. Plasticizers, such as phthalates and adipates, increase polymer flexibility by reducing intermolecular forces [3]. Stabilizers like UV absorbers and antioxidants can prevent degradation caused by heat, light, and oxidation [4]. Flame retardants inhibit combustion by disrupting the burning process [5]. Fillers and reinforcements, such as glass fibers and calcium carbonate, improve mechanical strength and reduce material costs [6]. Colorants, including inorganic pigments (e.g., titanium dioxide) and organic dyes, provide coloration and opacity [7]. Antimicrobial agents, such as silver nanoparticles, inhibit microbial growth in medical and food packaging applications [8]. Antistatic agents can minimize electrostatic buildup on plastic surfaces [9]. Other additives include lubricants, nucleating agents, impact modifiers, etc. In this work, we will mainly focus on the removal methods of brominated flame retardants (BFRs), phthalates, per- and polyfluoroalkyl substances (PFAS).

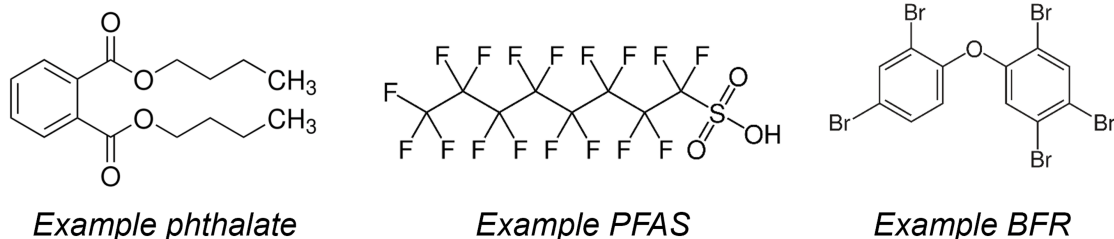


Figure 5.1: Example structures of a phthalate, a PFAS, and a BFR molecules.

Flame retardants are added to plastics to reduce flammability and improve fire safety. They are commonly used in electronic casings, building materials, textiles, and automotive components to meet fire resistance regulations [5]. Flame retardants can be categorized into halogenated and non-halogenated types. Brominated flame retardants (BFRs), such as polybrominated diphenyl ethers (PBDEs), are highly effective

due to their ability to interfere with combustion processes by releasing bromine radicals that suppress flames [10]. However, they are persistent organic pollutants with bioaccumulative properties. In response to environmental concerns, non-halogenated alternatives such as phosphorus-based and nitrogen-based flame retardants are increasingly being used [11]. Many flame retardants are either incorporated directly into the polymer matrix or applied as coatings on the plastic surface.

Phthalates are plasticizers added to polymers, primarily polyvinyl chloride (PVC), to improve flexibility, durability, and workability [12]. They are found in a vast range of consumer products, including vinyl flooring, medical tubing, shower curtains, and food packaging. Phthalates are esters of phthalic acid with varying alkyl chain lengths determining their volatility and migration potential. Short-chain phthalates, such as dimethyl phthalate (DMP), are more volatile and can evaporate into the air, whereas longer-chain phthalates, like di(2-ethylhexyl) phthalate (DEHP), tend to leach from plastics into surrounding environments over time [12, 13]. Phthalates are often physically integrated into plastics rather than chemically bound, which means they can migrate out of products through wear, heating, or contact with liquids. Due to potential endocrine-disrupting effects, regulatory agencies have restricted the use of certain phthalates in children's toys, cosmetics, and medical devices, prompting the development of alternative plasticizers such as citrate- and adipate-based compounds [14].

Per- and Polyfluoroalkyl Substances (PFAS) are a class of synthetic chemicals used in plastics to impart water, oil, and stain resistance [15]. Their strong carbon-fluorine bonds make them highly resistant to heat, chemicals, and degradation. PFAS have been widely used in nonstick cookware coatings, grease-resistant food packaging, stain-resistant textiles such as carpets and outdoor apparel, and firefighting foams. While their hydrophobic and oleophobic properties make them indispensable for many applications, their environmental persistence and bioaccumulation pose significant health risks, including links to cancer, liver toxicity, and immune system disruption [16]. PFAS can be introduced into the environment through industrial wastewater, landfill leachate, and household product use, leading to widespread contamination of water sources [17]. Increasing regulatory scrutiny has prompted research into alternative fluorine-free coatings and improved methods for PFAS removal from contaminated environments [18].

In plastic recycling processes, many such additives become contaminants since

industrial standards regulates maximum concentration of these chemicals in pure polymers. Computational property prediction and solvent screening approaches offer promising solutions for selectively removing harmful additives while maintaining the integrity of the base polymer, enabling more sustainable plastic recycling and reuse. In this Chapter, we introduce strategies to remove contaminants from plastic waste by leveraging computational predictions of contaminant partitioning in a broad range of solvents.

## 5.2 Computational framework

Two contaminant removal methods are presented in Figure 5.2. Leaching is a commonly employed method for the removal of undesirable chemicals from industrial products. This process involves the immersion of targeted materials into a solvent, facilitating the extraction of contaminants from the polymer matrix. Leaching is often utilized in environmental remediation and recycling efforts, as it allows for the selective removal of harmful additives that may pose ecological or health risks. In STRAP processes, polymers are often first dissolved in carefully selected solvents, and then precipitated by decreasing temperature or adding a nonsolvent to the solution. Therefore, if properly designed, the STRAP steps can be directly used for contaminant removal via selected precipitation of the polymer. Simultaneous recycling of pure polymer resins and contaminant removal can be integrated in a STRAP process.

The efficiency of contaminant removal depends on the partitioning behavior of contaminant molecules in the two phases. Partition coefficient,  $\log P$ , describes the distribution of a contaminant between the two immiscible phases. Equation 5.1 shows the definition of partition coefficient of contaminant molecules in the two phases, which is the logarithm of the ratio of contaminant concentrations in solvent phase versus polymer phase.

$$\log P = \log \frac{[\text{contaminant}]_{\text{solvent}}}{[\text{contaminant}]_{\text{polymer}}} \quad (5.1)$$

A positive partition coefficient ( $\log P > 0$ ) indicates that the contaminant is more likely to remain in the solvent phase, while a negative value ( $\log P < 0$ ) suggests it prefers to stay in the solid matrix. In the context of contaminant removal from plastics, understanding the partition coefficient is essential for the design of a successful leaching process, as it helps predict the efficiency of contaminant removal and

determines the selection of appropriate solvents for targeted compounds. Here, we treat a solid polymer as a liquid phase based on the assumption that contaminants partition into the amorphous region of a solid polymer with an affinity that can be quantified via  $\log P$  to guide solvent selection.

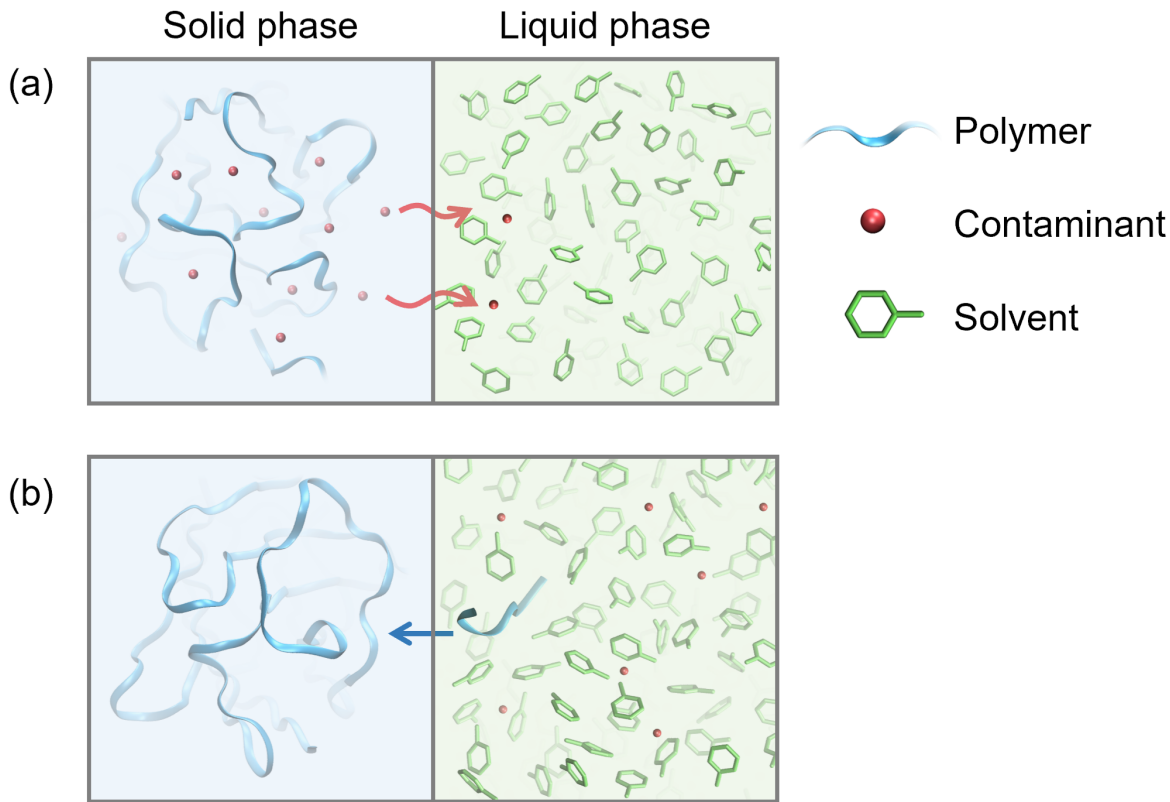


Figure 5.2: Molecular-scale illustrations of two contaminant removal strategies. (a) Leaching, where contaminant molecules migrate from solid polymer phase into liquid solvent phase. (b) Simultaneous STRAP and contaminant removal, it first dissolves the polymer and contaminant together in a solvent, and then selectively precipitate the polymer into solid phase.

Different solvent selection criteria are developed based on the characteristics of the two contaminant removal processes. These selection criteria involve property predictions of contaminant miscibility with solvents, contaminant partition coefficient, and polymer solubilities in the solvents. The leaching process requires:

1. The selected solvent must be miscible with contaminants;

2. Contaminants should have positive partition coefficients ( $\log P > 0$ ), with higher values preferred;
3. Ideal solvent candidates will swell but not dissolve the polymer.

For the simultaneous STRAP and contaminant removal process, the requirements are:

1. The solvent can dissolve both the polymer and the contaminants;
2. The solvent does not dissolve non-target compounds, such as other polymers in the plastics;
3. Contaminants have positive partition coefficients, and higher values are preferred;
4. Precipitation is feasible, either by using a nonsolvent or via strong temperature dependence of polymer solubility.

Since additives in plastic products are often mixtures of a set of similar chemical compounds, and most of these chemical families include a wide range of different substances, it is challenging to perform computational predictions on every exact chemical structures. To conduct feasible property calculations, we first need to select a set of representative chemicals, then use their molecular structures to perform predictions of interest. In this work, the representative chemicals are selected based on common compounds reported in literatures. Their structures then serve as inputs to the conductor-like screening model for real solvents for property calculations.

Since additives in plastic products typically consist of mixtures of structurally similar compounds, and many of these chemical families include a broad range of substances, performing computational predictions on every individual structure is impractical. To enable feasible property calculations, a representative set of chemicals must first be selected, which can then serve as the inputs to predictive models. In this work, representative chemicals are chosen based on commonly reported compounds in the literature. We then utilize the conductor-like screening model for real solvents (COSMO-RS) to predict miscibility, solubility, and partition coefficient as mentioned above.

Computational property predictions involve several steps. The selected molecular structures will first be used as inputs to density functional theory calculations to

obtain the screening charge density profiles. This step includes a geometry optimization in implicit water using the conductor-like polarizable continuum model and a single-point calculation in the infinite dielectric constant limit, and is performed with Gaussian 16 at the BVP86/TZVP/DGA1 level of theory[19]. Then COSMO-RS statistical thermodynamics calculations will use the screening charge densities to calculate the chemical potentials of the compounds [20]. Polymer solubilities, solvent miscibility, and contaminant partition coefficients were calculated via solid-liquid and liquid-liquid equilibrium calculations [21, 22]. All these COSMO-RS calculations were performed using the COSMOtherm 19 software with the BP\_TZVP\_19 parameterization [23].

## 5.3 Results and discussion

### 5.3.1 Case study: BFR removal from plastic products

Brominated flame retardants (BFRs) are synthetic chemicals widely used as additives in plastic materials, particularly in the electrical and electronic industries, to reduce product flammability. Exposure to BFRs has been associated with serious health concerns, including cancer, neurobehavioral disorders, and reproductive issues [10]. However, traditional recycling methods of these plastic products, such as mechanical recycling or incineration, are not able to separate BFRs from the target polymer resins, and may pose significant environmental and health risks by releasing hazardous halogenated compounds. In this section, we use computational methods to perform solvent screening and identify solvent candidates that can remove BFRs from common polymers in plastic materials. Figure 5.3 shows the BFRs and their chemical structures.



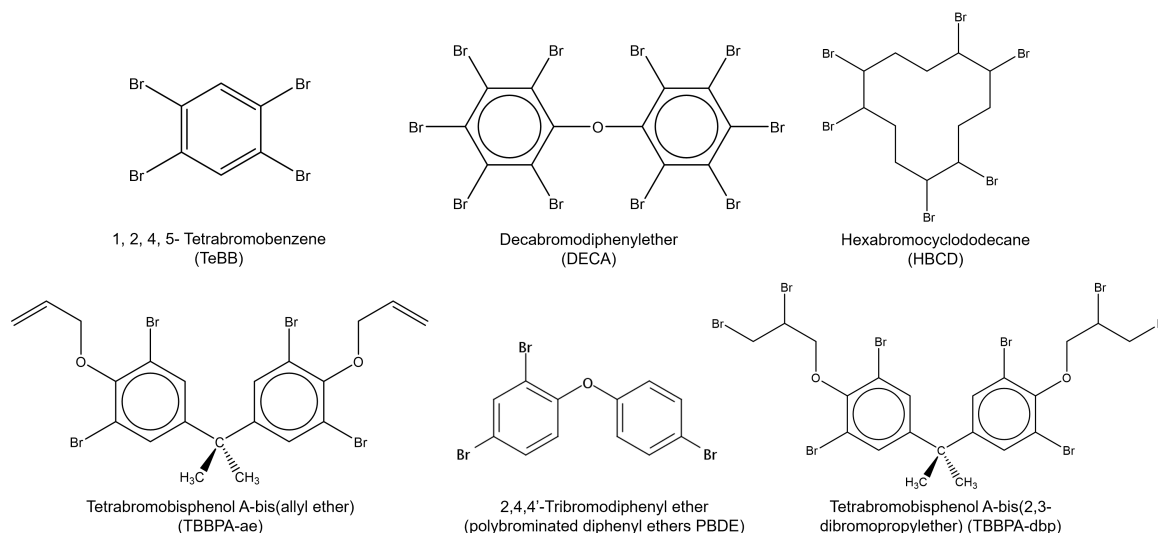


Figure 5.3: Chemical structures of some example brominated flame retardants.

Several studies have reported the experimental extraction and sorption of BFRs from some common polymers including polystyrene (PS), polypropylene (PP), and polyethylene terephthalate (PET) [24, 25]. Based on these BFRs and polymers, we conducted computational predictions on the partition coefficients of BFRs and solubilities of polymers in 60 common solvents and compare our prediction results with the experimental observations in the literatures. Table 5.1 presents data on the extraction of these BFRs from different polymers under specific conditions and compared literature experimental results with our computational log  $P$  predictions. Soxhlet extraction at 90°C was used for hexabromocyclododecane (HBCD) and tetrabromobisphenol A (TBBPA) derivatives in PS. The literature experiments showed limited extraction of HBCD from PS with a solvent mixture of toluene and 1-propanol. The positive log  $P$  values, however, suggest that this extraction should be feasible, which was not supported by the experiment. But the relatively low value (log  $P < 1$ ) indicate moderate extraction capability, which partially match the experimental outcome. All other results showed high consistency between computational predictions and experimental observations. Low extraction behavior of 1-propanol for removing TBBPA-bisallylether (TBBPA-ae) was captured by the negative value of log  $P$  prediction. Acetonitrile showed effective extraction for TBBPA-bis-(2,3-dibromopropylether) (TBBPA-dbp) in PS, aligning with its higher predicted log  $P$  values (2.6). For polybrominated diphenyl ethers (PBDE), four identified effective solvents with positive log  $P$  values were supported by sorption/desorption experiments at room temper-

ature. Overall, the data suggest that computational log P predictions reasonably correlate with experimental findings, highlighting the potential of computational guidance to solvent selection in BFR removal processes.

Table 5.1: Comparison of our log P calculation results and literature experiment observations of BFR removal from several different polymers. Red color indicate inconsistency between computational data and experimental results, green color means they align with each other.

BFR	Polymer	Condition	Technique	Solvents	
				Literature Experiments	Our logP prediction
HBCD	PS	90 °C	Soxhlet extraction	Toluene + 1-Propanol (Low extraction)	0.8, 0.2
TBBPA-ae	PS	90 °C	Soxhlet extraction	1-Propanol (Low extraction)	-0.8
TBBPA-dbp	PS	90 °C	Soxhlet extraction	Acetonitrile	2.6
	PET			Acetonitrile	1.1
Tri-PBDE	PE	RT	Sorption/Desorption	Toluene	1.4
	PS			EthylAcetate	1.1
	PP			Toluene	1.6

### 5.3.2 Case study: phthalates removal from PVC

Phthalates are a family of synthetic chemical compounds used in plastics, solvents, and personal care products. These colorless, odorless, and oily liquids have low volatility and do not chemically bind to the materials they are added to [26]. In plastic products, phthalates are widely used as plasticizers in the production of flexible and durable plastic materials, particularly polyvinyl chloride (PVC) [27]. By embedding themselves between polymer chains, phthalates reduce rigidity and enhance the flexibility, workability, and longevity of plastic products. In this section, we use computationally predicted properties to identify suitable solvents that can remove phthalates from PVC resins via the leaching process.

Since there are hundreds of different phthalate compounds, selecting a representative set of structures is essential for practical analysis and computational modeling. These representative phthalates were chosen based on their prevalence in commercial applications, structural diversity, and relevance to environmental and health concerns [13]. By focusing on a subset of commonly used phthalates, we can effectively predict their properties and interactions with plastic resins and in the meantime maintain the generalizability of the findings. Table 5.2 presented the eight selected phthalates for this study and their common applications in commercial products based on literatures [13, 28].

To identify suitable solvents that facilitate the leaching of phthalate, we performed COSMO-RS predictions on the following properties: partition coefficients of these phthalates in solvent phases versus PVC phase, miscibility of phthalates and the solvents, and PVC solubility at multiple temperatures in the solvents. A library of 60 common solvents were considered. Table 5.3 presented the computational prediction results for some solvent candidates. The ideal solvent should meet several standards of these properties. First, it should be miscible with all eight phthalate compounds considered. Second, all phthalates should have positive partition coefficient values for these solvents, and higher average values preferred. Additionally, we also require that PVC solubility at room temperature must be low in the solvent, but can be increased when temperature is elevated. This is to guarantee that PVC resins are not dissolved by the solvent, but can be swelled to enhance the contact between the solvent and the phthalates. Based on the prediction data, 9 solvents meet the  $\log P > 0$  and miscibility requirements: chloroform, tetrahydrofuran, tetrahydropyran, 2,3-dihydropyran, acetone, toluene, ethyl acetate, o-xylene, and diphenyl ether. Among these candidates, 3 solvents satisfy the PVC solubility requirements: toluene, o-xylene, and diphenyl ether. O-xylene was selected for experiments since it has a competitive mean  $\log P$  value (0.61) while keeps PVC solubility very low at room temperature.

Table 5.2: The phthalates considered in this work, and their applications in plastic products [28].

Phthalates	Usage
BBP butyl benzyl phthalate	Vinyl tiles, food conveyor belts, artificial leather, automotive trim, traffic cones
DBP di-n-butyl phthalate	PVC plastics, latex adhesives, cosmetics (most common phthalate added to nail polish), personal care products, cellulose plastics, solvent for dyes
DEHP di-(2-ethylhexyl) phthalate	Building products (wallpaper, wire and cable insulation), car products (vinyl upholstery, car seats), clothing (footwear, raincoats), food packaging, children's products (toys, grip bumpers), medical devices, most widely added phthalate to PVC to make products flexible
DEP diethyl phthalate	Personal care products, most common phthalate added to enhance fragrance, cosmetics.
DiDP di-isodecyl phthalate	PVC plastics, covering on wires and cables, artificial leather, toys, carpet backing, pool liners
DiNP di-isononyl phthalate	Garden hoses, pool liners, flooring tiles, tarps, toys (most common phthalate added as a softener in the manufacture of toys and childcare products - bath toys, drinking straws, and rubber ducks)
DnHP di-n-hexyl phthalate	Dipmolded products, tool handles, dish-washer baskets, flooring, vinyl gloves, flea collars, conveyer belts used in food processing
DnOP di-n-octyl phthalate	Garden hoses, pool liners, flooring tiles, tarps, seam cements, bottle cap liners, conveyor belts

Table 5.3: COSMO-RS prediction results for solvent screening of phthalates removal from PVC. The elevated temperature  $T_h$  is defined to be 1°C lower than the boiling point (BP) of the solvent, with an upper bound of 120°C.

Solvent	BP (°C)	Th (°C)	all logP > 0	mean logP	misci. w. phlts		PVC solub (wt%)	
					RT	Th	RT	Th
chloroform	61.1	60.1	yes	1.94	yes	yes	1.1	4.2
tetrahydrofuran	65	64.0	yes	1.21	yes	yes	8.9	19.1
tetrahydropyran	88	87.0	yes	0.99	yes	yes	3.9	17.9
2,3-dihydropyran	86	85.0	yes	0.88	yes	yes	1.9	13.6
acetone	56	55.0	yes	0.81	yes	yes	10.9	19.8
toluene	110.6	109.6	yes	0.72	yes	yes	0.7	14.8
ethyl acetate	77.1	76.1	yes	0.71	yes	yes	4.5	16.3
o-xylene	144.5	120.0	yes	0.61	yes	yes	0.5	15.5
triethylamine	89	88.0	no	0.38	yes	yes	0.5	4.7
diphenyl ether	258	120.0	yes	0.29	yes	yes	0.3	8.8
dimethyl sulfoxide	189	120.0	no	0.23	no	yes	8.4	33.2
hexane	68.7	67.7	no	-0.04	yes	yes	0.1	0.6
tert-butanol	82.4	81.4	no	-0.04	yes	yes	0.2	3.3
ethanol	78.2	77.2	no	-0.32	yes	yes	0.2	2.8
dodecane	216.3	120.0	no	-0.45	no	yes	0.0	2.0
acetic acid	117.9	116.9	no	-0.77	no	yes	0.1	5.2
ethylene glycol	197.3	120.0	no	-2.12	no	no	0.0	1.6
water	100	99.0	no	-8.02	no	no	0.0	0.0

To test and verify the phthalate removal ability of o-xylene from PVC resins, we conducted two sets of experiments on two different physical mixtures of PVC and phthalate. Sample 1 is a mixture of PVC powder and liquid butyl benzyl phthalate (BBP) with a mass ratio of 2.5:1. This ratio was determined based on the typical concentration of phthalate additives in industrial PVC materials [29]. The mixture was extruded and cut into short pieces. Sample 2 used the same mixture, but the

extruded material was hot pressed into a mold as an additional processing step. Both samples were placed in o-xylene in the leaching experiment, which include 3 steps. Step 1 and 2 are both 1-hour leaching at room temperature, step 3 is another 1 hour at 130°C.

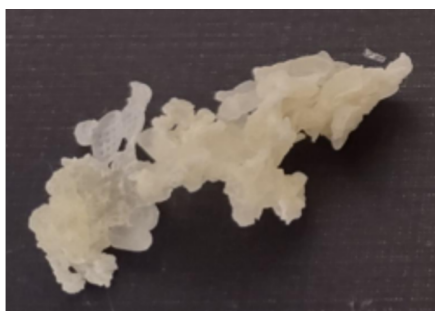
Sample 1



Sample 2



Before experiment



After experiment

Figure 5.4: Photos of the experimental material before and after the phthalate removal experiments. Sample 1 is an extruded material based on the mixture of PVC powder and liquid BBP. Sample 2 is the extruded material after an additional processing step of hot pressing.

Table 5.4 and 5.5 show the experimental measurement of released phthalate from the leaching experiments of sample 1 and sample 2 respectively. For sample 1, 89.1% of the phthalate was removed in the 3-hour experiment. Since sample 2 went through an additional processing step of hot pressing, only 75.2% was removed from the material. These results validated the ability of o-xylene of phthalate removal from PVC resins. Note that these experiments serve as proof of concept of the selected solvent and our computational methods, and the operation conditions such as time and temperature can be further investigated to improve the efficiency of the process.

Table 5.4: Experimental phthalate removal result for sample 1.

Step number	Phthalate (g)	Percent recovered
1	0.298	36.4%
2	0.160	19.6%
3	0.271	33.1%
Total	0.730	89.1%

Table 5.5: Experimental phthalate removal result for sample 2.

Step number	Phthalate (g)	Percent recovered
1	0.231	28.9%
2	0.107	13.4%
3	0.263	32.9%
Total	0.602	75.2%

### 5.3.3 Case study: PFAS removal from LDPE

Per- and polyfluoroalkyl substances (PFAS) are a diverse group of synthetic fluorinated compounds known for their remarkable stability, water and oil repellency, and

resistance to heat and chemical degradation [15]. These properties have made PFAS essential in applications such as nonstick cookware, waterproof fabrics, grease-resistant food packaging, and firefighting foams [16]. However, their strong carbon-fluorine bonds also make them highly persistent in the environment. Due to their bioaccumulative nature and potential health risks, PFAS contamination has become a significant global issue [16]. In this section, we use computational predictions to assist the design of PFAS removal process from plastic waste during recycling processes to avoid their reintroduction into the plastic packaging industry, particularly via post-consumer recycled resins [18].

Although thousands of PFAS have been identified by the US EPA [30], their detection via experimental approaches have been limited. However, the FDA have been successful at detecting 33 PFAS concentration levels in food samples purchased at grocery stores in the US [31, 32]. Therefore, in this work, we apply our contaminant removal strategy to this subset of PFAS to show the efficacy of our framework.

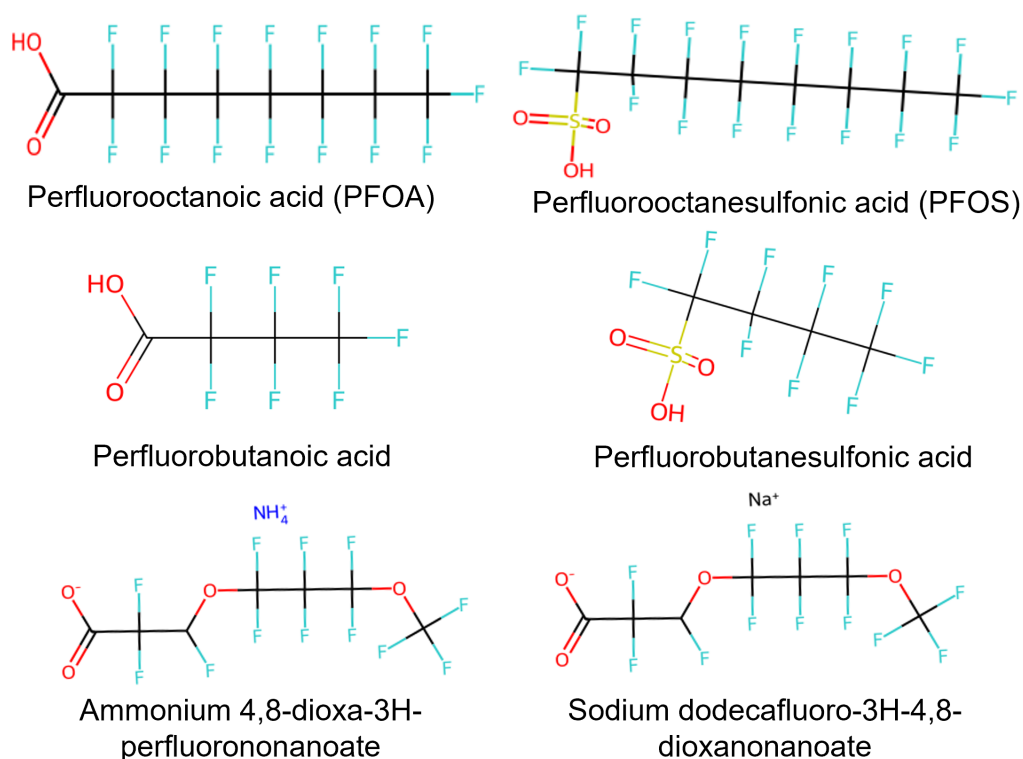


Figure 5.5: Examples of some PFAS compounds and their chemical structures



The 33 common PFAS identified by FDA and a library of 60 common solvents were considered. Figure 5.5 shows some example PFAS compounds and their chemical structures. Low-density polyethylene (LDPE) was selected as the reference polymer. We performed COSMO-RS predictions on the following properties: partition coefficients of these PFAS in solvent phases versus LDPE phase, miscibility of PFAS and the solvents, and LDPE solubility at multiple temperatures in the solvents. We require that the solvent must be miscible with all 33 PFAS, and their partition coefficient should also have  $\log P > 0$ . Besides, we also need LDPE solubility to be low at room temperature, but can be higher at an elevated temperature. We divided the 33 PFAS compounds into 4 different groups, and identified solvents that facilitate PFAS removal from LDPE resins. Table 5.6 shows the solvent screening and property calculation results. Tetrahydropyran (THP) was selected for group 1 and 2 as it has excellent mean  $\log P$  values while keeping LDPE solubility low at room temperatures. Toluene is the choice for group 2 and 3, since it satisfies positive  $\log P$  requirements and shows strong temperature dependence of LDPE solubility. This result can guide the experiment of PFAS removal from LDPE resins. Apart from the subset of PFAS identified by FDA, the entire PFAS family includes thousands of different substances. We have an ongoing research that considers 15000 PFAS compounds and aims to find selective solvents for them from a library of over 1000 solvents. The PFAS compounds were divided into 7 groups and solvent screening was performed. Some selected example results are presented in Table 5.7.

Table 5.6: Solvent screening result for the 4 groups of 33 PFAS identified by FDA.

Group	Number of PFAS	Identified solvent	Mean $\log P$	LDPE solubility at RT	LDPE solubility at Th
1	12	THP	4.9	0.1 wt%	7.3 wt% (64°C)
2	10	THP	5.1	0.1 wt%	7.3 wt% (64°C)
3	3	Toluene	0.9	0.1 wt%	22.6 wt% (109.6°C)
4	8	Toluene	0.8	0.1 wt%	22.6 wt% (109.6°C)

Table 5.7: Example results of solvent selection for a more general study that divided 15000 PFAS compounds into 7 groups.

Groups	Example representative PFAS	Examples of selective solvents
1	Perfluoropropyl hydrogen sulfate	THP
2	Hexafluorobenzene	Triethylamine, THP
3	2-(1,1,2,2-Tetrafluoroethoxy) naphthalene	n-methyl-2-pyrrolidinone, pyridine, naphthalene, acetylacetone, benzaldehyde
4	Ethyl 2,3,4,4,4-pentafluorobut-2-enoate	triethylamine, hexamethylphosphoramide, diglyme, isophorone, n-methyl-2-pyrrolidinone
5	2,2,3,3,4,4,4-Heptafluoro-N-undecylbutanamide	benzaldehyde, chlorobenzene, 1,4-dimethylbenzene, triethylamine, pyridine
6	2,3,5,6-tetrafluoropyridin-4-ol	Triethylamine, THP
7	1,1,1,3,3-Pentafluoropropane	cyclohexanol, chlorobenzene, acetylacetone, 1,4-dimethylbenzene, dipentene

### 5.3.4 Case study: ink removal from printed multilayer plastic films

In this section, STRAP was applied to a printed flexible multilayer plastic film to recover and produce transparent polymer resins after incorporating a deinking step. The target film is a post-industrial oriented polyester film composed of PE, EVOH, and PET with polyurethane (PU) inks (Figure 5.6). A challenge with this specific plastic waste feedstock is how and at what stage of the process should the ink components be removed. Different surfactant solutions and PU-selective solvents were considered to achieve the recovery of the polymer fractions without any coloration.

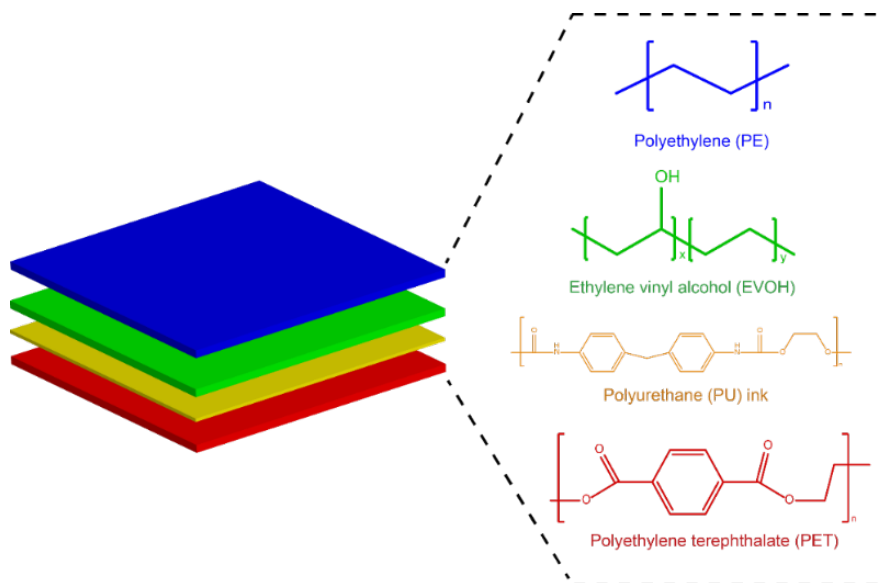


Figure 5.6: Simplified structure of a printed multilayer film composed of PE, EVOH, PET, and PU-based inks, manufactured by Amcor

Following our previous work, we used a combination of Hansen Solubility Parameters (HSPs) and the Conductor-like Screening Model for Real Solvents (COSMO-RS) to identify solvents for STRAP [33, 34, 35]. Figure 5.7 summarizes the computational tools used in this work. HSPs are three parameters associated with each compound (polymer or solvent) that account for dispersion, polar and hydrogen-bonding forces [36]. The values of these three parameters define the coordinates of a compound in HSP space. Each polymer has an additional radius parameter,  $R_0$ , that defines a sphere in HSP space, as shown in Figure 5.7(a). Only solvents with HSPs within this sphere (such that the distance in HSP space,  $R_a$ , between the polymer and solvent HSP values is less than  $R_0$ ) are expected to dissolve the polymer. Tabulated, experimentally determined HSP values for polymers and solvents were obtained from literature sources [36, 37, 38]. COSMO-RS uses statistical thermodynamic methods to compute the equilibrium properties of multicomponent systems based on the screening charge density that arises at each compound's molecular surface due to the polarization of the medium, as illustrated in Figure 5.7(b) [21]. Screening charge density profiles were obtained from density functional theory (DFT) calculations performed using Gaussian 16 at the BVP86/TZVP/DGA1 level of theory [19]. Screening charge densities were then used to predict polymer solubilities via a solid-liquid equilibrium calculation using the *COSMOtherm 19* software with the BP\_TZVP\_19

parameterization [35, 39, 22]. This solubility calculation requires the polymer melting temperature and an experimentally measured solubility in a reference solvent as input, which were obtained using data from our previous work [35].

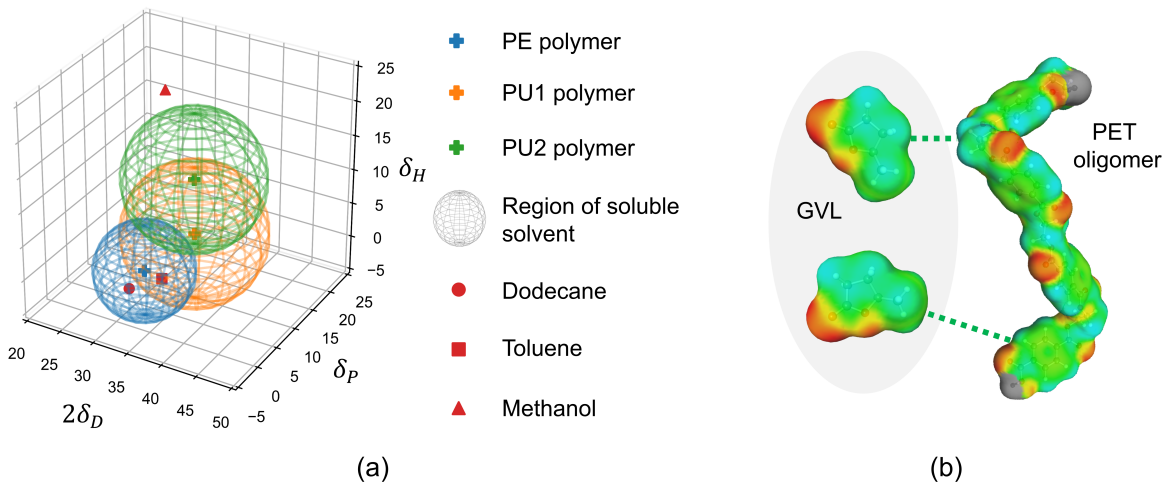


Figure 5.7: Computational methods used in this work. (a) Screening of PE-selective solvents in the presence of PU-based inks using HSPs. The HSPs for the PE polymer, two representative PU polymers, and 3 example solvents are indicated as points in HSP space, with the soluble regions for each polymer drawn as spheres centered on the corresponding polymer HSPs. Dodecane lies within the PE sphere but outside of the PU spheres and is thus predicted to be a selective solvent for PE. (b) COSMO-RS screening charge distributions (colored surfaces) of GVL and a PET oligomer. Oligomer molecules with end groups neglected (gray surface) are used to represent the chemical properties of longer polymer chains. The intermolecular interactions between polymers and solvents are quantified by the interaction of screening charges, as schematically indicated by dashed lines.

In our previous work, we successfully recovered the main constituent polymers (PE, EVOH, and PET) from a transparent multilayer film through a STRAP process in which PE was first dissolved by toluene, EVOH was dissolved by a DMSO/water mixture, and PET was recovered as the only remaining resin [34]. The printed film considered in this work consists of the same three polymers with an additional PU-based ink. Therefore, we sought to modify the prior STRAP process by using computational tools to identify new solvents that remain selective to the target polymers in the presence of the ink, as no ink removal was observed with different surfactant solutions.

The first step is to find a selective solvent for the PE component of the printed film. Since the specific molecular structure of the PU-based ink is unknown, we cannot directly predict ink solubility with molecular-scale modeling. Therefore, we first conducted quantitative solubility predictions using COSMO-RS for the three known polymers to identify potential selective solvents, then used qualitative HSP calculations to eliminate solvents likely to dissolve the PU-based ink. Table 5.8 shows predicted solubilities for PE, EVOH, and PET in 30 common solvents at elevated temperatures. We define PE-selective solvents as solvents with a predicted PE solubility greater than 10 wt% and predicted EVOH and PET solubilities that are each less than 5 wt%. Four PE-selective solvents were identified: toluene, dodecane, heptane, and diphenyl ether. Since information on the ink structure is limited, we collected HSP data for 11 different PU resins to determine the potential of these four solvents to dissolve the ink. Table 5.9 presents HSP data for these PU resins and the 4 solvents studied and Table 5.10 reports calculated values of  $R_a/R_0$ . Based on these data, toluene is predicted to dissolve ( $R_a/R_0 < 1$ ) 4 of the 11 PU resins and diphenyl ether is predicted to dissolve 7, whereas dodecane and heptane are not predicted to dissolve any of the PU resins. Therefore, dodecane and heptane are possible computationally identified PE-selective solvents for the printed film. Dodecane was finally selected for experiments since it has a higher predicted PE solubility than heptane. The selectivity of this solvent was verified experimentally.

The second step is to find an EVOH-selective solvent after PE dissolution. In our previous STRAP process, we used a mixture of 60% DMSO-40% water (v/v) to selectively dissolve EVOH but not PET [34]. We thus considered whether the ink will dissolve in this solvent system. HSP calculations were again performed for this solvent mixture and the 11 PU resins with results shown in Table 5.10. None of the 11 PU polymers are expected to dissolve in this solvent mixture. Therefore, the same 60% DMSO-40% water (v/v) solvent system was used in experiments and selective EVOH dissolution was observed.

The final step is to remove the PU-based ink from the remaining PET resin after PE and EVOH separation. We performed HSP calculations to identify solvents that could dissolve PU but not PET. Since the HSP data for the different PU resins varied substantially, we identified potential PU-selective solvents that are predicted to dissolve at least 5 of the 11 PU resins without dissolving PET. Table 5.11 shows HSP calculations for solvents that fit these criteria. Among these solvents, we noted GVL

as an appealing, biodegradable green solvent with low toxicity [40]. The  $R_a/R_0$  value of GVL to PET (1.02) is very close to 1, which indicates that it may dissolve PET at elevated temperatures. We thus computed temperature-dependent PET solubilities in GVL using COSMO-RS, as shown in Figure 5.8. Using a 5 wt% solubility threshold to distinguish good and poor solvents, we predict that the temperature should be below 125 °C to avoid substantial dissolution of PET in GVL. Experiments have verified that PET can dissolve in GVL above 165 °C but not at 125 °C, which aligns with our computational predictions.

Table 5.8 presents the COSMO-RS solubility predictions for PE, EVOH and PET in 30 common lab solvents. The temperature used for each prediction was determined by the solvent: the temperature was selected to be just below the boiling point of the solvent, but without exceeding 120 °C. This maximum value is to avoid melting or thermal degradation of the polymers. Bold solvents are identified as PE-selective, which are predicted to dissolve PE but not EVOH or PET.

Table 5.8: COSMO-RS solubility predictions for PE, EVOH and PET in 30 common solvents.

Solvent	T (°C)	EVOH solub (wt%)	PE solub (wt%)	PET solub (wt%)
methanol	63.6	0.8	0.1	0.0
dichloromethane	39.0	0.0	0.1	0.8
ethylene glycol	120.0	10.6	0.9	0.0
acetone	55.0	0.2	0.3	0.7
isopropanol	81.3	1.4	1.6	0.0
1-propanol	96.2	4.1	4.2	0.1
<b>toluene</b>	109.6	0.3	22.6	2.5
chloroform	60.1	0.0	0.6	1.0
tetrahydrofuran	64.0	0.9	1.7	0.8
tetrahydropyran	87.0	1.1	7.3	0.8
cyclohexane	79.7	0.0	6.9	0.0
<b>heptane</b>	97.5	0.0	15.3	0.0
triethylamine	88.0	7.7	8.7	0.0
1,2-propanediol	120.0	12.4	3.2	0.0
dimethyl sulfoxide	120.0	35.3	5.3	8.3
hexane	67.7	0.0	3.1	0.0
acetylacetone	120.0	6.6	8.2	2.0
tert-butanol	81.4	0.9	2.1	0.0
ethyl acetate	76.1	0.3	1.6	0.5
isopropylamine	30.7	11.7	0.1	0.0
<b>diphenyl ether</b>	120.0	0.4	18.5	1.4
<b>dodecane</b>	120.0	0.0	32.5	0.0
N,N-dimethylformamide	120.0	30.8	16.2	18.4
2,3-dihydropyran	85.0	0.1	5.0	0.7
methylacetate	55.8	0.1	0.3	0.2
ethanol	77.2	1.8	0.9	0.0
cyclohexanol	120.0	7.7	22.1	0.3
2-butanone	78.5	0.8	2.3	1.4
water	99.0	0.0	0.0	0.0
benzene	79.0	0.0	3.1	0.9

Table 5.9 shows the HSP data for selected solvents and polymers obtained from literature sources.<sup>3-4</sup> Note that the DMSO/water mixture has a composition of volume ratio 60%:40%, which is equivalent to a molar ratio of 27.56%:72.44%. The molar ratio was used to calculate HSP values.

Table 5.9: HSP data for some solvents, PET, and 11 PU polymers.

Compound	Dispersion	Polarity	Hydrogen bonding	$R_0$
toluene	18	1.4	2	\
dodecane	16	0	0	\
heptane	15.3	0	0	\
diphenyl ether	19.6	3.2	5.8	\
60% DMSO- 40% water (v/v)	16.3	16.1	33.5	\
GVL	15.5	4.7	6.6	\
PET polymer	18.7	6.3	6.7	6.5
	18.1	9.3	4.5	9.7
	17.9	6.9	3.7	2.7
	17.7	10.6	11.6	9.5
	19.1	12.2	9.9	8
	21.54	14.94	12.28	16.78
PU polymers	16	13.1	9.2	11.4
	20.6	7.8	11.6	13.1
	19.4	7.4	6	9.8
	17.9	9.6	5.9	8.2
	18.7	9.6	9.9	8.2
	19.9	8.1	6	9.8

Table 5.10 shows the calculated values of  $R_a/R_0$  for the solvent systems and 11 different PU polymers. If the value of  $R_a/R_0$  is larger than 1, the solvent should not dissolve the polymer; if it is less than 1 (indicated by bold values in the table),



the solvent can dissolve the polymer. In this table, toluene, diphenyl ether and GVL are predicted to dissolve some PU polymers, while dodecane, heptane and the DMSO/water mixture are not predicted to dissolve any PU polymers. This DMSO/water mixture is the same system as that in Table 5.9.

Table 5.10: HSP calculations for some solvents and 11 PU resins

Solvent	toluene	dodecane	heptane	diphenyl ether	DMSO/water mixture
$R_a/R_0$ for 11 PU	<b>0.85</b>	1.15	1.21	<b>0.71</b>	3.09
	2.13	3.22	3.48	2.02	11.60
	1.40	1.69	1.73	1.07	2.39
	1.70	2.11	2.18	1.24	3.07
	1.10	1.33	1.37	<b>0.83</b>	1.41
	1.26	1.40	1.41	1.11	2.14
	<b>0.97</b>	1.28	1.34	<b>0.59</b>	1.90
	<b>0.79</b>	1.19	1.28	<b>0.43</b>	3.01
	1.11	1.45	1.51	<b>0.88</b>	3.47
	1.40	1.81	1.88	<b>0.95</b>	3.04
	<b>0.89</b>	1.30	1.39	<b>0.50</b>	3.01

Table 5.11: HSP calculations for solvents considered for ink removal from PET

Solvent	$R_a/R_0$ to PET	$R_a/R_0$ to 11 PU											
acetone	1.17	0.61	2.52	0.67	1.00	0.83	0.32	0.88	0.86	0.61	0.86	0.93	
DMSO	1.65	0.94	4.28	0.65	0.55	0.40	0.52	0.75	1.03	0.99	0.83	1.00	
DMF	1.40	0.85	3.80	0.33	0.50	0.50	0.31	0.66	0.93	0.84	0.62	0.94	
cyclohexanol	1.17	1.08	3.79	0.72	1.19	0.82	0.91	0.58	0.93	1.15	0.86	1.01	
GVL	1.02	0.75	2.23	0.94	1.36	1.00	0.78	0.90	0.84	0.84	1.06	0.96	

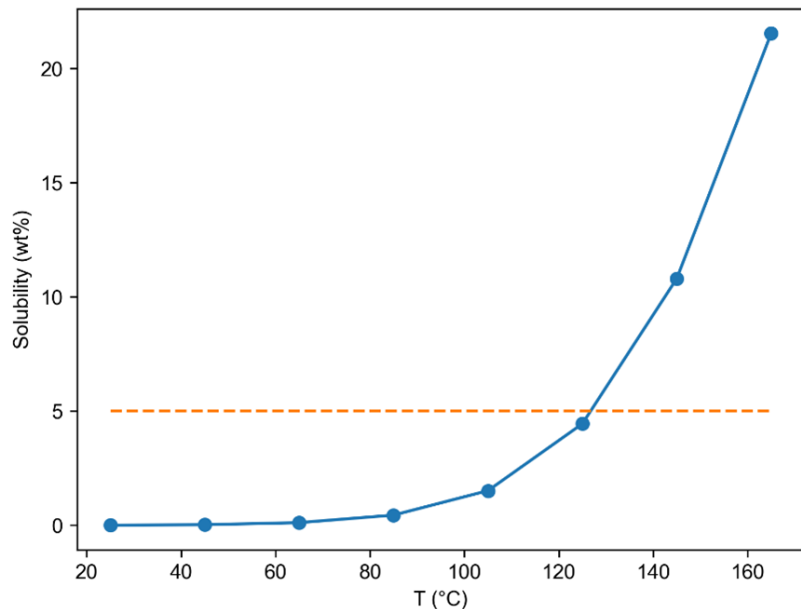


Figure 5.8: Temperature-dependent solubility prediction of PET in GVL. Dashed line is the dividing value to distinguish between a good solvent and a poor solvent (5 wt%).

The flexible printed multilayer film composed of PE, EVOH, PET, and PU-based inks was processed through STRAP to recover all polymer components. Table 5.12 discloses the yield of each component, including the ink residue (black and white) recovered after the ink removal step. Figure 5.9 shows solvents, temperatures, and dissolution times for each step. In our approach, the PE and EVOH are dissolved and recovered, leaving the PET and ink components behind. This was done to minimize coloration of the PE and EVOH streams by carrying out the ink removal step for the PET at the end. Polymer precipitation was achieved by reducing the solvent temperature and not by the addition of antisolvents. In our previous work this was demonstrated to be beneficial both economically and environmentally [34]. Due to the high percentage of PE in the printed film, an additional PE dissolution step was required to recover most of the polymer and clean out the experimental set up. This additional PE dissolution step was done in every experiment in Table 5.12, which allowed for an average PE yield of  $61.78\% \pm 1.74\%$ . As seen in Table 5.12, the overall mass balance from the STRAP experiments was  $88.66 \pm 0.53$  wt%. We found that the material that was not recovered after STRAP was left behind in our equipment, mostly in the round bottom flasks and filters. The overall mass balance improved

when accounting for the material lost in the equipment which was around 8 wt% of the plastic feed. Furthermore, part of the ink (mostly yellow color) can be recovered via distillation of the GVL, around 3 wt% (Table S6). The overall mass balance can be near 100 wt% of the starting material, considering the average recovery of PE, EVOH, and PET presented in Table 5.12. This gives indication that when dealing with flexible plastics that have been shredded, material will be left behind in the equipment which should be considered when thinking about larger scale systems. Furthermore, it was challenging for us to predict and measure consistent amounts of material lost in the equipment, since it depends on multiple factors like plastic size, stirring rates, and it is subject to however the material is handled by the person conducting the batch experiment.

Table 5.12: Yield of components from a printed multilayer film with the STRAP process. The component yields are the recovered mass of each component divided by the multilayer feed mass in each experiment. The overall mass balance can be improved to near 100 wt% when accounting for material left in the equipment and residual ink in the deinking solvent.

Experiment	Component Yield (wt%)				Overall Mass Balance (wt%)
	PE	EVOH	PET	Black and White Ink Residue	
1	59.82%	7.70%	19.80%	1.36%	88.66%
2	62.36%	6.94%	17.55%	2.13%	88.98%
3	63.15%	7.74%	18.20%	0.61%	89.70%
Average	61.78%	7.46%	18.52%	1.36%	88.66%
STDEV	1.74%	0.45%	1.16%	0.76%	0.53%

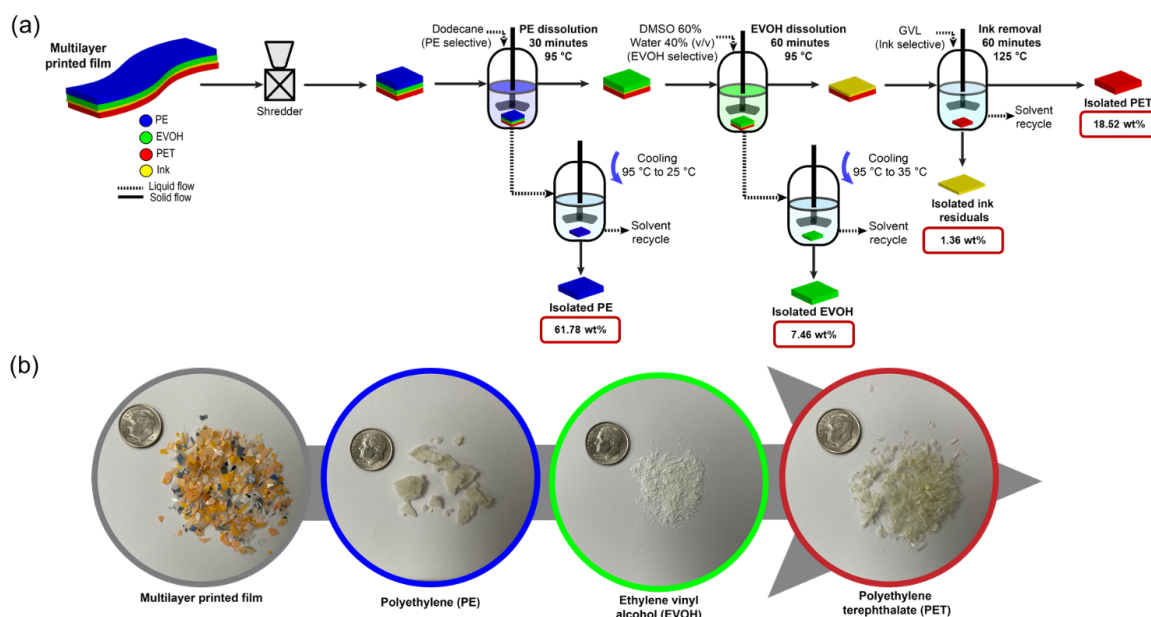


Figure 5.9: (a) Solvent-targeted recovery and precipitation (STRAP) of a printed multilayer film composed of PE, EVOH, PET, and PU-based inks, (b) Photos of each polymer after the STRAP process.

The main colors in the PU inks were black, white, and yellow. PUs are commonly used as adhesives in multilayer packaging materials and as binders in printing inks for plastic substrates [41, 42]. The ink separation step uses GVL, which is a PU and PET-selective solvent, as it was determined with our computational predictions. The PET was not dissolved in the ink removal step since the temperature was 125 °C and PET has a measured experimental solubility of 0.025 wt% at this temperature. Under these conditions, deinking was observed for all colors (Figure 5.10). White and black ink components were dispersed in the GVL after the deinking time was completed, while the yellow component was dissolved (Figure 5.10). It was observed that deinking of the PET improved with time and sequential deinking steps, with optimal removal taking up to 2 to 3 hours. According to a recent study, at 125 °C PET swelling occurs [43] which could play a role in the release of white and black ink components since a dissolution of those colors was not observed. The white and black pigment residues were recovered by filtration and the dissolved yellow ink residues were recovered by distillation of the GVL.

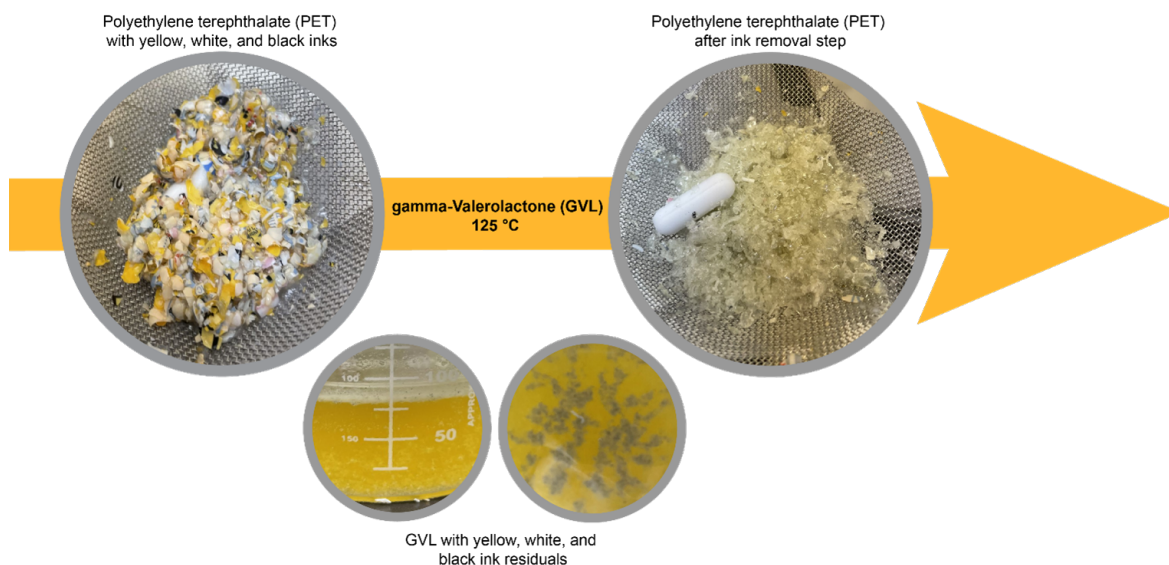


Figure 5.10: STRAP deinking step with gamma-valerolactone (GVL) to separate white, black, and yellow ink from PET of a printed multilayer film.

In ink formulations, inorganic and/or organic pigments are used. For example, in a white ink, titanium dioxide ( $\text{TiO}_2$ ) pigment is commonly used. Researchers have disclosed the use of o-dichlorobenzene and o-xylene to remove  $\text{TiO}_2$  from PE, but they were only able to remove 15% of the colorant [44]. Some of the solvents that have been used to target colors and pigments have been organic solvents and some have been chlorinated compounds, which raises concerns about toxicity, safe handling, and environmental impact [45, 46]. In our study, we have been able to demonstrate the use of a green solvent, GVL, to efficiently clean PET from black, white, and yellow ink; this by using a combination of dissolution and ink dispersion in the solvent.

## 5.4 Summary

The removal of contaminants from plastic products is a critical challenge for improving plastic recycling efficiency and ensuring the safety of recycled materials. We have developed computational approaches for predicting polymer solubility and guiding solvent selection to facilitate contaminant removal. By leveraging molecular models, it is possible to identify suitable solvents that selectively dissolve target additives and recover high-quality target polymer resins. The research presented in this chapter focused on using computational property prediction as a powerful tool for designing

more effective and sustainable recycling processes. Specifically, the application of solubility models and solvent screening techniques can optimize dissolution-based recycling, leading to higher-purity recovered polymers and reduced environmental impact. Case studies on the removal of brominated flame retardants (BFRs), phthalates, PFAS, and pigments demonstrate the versatility of this approach across different contaminant classes. A STRAP process with ink removal to recover the constituent polymers of a printed flexible multilayer plastic film was also presented. The deinking step removed all colors and obtain clear PE, EVOH, and PET that could be recycled for different applications. The computational modeling tools allowed for the selection of polymer-selective solvents in the presence of the inks and for the selection of solvents to develop an ink removal step. By combining computational tools with experiments, this research paves the way for more efficient contaminant removal strategies in plastic recycling processes, promoting a circular economy for plastic materials. Moving forward, further integration of computational modeling with experimental validation will enhance the predictive accuracy of solubility models and expand their applicability to a wider range of plastic waste streams. Other additive compounds in plastic products (such as stabilizers, plasticizers, modifiers, pigments, fillers, and processing aids) can also be taken into consideration with a similar approach.

## 5.5 References

- [1] Geoffrey Pritchard. *Plastics additives: an AZ reference*, volume 1. Springer Science & Business Media, 2012.
- [2] Rudolph D Deanin. Additives in plastics. *Environmental health perspectives*, 11:35–39, 1975.
- [3] George Wypych. *Handbook of plasticizers*. ChemTec Publishing, 2004.
- [4] Norman S Allen and Michele Edge. Perspectives on additives for polymers. 1. aspects of stabilization. *Journal of Vinyl and Additive Technology*, 27(1):5–27, 2021.
- [5] M Wensing, E Uhde, and T Salthammer. Plastics additives in the indoor environment—flame retardants and plasticizers. *Science of the total environment*, 339(1-3):19–40, 2005.

- [6] Marino Xanthos. *Functional fillers for plastics*. John Wiley & Sons, 2010.
- [7] Robert A Charvat. *Coloring of plastics: Fundamentals*. John Wiley & Sons, 2003.
- [8] Niall D'arcy. Antimicrobials in plastics: a global review. *Plastics, Additives and Compounding*, 3(12):12–15, 2001.
- [9] George Wypych and Jurgen Pionteck. *Handbook of antistatics*. Elsevier, 2016.
- [10] Isao Watanabe and Shin-ichi Sakai. Environmental release and behavior of brominated flame retardants. *Environment international*, 29(6):665–682, 2003.
- [11] Linda S Birnbaum and Daniele F Staskal. Brominated flame retardants: cause for concern? *Environmental health perspectives*, 112(1):9–17, 2004.
- [12] AP Tüzüm Demir and S Ulutan. Migration of phthalate and non-phthalate plasticizers out of plasticized pvc films into air. *Journal of applied polymer science*, 128(3):1948–1961, 2013.
- [13] Alireza Afshari, Lars Gunnarsen, Per Axel Clausen, and V Hansen. Emission of phthalates from pvc and other materials. *Indoor air*, 14(2), 2004.
- [14] Leonard G Krauskopf. How about alternatives to phthalate plasticizers? *Journal of vinyl and additive technology*, 9(4):159–171, 2003.
- [15] Juliane Glüge, Martin Scheringer, Ian T Cousins, Jamie C DeWitt, Gretta Goldenman, Dorte Herzke, Rainer Lohmann, Carla A Ng, Xenia Trier, and Zhanyun Wang. An overview of the uses of per-and polyfluoroalkyl substances (pfas). *Environmental Science: Processes & Impacts*, 22(12):2345–2373, 2020.
- [16] Ziyad Abunada, Motasem YD Alazaiza, and Mohammed JK Bashir. An overview of per-and polyfluoroalkyl substances (pfas) in the environment: Source, fate, risk and regulations. *Water*, 12(12):3590, 2020.
- [17] Zhiming Zhang, Dibyendu Sarkar, Jayanta Kumar Biswas, and Rupali Datta. Biodegradation of per-and polyfluoroalkyl substances (pfas): A review. *Biore-source technology*, 344:126223, 2022.
- [18] Erica Gagliano, Massimiliano Sgroi, Pietro P Falciglia, Federico GA Vagliasindi, and Paolo Roccaro. Removal of poly-and perfluoroalkyl substances (pfas) from

water by adsorption: Role of pfas chain length, effect of organic matter and challenges in adsorbent regeneration. *Water research*, 171:115381, 2020.

- [19] MJ Frisch, GW Trucks, HB Schlegel, GE Scuseria, MA Robb, JR Cheeseman, G Scalmani, VPGA Barone, GA Petersson, HJRA Nakatsuji, et al. Gaussian 16 revision c. 01, 2016. *Gaussian Inc. Wallingford CT*, 1:572, 2016.
- [20] Andreas Klamt and GJGJ Schüürmann. Cosmo: a new approach to dielectric screening in solvents with explicit expressions for the screening energy and its gradient. *Journal of the Chemical Society, Perkin Transactions 2*, (5):799–805, 1993.
- [21] Andreas Klamt. Conductor-like screening model for real solvents: a new approach to the quantitative calculation of solvation phenomena. *The Journal of Physical Chemistry*, 99(7):2224–2235, 1995.
- [22] Andreas Klamt, Frank Eckert, Martin Hornig, Michael E Beck, and Thorsten Bürger. Prediction of aqueous solubility of drugs and pesticides with cosmo-rs. *Journal of computational chemistry*, 23(2):275–281, 2002.
- [23] Andreas Klamt, Volker Jonas, Thorsten Bürger, and John CW Lohrenz. Refinement and parametrization of cosmo-rs. *The Journal of Physical Chemistry A*, 102(26):5074–5085, 1998.
- [24] Abdel mnim Altwaiq, Marion Wolf, and Rudi Van Eldik. Extraction of brominated flame retardants from polymeric waste material using different solvents and supercritical carbon dioxide. *Analytica Chimica Acta*, 491(1):111–123, 2003.
- [25] M Singla, J Díaz, F Broto-Puig, and S Borrós. Sorption and release process of polybrominated diphenyl ethers (pbdes) from different composition microplastics in aqueous medium: Solubility parameter approach. *Environmental pollution*, 262:114377, 2020.
- [26] Russ Hauser and AM Calafat. Phthalates and human health. *Occupational and environmental medicine*, 62(11):806–818, 2005.
- [27] Ursel Heudorf, Volker Mersch-Sundermann, and Jürgen Angerer. Phthalates: toxicology and exposure. *International journal of hygiene and environmental health*, 210(5):623–634, 2007.



- [28] Yufei Wang and Haifeng Qian. Phthalates and their impacts on human health. In *Healthcare*, volume 9, page 603. Multidisciplinary Digital Publishing Institute, 2021.
- [29] Charlotte Henkel, Thorsten Hüffer, and Thilo Hofmann. The leaching of phthalates from pvc can be determined with an infinite sink approach. *MethodsX*, 6:2729–2734, 2019.
- [30] United States Environmental Protection Agency. Pfas strategic roadmap: Epa’s commitments to action 2021–2024. *Environmental Protection Agency*, 20460, 2021.
- [31] Susan Genualdi, Jessica Beekman, Katherine Carlos, Christine M Fisher, Wendy Young, Lowri DeJager, and Timothy Begley. Analysis of per-and poly-fluoroalkyl substances (pfas) in processed foods from fda’s total diet study. *Analytical and bioanalytical chemistry*, 414(3):1189–1199, 2022.
- [32] Susan Genualdi, Wendy Young, Lowri DeJager, and Timothy Begley. Method development and validation of per-and polyfluoroalkyl substances in foods from fda’s total diet study program. *Journal of Agricultural and Food Chemistry*, 69(20):5599–5606, 2021.
- [33] Theodore W Walker, Nathan Frelka, Zhizhang Shen, Alex K Chew, Jesse Banick, Steven Grey, Min Soo Kim, James A Dumesic, Reid C Van Lehn, and George W Huber. Recycling of multilayer plastic packaging materials by solvent-targeted recovery and precipitation. *Science advances*, 6(47):eaba7599, 2020.
- [34] Kevin L Sánchez-Rivera, Panzheng Zhou, Min Soo Kim, Leonardo D González Chávez, Steve Grey, Kevin Nelson, Shao-Chun Wang, Ive Hermans, Victor M Zavala, Reid C Van Lehn, et al. Reducing antisolvent use in the strap process by enabling a temperature-controlled polymer dissolution and precipitation for the recycling of multilayer plastic films. *ChemSusChem*, 14(19):4317–4329, 2021.
- [35] Panzheng Zhou, Kevin L Sánchez-Rivera, George W Huber, and Reid C Van Lehn. Computational approach for rapidly predicting temperature-dependent polymer solubilities using molecular-scale models. *ChemSusChem*, 14(19):4307–4316, 2021.

- [36] Charles M Hansen. *Hansen solubility parameters: a user's handbook*. CRC press, 2007.
- [37] Muhammad Azam Rasool and Ivo FJ Vankelecom.  $\gamma$ -valerolactone as bio-based solvent for nanofiltration membrane preparation. *Membranes*, 11(6):418, 2021.
- [38] Steven Abbott and Charles M Hansen. *Hansen solubility parameters in practice*. Hansen-Solubility, 2008.
- [39] Frank Eckert and Andreas Klamt. Fast solvent screening via quantum chemistry: Cosmo-rs approach. *AIChE Journal*, 48(2):369–385, 2002.
- [40] Florian Kerkel, Marta Markiewicz, Stefan Stolte, Eva Müller, and Werner Kunz. The green platform molecule gamma-valerolactone—ecotoxicity, biodegradability, solvent properties, and potential applications. *Green Chemistry*, 23(8):2962–2976, 2021.
- [41] J Sutter, V Dudler, and R Meuwly. Packaging materials 8. printing inks for food packaging composition and properties of printing ink. *ILSI Europe Report Series*, 2011.
- [42] John Dixon. *Packaging materials: 9. multilayer packaging for food and beverages*. 2011.
- [43] Wenjun Chen, Yuechao Yang, Xue Lan, Baolong Zhang, Xiaogang Zhang, and Tiancheng Mu. Biomass-derived  $\gamma$ -valerolactone: efficient dissolution and accelerated alkaline hydrolysis of polyethylene terephthalate. *Green Chemistry*, 23(11):4065–4073, 2021.
- [44] T Vuorinen, H Joki, and O Härkki. Report: Colour removal from recycled plastics. *VTT Technical Research Centre of Finland: Espoo, Finland*, 2016.
- [45] Ana M Ferreira, Isa Sucena, Vanessa Otero, Eva Mariasole Angelin, Maria João Melo, and João AP Coutinho. Pretreatment of plastic waste: Removal of colorants from hdpe using biosolvents. *Molecules*, 27(1):98, 2021.
- [46] MC Garrigós, F Reche, ML Marin, K Pernias, and A Jiménez. Optimization of the extraction of azo colorants used in toy products. *Journal of Chromatography A*, 963(1-2):427–433, 2002.

## Chapter 6

# Conclusion and future research

In this chapter, we summarize the key contributions of the studies described before, and provide a detailed discussion on potential research directions that can further extend and improve these projects.

### 6.1 Contributions

*A joint computational and experimental workflow for temperature-dependent polymer solubility predictions in various solvent systems.* We developed a computational polymer solubility prediction workflow that combines a series of computational approaches including molecular dynamics (MD) simulations, conformational sampling, density functional theory calculations, and the conductor-like screening model for real solvents (COSMO-RS). We incorporated experimental reference inputs to perform model calibrations and validations, thus achieved rapid and reliable calculations. This workflow has filled the research gap of quantitative solubility predictions for polymers.

*Establishment of a large-scale computational polymer solubility database.* Based on the joint workflow, a polymer solubility database that includes 11 common polymers in the packaging industry and 1007 solvents have been established. The solubility prediction data has guided and assisted the design of several lab-scale experiments that successfully separated and recycled post-industrial multilayer plastic films. A computational tool of efficient solvent screening for selective polymer dissolutions was developed based on the database. This solubility database is also made publicly accessible online.

*A fast computational framework for the design and optimization of dissolution-based plastic recycling processes.* We combined the polymer solubility database, solvent screening tool, process simulation models, techno-economic analysis, and life-cycle assessment to develop this computational framework that is capable of testing different polymer separation sequences and solvent selections. It can provide suggestions on favorable processes and offer numerical metrics on the economics and environmental impacts of the proposed processes.

*Development of new plastic recycling processes on real-world commercial products.* We have demonstrated the application of our computational tools to develop experimental recycling of several post-industrial multilayer plastic films. We also showed successful separation and recovery of pure polymer resins from mixed plastic waste that was composed of up to ten polymers. We also applied our computational models and proved novel feasible methods on contaminant removal of recycled plastic products.

## 6.2 Future research directions

### 6.2.1 Improvement and extension of current property prediction workflow for polymer-solvent systems

Our current joint computational and experimental workflow for polymer solubility prediction can be further improved and extended in the following several aspects: (1) to include more polymers and solvents; (2) to consider other compounds in dissolution-based plastic recycling processes, such as additives, pigments, and contaminants; (3) to consider properties other than just solubility; (4) to develop better prediction models with higher accuracy and deeper understanding of resin-specific properties.

The current established polymer solubility database includes 11 common polymers in the packaging industry and 1007 solvents. Apart from the packaging industry, other industrially relevant polymers and biopolymers such as lignin that must be solubilized prior to depolymerization can also be considered.

In the previous chapter, we have discussed contaminant removal methods that involve BFR, phthalates, PFAS, and PU-based printed ink. More generally, other additive compounds in plastic products could also be considered in similar approaches. A more comprehensive study on different types of additive molecules should include

flame retardants, plasticizers, stabilizers, modifiers, pigments, fillers, antistatic agents and processing aids [1]. These additives are often large families of many different chemicals, their property studies will require not only molecular-scale models, but also group-based classification and prediction methods.

Other directions include solution properties other than solubility, such as viscosity, that will influence the design of solvent-mediated recycling methods [2]. For example, thermodynamic models to understand solubility are also useful for understanding the thermodynamics of precipitation as a method to recover dissolved polymer resins from solution. However, polymer crystallization during precipitation depends upon the thermodynamics of nucleation, which remains challenging to predict [3]. The kinetics of polymer crystallization during precipitation can likewise greatly affect the properties of the recycled materials. For example, crystallization temperature, cooling rate, and the application of high shear strain are typical factors to control the crystal structure and morphology of polymers [3]. Therefore, both thermodynamic and kinetic factors need to be considered in process design.

Another challenge is to treat variations in polymer solubility associated with molecular weight, crystallinity, and other resin-specific properties [4]. More complicated polymers will have additional parameters to consider. For example, copolymers may have different monomer ratios and structural arrangements (block/alternating/random copolymers). Polymers that have chiral carbons in its repeating units will have different tacticities (isotactic/syndiotactic/atactic polymers) that can affect polymer properties. Integration of these parameters into our models will not only improve the accuracy and applicability of our computational methods, but also help to understand different factors that could affect polymer-solvent interactions. This will also benefit the manufacturing of recycled plastic products, as rheological and thermal behaviors of the products are also often related to these parameters [5].

Since the thermodynamic properties of solvents, polymers, and impurities largely influence the operating conditions of the recycling process and its overall economic and environmental performance, another important challenge is the co-design of solvents and of the recycling process, particularly when diverse polymers and impurities are present in the input waste feedstock [6].

### 6.2.2 Identification of green alternative solvents for solvent-mediated processes

The solubility prediction model and polymer solubility data can be combined with toxicity assessment of solvent candidates to look for green solvents as alternatives to current existing processes. This is not limited to dissolution-based plastic recycling processes, but to more general chemical processes that involve polymer-solvent systems.

Green solvents reported in the literature include switchable hydrophilicity solvents [7, 8, 9], ionic liquids [10], natural eutectic solvents [11], supercritical fluids [12], and organic solvents from natural sources [13]. However, the lack of physics-based solubility predictive models for these solvents places a limitation on their application. A comprehensive framework that screens solvents based on solubility, toxicity, environmental impact, government regulations, and costs is lacking in the literature. Also, more detailed tradeoff analysis between environmental impact and cost associated with solvent choice is needed.

Solvents' octanol-water partition coefficient ( $\log P$ ) is a key indicator of solvent toxicity, reflecting the bioaccumulation tendencies [14]. It represents the equilibrium ratio of a chemical's concentration in octanol (hydrophobic or non-polar phase) and water (hydrophilic or polar phase) [15]. Multiple models exist regarding the prediction of this property: the quantitative structure-retention relationship models [16], the solvation model based on electronic density and COSMO-RS methods [17], and physics-informed machine learning models [18].

Apart from toxicity properties, there are many systematic guides on the evaluation of green solvents. The pharmaceutical industry has actively sought green solvents for industrial purposes based on such quantitative metrics. Notable guides for solvent selection include the GlaxoSmithKline (GSK) [19], the ACS Green Chemistry Institute Pharmaceutical Roundtable (ACS GCI-PR) [20], and the AstraZeneca (AZ) [21]. The GSK guideline categorizes 111 solvents under six categories, with an additional one for legislative restrictions. AZ and ACS GCI-PR rank 46 and 63 solvents on a scale of 1 to 10, focusing on Health, Safety, and Environment (HSE) metrics.

Similarly, governmental regulatory bodies, such as the EU's Registration, Evaluation, Authorization, and Restriction of Chemical Regulation (REACH) initiative and the US EPA through the Toxic Substance Control Act (TSCA), aim to regulate toxic solvents to protect human health and the environment [22, 23, 24]. For instance,

the REACH restricts both common and uncommon chemicals, including benzene and toluene. The TSCA empowers the EPA to demand full disclosure of processes related to the use of chemical substances contained in the restricted list of chemicals. Additionally, frameworks like the Chemical Hazards and Toxic Substances (OCHA) framework strive towards similar goals, but rather than enforcing restrictions on chemicals; they focus on implementing operational standards for safe handling of chemicals.

As described above, there are plenty of resources on solvent toxicity assessment that could be integrated into our solvent screening workflows. A systematic approach that combines the data from these different resources and provide suggestions based on both dissolution preference and toxicity requirement of the process is needed.

### **6.2.3 Computational tool development for all-atom MD simulations of complex polymers**

Due to the large molecular size of polymer chains, MD simulations of polymers also employ coarse-grained models. However, the computational workflows developed in this work require MD simulations of polymer-solvent system to provide exact all-atom information of the molecules as the input to DFT and COSMO-RS calculations. To facilitate large-scale calculations of polymer solubilities in various solvents, simplified models have been utilized to approximate polymer molecule behavior in solution systems [25]. For example, short oligomers with terminal groups deactivated were used to represent much longer polymer chains, which is based on the hypothesis that multiple oligomers' COSMO-RS screening charge distribution profiles can reflect the actual distribution profile of a polymer [26]. However, many related work were needed to support such modeling. The conformational sampling methods and prediction convergence study presented in previous chapters were both used to connect oligomer models with polymer behaviors.

As computing technology advances, there are more studies that use all-atom MD simulations for polymers in recent years [27, 28, 29]. All-atom MD simulations for large polymers may help us understand the effects of molecular weight, crystallinity, and concentration on polymer-solvent interactions. For more complicated polymers, such as copolymers and tactic polymers, all-atom simulations can also help to study how monomer ratios, arrangements, and tacticity may affect the properties of the molecule.

Current computational tools that can prepare molecular topologies and initial configurations for polymers often have many limitations. For example, CHARM-GUI polymer builder can build polymer molecules with pre-defined monomer units, but it is only applicable to default structures within its database [30]; PolyParGen can divide large molecules into substructures and combine them to obtain the simulation files for the whole molecules, but it is only limited to OPLS-AA and AMBER force fields [31]; pyPolyBuilder is able to build topologies and initial configurations of arbitrary supramolecules based on their constituent building blocks, but it is based on GROMOS united atom force field [32]; HTPolyNet is a Python package to generate all-atom realizations of amorphous crosslinked polymers, but it is only designed for General Amber Force Field [33]. Therefore, a more general computational tool for polymer topology preparation is needed.

#### **6.2.4 Supercritical fluids as tunable solvents and pressure effect on polymer-solvent interactions**

Although a lot of different temperatures have been considered, most systems we studied in this work are at ambient pressure. Thermodynamically, an important factor that influences both  $\Delta H_{\text{mix}}$  and  $\Delta S_{\text{mix}}$  is solvent density [34, 35]. In a homogeneous solution, the contribution of pairwise interactions to  $\Delta H_{\text{mix}}$  is roughly proportional to density, which approximately determines the number of interactions per volume. Increasing solvent density for a system with favorable polymer-solvent interactions can thus increase polymer solubility [35]. However, if there are large differences in the densities of the solvent and polymer, the corresponding change in volume upon mixing also contributes to  $\Delta S_{\text{mix}}$  [34]. Unlike the combinatorial entropy, which always promotes mixing, the noncombinatorial contribution to the entropy of mixing due to this density difference disfavors mixing by reducing the entropy of the lower-density (typically solvent) component. This behavior leads to phase separation at temperatures above the lower-critical solution temperature; at high temperatures, the solvent density decreases to a much greater degree than the polymer density and the noncombinatorial entropy is highly unfavorable. The impact of solvent density on polymer solubility has motivated interest in supercritical fluids as solvents for polymer dissolution [36]. Unlike normal solvents, which are nearly incompressible, the density of a supercritical fluid can vary from gas-like to liquid-like by manipulating the pressure. Increasing the pressure of a supercritical fluid such that its density



approaches that of a target polymer will drive dissolution by reducing the unfavorable noncombinatorial entropy [35]. Pressure variations can also lead to differences in solubility for polymers with similar chemical properties but distinct densities (*e.g.*, low vs. high density polyethylene) [37]. The addition of pressure as a knob to tune the properties of supercritical fluids has motivated the use of solvents with low critical temperatures and pressures, such as carbon dioxide, ethylene propane, and butane, to dissolve and purify polymers.

Predictive methods for solubility in supercritical fluids are also less established than for typical solvents. Current methods rely on equation-of-state models, such as the perturbed chain-statistical associating fluid theory (PC-SAFT) equation of state [38], and some recent methods have developed machine-learning methods or extended COSMO-RS models appropriate for predicting solubility in supercritical carbon dioxide, [39] but more generalizable methods are needed.

## 6.3 References

- [1] Geoffrey Pritchard. *Plastics additives: an AZ reference*, volume 1. Springer Science & Business Media, 2012.
- [2] Rita Kol, Tobias De Somer, Dagmar R D’hooge, Fabian Knappich, Kim Ra-gaert, Dimitris S Achilias, and Steven De Meester. State-of-the-art quantifica-tion of polymer solution viscosity for plastic waste recycling. *ChemSusChem*, 14(19):4071–4102, 2021.
- [3] NM Nurazzi, MNF Norrrahim, SS Shazleen, MM Harussani, FA Sabaruddin, and MRM Asyraf. Introduction to polymer crystallization. *Polymer Crystallization: Methods, Characterization and Applications*, pages 1–12, 2023.
- [4] Beth A Miller-Chou and Jack L Koenig. A review of polymer dissolution. *Progress in polymer science*, 28(8):1223–1270, 2003.
- [5] Michael Rubinstein and Ralph H Colby. *Polymer physics*. Oxford university press, 2003.
- [6] Aurora del C Munguía-López, Panzheng Zhou, Ugochukwu M Ikegwu, Reid C Van Lehn, and Victor M Zavala. A fast computational framework for the design

of solvent-based plastic recycling processes. *Systems and Control Transactions*, 3:814–819, 2024.

- [7] Chiara Samorì, Daniele Cespi, Paola Blair, Paola Galletti, Danilo Malferrari, Fabrizio Passarini, Ivano Vassura, and Emilio Tagliavini. Application of switchable hydrophilicity solvents for recycling multilayer packaging materials. *Green Chemistry*, 19(7):1714–1720, 2017.
- [8] Yanhui Zhang, Ruiyu Fu, Qingxin Lu, Tingze Ren, Xiaoli Guo, and Xin Di. Switchable hydrophilicity solvent for extraction of pollutants in food and environmental samples: A review. *Microchemical Journal*, 189:108566, 2023.
- [9] Igor T Cunha, Meghan McKeeman, Maedeh Ramezani, Kayleigh Hayashi-Mehedy, Alana Lloyd-Smith, Marco Bravi, and Philip G Jessop. Amine-free co<sub>2</sub>-switchable hydrophilicity solvents and their application in extractions and polymer recycling. *Green Chemistry*, 24(9):3704–3716, 2022.
- [10] Mood Mohan, Jay D Keasling, Blake A Simmons, and Seema Singh. In silico cosmo-rs predictive screening of ionic liquids for the dissolution of plastic. *Green Chemistry*, 24(10):4140–4152, 2022.
- [11] Samuel C Pestana, João N Machado, R Domingos Pinto, Bernardo D Ribeiro, and Isabel M Marrucho. Natural eutectic solvents for sustainable recycling of poly(ethyleneterephthalate): closing the circle. *Green Chemistry*, 23(23):9460–9464, 2021.
- [12] Ben Said Anouar, Cécile Guinot, Jean-Christophe Ruiz, Frédéric Charton, Patrice Dole, Catherine Joly, and Chalamet Yvan. Purification of post-consumer polyolefins via supercritical co<sub>2</sub> extraction for the recycling in food contact applications. *The Journal of Supercritical Fluids*, 98:25–32, 2015.
- [13] Benedikt Hanschmann. Precipitation of polypropylene and polyethylene terephthalate powders using green solvents via temperature and antisolvent-induced phase separation. *Advances in Polymer Technology*, 2023(1):7651796, 2023.
- [14] Rebecca Renner. The kow controversy, 2002.
- [15] Gregor Cevc. Partition coefficient vs. binding constant: How best to assess molecular lipophilicity. *European Journal of Pharmaceutics and Biopharmaceutics*, 92:204–215, 2015.

- [16] Jun-Qin Qiao, Xiao-Lan Liu, Chao Liang, Ju Wang, Hong-Zhen Lian, and Li Mao. Prediction of the n-octanol/water partition coefficients of basic compounds using multi-parameter qsrr models based on is-rplc retention behavior in a wide ph range. *Molecules*, 28(5):2270, 2023.
- [17] David Van der Spoel, Sergio Manzetti, Haiyang Zhang, and Andreas Klamt. Prediction of partition coefficients of environmental toxins using computational chemistry methods. *ACS omega*, 4(9):13772–13781, 2019.
- [18] Qiang Zhu, Qingqing Jia, Ziteng Liu, Yang Ge, Xu Gu, Ziyi Cui, Mengting Fan, and Jing Ma. Molecular partition coefficient from machine learning with polarization and entropy embedded atom-centered symmetry functions. *Physical Chemistry Chemical Physics*, 24(38):23082–23088, 2022.
- [19] Richard K Henderson, Concepción Jiménez-González, David JC Constable, Sarah R Alston, Graham GA Inglis, Gail Fisher, James Sherwood, Steve P Binks, and Alan D Curzons. Expanding gsk’s solvent selection guide—embedding sustainability into solvent selection starting at medicinal chemistry. *Green Chemistry*, 13(4):854–862, 2011.
- [20] Denis Prat, John Hayler, and Andy Wells. A survey of solvent selection guides. *Green Chemistry*, 16(10):4546–4551, 2014.
- [21] Louis J Diorazio, David RJ Hose, and Neil K Adlington. Toward a more holistic framework for solvent selection. *Organic Process Research & Development*, 20(4):760–773, 2016.
- [22] Indumathy Jagadeeswaran and Harini Sriram. Eu 1907/2006—registration, evaluation, authorisation and restriction of chemicals. In *Medical Device Guidelines and Regulations Handbook*, pages 237–260. Springer, 2022.
- [23] Linda Schierow. Toxic substances control act. *Environmental Laws: Summaries of Statutes Administered by the Environmental Protection Agency*, page 89, 2001.
- [24] Linda-Jo Schierow. The toxic substances control act (tsca): implementation and new challenges. Congressional Research Service, Library of Congress, 2008.
- [25] Panzheng Zhou, Jiuling Yu, Kevin L Sánchez-Rivera, George W Huber, and Reid C Van Lehn. Large-scale computational polymer solubility predictions and

applications to dissolution-based plastic recycling. *Green Chemistry*, 25(11):4402–4414, 2023.

- [26] Jens Kahlen, Kai Masuch, and Kai Leonhard. Modelling cellulose solubilities in ionic liquids using cosmo-rs. *Green Chemistry*, 12(12):2172–2181, 2010.
- [27] Yoshihiro Hayashi, Junichiro Shiomi, Junko Morikawa, and Ryo Yoshida. Radonpy: automated physical property calculation using all-atom classical molecular dynamics simulations for polymer informatics. *npj Computational Materials*, 8(1):222, 2022.
- [28] Raashiq Ishraaq and Siddhartha Das. All-atom molecular dynamics simulations of polymer and polyelectrolyte brushes. *Chemical Communications*, 60(48):6093–6129, 2024.
- [29] Kazuo Yamada and Nobuyuki Matubayasi. Chain-increment method for free-energy computation of a polymer with all-atom molecular simulations. *Macromolecules*, 53(3):775–788, 2020.
- [30] Sunhwan Jo, Taehoon Kim, Vidyashankara G Iyer, and Wonpil Im. Charmm-gui: a web-based graphical user interface for charmm. *Journal of computational chemistry*, 29(11):1859–1865, 2008.
- [31] Makoto YABE, Kazuki MORI, Kazuyoshi UEDA, and Minoru TAKEDA. Development of polypargen software to facilitate the determination of molecular dynamics simulation parameters for polymers. *Journal of Computer Chemistry, Japan-International Edition*, 5:2018–0034, 2019.
- [32] Mayk C Ramos, Patrick K Quoika, Vitor AC Horta, Douglas M Dias, Elan G Costa, Jorge LM do Amaral, Luigi M Ribeiro, Klaus R Liedl, and Bruno AC Horta. pypolybuilder: automated preparation of molecular topologies and initial configurations for molecular dynamics simulations of arbitrary supramolecules. *Journal of Chemical Information and Modeling*, 61(4):1539–1544, 2021.
- [33] Ming Huang and Cameron F Abrams. Htpolynet: A general system generator for all-atom molecular simulations of amorphous crosslinked polymers. *SoftwareX*, 21:101303, 2023.

- [34] Donald Patterson. Polymer compatibility with and without a solvent. *Polymer Engineering & Science*, 22(2):64–73, 1982.
- [35] Christopher F Kirby and Mark A McHugh. Phase behavior of polymers in supercritical fluid solvents. *Chemical Reviews*, 99(2):565–602, 1999.
- [36] Mark McHugh and Val Krukonis. *Supercritical fluid extraction: principles and practice*. Elsevier, 2013.
- [37] BM Hasch, S-H Lee, MA McHugh, JJ Watkins, and VJ Krukonis. The effect of backbone structure on the cloud point behaviour of polyethylene-ethane and polyethylene-propane mixtures. *Polymer*, 34(12):2554–2558, 1993.
- [38] Pedro Arce and Martín Aznar. Modeling the phase behavior of commercial biodegradable polymers and copolymer in supercritical fluids. *Fluid phase equilibria*, 238(2):242–253, 2005.
- [39] Edgar T de Souza Jr, Paula B Staudt, and Rafael de P Soares. Prediction of solid solubility in supercritical carbon dioxide using a pairwise surface contact equation of state—cosmo-sac-phi. *The Journal of Supercritical Fluids*, 191:105765, 2022.